UNIVERSITÀ
DEGLI STUDI
FIRENZE

DOTTORATO DI RICERCA IN
Area del Farmaco e Trattamenti Innovativi
Curriculum Scienze Farmaceutiche

CICLO **XXXIV**

COORDINATORE Prof.ssa Carla Ghelardini

Drug design, synthesis and biological/structural evaluation of hybrids targeting proteins and nucleic acids involved in pathological processes

Settore Scientifico Disciplinare CHIM/08

Dottorando
Dr. Andrea Petreni

Tutore scientifico
Prof. Claudiu T. Supuran

Tutore teorico
Prof. ssa Paola Gratteri

Coordinatore
Prof.ssa Carla Ghelardini

(firma)

Anni 2018-2021

ABSTRACT

The main goal of this PhD thesis has been the creation of new multi-target derivatives which interact simultaneously with multiple targets implicated in a pathology. The multi-target strategy has become more widespread in the twenty-first century where year after year there has been an increasing number of compounds approved by the FDA and EMA that have this type of characteristics. The main advantages are a better patient compliance, a reduction of drug-drug interactions, a simpler pharmacokinetics, and a synergistic effect.

The multi-target drug-design projects here proposed have a common base that is a portion in the compound structures to modulate the activity of human carbonic anhydrases (hCAs). CAs have been found in countless species, including bacteria, protozoa, fungi, mammals and thus human. Eight families, indicated with Greek letters (α, β, γ, δ, ζ, η, θ and ι), have been discovered from unrelated gene families. Among these, only α-class CAs are present in human and are distinguished in 15 different isoforms, of which 12 are catalytically active (hCAs I, II, III, IV, VA/B, VI, VII, IX, XII, XIII, XIV). As all CAs, hCAs catalyse the hydration of carbon dioxide into bicarbonate and protons, playing a variety of pivotal physiological roles in human body, which are related to this apparently simple reaction: respiration, pH and CO_2 homeostasis, transport of CO_2/HCO_3^- and a multitude of biosynthetic reactions involved in crucial metabolic pathways such as gluconeogenesis, lipogenesis, ureagenesis, bone resorption, calcification, and carcinogenesis. Abnormal levels or activities of hCAs have been associated to a multitude of human diseases which increased the interest of the scientific community for the design of hCAs inhibitors or activators with biomedical applications.

In a first project we proposed the inclusion of a 5-fluorouracil (5-FU) moiety, a chemotherapeutic agent, into the structure of different types of validated inhibitors of CAs IX and XII, that are cancer-associated isoforms and valuable antitumor targets. Most sulfonamide derivatives efficiently inhibit the target CA IX and CA XII, while the 5-FU coumarin derivatives showed a potent and totally selective inhibitory action against the cancer-related CAs over off-target CA I and II. A subset of potent inhibitors showed effective *in vitro* antiproliferative and proapoptotic action against several cancer cell lines corroborating the potential of 5-FU CAIs for the design of new effective anticancer strategies.

The second proposed project is also aimed at obtaining new antitumor derivatives upon a multi-target approach. Again, sulfonamide and coumarin CAIs were hybridized with a berberine scaffold, a natural compound shown to be able to stabilize G-quadruplex (G4) structures. The latter are non-canonical DNA folding, found in guanine-rich sequences, such as single-stranded terminal segment of telomeres and numerous proto-oncogenic genes (*e.g.* C-kit and C-myc). G4 stabilization inhibits the action of telomerases (overexpressed in 85% of tumors and making cancer cells semi-immortal), and the transcription of C-kit and C-myc. Berberine was linker to CAI portions by different length spacer and 1,2,3-triazole linker produced by Click Chemistry. The compounds demonstrated relevant inhibitory potency and often selectivity against the tumor-associated CAs over off-target ones. Further, all hybrid compounds showed to stabilize the target G4 foldings (c-kit > telomer > c-myc > off-target DNA folding) more efficiently than lead berberine. In this project I have also dedicated to crystallization studies, that were set to attain the 3D structure of the G4 folding in complex with the hybrid inhibitors. To date, we succeeded in solving the Tel23 structure (mimicking the telomer G4) in complex with a sulfonamide berberine hybrid (PDB code 7PNL).

The third proposed project also applies a multi-target approach to produce innovative agent endowed with a potent precognitive action for the symptomatic treatment of neurodegenerative disorders, such as Alzheimer's disease (AD). CA activators of the amine/amino acid type were merged with tacrine, the first drug approved by the FDA for the treatment of AD, that effectively inhibits acetylcholinesterase and butyrylcholinesterase. Two series of hybrids were designed according to the type of linker (amide or amine) connecting tacrine with the CAAs. Extended SAR were worked out with the wide set of derivatives as activators of many CNS CA isoforms and inhibitors of cholinesterases, identifying a multitude of potent dual modulators. The 3 best derivatives were evaluated by a procognitive test in mice and even showed that the multi-target compounds are more effective than the co-administration of D-Phe, as a standard and potent CAA, and tacrine.

During my Ph.D. period, I also performed a multitude of kinetic studies with inhibitors and activators of several isoforms of CA belonging to the classes α, β, γ and ι. These studies allowed to draw up the inhibition or activation profiles of hundreds of derivatives from collaborators of us. Additionally, I performed the *ex-novo* complete kinetic characterization of the new ι-CA isoforms identified in a Gram-negative bacterium *Burkholderia territorii*.

TABLE OF CONTENTS

List of Abbreviations and Acronyms

Aβ	Amyloid β-peptide
AAZ	Acetazolamide
Ach	Acetyl choline
AChE	Acetyl Choline Esterase
AD	Alzheimer's disease
AE2	Anion Exchangers
AG	Anchoring Group
APP	Amiloyd precursor protein
BACE	Beta Secretase
BBB	Blood brain barrier
BRZ	Brinzolamide
BtcCA-ι	*Burkholderia territorii* **CA-ι**
BuChE	Butirryl Cholinesterase
BZA	Benzolamide
CA	Carbonic Anhydrase
CAI	Carbonic Anhydrase Inhibitor
CAAs	Carbonic Anhydrase Activators
CARPs	CA-Related Proteins
CLX	Celecoxib
CNS	Central Nervous System
CSF	Cerebro spinal fluid
DBU	Diazabicycloundecene
DCP	Dichlorophenamide
DCM	Dichloromethane
DIPEA	Di-isopropyl ethyl aminw
DMF	Dimetilformammide
DMAP	4-Dimethylaminopyridine
DNA	Desoxyribonucleic acid
DTCs	Dithiocarbamates
DZA	Dorzolamide
EDCI	1-Ethyl-3-(3-
EhiCA	*Entamoeba histolytica*
EPSP	Excitatory postsynaptical potential
ERK	Extracellular signal-regulated kinases
EZA	Ethoxzolamide
FRET	Fluorescence Resonance Energy Transfer
5-FU	5-Fluorouracil
G4	G-Quadruplex
GIST	Gastrointestinal Stromal Tumours
GLUT-1	Glucose transporter 1
hpαCA	*H. pylori* α-Carbonic Anhydrase
hpβCA	*H. pylori* β-Carbonic Anhydrase
hCA	Human Carbonic Anhydrase
HIF-1	Hypoxia inducible factor 1
HJ	Holliday Junctions
HOBT	Hydroxybenzotriazole
IC_{50}	Half Maximal Inhibitory
IND	Indisulam
K_A	Activation Constant
K_I	Inhibition Constant
LdcCA	*Leishmania chagasi* Carbonic Anhydrase
MgCA	*Malassezia globosa* Carbonic Anhydrase
MPD	2-metil-2,4-pentandiole
MR	Molecular Replacement
MZA	Methazolamide
NBCe1	Sodium-bicarbonate Transporters
NFT	Neuro Fibrillary Tangles
NHE1	Sodium-proton Exchangers
OPs	Organo Phosphorus
PDB	Protein Data Bank
PEG	Polyethylenglicole
PEN2	Presenilin Enhancer 2
pK_i	Inhibition Binding Constants
PTSD	Post Traumatic Stress Disorders
ROS	Reactive Oxygen Species
RTK	Receptor Tyrosine Kinase
RY	Ryanodine
SA	Sulfanilamide
SAC	Saccharin
SAR	Structure-Activity Relationship
SG	Sticky Group
SI	*Selectivity Index*
SLP	Sulpiride
SLT	Sulthiame
SP	Senile Plaques
TBAF	Tetra Butyl ammonium fluoride
TEA	Triethylamine
TERT	Telomerase reverse trascriptase
TFA	Trifluoroacetic Acid
THF	Tetrahydrofuran
TPM	Topiramate
VchCA	*Vibrio cholerae* Carbonic Anhydrase
VLX	Valdecoxib
ZBG	Zinc Binding Group
ZNS	Zonisamide

PART I: INTODUCTION

CHAPTER 1. CARBONIC ANHYDRASES: CLASSIFICATION, BIOCHEMISTRY, AND STRUCTURE

Carbonic anhydrases (CAs, EC 4.2.1.1) exist in eukaryotes and prokaryotes as a superfamily of phylogenetically ubiquitous metalloenzymes.[1-15] The omnipresence of CAs is due to the catalysis of an easy physiologically essential reaction for living beings,[1] that is the reversible hydration of carbon dioxide to bicarbonate and proton (Equation 1).

$$CO_2 + H_2O \leftrightharpoons HCO_3^- + H^+ \qquad \text{(Eq.1)}$$

Usually, this reaction happens slowly at the pH values typically found in most tissues and organisms (turnover number - k_{cat} - of 10^{-1} s^{-1}). Thus, CAs are evolved to catalyze the carbon dioxide hydration to manage the large CO2 loads produced by most organisms, making the reaction substrates readily available for physiologic processes and managing acid-base equilibria.[1-3] Consequently, CAs are found in organisms of all life kingdoms (Animalia, Plantae, Fungi, Protista, Bacteria, and Archaea), becoming among the fastest enzymes known which effectively accelerate the speed of the reaction to 10^6 s^{-1}.[16]

In a lot of organisms, CAs are involved in the essential physiological processes of respiration, transport of CO_2/HCO_3^-, pH and CO_2 homeostasis and a range of biosynthetic reactions.[1-4] Moreover, in mammals, CAs promotes the metabolic reactions such as gluconeogenesis, secretion of electrolytes in many tissues/organs, ureagenesis, lipogenesis, bone resorption, calcification and tumorigenicity.[17-26] In algae, cyanobacteria and plants, these enzymes are implicated in photosynthesis,[6-9] whereas in diatoms CAs play a pivotal role in CO_2 fixation and SiO_2 cycle.[11] In pathogen microorganisms, such as bacteria, protozoa and fungi, CAs were shown to be crucial for the growth, virulence or acclimatization of the parasites in the hosts.[12]

1.1 Classification of carbonic anhydrases

The CAs are classified in eight evolutionarily unrelated families (α-, β-, γ-, δ-, ζ-, η-, θ-, and ι-CAs) that are distinguished by different structural properties and phylogenetic distribution (Table 1).[1-15]

The α-CAs have been identified in vertebrates, protozoa, algae, corals, bacteria, and green plants.[1,12] The β-CAs are present in bacteria, fungi, archaea, algae, and chloroplasts of both mono- and dicotyledons.[12,27,28] The γ-CAs were found in archaea, bacteria, and plants.[9] The δ-CAs are encoded in marine phytoplankton, such as haptophytes, dinoflagellates, diatoms, and chlorophyte prasinophytes,[8] whereas ζ-CAs have been identified only in marine diatoms.[4] A unique η-CA were detected to date in the protozoa *Plasmodium falciparum*.[7] The θ-Cas seem to be present in the marine diatom *Phaeodactylum tricornutum*.[11] The first ι-CA was identified in the marine diatom *Thalassiosira pseudonana*,[5] and more recently it was also found in Gram-negative bacterium *Burkholderia territorii*. [13-16, 29]

Table 1. Structural features and phylogenetic distribution of the eight evolutionarily unrelated families: α-, β-, γ-, δ-, ζ-, η-, θ- and ι-CAs.

Family	Metal atom	Coordinated residues	Quaternary structure	Organisms
α	Zn^{2+}	His, His, His	Monomer, dimer	Vertebrates, bacteria, protozoa, fungi, green plants, algae, and corals
β	Zn^{2+}	His, Cys, Cys	Dimer, tetramer, octamer	Bacteria, protozoa, fungi, archaea, algae, and chloroplasts of mono- and dicotyledons.
γ	Zn^{2+}, Fe^{2+}, Co^{2+}	His, His, His	Trimer	Archaea, bacteria, and plants
δ	Zn^{2+}, Cd^{2+}, Co^{2+}	His, His, His	Not available	Marine phytoplankton
ζ	Cd^{2+}, Zn^{2+}	His, Cys, Cys	Trimer	Marine diatoms
η	Zn^{2+}	His, His, Gln	Not available	Plasmodium spp.
θ	Zn^{2+}	His, Cys, Cys	Dimer	Marine diatoms
ι	Not available	Not avalailable	Not available	Marine diatoms, and bacteria

A broad collection of kinetic and X-ray crystallographic data allow a detailed awareness of the structure-function relationship in the CAs superfamily.[2,16] These metalloenzymes are catalytically

effective when a metal ion is bound within the active site cavity. The catalytic portion frequently includes a metal(II) ion in a tetrahedral geometry, three coordinated amino acid residues, and a water molecule/hydroxide ion completing the coordination sphere around the metal atom. Zn(II) is the metal ion spread in all CA genetic families, but it can be exchanged with Cd(II) in ζ-CAs,[4] and Fe(II) is presumably present in γ-CAs in anaerobic conditions.[8] A Co(II) ion can replace the zinc ion in several α-CAs not giving a significant loss of the catalytic efficiency.[8]

1.2 Catalytic mechanism of carbonic anhydrases

In all CA classes, the catalytic mechanism is verified in two steps (Eq. 2 and 3).

$$E\text{-}M^{2+}\text{–}\ OH^{-} + CO_2 \rightleftarrows E\text{-}M^{2+}\text{–}\ HCO_3^{-} + H_2O \rightleftarrows E\text{-}M^{2+}\text{–}H_2O + HCO_3^{-} \qquad \text{(Eq.2)}$$

$$E\text{-}M^{2+}\text{–}\ H_2O + B \rightleftarrows E\text{-}M^{2+}\text{–}\ OH^{-} + BH^{+} \qquad \text{(Eq. 3)}$$

The metal hydroxide ($E\text{-}M^{2+}\text{-}OH^{-}$) is the catalytically active species of the enzyme. At neutral pH, in the first step of the reaction, this species acts as a strong nucleophile against the CO_2 molecule bound in a hydrophobic pocket nearby, with consequent formation of HCO_3^{-}. Therefore, the bicarbonate ion is displaced by a second water molecule and released outwards (Eq. 2). When a water molecule is bound to the zinc ion ($E\text{-}M^{2+}\text{-}H_2O$), the enzyme is in its acidic, catalytically inactive form. In the second and rate-determining step, the catalytically active metal hydroxide species is regenerated by a proton transfer reaction from the metal-bound water to an exogenous proton acceptor or an active site residue (B).[1-3] The overall catalytic mechanism is shown in Figure 1A. In the catalytically very active isozymes, (such as the human isoforms II, IV, VI, VII, IX, XII, XIII, and XIV), the proton transfer process is assisted by a Histidine residue placed at the entrance of the active site (H64 known as "proton shuttle residue"), or by a cluster of Histidines (Figure 1B), which protrudes from the rim of the active site to the surface of the enzyme, thus assuring efficient proton-transfer pathways.[2] The absence of His64 in other CAs significantly decreases their catalytic efficiency.

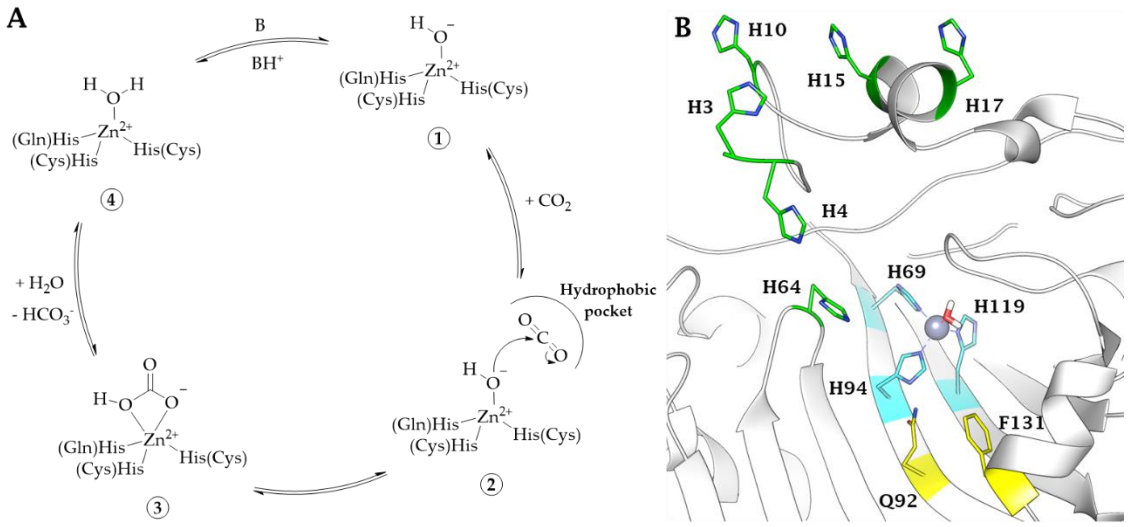

Figure 1. (A) Schematic representation of the CA catalytic mechanism; (B) His64, known as "proton shuttle residue" and cluster of His residues which ensure an efficient proton-transfer pathway (shown in hCA II, PDB 3KKX).

A catalytic turn-over reaching k_{cat}/K_M values over 10^8 M^{-1} x s^{-1} in some α- and ζ-CAs places CAs among the most efficient natural catalysts.[30] This efficient catalysis is also due to a peculiar architecture common among all CA families that differentiates the active site in two very different environments: one made of hydrophobic amino acids and the other lined by hydrophilic residues.[16,30] Indeed, the hydrophobic part could have the role of entrapping the CO_2 molecule while the hydrophilic one could represent the escape outwards of the polar species produced by the CO_2 hydration reaction.[2] The latter process was demonstrated at least for the protons, adjuvated in their moving towards outside of the cavity by a network of water molecules and Histidine residues.[3]

1.3 Characteristics of the major families of carbonic anhydrases

1.3.1 α-Carbonic anhydrases

α-CAs are spread in vertebrates, algae, protozoa, corals, green plants and bacteria. A great deal of studies enabled to identify sixteen different isozymes in mammals, and several other isozymes in non-mammalian vertebrates.[1,2] Unquestionably, the most important α-CAs subset is represented by the fifteen isoforms identified to date in *Homo sapiens* (Table2).[1-3,16]

Table 2. Organ/Tissue Distribution, Subcellular Localization, CO_2 Hydrase Activity, and Diseases in which each isoform is involved.

hCA	Organ/tissue distribution	Subcellular localization	k_{cat}/K_M ($M^{-1}s^{-1}$)	Diseases in which the isoform is involved
CA I	Erythrocytes, gastrointestinal tract, eye, CNS (motoneurons)	Cytosol	5.0×10^7	Retinal/cerebral edema, neurodegenerative diseases
CA II	Erythrocytes, eye, gastrointestinal tract, bone osteoclasts, kidney, lung, testis, brain (choroid plexus, oligodendrocytes, astrocytes, and	Cytosol	1.5×10^8	Glaucoma, edema, epilepsy, altitude sickness, cancer, neurodegenerative diseases
CA III	Skeletal muscle, adipocytes	Cytosol	2.5×10^5	Oxidative stress
CA IV	Kidney, lung, pancreas, colon, heart muscle, eye, brain (brain capillaries, BBB, thalamus, and hippocampus)	Membrane-bound	5.1×10^7	Glaucoma, retinitis pigmentosa, stroke, neurodegenerative disease
CA VA	Liver, CNS (astrocytes and neurons)	Mitochondria	2.9×10^7	Obesity, diabetic cerebrovascular and neurodegenerative disease
CA VB	Heart and skeletal muscle, pancreas, kidney, spinal cord, gastrointestinal tract, CNS (astrocytes and neurons)	Mitochondria	9.8×10^7	Obesity, neurodegenerative disease
CA VI	Salivary and mammary glands	Secreted	4.9×10^7	Cariogenesis
CA VII	CNS (pH regulation)	Cytosol	8.3×10^7	Epilepsy, neuropathic pain, neurodegenerative disease
CA IX	Tumors, gastrointestinal mucosa	Transmembrane	5.4×10^7	Cancer
CA XII	Renal, intestinal, reproductive epithelia, eye, tumors	Transmembrane	3.5×10^7	Cancer, glaucoma
CA XIII	Kidney, brain, lung, gut, reproductive tract	Cytosol	1.1×10^7	Sterility
CA XIV	Kidney, brain, liver, skeletal muscle	Transmembrane	3.9×10^7	Epilepsy, retinopathies

These isoenzymes differ by molecular features, expression levels, kinetic properties, distribution in organs and tissues, oligomeric arrangement, cellular localization and response to different classes of inhibitors.[1-3] Catalytically active isoforms are twelve(I, II, III, IV, VA, VB, VI, VII, IX, XII, XIII, XIV), while the remaining three (VIII, X, XI), called CA-related proteins (CARPs), have no catalytic activity as they lack the zinc ion in the active site and one or more Histidine residues usually belonging to its coordination sphere.[1-3] Human CAs can be grouped into four different subsets depending on their subcellular localization (Figure 2). CA I, II, III, VII, VIII, X, XI, XIIII are cytosolic proteins, CA VA and VB are present in the mitochondrial matrix, CA VI is a secreted enzyme, CA IV is a glycosylphosphatidylinositol (GPI)-anchored protein, and CA IX, XII and XIV are trans-membrane isoforms.[32] These enzymes are broadly distributed in many organs and tissues where they are involved in a plethora of essential physiological processes. Thus, their dysregulated expression and/or abnormal activity can result in severe pathological conditions (Table 2).

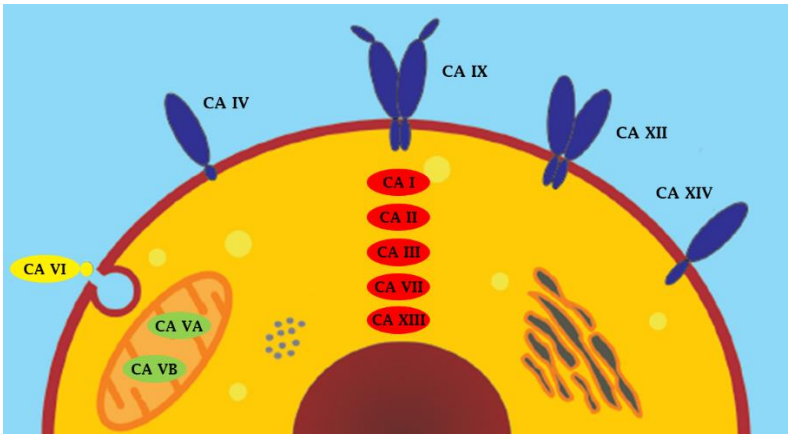

Figure 2. Schematic illustration of domain composition and subcellular localization of catalytically active human α-CAs.

All 3D structure of all catalytically active human isoforms are contained in PDB[31] database contains the 3D structures, except CA VA and VB. These enzymes maintain common structural attributes independently on their subcellular localization. Indeed, in agreement with the high sequence identity among hCA isoforms, structural studies have demonstrated that all these enzymes share the same fold characterized by a central ten-stranded β-sheet, surrounded by α- and 3_{10}- helices and additional β-strands (Figure 3A). The active site is in a large conical cavity, about 15 Å deep, at the base of which the zinc ion is located, coordinated by three conserved histidine residues (H94, H96, and H119) and the solvent molecule/hydroxide ion.

The Zn^{2+}-bound water molecule/hydroxide ion is involved in a network of hydrogen bonds that increase its nucleophilicity (Figure 3B).

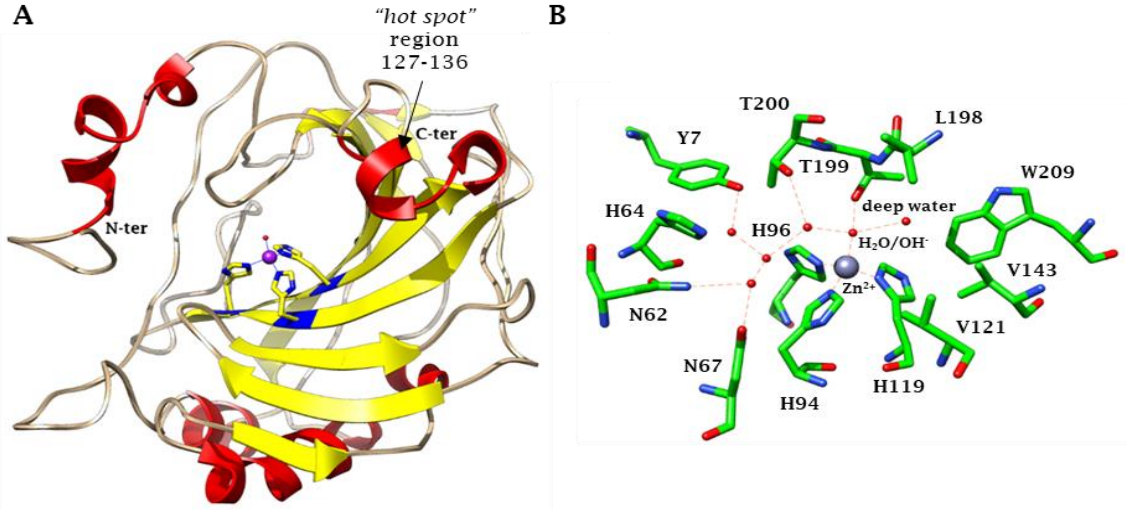

Figure 3. (A) Ribbon diagram of hCA II structure (PDB code 1CA2), which has been chosen as representative CA isoform. The active site Zn^{2+} coordination is also shown. Helix and β-strand regions are colored in red and yellow, respectively. (B) View of CA II active site. The Zn^{2+} is tetrahedrally coordinated by the three catalytic Histidines and a water molecule/hydroxide ion, which is engaged in a well-defined network of hydrogen bonds. Water molecules are indicated as red spheres.

In particular, it establishes a hydrogen bond with the hydroxyl moiety of the conserved T199 residue and with two water molecules, located on two opposite sides: the first one also called the "deep water", is located in a hydrophobic cavity delimited by conserved residues V121, V143, L198, and W209, while the second one is in a hydrophilic environment toward the entrance of the active site (Figures 3B and 4A). These two peculiar active site environments are supposed to be responsible for the rapid catalytic cycle of CO_2 to bicarbonate; in fact, the hydrophobic region is necessary to take the CO_2 substrate and orient the carbon atom for the nucleophilic attack by the zinc-bound hydroxide (Figure 4B), while the hydrophilic region creates a well-ordered hydrogen-bonded solvent network, which is necessary to allow the proton transfer reaction from the zinc-bound water molecule to the bulk solvent (Figure 4C).[16,30]

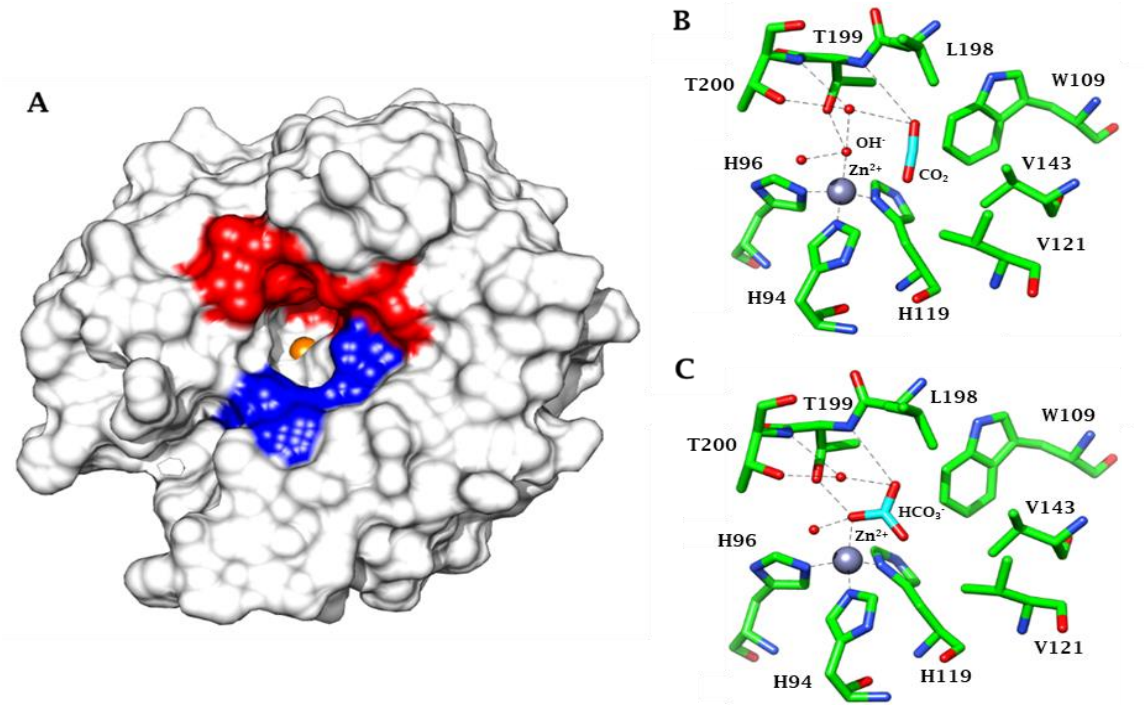

Figure 4. (A) Solvent accessible surface of CA II. Residues delimiting the hydrophobic half of the active site cleft are shown in red (I91, F131, V121, V135, L141, V143, L198, P202, L204, V207 and W209), while residues delimiting the hydrophilic one is shown in blue (N62, H64, N67 and Q92). The active site of CA II showing: (B) the position of CO_2 molecule (PDB code 2VVA), and (C) the binding of the bicarbonate ion (PDB code 2VVB). Zn^{2+} coordination and polar interactions are also reported.

A detailed comparison between all hCA isoforms reveals that the main sequence and structural differences between these enzymes are observed in the region 127-136 (Figure 3A), which thus has to be considered a "hot spot" in the structure-based drug design of selective hCA inhibitors.[30] The 12 catalytically active isoforms show also important differences in the quaternary structure; indeed, whereas CAs I-IV, VA, VB, VII, XIII, and XIV are monomers, CAs VI, IX, and XII are dimers. Interestingly, the dimeric interface is different in each one of these hCA dimers.

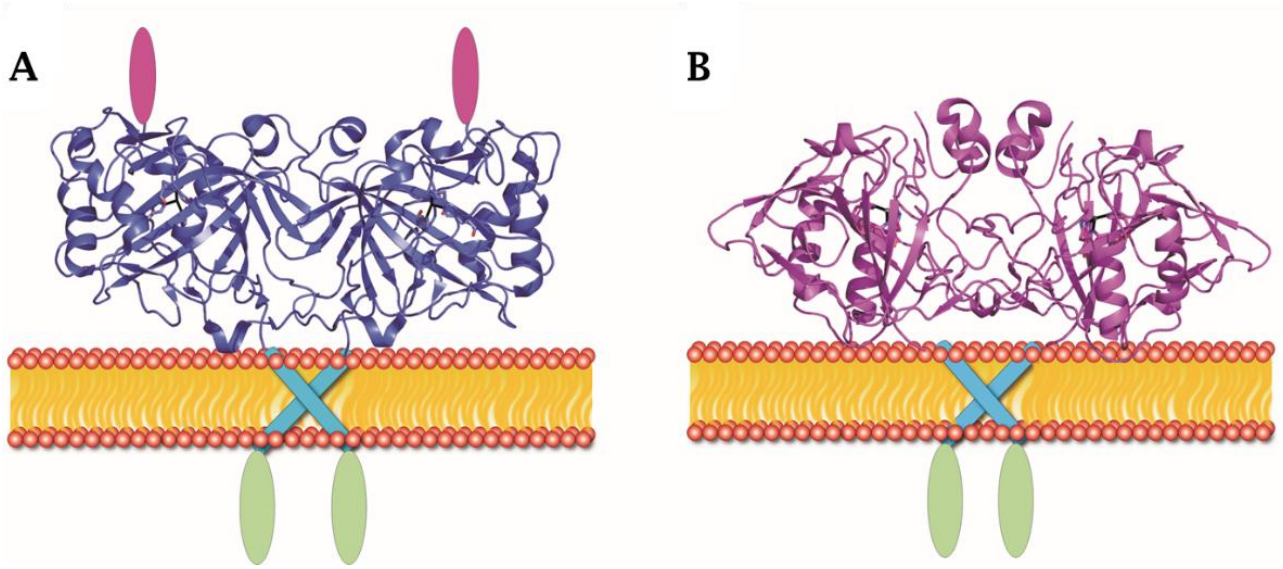

Figure 5. Proposed models of full-length CA IX (A)[32] and CA XII (B)[33] on the cell membrane. Both CA IX and CA XII contain an extracellular CA domain, a transmembrane region (cyan), and an intracellular tail (green). Additionally, CA IX contains a proteoglycan-like (PG) domain (magenta) at the N-terminus.

Differently, the bacterial α-CAs, such as those identified in *Sulfurihydrogenibium yellowstonense*, *Sulfurihydrogenibium azorense*, and *Neisseriagonorrhoeae*, are dimers formed by two identical active monomers.[12] Additionally, α-CAs possess a certain catalytic versatility that enables the fulfilment of several other hydrolytic processes presumably involving non-physiological substrates. These promiscuous reactions include the hydration of cyanate to carbamic acid (Equation 4), or of cyanamide to urea (Equation 5), the aldehyde hydration to gem-diols (Equation 6), the hydrolysis of carboxylic, sulfonic, and phosphate esters (Equations 7-10).[2]

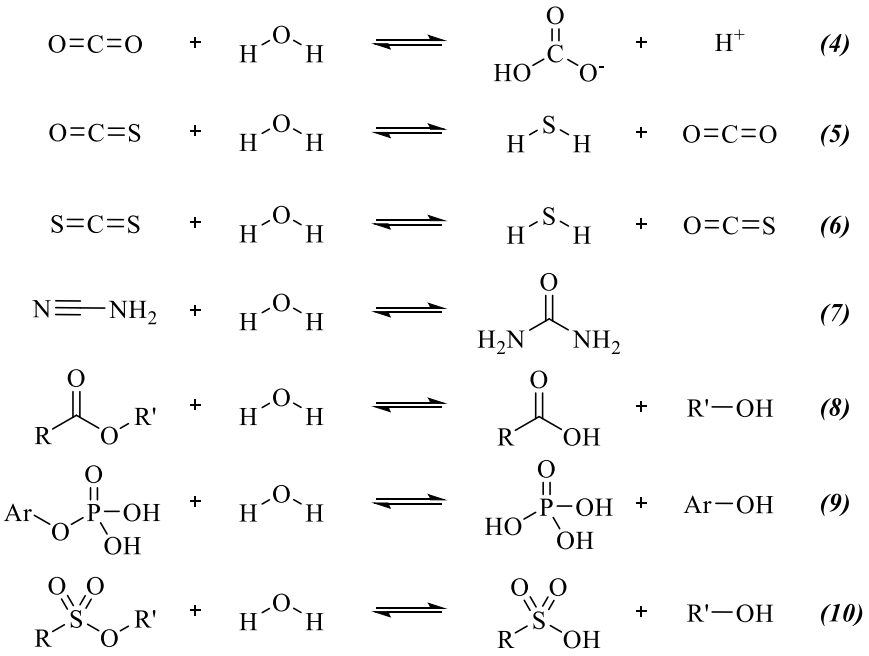

(4)

(5)

(6)

(7)

(8)

(9)

(10)

1.3.2 β-Carbonic anhydrases

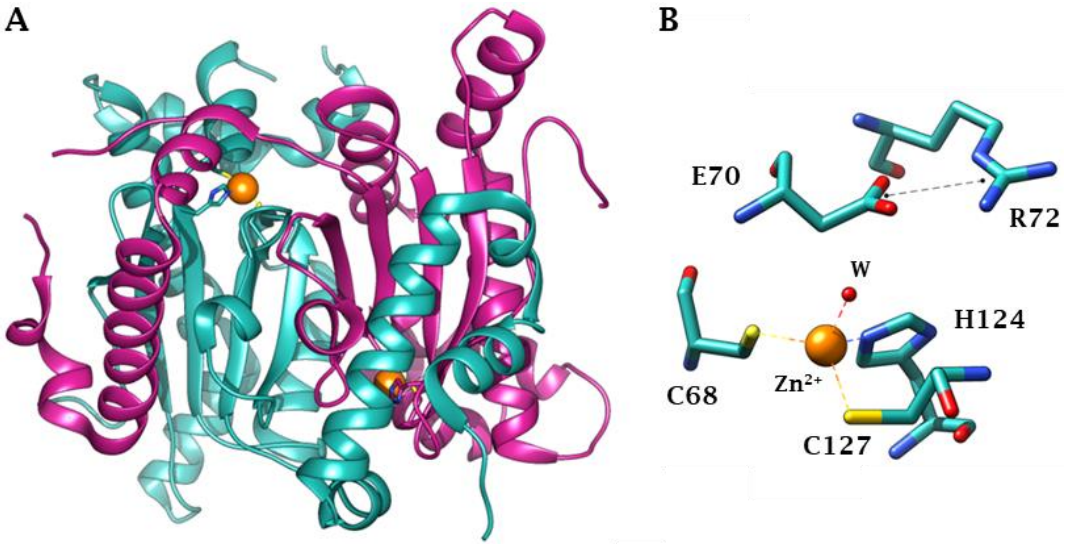

Figure 6. (A) Overall structure of a representative β-CA from fungi *Cryptococcus Neoformans* (Can2) dimer. One monomer is colored magenta, while the other one is colored sea green. The Zn^{2+} ions are shown as orange spheres. (B) The active site of Can2. Coordination of the active-site Zn(II) by C68, H124, C127, and a water molecule is shown by colored dashed lines, and the D70-R72 salt bridge is colored black.

The β-class CAs are widely distributed and identified in plants, bacteria, archaea, yeast, invertebrates and fungi.[10] Conversely from α-class isozymes, β-CAs are oligomers formed by two or more identical subunits, generally dimers, tetramers, and octamers (Figure 6A).[34] The active site exists at the dimer interface and contains hydrophobic and hydrophilic areas similar to hCAs. The residues of the catalytic triad are highly conserved among β-CA isoforms: the Zn(II) ion is coordinated by two cysteine residues, a residue of His and the carboxyl group of a residue of Asp or, alternatively, a water molecule/hydroxide ion (Figure 6B and Figure 7).

At a pH of 7.5 or lower, the β-CA active site, formed by residues belonging to two different subunits, is "closed" (type II enzyme), since the carboxyl group of the aspartic acid of the conserved dyad arginine-aspartate coordinates the zinc ion, thus completing the coordination sphere (Figure 7A). At pH values higher than 8.3, the aspartate and arginine of this dyad form a salt bridge leading the enzyme in its "open" active form (type I enzyme).[10,16,24] A molecule of water/hydroxide ion completes the tetrahedral geometry coordination pattern around the metal ion (Figure 7B). The catalytic mechanism of β-CAs with the active site in the "open" form is rather similar to α-class enzymes.

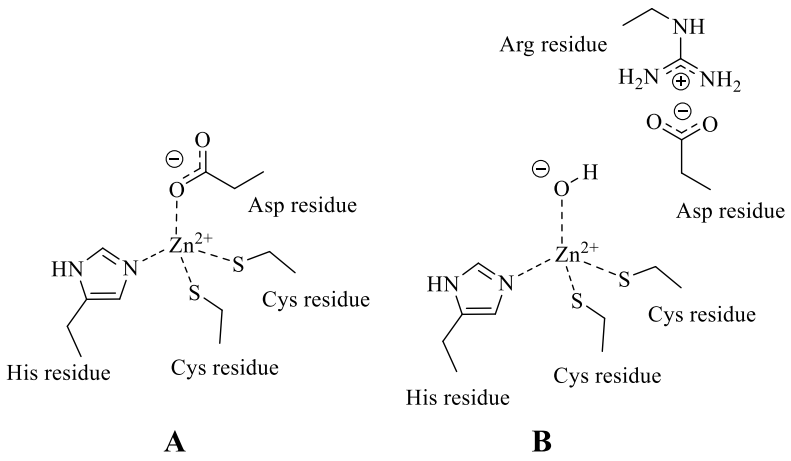

Figure 7. Inactive (A) and active (B) forms of β-CAs active sites.

1.3.3 γ-Carbonic anhydrases

Until now, γ-class CAs have been identified in plants, archaea and bacteria[9] Cam, the carbonic anhydrase from the methanearcheon *Methanosarcina thermophila*, is the prototype of the γ-class.[35] The crystal structure of Cam showed that one monomer consists of seven complete turns of a left-handed parallel β-helix topped by a short α-helix, followed by a second C-terminal α-helix which is positioned antiparallel to the axis of the β-helix (Figure 8A).[35] Each face of the beta-helix is included of parallel beta-strands, containing two or three residues each, and is connected to the subsequent face by a 120° turn, so that the cross-section of the β-helix resembles an equilateral triangle. Each turn of the β-helix contains two type II β-turns positioned between strands 1 and 2 and between strands 2 and 3 and is completed by a loop, connecting strand 3 with strand 1 of the next turn. The interior of the helix is dominated by hydrophobic interactions between aliphatic side chains of residues originating from equivalent positions in adjacent turns of the helix. The active enzyme is a homotrimer resulting from the packing of three left-handed β-helices with the axis all parallel (Figure 8B and 8C). Three residues, R59, D61, and D76, are important amino acids for *trimer* formation. R59 forms a salt bridge with D61 of the same monomer and D76 of another monomer. These three residues are almost entirely conserved in all γ-CAs sharing homology with Cam.

The active site is localized at the interfaces between two subunits. In the active site a Zn(II) ion is coordinated by H81 and H122, which extend from equivalent positions of the adjacent turn of one monomer, and by H117 located in an adjacent monomer (Figure 8C). Two water molecules complete the zinc coordination sphere forming a distorted trigonal bipyramidal geometry. The two water molecules are within hydrogen bond distance of the side chain of Q75 and E62.[16,35]

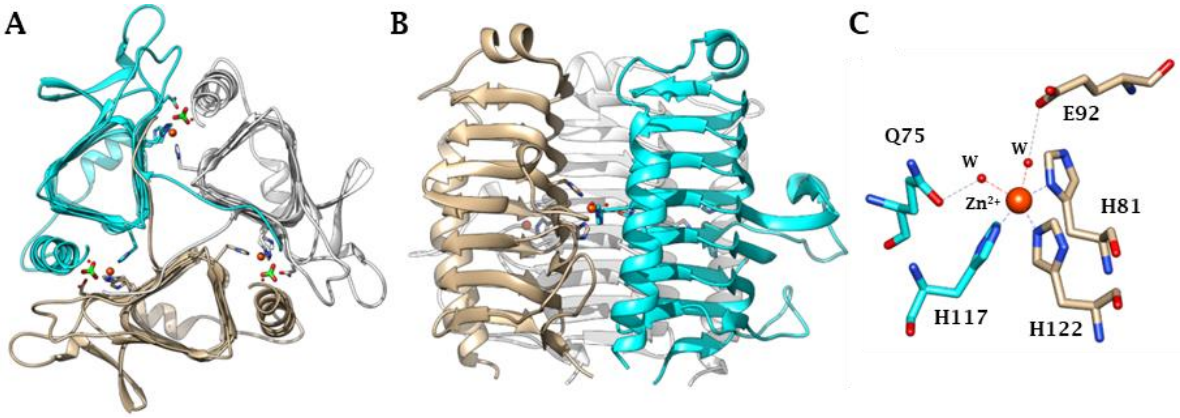

Figure 8. Ribbon representation of the Cam trimer. (A) Top view of the enzyme / HCO_3^- complex (PDB: 1QRL). (B) Side view (PDB: 1QRG). The overall fold is a left-handed β-helix, consisting of three untwisted, parallel β-sheets connected by left-handed crossovers. (C) Metal coordination within the active site which consists of a distorted trigonal bipyramidal geometry. Residues belonging to different subunits are depicted using different colours.

CHAPTER 2. CARBONIC ANHYDRASES AS DRUG TARGETS

2.1. Human carbonic anhydrases

The first isoforms to have been studied as drug-targets are human Cas, they have been from both the inhibition and activation perspectives.[1] Human CA inhibitors (CAIs) have written a long pharmacological history in many fields due to the involvement of CAs in a variety of important physio/pathological processes such as pH regulation, calcification, respiration, lipogenesis, gluconeogenesis, or tumorigenesis.[18-27] In contrast, CA activators have been much less studied to date, but in this thesis will see how they too will have some relevance.[16,36] Indeed, as a subset of CAs is abundant in the brain and was shown to be activatable by drug-like compounds, the possibility to design agents that enhance cognition has been recently emerging, with potential therapeutic applications in aging and neurodegenerative diseases.[1-4,16]

CAIs of the sulfonamide/sulfamate type have been long used as diuretics, systemic anti-convulsants, topically acting anti-glaucoma agents, or for the treatment of altitude sickness.[1,18-27,37] More recently CAIs have shown promising results as anti-obesity, anti-inflammatory, anti-neuropathic pain, and anti-tumor agents/diagnostic tools.[16-27]

The first-generation of CAIs shows an isoform mixed inhibitory activity, which leads to serious side effects for all pathologies in which they are used.[3] Hence, in the last decades, some innovative strategies were adopted to produce isoform-selective sulfonamide-like derivatives as well as new classes of isoform-specific CAIs were produced which showed alternative mechanisms of action. Understanding the factors governing selective inhibition of the single isoforms is clearly of pivotal importance and represents the breakthrough step to yield potential drugs that avoid the serious side effects due to promiscuous inhibition in the treatment of all pathologies in which CAIs will be employed.[3] In fact, the great potential of hCAs as drug targets resides in the wide multitude of diseases that can be targeted by selectively modulating the different isoforms.[37-61]

CA I is abundantly expressed in red blood cells and colon but is still considered an "orphan target" as it remains an "obscure object" for medicinal chemists.[13,35] Further difficulties have been encountered in developing CA I selective inhibitors.[1] However, several pieces of evidence

have demonstrated that CA I is involved in some types of anemia and chronic acidosis, diabetic macular edema and the proliferative diabetic retinopathy.[13,28]

The deregulation of the activity of the most physiologically relevant CA II has important pathological consequences in one or more tissues, such as glaucoma, edema, epilepsy, and is also involved in other pathologies such as acute mountain sickness[22] and, apparently, atherosclerosis[21] and osteoporosis.[28] CA II is also a target for imaging in various pathological conditions, in organs where the enzyme is present, such as the brain and cerebrospinal fluid or the gastrointestinal tract.[13]

Inhibition of CA III has not been determined to be advantageous for treating several diseases.[13] On the contrary, several natural and non-natural amino acid and aromatic/heterocyclic activators of CA III have been discovered, which might increase the defense mechanism against reactive oxygen species (ROS) in hepatocytes especially in the case of hepatotumorogenesis or infection by hepatitis B or C virus or might be beneficial therapeutics aimed to treat obesity.[28,37] However, because CA III has recently been proposed to be associated with acute myeloid leukemia and the progression of liver carcinoma, CA III specific inhibitors may have potential against in tumor proliferation and invasiveness in myeloid and liver tissue.[50]

CA IV was proven to be a promising drug target in the treatment of glaucoma, inflammation, retinis pigmentosa, some types of brain cancers and stroke.[35-38]

The involvement of CA VA and VB in *de novo* lipogenesis and the clear indications that the antiepileptic drugs topiramate and zonisamide (also potent inhibitors of the mitochondrial CAs) elicit significant weight loss in obese patients suffering with epilepsy led pharmaceutical companies to show interest in hCA V enzymes as novel drug targets for the treatment of obesity.[40] Activators of CA V (probably CA VB) might have clinical potential in diabetes, due to the implication of CA V in glucose-mediated insulin secretion from pancreatic β-cells.[28] CAVA has been also recently proposed as a specific target for prevention of diabetic cerebrovascular pathology.[13]

It could be speculated that the caries-inducing effect of CA VI is a result of enzymatic activity, and thus the inhibition of CA VI could reduce carcinogenesis. A CA inhibitor might be added

to oral hygiene products, such as toothpaste, mouthwash, tooth varnish, and chewing gum, to reduce the risk for the formation of enamel caries lesions.[43,44]

CA VII might represent a safe drug-target in the treatment of febrile seizure or eventually other epileptiform diseases as it is involved these pathologies and almost uniquely expressed in the central nervous system (CNS).[28,45] As the treatment with acetazolamide in combination with midazolam synergistically reduces neuropathic allodynia after spinal nerve damage,[47] CA VII together with CA II may represent a new drug target for managing neuropathic pain. Considering the importance of pH and ion homeostasis in reproductive organs to ensure a normal fertilization, the use of CA XIII inhibitors could be used for the development of anti-contraceptive agents.[55]

Data are available on the involvement of CA XIV in some retinopathies and epileptogenesis, which make CA XIV inhibitors useful agents for the management of such diseases.[57]

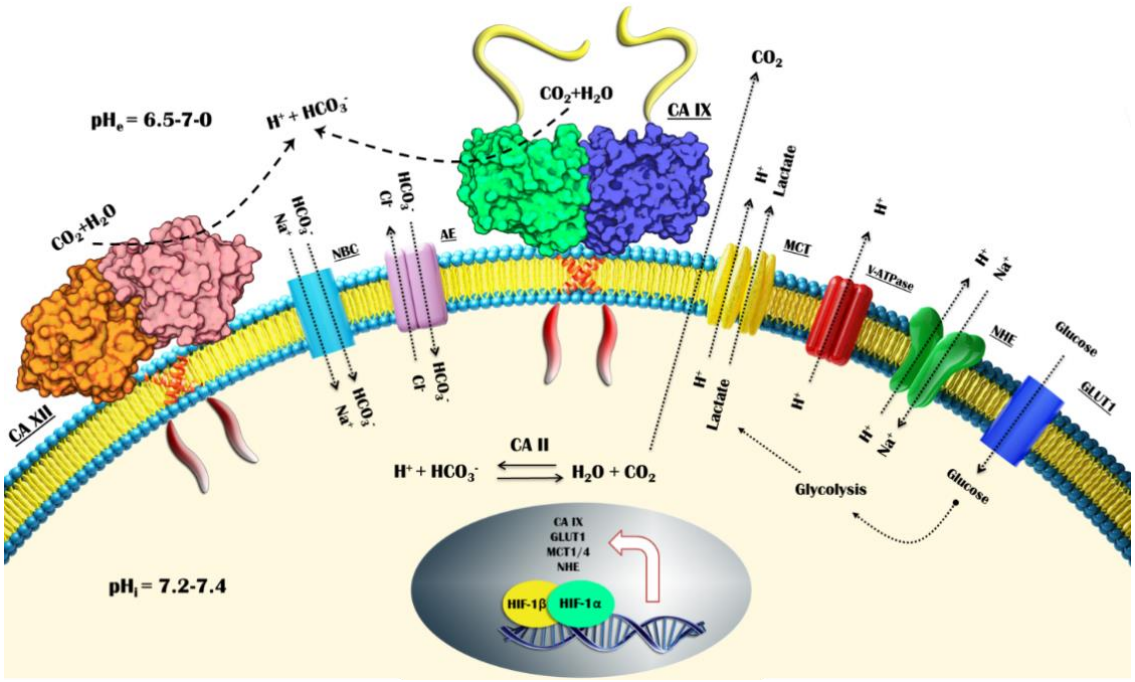

Figure 9. pH modulation machinery in hypoxic tumor cells. HIF-1 upregulates the expression of glucose transporters (GLUT1), glycolytic enzymes and proteins involved in pH regulation: monocarboxylate transporter (MCT), V-type H^+ATP (V-ATPase), Na^+/H^+ exchanger (NHE), bicarbonate co-transport (NBC), anion exchanger (AE), carbonic anhydrase IX (CA IX) and XII (CA XII).

The CA IX and XII were consistently validated as drug-targets and markers of disease progression in many solid tumors.[26,51,52] Overexpression of tumor-associated CAs is part of tumor cells adaptive responses to hypoxic conditions.[51] In fact, the inadequate delivery of oxygen to tumor cells (hypoxia) does induce a shift to glycolytic metabolism. The high glycolytic rate of tumor cells leads to increased production of acid metabolites, including lactate, carbon dioxide, and protons that creates an intracellular acidosis (pH_i) incompatible with the basic cellular functions. To survive and reduce intracellular acidification, cells activate complex molecular mechanisms involving ion exchangers, pumps, transporters, and carbonic anhydrases, which maintain a slightly alkaline pH_i acidifying the extracellular environment (pH_e) (Figure 9).[26]

CA IX was even more studied in this context being almost uniquely overexpressed in hypoxic tumors by the major pathway of HIF-1 transcription factor and serving as a prognostic/predictive factor for hypoxic, aggressive, and malignant tumors.[32,52] Nonetheless, both CA IX and XII were shown to be involved in chemoresistance, tumor cell migration, invasion, and maintenance of cancer cell stemness.[16,26]

Besides, CA IX and XII were lately identified to be overexpressed in inflamed tissues, being likely implicated in the acidification marking these tissues.[42] Furthermore, CA XII is also a validated target for the treatment of glaucoma.[37]

The 3D structures are available for all human isoforms except CA VA and VB and are of significant importance for structure-based drug design campaigns for yielding disease-targeting CA selective modulators.[62-71]

2.2 Carbonic anhydrases from pathogens

CAs are also emerging as innovative targets for the development of anti-infective agents with novel mechanisms of action to overcome cross-resistance shown against various existing anti-microbial drugs. A *plethora* of α-, β-, γ-CAs were cloned and characterized in many bacterial, fungal and protozoan pathogens and were shown to be promising anti-infective targets, though to date no CAI as anti-microbial agent is available for clinical use. CAs are essential in the pathogens life cycle and their inhibition can lead to growth impairment and defects.[18,72] One of the best-studied bacterial α-CA is the one from the gastric pathogen provoking ulcer and gastric cancer, *Helicobacter pylori*.[73-75] In fact, the genome of *H. pylori* encodes two CAs with different subcellular localization: a periplasmic α-class CA (hpαCA) and a cytoplasmic β-class CA (hpβCA).[73-75] These two enzymes were shown to be catalytically efficient, exhibiting an almost identical activity as the human isoform hCA I in the CO_2 hydration reaction, and are highly inhibited by many clinically used sulfonamides/sulfamates.[75] Since the efficacy of *H. pylori* eradication therapies currently employed has been decreasing due to drug resistance and side effects of the commonly used drugs, the dual inhibition of α- and/or β-CAs of *H. pylori* could be applied as an alternative therapy against the infection or for the prevention of gastroduodenal diseases provoked by this widespread pathogen.[74,75]

Vibrio cholerae is a Gram-negative bacterium, the causative agent of cholera, that colonizes the upper small intestine where sodium bicarbonate, an inducer of virulence gene expression, is present at a high concentration. *V. cholera* utilizes the CA system to accumulate bicarbonate into its cells, thus suggesting a pivotal role of these metalloenzymes in the microbial virulence.[76] *V. cholera* encodes CAs of three distinct classes, which are called VchCA (α-CA), VchCAβ and VchCAγ. These enzymes are efficient catalysts for CO_2 hydration.[76,77]

CAs are also abundantly spread in fungi and yeasts.[24,78-83] *Saccharomyces cerevisiae*,[82] *Candida albicans*[78-81], and *Candida glabrata*[79,80] have only one β-CA, whereas multiple copies of β-CA- and α-CA-encoding genes were reported in other fungi.[81] A recent work demonstrated that these CAs play an important role in the CO_2-sensing of the fungal pathogens and the regulation of sexual development.[80] Finally, another yeast, which has been investigated in detail for the presence of CAs is *Malassezia globosa*, which induced the production of dandruff.[83] As the

above-mentioned fungi/yeasts, it contains only one β-CA, denominated MgCA. Few protozoan parasites have been investigated for the presence and druggability of CAs. The malaria-provoking *Plasmodium falciparum* encodes the unique example of η-CA identified to date.[10,81-86] An α-CA has also been cloned and characterized in the unicellular protozoan *Trypanosoma cruzi*, the causative agent of Chagas disease.[77-88] The enzyme (TcCA) has a very high catalytic activity for the CO_2 hydration reaction, being similar kinetically to the human isoform hCA II.

In addition, another β-CA from the unicellular parasitic protozoan *Leishmania donovani chagasi* (LdcCA), which causes visceral leishmaniasis was identified, cloned and characterized.[8]

2.3 Main categories of carbonic anhydrase inhibitors

The mechanisms through which CAs are inhibited or activated have been studied for long time and are well-known processes. Nonetheless, new discoveries in the field are continually emerging.[3,90-130] Four inhibition mechanisms have been kinetically and structurally validated, while a significant subset of CA inhibitors lacks mechanistic characterization yet. A superimposition of compounds binding to the representative CA II by four distinct inhibition mechanisms is depicted in Figure 10 and classification is reported below:

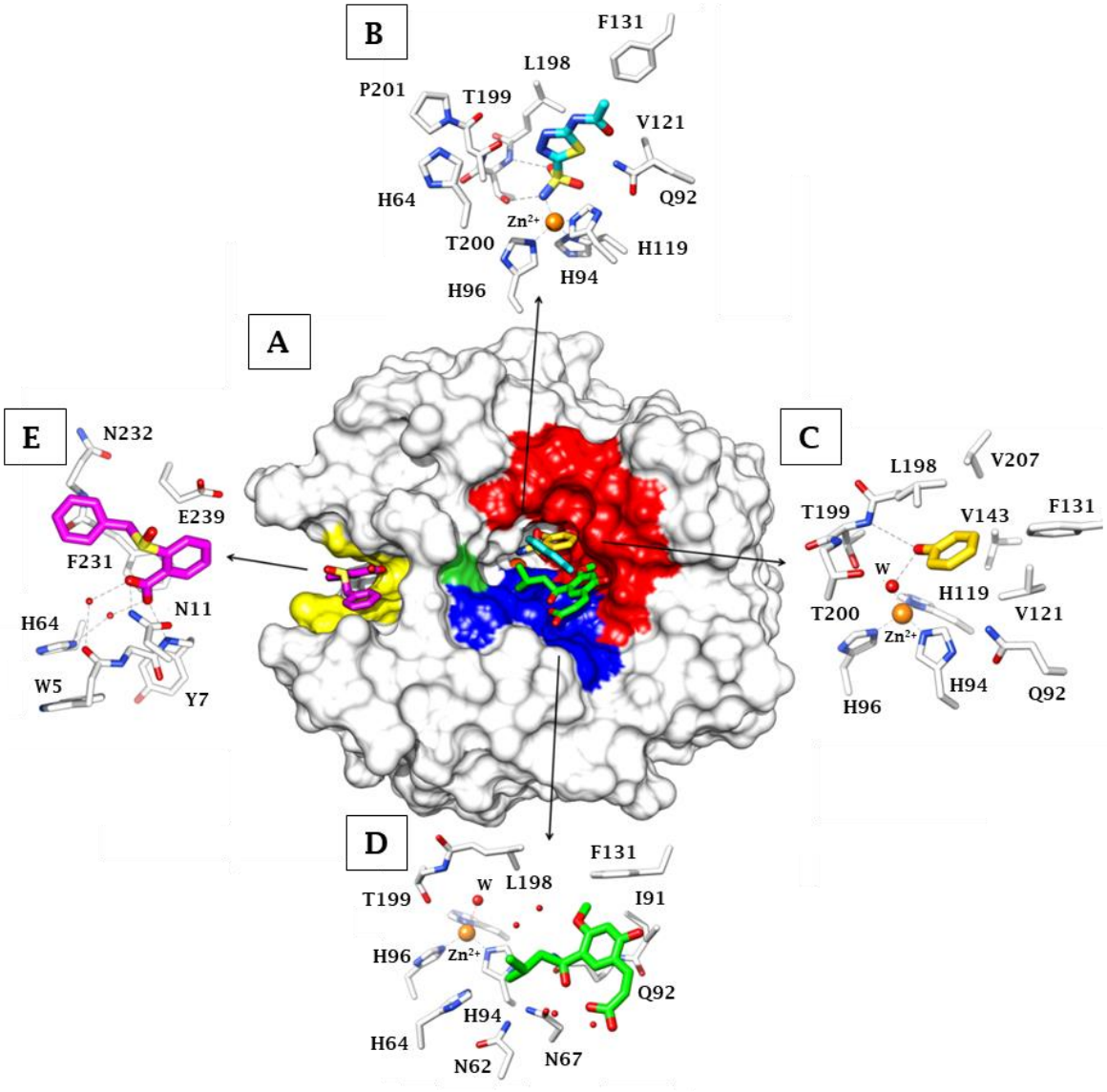

Figure 10. (A) hCA II active site with three superimposed inhibitors: acetazolamide (blue); phenol (yellow), hydrolyzed natural product coumarin (green). The hydrophobic half of the active site is colored in red, the hydrophilic one in blue. His64, the proton shuttle residue is in green (surface representation) (PDB files codes:

3HS4, 3F8E, 4QY3). The hydrophobic adjacent pocket where inhibitors bind outside the active site is shown in yellow with a benzoic acid derivative represented in magenta. The detailed interactions for the binding of the four inhibitors, with their different inhibition mechanisms, are shown in (B) for acetazolamide, (C) for phenol, (D) for the 2-hydroxy-cinnamic acid derivative, and (E) for the benzoic acid derivative.

a) the zinc-binders, among which inorganic anions, sulfonamides, and their bioisosteres (sulfamides, sulfonates, sulfamates), monothiocarbamates, dithiocarbamates, xanthates, thioxanthenes, hydroxamates, carboxylates, phosphates, selenols, benzoxaboroles (Figure 10B).[94-114]

b) compounds that anchor to the zinc-bound water molecule/hydroxide ion, such as phenols, thiophenols, polyphenols, carboxylates, polyamines, 2-thioxocoumarins, sulfocoumarins (Figure 10C).[115-122]

c) compounds that occlude the entrance of the active site, namely coumarins and their bioisosteres (Figure 10D).[123-130]

d) compounds binding out of the active site (to date this inhibition mechanism has been shown uniquely for 2-(benzylsulfonyl)-benzoic acid – Figure 10E).[131] Compounds such as secondary/tertiary sulfonamides, N-substituted saccharin, imatinib, and nilotinib inhibit specific CA by an unknown mechanism of action.[132,133] Among these categories, compounds belonging to a, b and c classes are described more in-depth.

2.3.1 Zinc binders

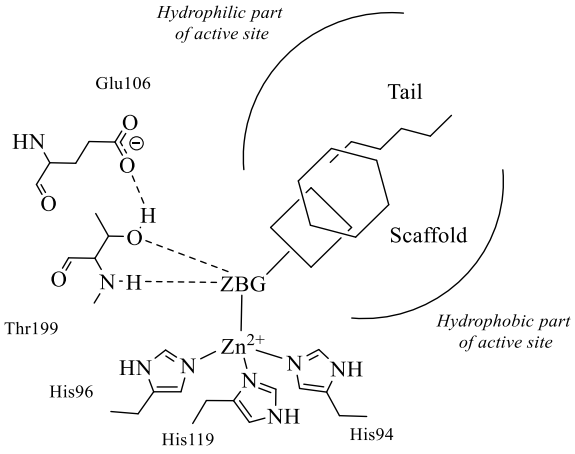

Figure 11. Schematic illustration of the key interactions between a zinc-binder and a representative human CA active site.

Compounds containing a zinc-binding group (ZBG) directly coordinate the metal ion with a tetrahedral or trigonal bipyramidal geometry, displacing the zinc-bound nucleophile (water molecule or hydroxide ion; Figure 11).[1-3,84] In addition, the ZBG interacts with various residues (i.e. such as with T199, a conserved residue in all α-CAs) nearby the metal ion, mainly by hydrogen bonds, whereas the scaffold of the inhibitor participates in several other interactions with the hydrophilic and/or hydrophobic areas of the active site. The sulfonamide group (R-SO_2NH_2) is the most important and widely used zinc-binding function for designing CAIs,[90-94] with at least 20 such compounds in clinical use for decades or clinical development in the last period (Figure 12).[90-96]

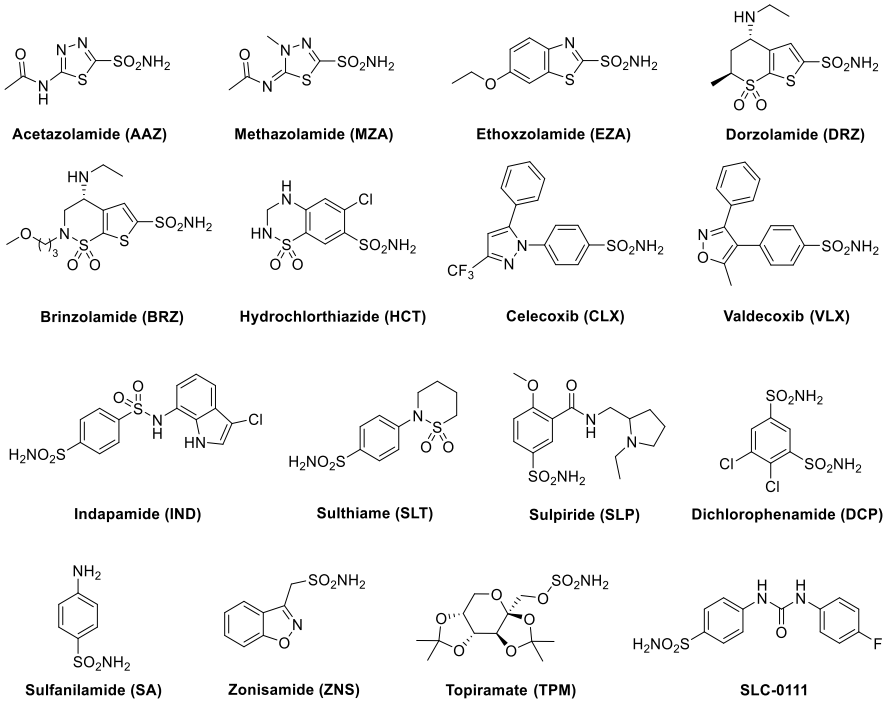

Figure 12. Examples of clinically used or studied sulfonamides.

A wealth of X-ray crystallographic evidence showed the binding mode of the zinc-binder-type CAIs, to which sulfonamides and their bioisosteres sulfamates and sulfamides belong. The latter binds in the deprotonated form to the Zn(II) ion from the enzyme active site, replacing the zinc-bound water molecule and retaining the tetrahedral coordination geometry (Figure 13).[1,2,93,94,96]

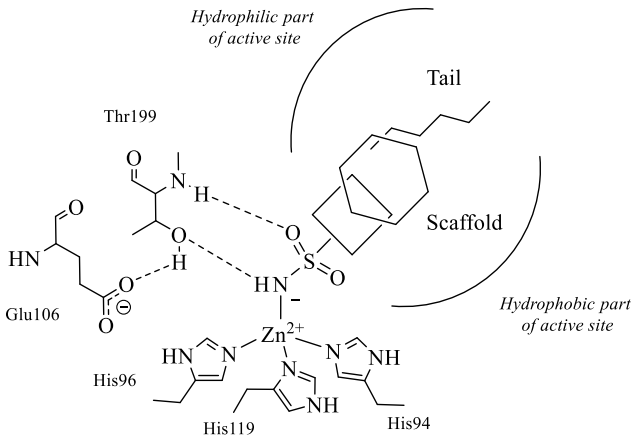

Figure 13. Schematic illustration of the key interactions between a primary sulfonamide and the hCA II active site as determined by X-ray crystallography.

It is commonly accepted that the sulfonamide group is the ideal ZBG for the CAs as it combines a negative charge of the deprotonated nitrogen with the positively charged zinc ion and, on the other hand, the presence of one proton on the coordinated nitrogen atom satisfies the hydrogen bond acceptor character of T199 OG1 atom.[1-3]

The first- and second-generation sulfonamide CAIs and their sulfamate/sulfamide analogs act as non-selective and rather efficient inhibitors of all CA isoforms. The consequence of this inhibition profile is the multitude of undesired side effects due to inhibition of isoforms not involved in the targeted pathology. This was and it is in fact the main drawback of the first- and second-generation CAIs, although they are still in clinical use.[1-3] As most differences among hCAs active site occur at the entrance of the cavity, compounds that would interact with that part may lead to isoform-selective inhibitors. Thus, the idea to attach "tails" to the scaffolds of the sulfonamide inhibitors emerged in 1999,[94-96] and indeed led to a certain degree of isoform selectivity already with the initial derivatives for which it has been proposed. Originally conceived for the design of water-soluble, antiglaucoma sulfonamides,[99-101] the tail approach was subsequently extended for the design of a multitude of CAIs possessing a variety of desired physicochemical properties, among which membrane impermeability,[101] enhanced liposolubility,[100] and more importantly, isoform-selective inhibitory profiles.[3] In fact, nowadays it is the most used synthetic approach for designing CAIs belonging to a variety of classes. The main outcome to date of the application of the tail approach is an ureidobenzenesulfonamide **SLC-0111** (Figure 12), selective inhibitor of CAs IX and XII over CAs I and II, which successfully completed Phase I clinical trials for the treatment of advanced, metastatic hypoxic tumors over-expressing hCA IX, and is currently in Phase Ib/II clinical trials in a multi-center, open-label study of oral in combination with gemcitabine (administered *i.v.*) in subjects affected by metastatic pancreatic ductal adenocarcinoma.[102,103]

Beyond sulfonamides, in the last period, a multitude of new ZBG for CAs have been identified, among which carboxylates,[108,109] hydroxamates,[110,111] phosphonates[112]. Lately crucial advances have been made in this field with mono- and dithiocarbammates,[104-106] xanthates,[106] thioxanthates,[106] boroles,[113] phosphonamidates,[112] and selenols[112] identified as novel zinc-binders. X-ray crystallographic evidence was achieved for dithiocarbamates (Figure 14A) and their derivatives,[104] hydroxamates,[110] some carboxylates,[108] one phosphonate,[110] and some

boroles (Figure 14B).[113] It should be stressed that a certain versatility was observed in the binding mode of some such ZBGs, with hydroxamates and boroles coordinating the metal ion in monodentate or bidentate manners.[94]

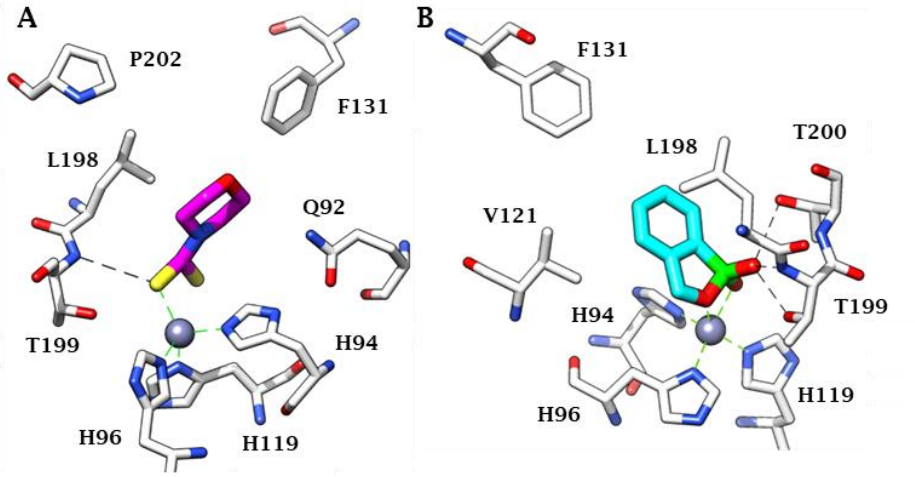

Figure 14. Active site view of the hCA II adduct with (A) a DTC (PDB 3P5A) and (B) benzoxaborole (PDB 5JQT).

2.3.2 Anchorage to the metal-bound water/hydroxide ion

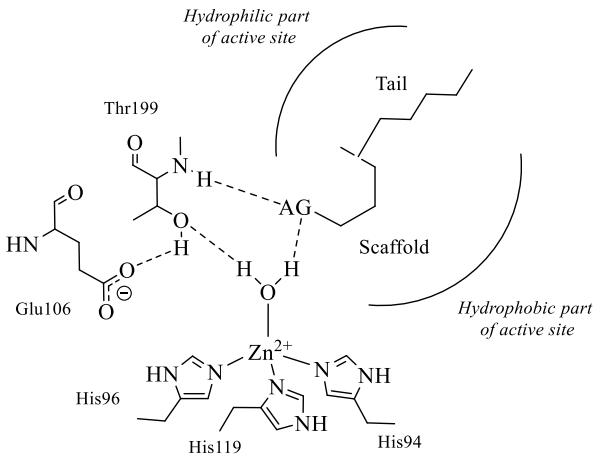

Figure 15. Compounds that anchor to the Zn(II)-coordinated water molecule/hydroxide ion. The anchoring group (**AG**) is of the phenol, amino, carboxylic acid, ester (COOR), sulfonate type.

Phenols, polyamines (*e.g.* spermine and spermidine), some carboxylates, sulfocoumarins (after having been hydrolyzed by the sulfatase activity of α-CAs to the corresponding hydroxyphenyl-ω-ethenylsulfonic acid), and thioxocoumarins have been chronologically shown to anchor to the zinc-bound water molecule/hydroxide ion by means of X-ray crystallography (Figure 15).[115-121,134] The anchoring is granted by an H-bond between the zinc-ligand and a precise anchoring group (AG) in the inhibitor of the OH, NH_2, COOH, $COOCH_3$, and SO_3H type. As in the case of zinc-binders, the ligand/target adduct is stabilized by further interactions the inhibitor scaffold establishes with amino acid residues from the active site.

The phenol is anchored to the Zn-bound hydroxide ion i.e. the major species at the pH of experimental conditions, by a hydrogen bond between the donor zinc bound hydroxide ion (E-M^{2+}– OH^-) and the ligand OH.[115] In addition, a second hydrogen bond involves the gate-keeping residue Thr199, whose backbone NH group participates in a second hydrogen bond with the phenol (Figure 16A).

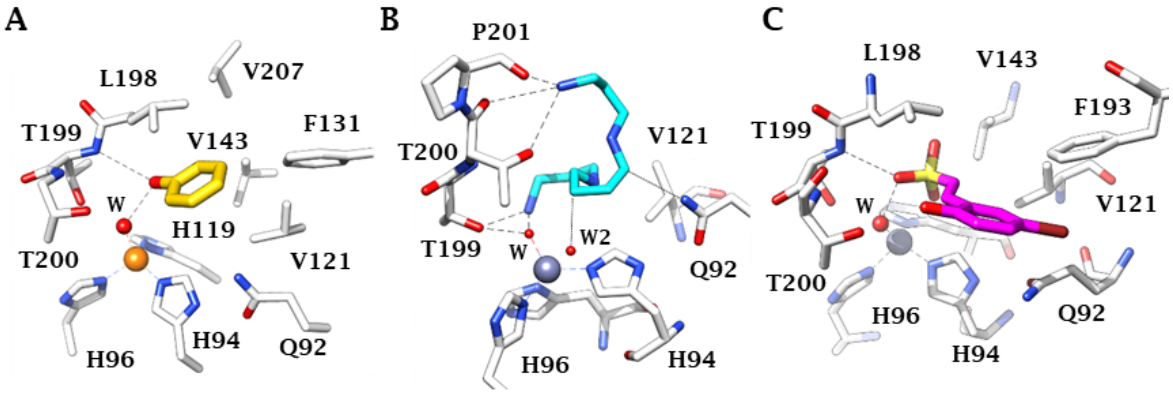

Figure 16. Active site view of the hCA II adduct with (A) phenol, (B) spermine (PDB 3KWA), and (C) hydroxyphenyl-ω-ethenylsulfonic acid deriving from sulfocoumarin hydrolysis (PDB 4BCW).

Spermine binds in a rather similar manner as phenol, although with a slightly different network of hydrogen bonding (Figure 16A).[117] Thus, one of the primary amine moieties of the inhibitor, probably as ammonium salt, anchors by means of a hydrogen bond to the zinc-coordinated water molecule/hydroxide ion, and also makes a second hydrogen bond with the side chain OH group of Thr199. The other terminal primary amine of spermine participates in hydrogen bonding with Thr200 and Pro201 (Figure 16B). The sulfonic acid from the hydrolyzed sulfocoumarin derivative was found to anchor to the Zn-bound hydroxide ion, thus making this CA inhibition mechanism much more general than initially considered when phenols were discovered as inhibitors (Figure 16C).[121]

2.3.3 Occlusion of the active site entrance

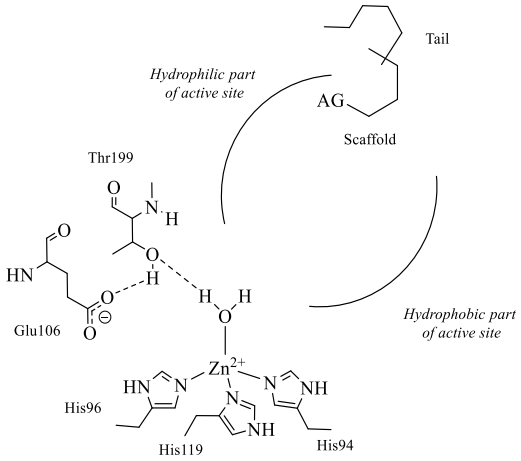

Figure 17. Schematic representation of compounds occluding the entrance to the active site. **AG** represents an anchoring group, of the phenol, carboxylic acid, or amide-type for sticking at the entrance of the active site cavity whereas the tail, when present, interacts with residues at the outer edge of the cleft.

The third main CA inhibition mechanism consists of the active site entrance occlusion (Figure 17). These inhibitors bind further away from the metal ion compared to the zinc binders in compounds anchoring to the zinc coordinated water molecule.[3,84] The occlusion of the entrance of the binding site cavity as inhibition mechanism, has been proposed for the first time for coumarins,[123] but thereafter other compounds such as the antiepileptic drug lacosamide,[124] 5- and 6-membered lactones and thiolactones or quinolinones[126-128] were observed to possess significant CA inhibitory properties probably sharing a common mechanism of action (Figure 18).

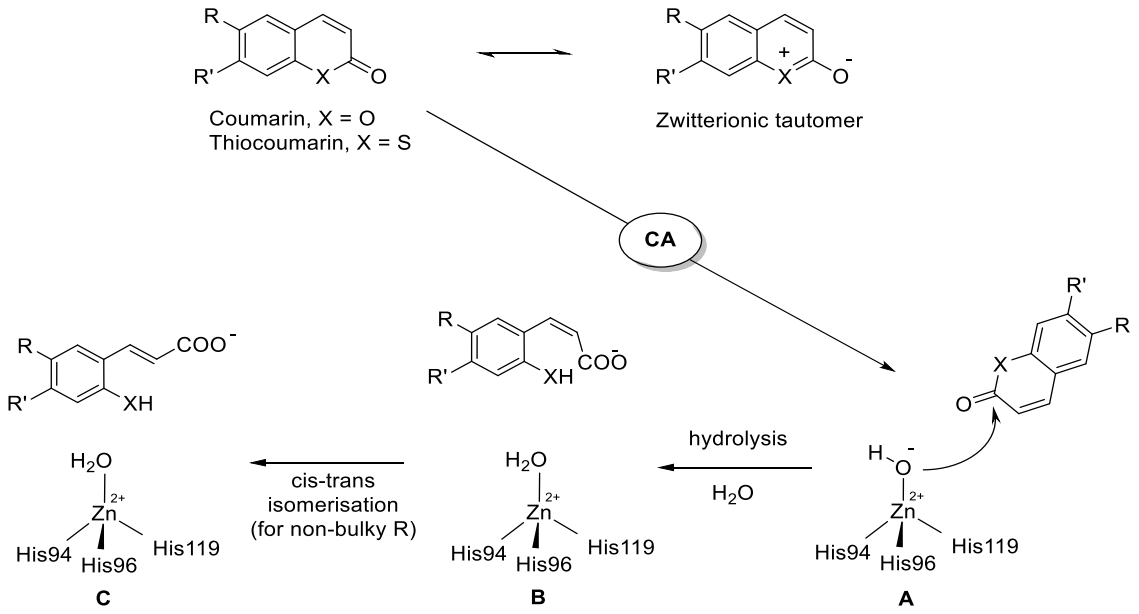

Figure 18. Proposed inhibition mechanism of CAs by coumarins/thiocoumarins, leading to *cis-* or *trans*-2-hydroxy/mercapto-cinnamic acids. A) Hydrolysis of the lactone ring. B) Movement of the hydrolysis product (as *cis* stereoisomer) towards the entrance of the active site cavity. C) *Cis-trans* isomerization of the hydrolysis product.[124]

X-ray crystallography studies primarily carried out on the coumarin derivatives isolated from the Australian plant *Leionema ellipticum* showed that coumarins (as the sulfocoumarins) acts as prodrug - at least- in human CAs and are hydrolyzed to the active species 2-hydroxycinnamic acids by the CA esterase activity (Figure 18).[120] In fact, unexpectedly the electron density data for the hCA II adduct with coumarins revealed that the actual inhibitory species is the coumarin hydrolyzed form that, depending on how bulky the moieties attached on the scaffold are, might bind as *cis* isomers (Figure 19A) or as *trans*-isomers (Figure 19B). Indeed, for the not bulky substitution pattern on the coumarin scaffold, the trans isomer was observed in the CA active site, whereas for bulkier such groups the isomerization did not occurThe most notable aspect of this inhibition mechanism is the fact that the inhibitors bind in an active site region where more significant differences in the amino acid compositions among hCAs occur.[1-3] This produces important consequences in the inhibition profiles exhibited by such a class of derivatives which showed a unique isoform-selective action. In fact, wide series of diversely substituted coumarin/thiocoumarin derivatives were investigated which reported significantly selective inhibition against isoforms such as CA IX, XII, XIII, and XIV over the ubiquitous CA I and II.[123-130]

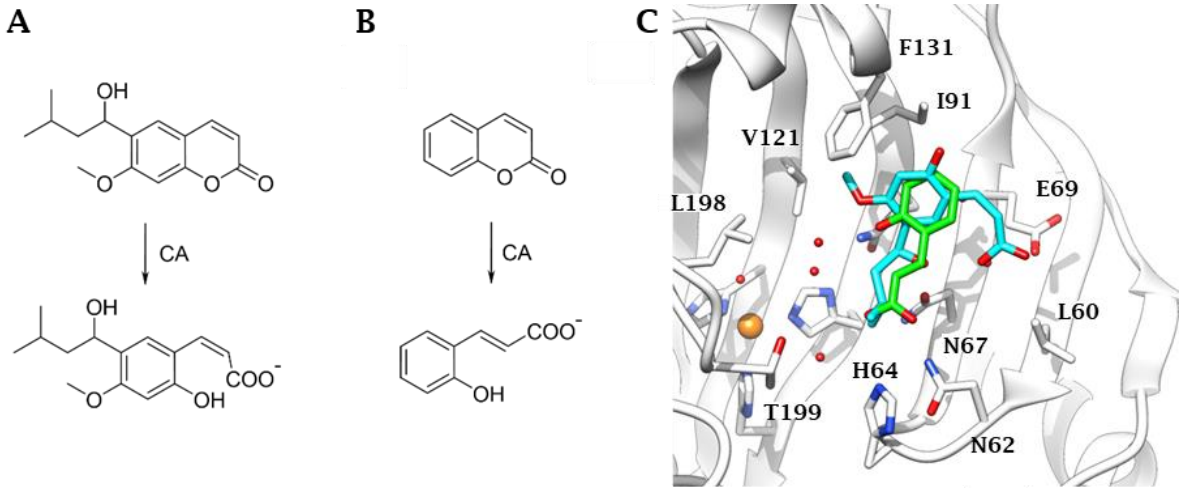

Figure 19. CA-mediated hydrolysis of (A) the coumarin extracted from *Leionema ellipticum* and (B) coumarin. (C) Active site view of the superimposed hCA II adducts with of the coumarins hydrolysis products shown in panel A (blue, PDB 3F8E) and B (green PDB 5BNL).

2.4 Carbonic anhydrase activators

CA activation with amino acids or biogenic amines, such as histamine, and peptides was reported in the early 40s, but it was validated only at the end of the 20th century.[1] Using methods such as stopped-flow kinetic assays, X-ray crystallography and spectroscopy, the CA activators (CAAs) were shown to take part in the catalytic cycle, as shown below in equation 10.[135-137]

$$EZn^{2+}–OH_2 + A \rightleftarrows [EZn^{2+}–OH_2 \cdot A] \rightleftarrows [EZn^{2+}–HO^- \cdot AH^+] \rightleftarrows EZn^{2+}–HO^- + AH^+ \quad \text{(Eq. 10)}$$

The CAA binds within the enzyme active site during the formation of the enzyme – activator complex. The activator participates in the rate-determining step of the catalytic cycle, which is the proton shuttling between the zinc coordinated water and the reaction medium. In many CA isoforms, His64 placed in the middle of the CA active site plays this role through its imidazole moiety with a pK_a in the range of 6-7.[36] In the enzyme-activator complexes, this proton transfer reaction is achieved more efficiently both by His64 and the activator molecule. The activator does not influence K_M (the affinity for the substrate) but affects the k_{cat} of the enzyme-catalyzed reaction, thus leading to the efficient formation of the nucleophilic species of the enzyme (EZn^{2+}–OH).[16,36]

To date, several X-ray crystal structures of CAAs bound to several hCA isoforms have been reported (Figure 20).[135-140] The Histamine–hCA II adduct crystallography was the first published such study,[135] and successively activators of the amines and amino acid type, such as L- and D-His, L- and D-Phe, D-Trp and L-adrenaline were studied by this technique.[3,16,135-140] All these activators bind in the same region of the CA active site, which has been denominated the activator binding site A; except D-Trp which interact in a bind site called activator binding site B (Figure 20).[36]In this position, at the entrance of the active site and not far away from His64, the activator participates in favorable interactions with several amino acid residues and water molecules, supplementing the proton shuttling effects of His64.It is supervising the activators and the coumarins binding sites are in fact superimposable, as shown in Figure 20.

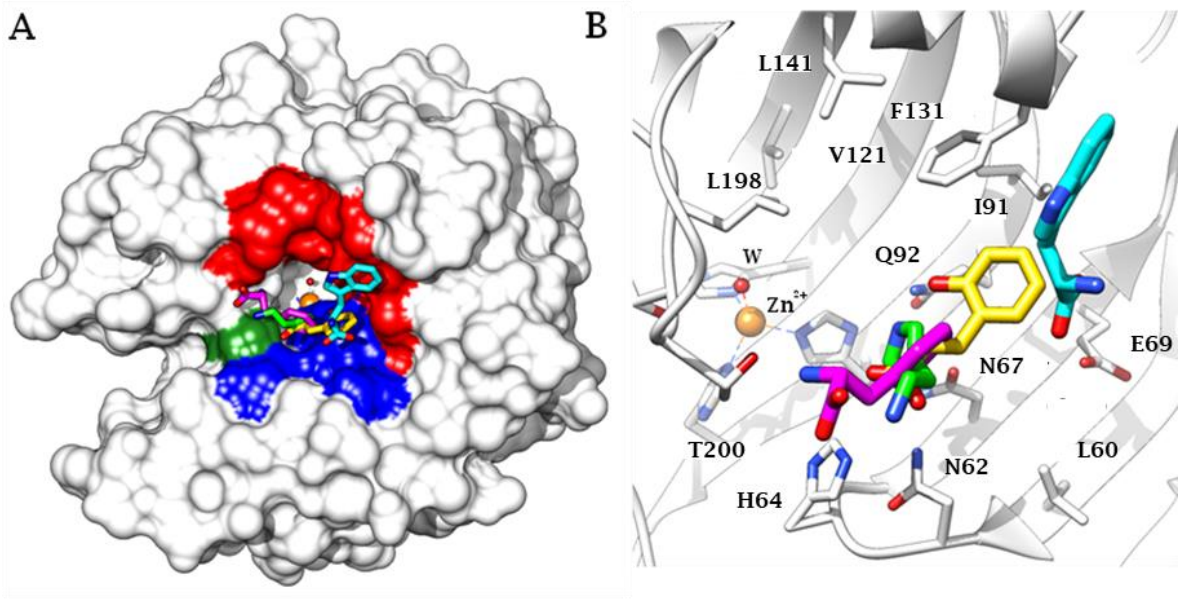

Figure 20. hCA II complexed with CAAs and the hydrolyzed coumarin (2-hydroxycinnamic acid). Histamine is shown in green (PDB 1AVN) D-Phe in magenta (PDB 2EZ7) and D-Trp in cyan (PDB 3EFI). 2-Hydroxycinnamic acid (in yellow, PDB 5BNL) is also superimposed to the hCA II – activator adducts. a) Complete view of the enzyme-ligands superimposed adducts. b) Active site view of the three activators and the hydrolyzed coumarin in a slightly different orientation, compared to panel A. A series of drug design studies are also available for CAAs, mainly using histamine and histidine as lead molecules.[3,36] Some of these compounds showed an increased affinity for many CA isoforms (compared to histamine), but the level of isoform selectivity achieved up to now is very poor.[3]

The present Ph.D. thesis mainly focused on tumor-associated hCAs IX and XII. The ligands that we have investigated act as zinc-binders and anchor to the zinc-bound water molecule/hydroxide ion. Moreover, we have studied the Cas present in brain, and, about the ligand, we focused on the Cas activator, less studied than CAI.

PART II – CHEMISTRY AND ENZYME KINETICS PROJECTS

CHAPTER 3. MULTITARGET APPROACHES APPLIED TO INHIBITORS AND ACTIVATORS OF HUMAN CARBONIC ANHYDRASES AS THERAPEUTICS AGAINST OF NEW DRUGS AGAINST DIFFERENT DISEASES.

3.1 Scope of the PhD thesis work

According to the classical approach, a drug should interact as much as possible with a single biological target. However, in recent years a trend reversal has been observed due to the increasing use of molecular hybrids.[141-144] These molecules incorporate in their structure pharmacophoric characteristics suitable for interaction with two or more biological targets. In fact, the complex network of biochemical processes involved in the pathogenesis of a disease, as in the case of cancers, is more effectively affected by molecules that hit multiple targets within the set of enzymes/receptors involved. Combination drug therapies could therefore be replaced by multifunctional molecules that minimize pharmacokinetic and metabolic problems that arise from taking multiple drugs simultaneously. Patient compliance improves, as do chemical or metabolic drug-drug interactions.[141-144] Similar to the combinatorial therapies from which it takes its inspiration, the multi-target approach does not necessarily require that the two targets have similar subcellular localization. For this reason, this thesis work addressed the design and synthesis of novel hybrid anticancer agents capable of acting on two distinct anticancer therapeutic targets. In detail, the goal of the first two projects is to obtain an anticancer agent that is able at the same time to inhibit the human Carbonic Anhydrases IX and XII associated with tumors and to stabilize the G-quadruplex structures, present at the level of telomeres in DNA; in one case, and in the second of these two projects, to insert a Fluorouracil moiety as antimetabolite drugs. In the third project, we decided to renew the interest toward the Carbonic Anhydrase Activators; insert them in complex with a Tacrine scaffold. The CAA part acts with the objective to restore the memory deficit[145]; while the tacrine interact with both Cholinesterase in order to maintain a valid cholinergic efflux in brain[146].

In addition, I performed further enzyme kinetic studies to characterize ex novo a new isoform: iota Ca. This CA was isolated for the first time by the marine diatom *Thalassiosira pseudonana* and the kinetic profile was evaluated on iota from the Gram-negative bacterium *Burkholderia territorii*.[13-15]

3.2 Inclusion of 5-fluorouracil in benzenesulfonamide CA IX/XII inhibitors produced a targeted action against MDA-MB-231 and T47D breast cancer cells (Series A).

Hypoxic induced cancer cells adapt their metabolism via a glycolytic shift, which decreases extracellular pH and modifies their genes expression pattern to survive in an environment incompatible for normal cell growth. [147-148] Among the membrane proteins overexpressed by hypoxic tumors to regulate pH are the carbonic anhydrases (CA, EC 4.2.1.1),[51] that catalyze the reversible hydration of carbon dioxide to bicarbonate ion and a proton. In this context, the transmembrane isoforms CA IX and XII participate in the pH regulation of the extracellular environment [25,51,149]. CA IX is not appreciably expressed in most normal tissues, while its up-regulation is associated with hypoxic cancer phenotypes, where it is strongly induced via the hypoxia inducible factor-1α (HIF-1α).[1,2,150] CA XII is also implicated in the extracellular acidification in many tumor types.[25-33] As a result, CA IX and XII are factors driving tumor growth, invasiveness, proliferation, metastasis, as well as resistance to radio- and chemotherapy.[151] This makes agents inhibiting CA IX and XII, in a selective manner, a valuable therapeutic for the targeting of the primary tumor growth, invasion metastasis, and the reduction of cancer stem cell population. [3,94,151]

The issue with sulfonamide-like CA inhibitors (CAIs), the main inhibitory chemotypes adopted for therapeutic purposes, is a promiscuous action against almost all isoforms encoded in humans, that results in non-selective targeting, and therefore undesired side effects.[1] In fact, the comparison of the 12 catalytically active human CAs demonstrates a high sequence homology within the active sites that increases the difficulties in the design of disease-targeted inhibitors.[152] Among the strategies adopted to bypass this issue are the optimization of CAIs (i.e. the tail approach,[3] whose application produced **SLC-0111**,[153] the first-in-class CAI entering clinical trials for the treatment of hypoxic tumors) or the use of alternative chemotypes, such as coumarin and bioisosters which use different chemotypes for enzymatic inhibition.[25,94]

As an application of the tail approach, we recently reported two series of uracil/adenine-tailed benzenesulfonamides as potent CA IX inhibitors (series 1 and 2, Figure 1).[154] Purine/pyrimidine-based scaffolds are considered privileged structures in the drug-design of bioactive compounds because of synthetic accessibility and ability to confer drug-like properties.[155,156] In particular, pyrimidines and purines are widely used as antitumor and

antiviral pharmacophores in medicinal chemistry, due their ability to interfere with the DNA functions in diverse manners.[157,158] A selection of the reported CAIs showed significant anti-proliferative activity against HT-29 colon cancer cell lines.[154]

As a continuation of the previous work, the uracil derivatives series is here developed by swapping the nitrogenous base to a 5-F-uracil (5-FU), a clinically used chemotherapeutic agent, to produce series 3 (Figure 21). A major number of benzenesulfonamide scaffolds as CAIs was investigated as well as coumarin cores to achieve a more targeted CA IX/XII inhibition. A subset of 5-FU CAIs was evaluated *in vitro* against eight cancer cell lines. The effects of the two more active compounds on the phases of cell cycle and annexin V-FITC-positive staining in breast T47D cells were thereafter assessed.

Results and Discussion

Drug design and chemistry

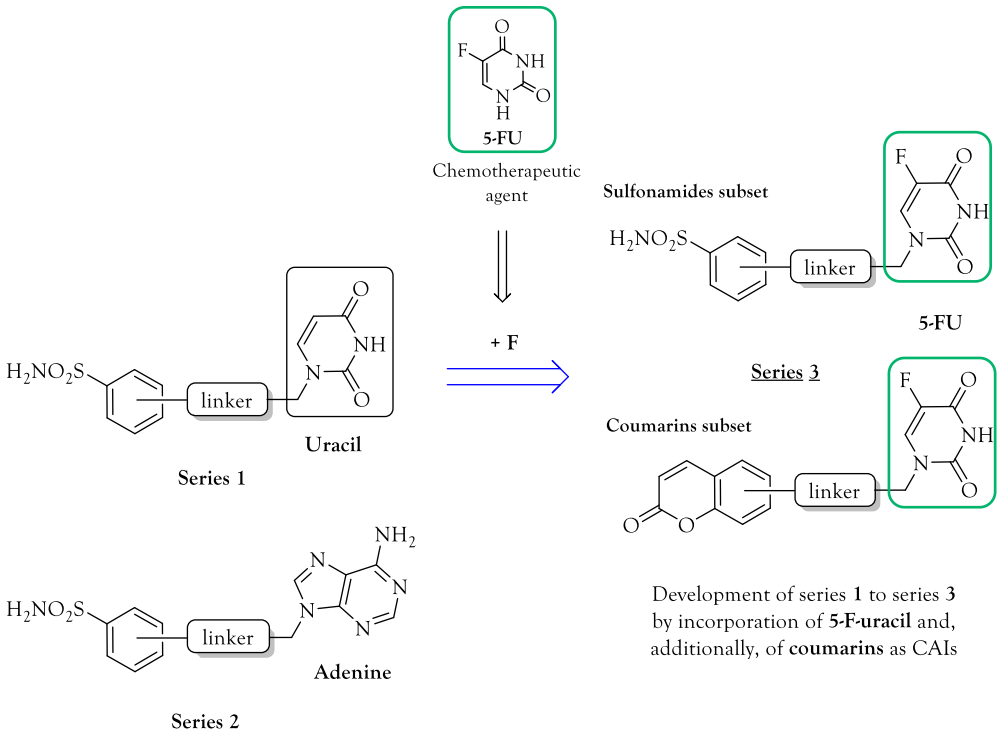

Figure 21. Drug-design of 5-fluorouracil derivatives as antitumor CAIs.

5-FU is widely used medication in the treatment of cancer.[159] Over the past 20 years, increased understanding of the mechanism of action of 5-FU, principally based on the inhibition of

thymidylate synthase, has led to the development of strategies that increase its anticancer activity. A molecular hybridization approach is here adopted combining 5-FU with CAI scaffolds to synergize the inhibition of the tumor-associated isozymes with intrinsic anticancer effects resulting by the pyrimidine pharmacophore.[160] 5-FU was incorporated through the N1 atom on a wealth of benzenesulfonamide structures by amide or triazole linkers to explore the chemical space within the target and off-target CAs binding sites. A small subset of ester, amide or triazole linked 5-FU coumarin derivatives was also produced to yield markedly selective CA IX/XII 5-FU-based inhibitors. In fact, coumarins act as prodrug which undergo a CA mediated hydrolysis and the formed species (*E*- or *Z*- cinnamic acid) accomplishes the enzymatic inhibition by occluding the entrance of the active site.[3,94] The latter is the most variable region, in terms of amino acid residues, among the human CAs. The cancer-related CAs were shown to be more prone to such a kind of inhibition mechanism than ubiquitous CAs.

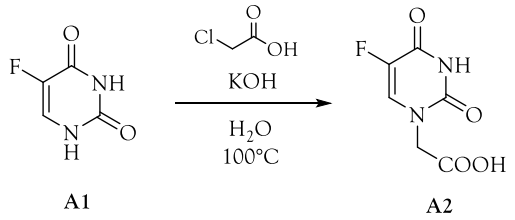

Scheme 1. Synthesis of intermediate A2.

Intermediate **A2** was provided by reacting 5-FU with chloroacetic acid in $KOH_{(aq)}$ (Scheme 1). The carboxylic acid **A2** was thus coupled with a variety of primary (**A3-A7**) and secondary (**A13-A18**) amine benzenesulfonamide derivatives using 1-ethyl-3-(3-dimethylaminopropyl)carbodiimide (EDCI) in presence of 1-hydroxybenzotriazole (HOBt) and 4-dimethylaminopyridine (DMAP) to yield amides **A8-A12** (Scheme 2) and **A19-A24** (Scheme 3) [15].

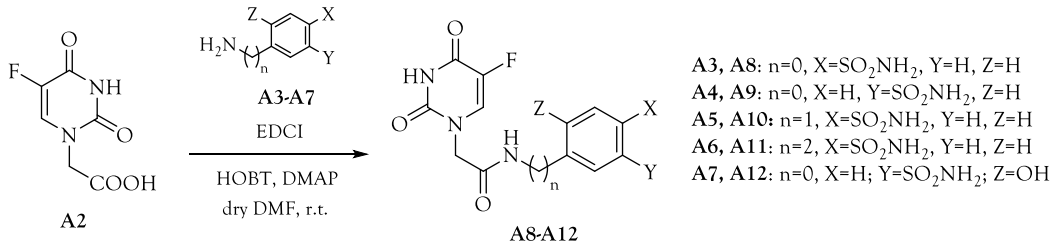

Scheme 2. Synthesis of amides **A8-A12**.

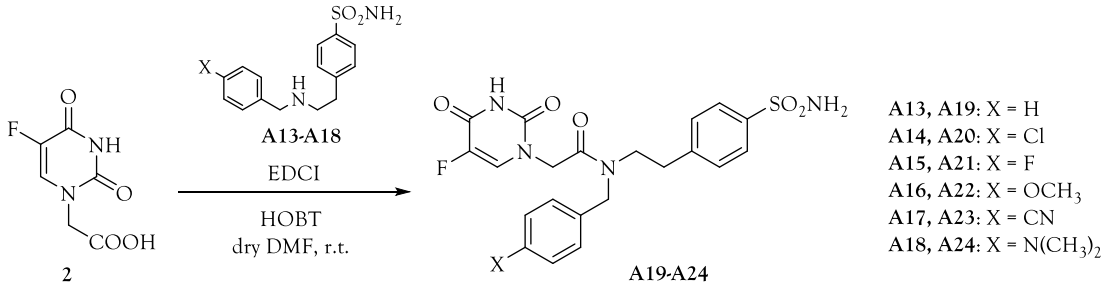

Scheme 3. Synthesis of amides **A19-A24**.

The triazole derivatives **(10a-d)** were generated by a Cu(I) catalyzed azide–alkyne cycloaddition (CuAAC) between the N1-propargyluracil **A27** and the freshly prepared azides **A30-A33** yielded by a Sand-Meyer reaction (Scheme 4). $CuSO_4$ and vitamin C were used to generate *in situ* the Cu(I) catalyst.

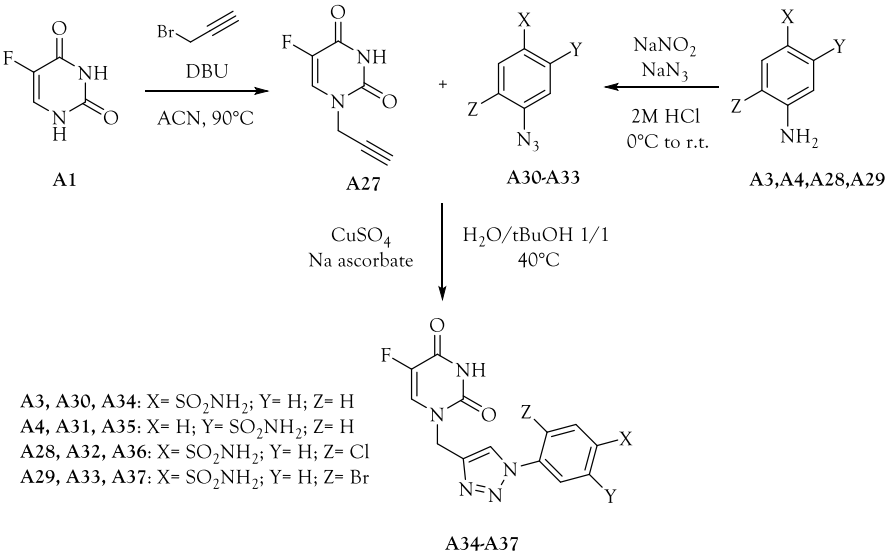

Scheme 4. Synthesis of triazoles **A34-A37.**

The coumarin derivatives **A40** and **A41** were prepared by coupling intermediate **A2** with 7-amino-4-methylcoumarin **A38** and umbelliferone **A39,** respectively, adopting again EDC as coupling agent. The CuAAC between alkyne **A27** and coumarin azide **A42** yielded triazole **A43**. Compounds **A8-A12, A19-A24, A34-A37, A40-A41, A43** were obtained in high yields and thoroughly characterized by ^{1}H-, ^{13}C-, ^{19}F-NMR and HRMS.

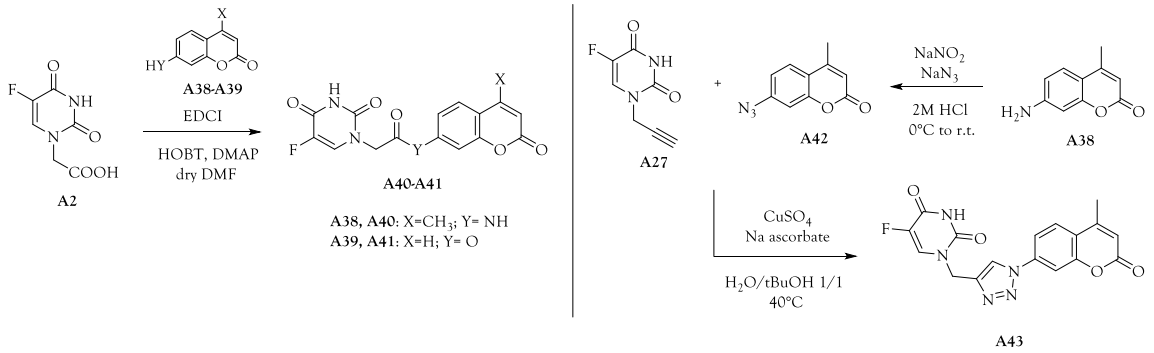

Scheme 5. Synthesis of coumarins **A40-A41** and **A43.**

Carbonic anhydrases inhibition

The CA inhibitory action of 5-FU compounds **A8-A12, A19-A24, A34-A37, A40-A41, A43**, was assessed against the cytosolic CA I and II (ubiquitous) and CA IX and XII (cancer-related) isoforms by a stopped flow CO_2 hydrase assay, in addition to acetazolamide (**AAZ**) as standard inhibitor.[161] The following structure–activity relationship (SAR) can be drawn up from the inhibition data reported in Table 3.

Table 3: Inhibition data of human CA isoforms I, II, IX and XII with 5-FU derivatives **A8-A12, A19-A24, A34-A37, A40-A41, A43** and the standard acetazolamide (**AAZ**) by a stopped flow CO_2 hydrase assay[161]. Compounds selected for *in vitro* anticancer assays are highlighted in gray.

Cmpd	K_I (nM)[a]			
	CA I	CA II	CA IX	CA XII
A8	323.5	6.8	4.8	4.7
A9	5158.3	81.5	44.7	66.3
A10	738.6	101.3	29.2	40.1
A11	299.3	19.6	24.8	7.0
A12	9679.8	9083.9	452.8	59.5
A19	207.6	0.59	3.5	2.9
A20	2965.0	34.8	4.2	6.2
A21	933.9	13.4	11.8	4.8
A22	727.4	8.0	1.9	9.0
A23	383.6	0.71	4.9	28.6
A24	581.9	5.1	26.8	15.5
A34	651.0	0.67	0.47	9.8
A35	8911.2	89.2	105.3	83.1
A36	656.1	2.4	11.2	8.4

A37	626.3	0.81	3.8	3.9
A40[b]	>10000	>10000	16.5	23.2
A41[b]	>10000	>10000	36.8	14.4
A43[b]	>10000	>10000	173.4	408.4
AAZ	250.0	12.5	25.0	5.7

a. Mean from 3 different assays, by a stopped flow technique (errors were in the range of ± 5-10 % of the reported values). b. Incubation time of 6h.

The cytosolic off-target CA I was the least inhibited isoform. The inhibition constants (K_Is) of the sulfonamide 5-FU derivatives spanned between 207.6 and 9679.8 nM. The *m*-substitution at the benzenesulfonamide scaffold produced the least CA I inhibition, such as in compounds **A9** (K_I of 5.1 μM), **A12** (K_I of 9.7 μM) and **A35** (K_I of 8.9 μM). Additionally, the *p*-chloro substituted secondary amide **A20** inhibited CA I by a micromolar value (K_I of 2.6 μM). The removal of the chlorine atom in the latter compound led instead to best CA I inhibitor that is **A19** (K_I of 207.6 nM). The elongation of the spacer between the benzenesulfonamide and the primary amide moiety reduced the CA I inhibitory activity passing from 0 **(A8)** to 1 **(A10)** carbon atom, while it is restored to a 300 nM value approximately when a second carbon atom unit was introduced **(A11)**. The most physiologically relevant isoform CA II was effectively inhibited by most 5-FU based sulfonamide derivatives. In fact, K_Is spanned in the range 0.59-34.8 nM, except for **A9** (K_I of 81.5 nM), **A10** (K_I of 101.3 nM) and **A35** (K_I of 89.2 nM), while **A12** barely inhibited CA II below 10 μM (K_I of 9.1 μM). Again, *m*-substitutions at the benzenesulfonamide core were detrimental for CA inhibition with respect to *p*-substitutions, as well as a 1-carbon atom linker between zinc-binding portion and amide linker **(A10)**. A subset of derivatives inhibited CA II in a subnanomolar range, that are the unsubstituted and *p*-CN benzyl amide compounds **A19** (K_I of 0.59 nM) and **A23** (K_I of 0.71 nM) and the *p*-triazole benzenesulfonamide derivatives **A34** (K_I of 0.71 nM) and **A37**, that is also substituted in *meta* by a bromine atom (K_I of 0.81 nM). Swapping the *p*-CN group with a chlorine atom **(A20)**, a fluorine atom **(A21)**, a methoxy group **(A22)** and a dimethylamino group **(A23)** reduced the CA inhibitory action by 7 to 50-fold.

The main antitumor target CA IX was also efficiently inhibited by most 5-FU sulfonamide derivatives with K_Is ranging between 0.47 and 44.7 nM. Uniquely, the *m*-substituted **A12** and **A20** induced inhibition above 100 nM, with K_Is of 452.8 and 105.3, respectively. A single

subnanomolar CA inhibitor was identified against CA IX, that is the triazole **A34**, whose K_I of 0.47 nM represents the best CA inhibition here reported. Among the N-benzyl substituted secondary amides **A19-A24**, the *p*-OCH_3 derivative **A22** stood out as most active one with a K_I of 1.9 nM. Notably, a significant subset of 5-FU CAIs inhibits CA IX more capably than the clinically used **AAZ** (K_I of 25.0 nM). CA XII, the second tumor-related CA, was inhibited by most sulfonamide CAIs reported here with an overall comparable range with CA II and IX, though with diverse SAR. K_Is spanned in the range 2.9-83.1 nM and no subnanomolar inhibition was detected. The worst K_Is, detected in the range 59.5-83.1 nM, are consistently associated with the *m*-substituted **A9**, **A12** and **A35**. The introduction of a 1-carbon atom linker between zinc-binding portion and amide linker (**A10**) decreased CA IX inhibition below the average as well (K_I of 40.1 nM). The N-benzyl substituted secondary amides showed a rather flat inhibitory trend with K_Is spanning in the range 2.9-28.6 nM. The best value is associated to the unsubstituted **A19** while the worst value is related to the *p*-CN substitution of **A23**. Among the triazole derivatives **A34-A37** the introduction of *m*-Br substituent on the benzenesulfonamide scaffold produced the best CA XII inhibition (K_I of 3.9 nM). In contrast, the 5-FU coumarin derivatives **A40-A41** and **A43** showed a potent and totally selective inhibitory action against the target CA IX/XII over CA I/II. In detail, the three compounds did not inhibit CA I and II, lower than 10 μM. Whereas, CA IX and XII were inhibited in similar ranges, 16.5-173.4 nM and 14.4-408.4 nM, respectively. However, while amide **A40** was the best CA IX inhibitor (K_I of 16.5 nM), CA XII turned out to be slightly more efficiently inhibited by ester **A41**. The triazole coumarin **A43** exhibited a decrease of efficacy against both cancer-related Cas. As for target/off-target CAs selectivity ratio of action of sulfonamide 5-FU derivatives, all compounds exhibited remarkable I/IX and I/XII inhibitory specificity, as the calculated selectivity index (*SI*) span the ranges 12.1-1385.1 and 13.4-478.2, respectively (Table 2). In contrast, only two distinct subsets of sulfonamide derivatives (approximately the half compounds) produced a preferred inhibition of the target CA IX and XII over the main off-target CA II. In detail, only the 1-carbon atom spacer derivative **A10**, the *m*-substituted **A12** and the N-benzyl amides **A20** and **A22** reported significant II/IX *SI* spanning between 3.5 and 20, that are greater than that measured for the standard **AAZ**. As for II/XII *SI* values, oddly the 1- and 2-carbon atoms spacer derivative **A10** and **A11**, the *m*-substituted **A12** and the N-benzyl amides **A20** and **A21** solely had values above 2, with that of **A12** even reaching the value of 153.

On the basis of the data of Table 3 and 4, coumarin **A40**, the sulfonamide CAIs showing the greatest II/IX *SI*, namely **A12**, **A20** and **A22**, and the unique subnanomolar CA IX inhibitor **A40** were chosen for assessing *in vitro* their antiproliferative action against a panel of cancer cell lines.

Table 4. Selectivity index (*SI*) calculated for human CA IX and XII over off-targets isoforms as ratio between K_Is.

Cmpd	*Selectivity Index (SI)*			
	I/IX	II/IX	I/XII	II/XII
A8	67.4	1.4	68.8	1.4
A9	115.4	1.8	77.8	1.2
A10	25.3	3.5	18.4	2.5
A11	12.1	0.8	42.8	2.8
A12	21.4	20.1	162.7	152.7
A19	59.3	0.2	71.6	0.2
A20	706.0	8.3	478.2	5.6
A21	79.1	1.1	194.6	2.8
A22	382.8	4.2	80.8	0.9
A23	78.3	0.1	13.4	<0.1
A24	21.7	0.2	37.5	0.3
A34	1385.1	1.4	66.4	0.1
A35	84.6	0.8	107.2	1.1
A36	58.6	0.2	78.1	0.3
A37	164.8	0.2	160.6	0.2
A40	>606.1	>606.1	>431.0	>431.0
A41	>271.7	>271.7	>694.4	>694.4
A43	>57.7	>57.7	>24.5	>24.5
AAZ	10.0	0.5	43.9	2.2

The corresponding nonfluorinated analog (uracil derivative, from series A) was previously reported and characterized for a subset of 5-FU derivatives, namely **A8-A12, A34-A37** and tested as inhibitor of CA I, II and IX.[154] Table 3 shows the K_I ratio against CA I, II and IX between each uracil derivative and its corresponding 5-FU analog. A significant enhancement in the CA inhibitory action was detected for most 5-FU compounds against CA II (ratio of 0.5-8.6) and CA IX (ratio of 1.0-69.8) compared to the uracil correspondents. As in most cases the increase was more intense against the target CA IX over CA II, it can be speculated that the

incorporation of a fluorine atom in position 5 of the nitrogenous base scaffold increases both potency and selectivity against the target CA IX.

Table 5. K_I ratio between 5-FU derivatives and corresponding non-fluorinated compounds from series A (uracil derivatives) when applicable.

Cmpd	K_I uracil derivative (series A) / K_I 5-FU derivative (series C)		
	CA I	CA II	CA IX
A8	2.0	2.6	5.3
A9	1.5	8.6	69.8
A10	2.1	4.9	13.9
A11	2.2	2.1	1.8
A12	1.0	0.5	1.0
A34	0.4	1.4	10.2
A35	0.5	4.3	4.4

X-ray crystallography

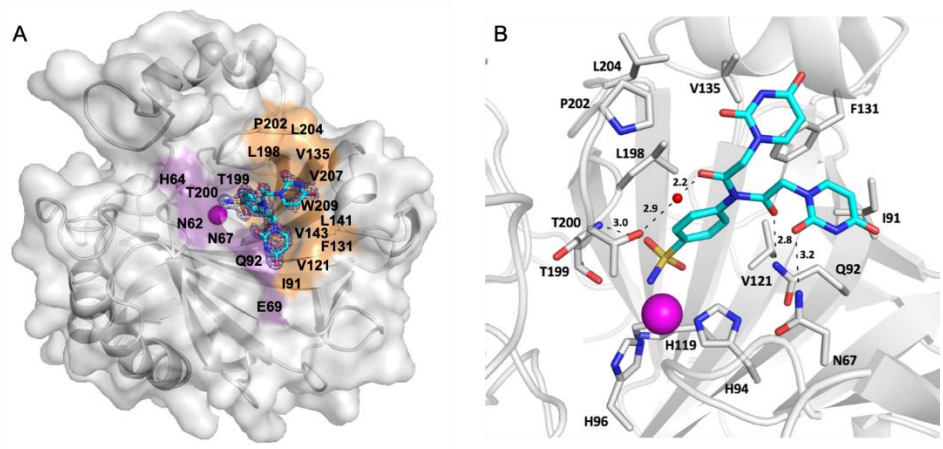

Figure 22. A) Surface representation of CA II in complex with compound **A** from series 1, the uracil (F-devoid) analog of compound **A8** (shown as cyan sticks). Hydrophobic and hydrophilic residues of the active site are labeled and colored orange and purple, respectively. B) Active site view of compound **A** binding. Hydrogen bonds are shown as black dashes with distances labeled in Å. X-ray crystallography was utilized to observe the binding to CA II of a representative compound from the pyrimidine series, compound **A** from series 1, the uracil (F-devoid) analog of compound **A8** from series 3. This structure was determined to a resolution of 1.4 Å (Table 6). As expected for a sulfonamide-based compound, the zinc-binding group (ZBG) displaced the active site zinc-bound water (ZBW) and bound directly to the zinc. The ZBG also formed a hydrogen bond between the sulfonamide

oxygen and backbone amide of T199 (3.0 Å). The tail component of compound **A** was observed to exhibit dual conformations, attributed to the freedom of rotation about the amide linker, resulting in one conformation oriented towards the hydrophobic side and another extending towards the hydrophilic side of the active site (Figure 22A). The minor tail conformation, oriented towards the hydrophobic pocket, exhibited a lower occupancy (43%) as indicated by the weaker electron density (Figure 22A). In the minor conformer, the carbonyl of the linker forms a hydrogen bond with a water that bridges to the side chain of T199 (2.2 and 2.9 Å, respectively; Figure 2B). In the major tail conformation, occupancy (55%), a hydrogen bond is formed between the linker carbonyl and side chain of Q92 (2.8 Å) in addition to the uracil moiety and side chain of N67 (3.2 Å) (Figure 22B). The additional hydrogen bonding is thought to stabilize the compound tail, resulting in the observed higher occupancy. Both conformations are further stabilized by interactions with active site residues F131, V135, L198, P202, L204 and F131, I91, V121 (Figure 22B).

Interestingly, the two orientations of compound **A** are reminiscent of the duel binding modes of a previously studied purine-based inhibitor, compound **B** from series 2, namely the adenine analog of **A11** from series 3. Compound **B** exhibited unique binding modes based on the CA isoform with the inhibitor tail orienting in the hydrophobic side in the active site of CA II and extending toward the hydrophilic side of the active site of CA IX-mimic. Despite a shift of the linker and tail portion of compound **A** by approximately 2-3 Å due to the steric hindrance of F131, these two binding modes of compound **B** are oriented similarly to the two observed conformations of compound **A** in CA II (Figure 23).

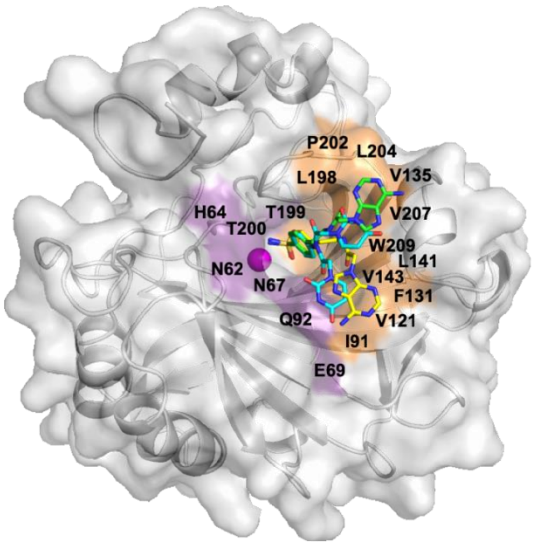

Figure 23. Overlay of compound **A** (cyan sticks) and compound **B**, an adenine derivate (adenine analog of **A11**) from series 2 (green sticks in CA II and yellow sticks in CA IX-mimic binding) in surface representation of CA II.

Table 6. X-ray crystallography statistics for structure of CA II in complex with compound **A**.

PDB Accession Code	CA II - A
	6VJ3
Space Group Cell Dimensions (Å;°)	$P2_1$ a = 42.5, b = 41.4, c = 72.2; β = 104.4
Resolution (Å)	32.2 – 1.4 (1.40 – 1.35)
Total Reflections	164,794
I/Iσ	12.9 (1.5)
Redundancy	3.1 (2.1)
Completeness (%)	98.0 (88.0)
Rcryst (%)	15.1 (27.2)
Rfree (%)	15.2 (28.4)
# of Protein Atoms	2069
# of Ligand Atoms	51
Ramachandran stats (%): favored, allowed, generously allowed	97.3, 2.7, 0.0
Avg. B factors ($Å^2$): Main-chain, Ligand, Solvent	15.8, 23.8, 25.7
rmsd for bonds, angles (Å,°)	0.007, 1.12

***In vitro* anti-proliferative activity**

Sulfonamides **A12**, **A20, A22, A34** and coumarin **A40** displayed efficient and/or selective inhibitory actions against the tumor-related isoforms CA IX and XII over the cytosolic off-target CA I and II (Tables 3 and 4). Accordingly, the five compounds were selected to be evaluated *in vitro* for their potential anti-proliferative activity, utilizing Sulforhodamine B colorimetric assay (SRB) as described by Skehan *et al.*

The anti-proliferative activities of **A12**, **A20, A22, A34** and **A40** were first evaluated in a preliminary screening against eight cancer cell lines, namely cervical (Hela), colon (Colo-205), lung (A-549), leukemia (HL-60), ovarian (SKOV-3), and breast (MDA-MB-231, MCF-7 and T47D) cancer cell lines. This initial assessment of antitumor activity tested each derivative in triplicate at 10 and 100 μM concentrations, and the data were presented as percentage cell viability caused by each tested compound (Figures 24 and 25).

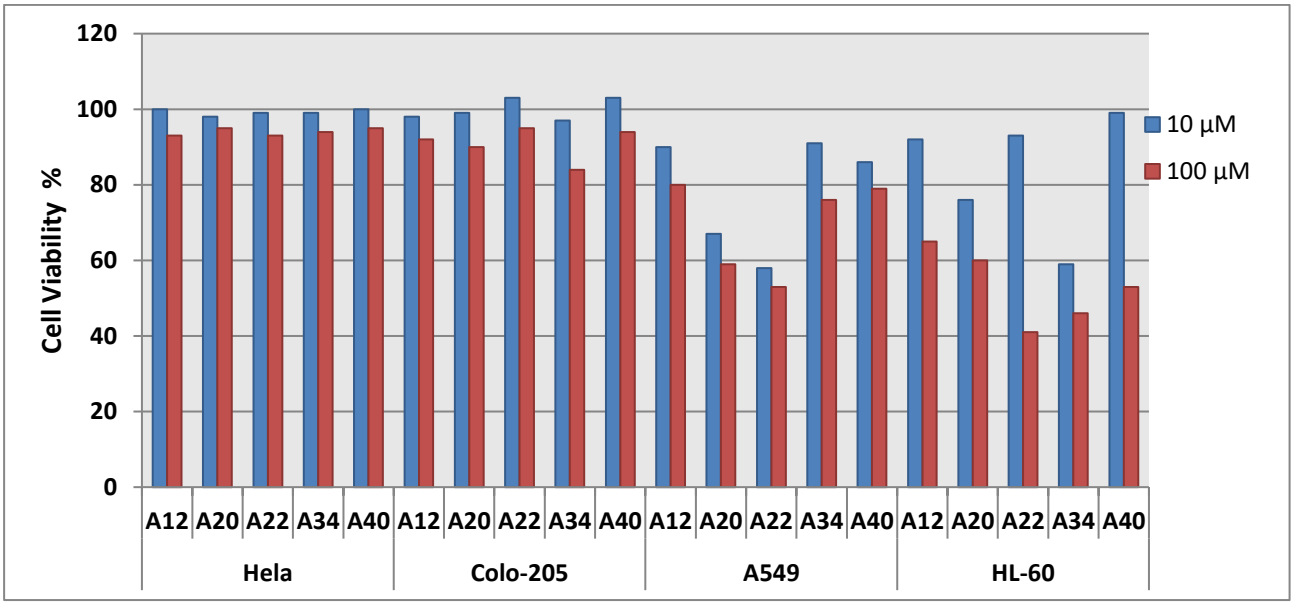

Figure 24. Anti-proliferative activity (cell growth inhibitory activity at 10 and 100 µM concentrations) of compounds **A12**, **A20, A22, A34** and **A40** against Hela, Colo-205, A549 and HL-60 cancer cell lines.

The tested derivatives showed different levels of growth inhibitory activity and possessed a distinctive pattern of selectivity toward the examined eight cancer cell lines. Close examination of the cell viability % in Figures 4 and 5 hinted out that breast cancer MDA-MB-231 and T47D cells were the most susceptible examined cell lines to the influence of the tested compounds, with cell viability % range of (49-61 and 36-58, respectively) at 10 µM and (34-41 and 49-61, respectively) at 100 µM (Figure 25). Moreover, lung A-549 and leukemia HL-60 cells were moderately affected by the tested compounds, with cell viability % range of (58-91 and 59-99, respectively) at 10 µM and (53-80 and 41-65, respectively) at 100 µM (Figure 24), whereas, the tested compounds (**A12**, **A20, A22, A34** and **A40**) displayed weak or no growth inhibitory activities towards cervical Hela, colon Colo-205, ovarian SKOV-3, and breast MCF-7 cancer cell lines.

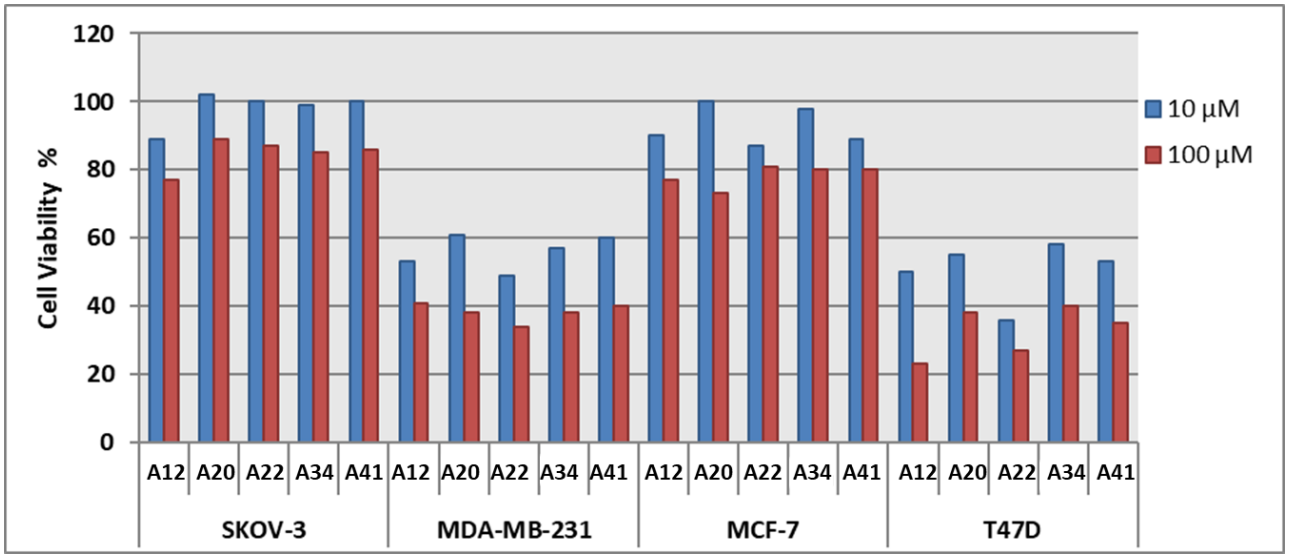

Figure 25. Anti-proliferative activity (cell growth inhibitory activity at 10 and 100 µM concentrations) of compounds **A12**, **A20, A22, A34** and **A40** toward SKOV-3, MDA-MB-231, MCF-7 and T47D cancer cell lines.

Therefore, the quantitative IC_{50} values were determined for sulfonamides **A12**, **A20, A22, A34** and coumarin **A40** against the most susceptible cancer cell lines in the preliminary screening (MDA-MB-231 and T47D), testing concentrations of 100, 10, 1, 0.1 and 0.01 µM for 72h (Table 7).

Table 7. IC_{50} of anti-proliferative activity of compounds **A12**, **A20, A22, A34** and **A40** against breast MDA-MB-231 and T47D cancer cell lines

Cmpd	IC_{50} (µM)[a]	
	MDA-MB-231	T47D
A12	25.46 ± 1.38	7.56 ± 0.29
A20	40.92 ± 1.59	18.86 ± 0.72
A22	6.86 ± 0.31	2.45 ± 0.07
A34	22.85 ± 0.91	33.51 ± 1.24
A40	32.04 ± 1.84	13.16 ± 0.71
Staurosporine	4.25 ± 0.16	4.52 ± 0.19

a. IC_{50} values are the mean ± S.D. of three separate experiments.

As indicated in Table 7, the tested compounds were more effective against T47D (IC_{50} range: 2.45±0.07–18.86±0.72 µM) than MDA-MB-231 cells (IC_{50} range: 6.86±0.31– 40.92±1.59 µM), except sulfonamide **10a** that exhibited enhanced activity against MDA-MB-231 cells (IC_{50} = 22.85 ± 0.91 µM) than T47D cells (IC_{50} = 33.51 ± 1.24 µM). As for the activity against T47D

cells, sulfonamides **4e** and **A22** emerged as the most potent analogues in this study with IC_{50} values of 7.56±0.29 and 2.45±0.07 μM, respectively. Besides, **A22** was the most efficient anti-proliferative agent herein reported, specifically against MDA-MB-231 cells with IC_{50} value of 6.86 ± 0.31 μM.

Cell Cycle Analysis

The efficient anti-proliferative impact of sulfonamides **A12** and **A22** on breast T-47D cancer cell line (Table 6) prompted a further investigation on their growth inhibitory action. The impact of both sulfonamides **A12** and **A22** on cell cycle distribution, after incubation with T-47D cells at their IC_{50} concentration (7.56 and 2.45 μM, respectively) for 24 h, was analyzed by a DNA flow cytometry assay (Figure 26).

The obtained results highlighted that, compared to control cells, breast cancer T-47D cells treated with **A12** and **A22** were arrested at the G2/M phase with an increase in cell population from 16.59% (control) to 26.83% and 35.47%, respectively. Moreover, the number of cells in the sub-G1 phase was dramatically increased from 2.41% (control) to 12.72% and 18.04%, respectively (Figure 26).

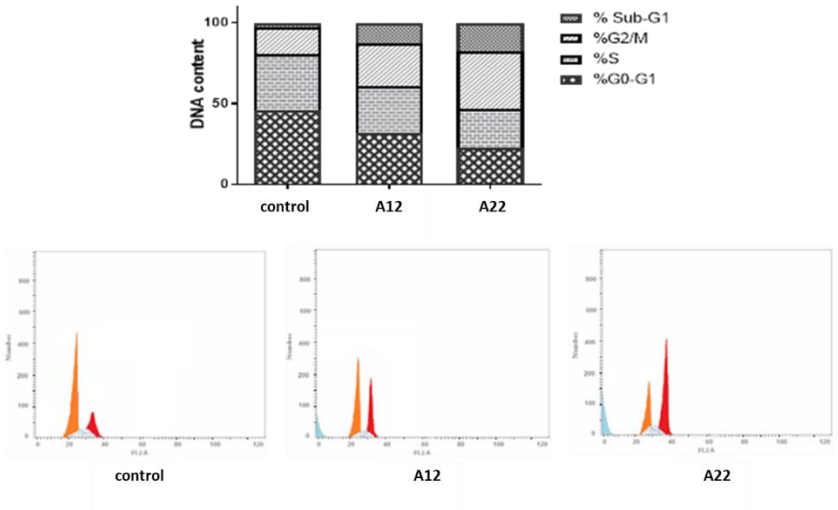

Figure 26. Effect of sulfonamides **A12** and **A22** on the phases of cell cycle of T47D cells.

Annexin V-FITC Apoptosis Assay

To determine whether the growth inhibitory action of sulfonamides **A12** and **A22** is consistent with the induction of apoptosis suggested by the elevated population of sub-G1 in the treated T-47D cells (Figure 26), Annexin V-FITC/PI double staining (AV/PI) apoptosis assay was carried out (Figure 27).

The results of this AV-FITC/PI assay revealed that incubation of T-47D cells with sulfonamides **A12** and **A22** resulted in an induction of apoptosis in these cells, that was evidenced *via* the marked elevation in the apoptotic cells percentage for the early apoptosis (from 0.39% to 3.59% and 7.31, respectively) and the late apoptosis (from 0.17% to 9.62% and 12.19, respectively) phases which represents about 23.6-fold and 34.8-fold total apoptosis increase, compared to the untreated control (Figure 27).

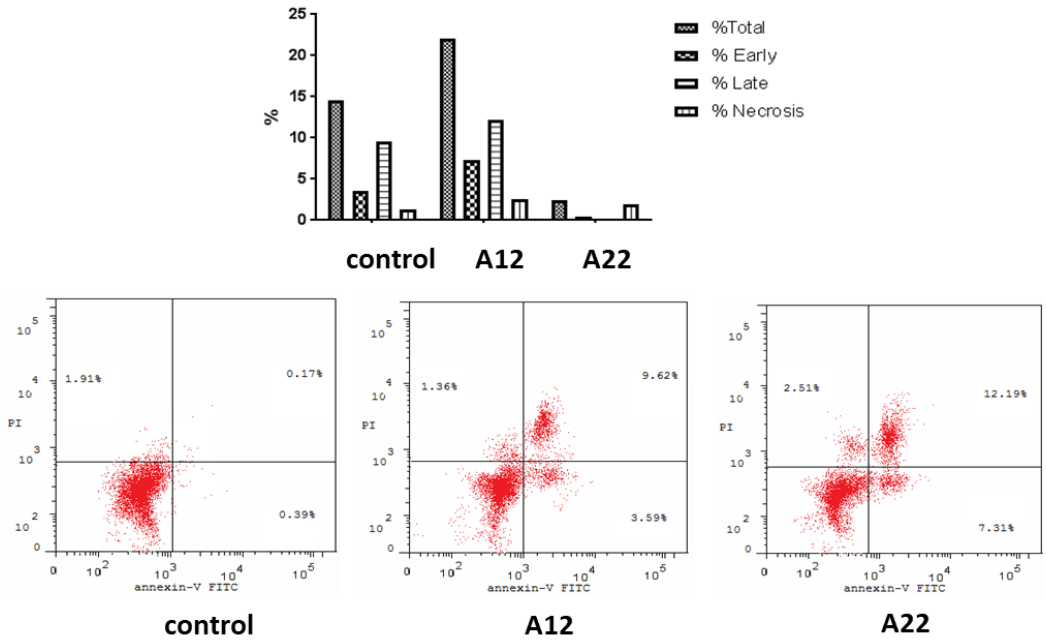

Figure 27. Effect of sulfonamides **A12** and **A22** on the percentage of annexin V-FITC-positive staining in breast T47D cells. The experiments were done in triplicates. The four quadrants identified as: LL, viable; LR, early apoptotic; UR, late apoptotic; UL, necrotic.

The addition of a fluorine atom in the structure of previously reported uracil benzenesulfonamide inhibitors of tumor-associated CAs produced a novel series of derivatives of 5-FU, a widely used medication in the treatment of cancer. A major number of

benzenesulfonamide scaffolds as CAIs was here investigated as well as coumarin fragments to achieve a more targeted CA IX/XII inhibition. Most sulfonamide derivatives efficiently inhibit the target CA IX (K_Is in the range 0.47-44.7 nM) and CA XII (K_Is in the range 2.9-83.1 nM), whereas the 5-FU coumarin derivatives **A40-A41** and **A43** showed a potent and totally selective inhibitory action against the target CA IX/XII over the off-target CA I/II. In contrast, while all sulfonamide compounds exhibited remarkable I/IX and I/XII inhibitory specificity, only two distinct subsets of sulfonamide derivatives produced a preferred inhibition of the target CA IX and XII over the main off-target CA II. When applicable, the comparison of K_I against CA I, II and IX between a 5-FU derivative and the corresponding nonfluorinated analog previously reported showed that the incorporation of a fluorine atom in position 5 of the nitrogenous base scaffold increases both potency and selectivity against the target CA IX. The X-ray solved crystal structure of CA II in adduct with a representative uracil derivative provided insights on the binding mode to the target of such pyrimidine derivatives. Coumarin **A40**, the sulfonamide CAIs showing the greatest II/IX *SI*, namely **A12**, **A20** and **A22**, and the unique subnanomolar CA IX inhibitor **A34** were chosen for assessing *in vitro* their antiproliferative action against a panel of eight cancer cell lines. The IC_{50} values, determined against the most susceptible cancer cell lines MDA-MB-231 and T47D, settle in a low to medium micromolar range (2.45±0.07– 18.86±0.72 μM and 6.86±0.31– 40.92±1.59 μM, respectively). A cell cycle analysis showed that **A12** and **A22**, the most active compounds, arrested T-47D cells mainly in the G2/M phase. Using an annexin V-FITC apoptosis assay, **A12** and **A22** were shown to induce an approximately 23.6-fold and 34.8-fold total increase in apoptosis, corroborating the concrete potential of these 5-FU CAIs for the design of new effective anticancer strategies.

The experimental procedures are reported in Chapter 5 and the data and results of this research were published in A. , et al. *Eur J Med Chem.* **2020**, 190, 112112.

3.3. Design, synthesis and biological evaluation of sulfonamide/coumarin CAI hybrids with berberine as a G-Quadruplex stabilizer to achieve new multi-target antitumor agents (Series B).

The G-Quadruplex is a non-canonical folding structure of deoxyribonucleic acid (DNA). DNA does not occur only in ordered structures held firmly in helical form. In some stretches it folds according to non-canonical structures including "hairpin" structures, Holliday junctions, triple helix DNA, i-motif and G-Quadruplex[162].

Hairpins are formed in stretches where the sequence is palindromic, meaning that it can be equally read in both directions (the sequence can also rearrange in a cross pattern). Holliday Junctions were observed by Robin Holliday to explain a particular case of genetic recombination and consist of four complementary double-helix strands so that they can overlap each other without base pairing errors.[162]

In other cases, DNA does not appear according to the canons described by Watson and Crick. The first to observe one of these cases was Hoogsteen, who in the early 60s described how bases, in a slightly acidic environment (it is no coincidence that it is at a similar pH of that outside the tumor cells), can bind in triplets instead of doublets; the most classic example is that between protonated cytosine-guanine-cytosine, C≡G-C+ that can determine the formation of a triple helix of DNA (Figure 28). However, the formation of the latter turns out to be favored by homopurinic, purine-only strands or homopyrimidinic, pyrimidine-only strands.[163]

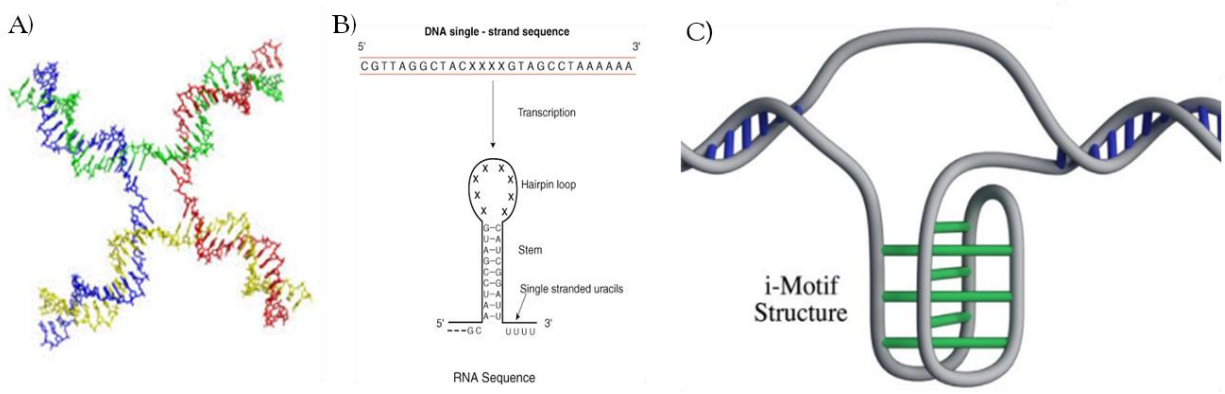

Figure 28. A) Holliday junction; B) Hairpin; C) i-Motif (C-quadruplex).

Non-canonical (Hoogsteen) base pairing can occur between bases of the same type such as A-A, G-G, T-T, C-C but also between different bases such as G-A or G-T.[163]

This structure has in the central region a certain negative electronic density that requires the presence of a monovalent cation to stabilize the structure. The most frequent cation is potassium (K+), both because it stabilizes the tetrad better than other ions and because it is found in greater quantities in the cellular environment (Figure 29). Other cations that can be found to stabilize the tetrad are always monovalent alkali metals: Na+, Rb+, Li+ and Cs+; Sodium and Rubidium stabilize more effectively than Lithium and Cesium.[164]

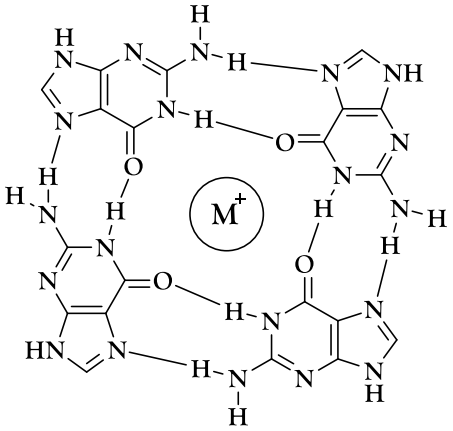

Figure 29. Tetrad arrangement in the presence of a metal cation.

The tetrads can be classified in several ways: they can be identified according to the number of filaments that form them, according to the loops, i.e., the links between the various strands, or according to the orientation of the filaments. The "strands" are the DNA sequences on which are located the guanosines that form the tetrad; in humans the 4 guanosines are all on the same strand, while in other species it has been seen that they can be on two or even four strands (even if in vitro 4 human strands have the ability to form tetrads if placed in ideal conditions). The orientation of the strands can be (Figure 30): parallel, when the 4 filaments all follow the same direction; antiparallel of the type 3+1, where 3 filaments follow one direction while the fourth goes to the opposite side; antiparallel of the type (2+2) where two adjacent filaments go in one direction and the other two follow the opposite one; finally, antiparallel always of the type (2+2) but where the filaments follow opposite directions in an alternating manner. [164,165]

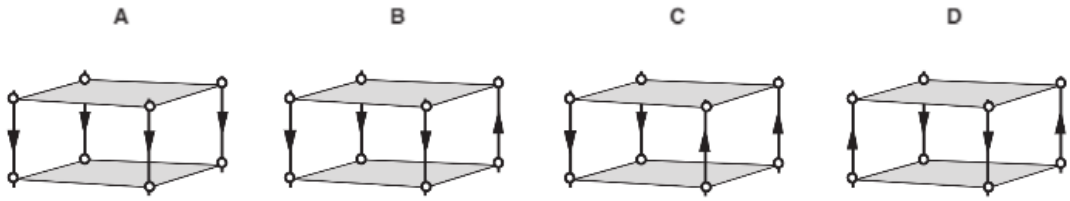

Figure 30. The possible orientations of the strands.

The loops that can be formed exist in four different conformations (Figure 31):

- edge-wise loop, also called lateral loop, connects two adjacent antiparallel strands and the nitrogenous residues composing it can also be single (≥1);
- diagonal loop connects two opposite antiparallel strands and in this case the nitrogen residues required are at least three (≥3);
- double-chain-reversal loop, also called propeller loop, connects two adjacent parallel filaments and requires at least two nitrogen residues (≥2);
- V-shaped loop requires one or more nitrogen residues (≥1) and is the most particular connection.

The latter type binds a phosphate- and deoxyribose-free guanosine with a guanosine present within the classical scaffold forming a bond ideally like a "V"; it appears in those structures in which the three guanosines included in the strands are in the *anti* conformation while the free one is in the *syn* conformation. The fact that it is released from the classical structure represents an interesting point within the G-quadruplexes because it results in a greater gap suitable for interaction with molecules with pharmacological activity.[166]

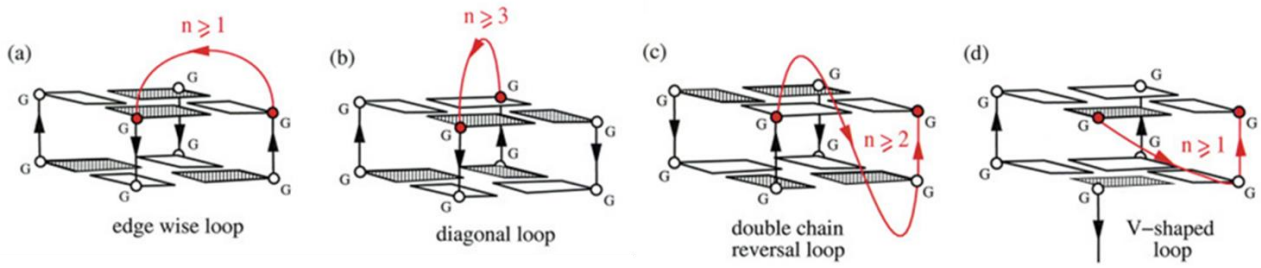

Figure 31. The four types of loops. Arrows indicate the 5'-3' trend; "n" the number of nitrogenous bases.

Finally, the last way of characterizing G-quadruplexes is based on the nature of the sequences; as far as single-stranded ones are concerned, they are assumed to have a sequence of the type GmLnGmLoGmLpGm, where the Gs indicate the guanosines that form the tetrads and "m" the number of them (often this number is between 3 and 5); L are all the bases found in the

loops, including the guanosines, and "n", "o", and "p" indicate the number of bases that make up the loops (these numbers range from 1 to 7). G-quadruplex sequences composed of two or four strands are identical to monomeric sequences but, simply, shorter in fact they contain one or two guanosine tracts; the other difference is that the latter are intermolecular, whereas single-stranded sequences are intramolecular.[164-166]

Various studies have confirmed that there are approximately 700000 hot sites within the human genome for the formation of these structures, and the most susceptible areas are telomeres and oncogene promoters. Oncogene promoters are regions within genes that promote uncontrolled growth and proliferation of malignant cells; under normal conditions they control the cell cycle and regulate apoptosis, but if they have undergone some mutation, they can lead the cell towards immortalization. The main genes involved in the formation of G4 structures are c-Myc, c-Kit1, c-Kit2, Bcl-2, H-ras1, H-ras2, K-ras, B-Raf, TERT, VEGF, TBA, HD22, and FMR1; most of these genes are involved in tumor development as oncogenes, which suggests that they too may be targets of small molecules in cancer therapy.[167]

Within telomeres, G4 structures are found in the single-stranded protrusion. They show a fair amount of variability at the topological level, and the structures that have been observed are as follows (Figure 32): anti-parallel-1 type basket, with anti-parallel strands and diagonal and lateral loops; parallel, with parallel strands and propeller loops; hybrid-1 and hybrid-2, with parallel and anti-parallel strands and propeller and lateral loops; anti-parallel-2 basket, with anti-parallel strands and diagonal and lateral loops but formed by only two tetrads.[167-168]

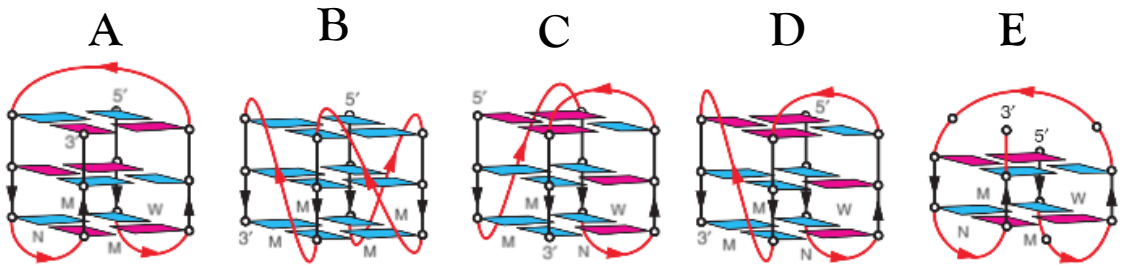

Figure 32. Examples of the possible conformations of G-quadruplexes in human telomeres. A) Antiparallel-1 basket; B) Parallel; C) Hybrid-1; D) Hybrid-2; E) Antiparallel-2 basket. Blue-colored guanosines are in *anti* conformation, whereas those in magenta are in *syn* conformation; N, M, W represent narrow, medium, and wide grooves.

The consequence of this is that it is difficult to determine which of these conformations will have the greatest biological value; however, by implanting sequences into *Xenopus laevis* oocytes, it has been determined that the most likely is the Hybrid-1 type form.[168]

Ligands

In 1991, Zahler and his collaborators demonstrated that it was possible to inhibit telomerase activity by stabilizing G-Quadruplexes, and thus many researches were directed towards the discovery of molecules that could interact with them.[169] The first problem encountered was to understand where the ligands could bind; initially, researchers thought that the ideal location was among the various tetrads of guanines, but subsequent studies showed that the central part of the tetrads remained unperturbed. The explanation lies in the fact that this type of conformation is very stable and compact. The entry of a molecule between the various planes of guanine needs a high energy cost because it causes the distortion of the structure in addition to the fact that inside there is a metal, which is difficult to displace.

These studies have led to the realization that the ligand can be arranged predominantly in three ways: above or below the tetrad, within or along the grooves (the areas comprising the bases that form the loops). In fact, position number 2 is the least likely and most energetically unfavorable.[169-170]

Among the possible ligands in the literature, our choice fell on berberine. A natural compound found in some plants of the genus *Berberis* and *Coptis* native to China. It has been used for centuries as an antimicrobial but at the end of the last century it was found to have inhibitory activity against telomerase. The two main groups of derivatives enclose berberine substituted in 13 and 9 respectively (**Z1** and **Z2**, Figure 33).; the latter shows a higher affinity toward G4 structures.[169]

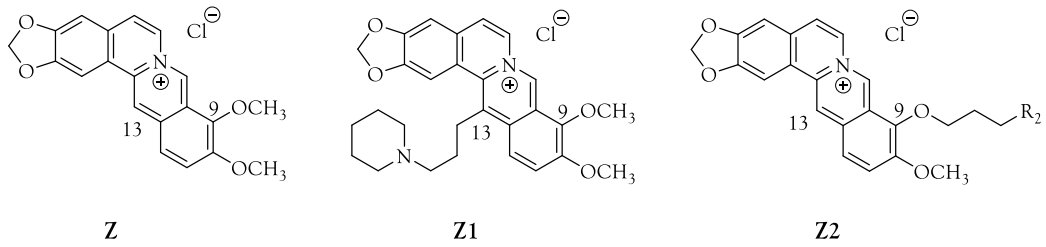

Z **Z1** **Z2**

Figure 33. Berberine **Z**, Berberine substituted **Z1** in 13 and Berberine **Z2** in 9.

Antitumorali

After the presentation about who binds the G4 structure, it is necessary to understand how the berberine derivatives stabilize these kinds of foldings and promote the cancer regression. Telomeres are found at the ends of chromosomes and contain non-coding DNA sequences, devoid of genetic information, but they act as protection to coding sequences. They are composed by a double helix made by TTAGGG sequences repeated for 2000-10000 bases and they end in a protrusion composed by 150-200 single stranded bases always with the TTAGGG sequence repeated several times. An important factor is their length: each cell division shortens the length of the telomere by a certain number of bases (due to the need to synthesize Okazaki fragments). After a series of divisions, the cell goes into senescence and the apoptotic mechanism that leads to programmed cell death is triggered. According to Hayflick's studies and calculations, the possible divisions are about 50. In germ cells there is the telomerase complex, an enzyme that among its various constituents has the TERT that is a reverse transcriptase able to attack in the 3' terminal part (the single stranded one) sequences of the type GGTTAG; this leads to the elongation or, however, to the maintenance of the length of the telomere avoiding apoptosis. In mature cells this mechanism is not active since TERT is inhibited, but if telomerases are overexpressed the cell becomes theoretically immortal since it never enters senescence. 85% of tumors show overexpression of telomerases. To prevent the action of this enzyme, it is necessary to stabilize the G-Quadruplexes, which do not allow the enzyme to anchor itself to the single DNA strand and lengthen the telomere again.[170-171] (Figure 34)

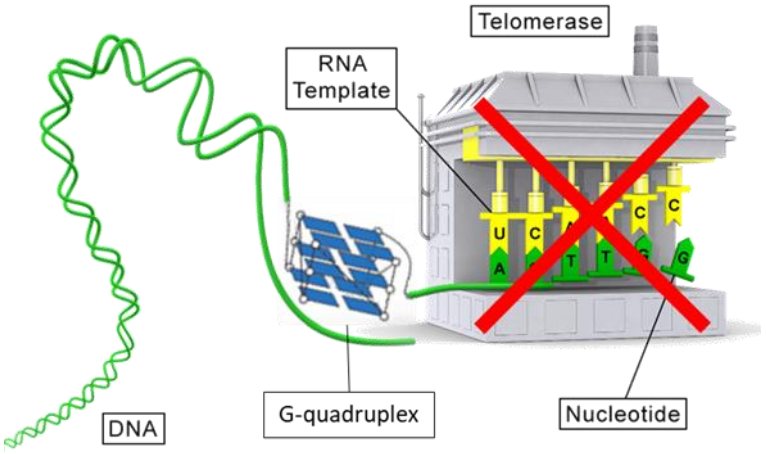

Figure 34. Mechanism of action of G4 to inhibit telomerase.

In addition to telomeric G4s, we also focus on those present in the c-kit and c-myc protooncogenes. Indeed, binding studies have also been conducted on those particular types of tetrads. In addition, crystallographic studies, to date, have been conducted in most cases against Tel23, however, in the latter part of my PhD I also performed crystallization tests on c-kit. The c-kit receptor (CD117) is a transmembrane protein with tyrosine kinase activity encoded by the oncogene c-kit. It is an important member of type III receptor tyrosine kinase family[172]. The human receptor tyrosine kinase (RTK) c-kit was identified and characterized in 1987 as the cellular homologue of the viral oncogene v-kit which was isolated in 1986 from a feline retrovirus[173]. Human c-kit proto-oncogene locates on chromosome 4q11～12 and has a total length of 90 kb. the c-kit receptor is composed of 976 amino acids (aa) divided into an extra-cellular domain with 519 aa, a trans-membrane domain with 23 aa, an intracellular tail of 433 aa consisting of a juxta-membrane domain and a tyrosine kinase domain inserted by about 80 amino acid residues[174]. C-kit was found in a plethora of compartments of our organism, infact, C-kit-dependent cell types include hematopoietic cells, germ cells, mast cells, melanoma cells and the gastrointestinal tract cajal cells. C-kit signaling plays a very important role in regulation of the red blood cell production, lymphocyte proliferation, mast cell development and function, melanin formation, and gamete formation. Human c-kit receptor loss of function mutations can cause autosomal mottle disease. Gain of function mutations can be found in GIST (>90%), mast cell tumor (>70%), nasal T-cell lymphomas (>17%), seminoma / dysgerminoma (> 9%) and acute myeloid leukemia (>68%).[175-176] One of the strategies

hypothesized, to act against the overexpression of c-kit receptors in this type of tumors, is to go to stabilize the g-4 structures that are formed in the proto-oncogenes c-kit (the same strategy that is used against telomerase) in order to avoid gene transcription.

Drug-design

The phenomenon of development of drug resistance, the main cause of possible therapeutic failure, has led towards the use of customizable polypharmacies, made with drugs that act on different cellular mechanisms, mutually increasing their effectiveness and reducing their respective dosage (with a decrease in the intensity of adverse effects). Research is moving towards the discovery of molecules with innovative targets to give a wide variability of choice on the drugs to be used in case of manifestation of resistance.

The new anticancer therapies should have a reduced toxicity (improving patient compliance to treatment), prevent and prevent the phenomena of resistance and should also be valid against most cancers.

Considering what has been said in the introductory chapters in relation to CA IX/XII and G4 targets, the objective of this thesis is to design target-specific molecular hybrids against hypoxic tumors, containing a selective inhibitor of CA IX and XII, and a pharmacophore capable of stabilizing non-canonical DNA structures called G-Quadruplex.

Inhibition of CA IX and XII is now a validated therapeutic approach to inhibit growth, invasiveness and metastasis of primary tumors, and to reduce the population of cancer stem cells. On the other hand, it has been shown that 85% of tumors possess active telomerase systems. G-quadruplexes, found at the single-stranded end of telomeres, inhibit telomerase activity allowing the cell to move toward senescence and subsequently apoptosis. Stabilization of G4 inhibits telomerase reactivation and causes apoptosis of the cancer cell.

The hybrid molecules reported in this thesis work were designed to incorporate Carbonic Anhydraseinhibitory pharmacophores on chromophore scaffolds known to interact with G4.

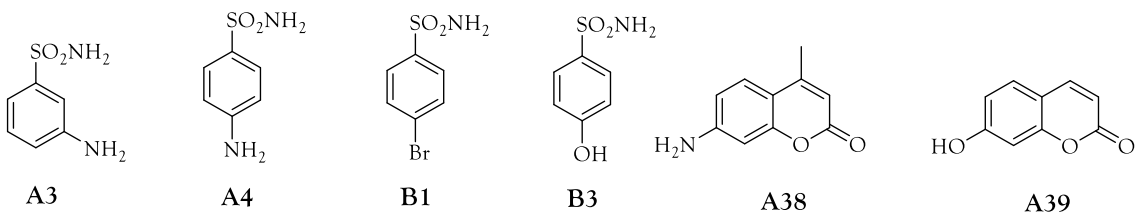

Figura 36. Sulfonamide or coumarin scaffold used as inhibitory CA portion in the hybrids.

The CA inhibitory portion is either sulfonamide or coumarin in nature (Figure 35). While coumarin derivatives almost distinctly delineate a selective of inhibitory action toward CA IX and XII as opposed to I and II, sulfonamides are known to result in a more promiscuous action. Despite this, sulfonamides bring greater solubility to the molecule. It should also not be forgotten that the incorporation of the G4-binding portion represents an application of the "tail approach" on the scaffold bearing the sulfonamide. Considering the steric encumbrance represented by the polycyclic structures used as G4 ligands (considered tail of the CA inhibitor), the reduced size of the catalytic sites of CA I and II (compared to IX and XII) may not allow an appropriate binding and equally delineate a selectivity of action.

Regarding the G4-binding portion, we opted for the berberine core, as previously explained. The two types of designed hybrids are the follows (Figure 36):

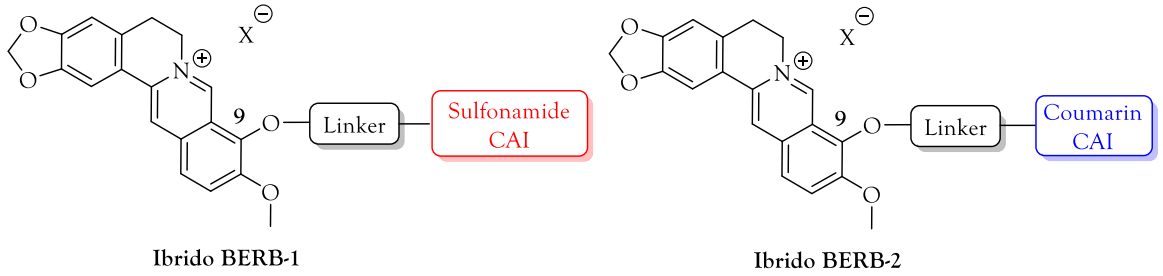

Figure 36. Two types of projected hybrids.

Recently, berberine has been shown to bind and stabilize human telomeric G4 with micromolar order constants.

Click chemistry, or Huisgen's 1,3-dipolar azide-alkyne cycloaddition, is a synthetic approach that is widely used today, particularly in pharmaceutical chemistry. It allows to connect two distinct portions of the molecule through a stable linker and not separable under physiological conditions, such as 1,2,3-triazole 1,4-disubstituted if catalyzed by Cu (I) (the reaction with ruthenium-based catalysts generates instead triazole 1,5-disubstituted). The only requirement is the presence in the two fragments of a terminal alkyne function and an azide function. The click chemistry reaction is rapid, simple to purify and versatile, so much so that it tolerates a wide variety of substituents, solvents and temperatures. 1,2,3-triazole is considered an amide group biosubstrate with a moderate dipolar character, hydrogen bond acceptor and donor properties, and an aromatic character useful for establishing π-type interactions with its receptor

counterpart[177]. For these reasons, the triazole-type linker was from the outset the first choice regarding the connection between the berberin core and CAIportion.[178]

Synthesis

To start the click chemistry, we need on our intermediates various azides ad alkynes. The first intermediates that we show are of sulfonamide tipe. We treated different sulfonamides **A3-A4** in a Sandemayer reaction to obtain the respective azides **A30** and **A31**. The alkynes were obtained from two different sulfonamides **B1** and **B3**; the first one **(B2)** through a Sonogashira reaction and the second one **(B4)** through a reaction with propargyl bromide and potassium carbonate in dry DMF.

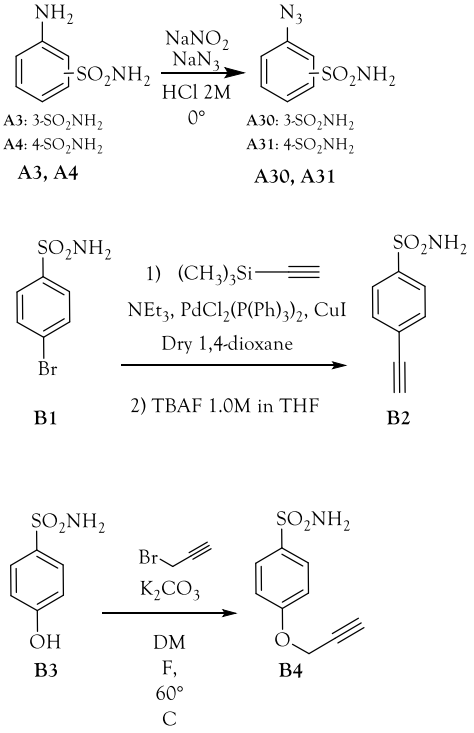

Scheme 6. Synthesis of sulfonamide intermediates **A30, A31, B2 and B4**.

The second types of intermediated that we have synthetized are of coumarin scaffold. We treated the umbelliferone **A39** with 3 different dibromoalkanes with 3 to 5 carbon spaces in carbonate and DMF at 80° degrees and than, without purification, we put them **(B5-B7)** in DMF and sodium azide to obtain the compounds **B8-B10**. The same **A39** was also reacted in carbonate and DMF with 3 different propargyl bromide from 3 to 5 unit carbon atoms,

obtaining the intermediates **B11-B13**. One more azide A42 was derived by treating the coumarin **A38** in the same conditions of compounds **B5-B7**.

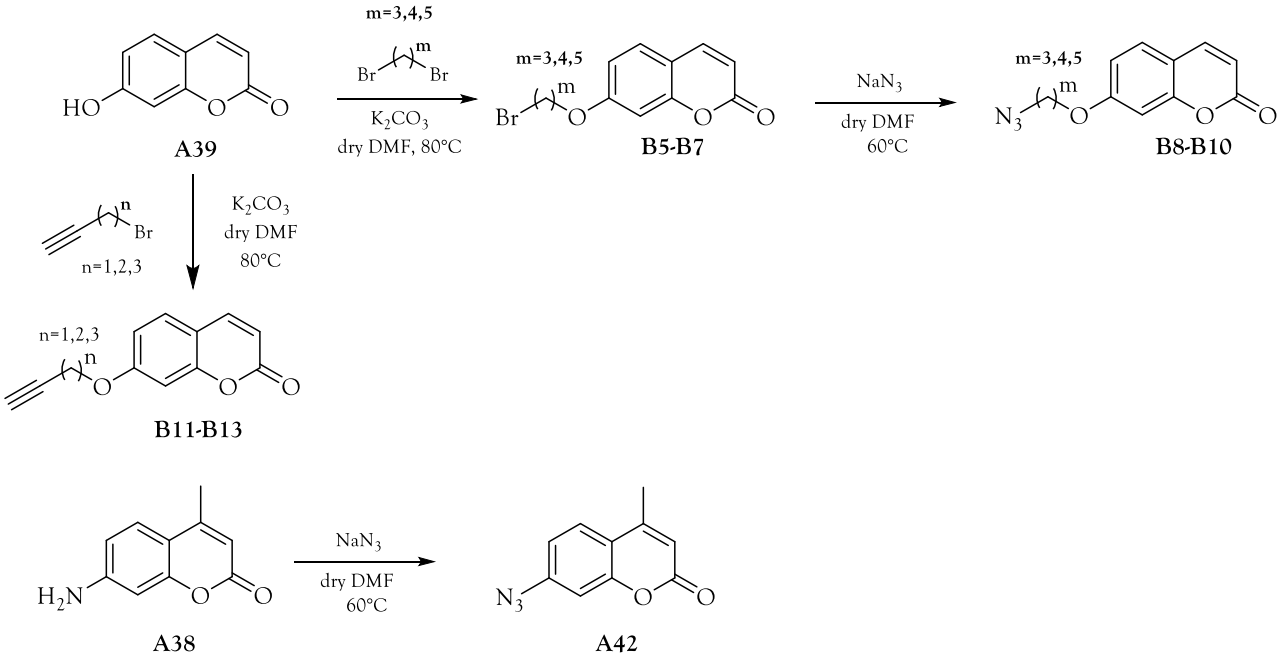

Scheme 7. Synthesis of coumarin intermediates **B8-B13** and **A42**.

The last group of intermediates are the berberines. First, is necessary to do the selective demethylation of berberine to berberrubine **(B14)** in position 9; obtained at high pressure and high temperature without solvent for 2 hours. Very interesting is that berberine is a yellow powder while berberrubine powder is red, just like the name suggests. This modification is probably due to the rearrangement of the electronic configuration after loss of permanent charge on nitrogen; instead, the following NMR spectra show that, on the aromatic portion, there is a significant change.

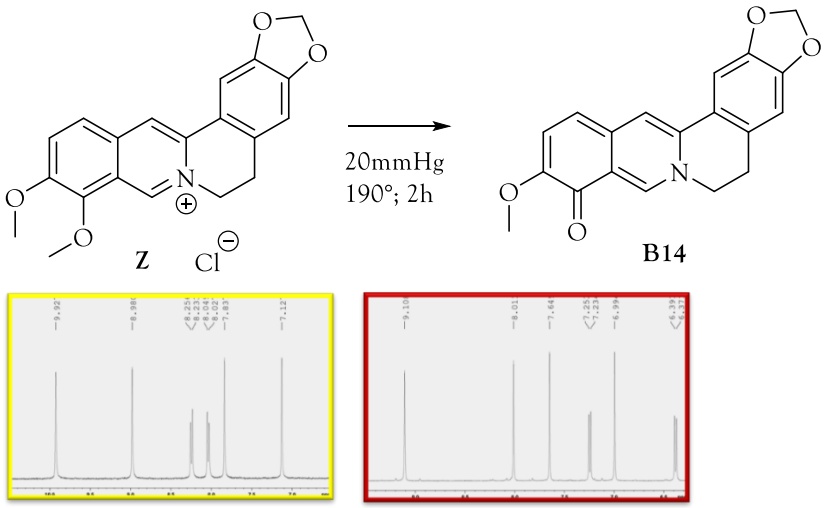

Scheme 8. Synthesis of berberrubine **B14.** Comparison between the aromatic part of berberine and berberrubine.

Subsequently, we treated berberrubine in the same way of coumarins to obtain azides and alkynes, with propargyl bromide in dry DMF at 60° to give the compounds **B23-B24**. For the compounds **B15-B18** we incorporated a bromoalkyl linker on the berberrubine scaffold then converted into the respective azides (**B19-B22**).

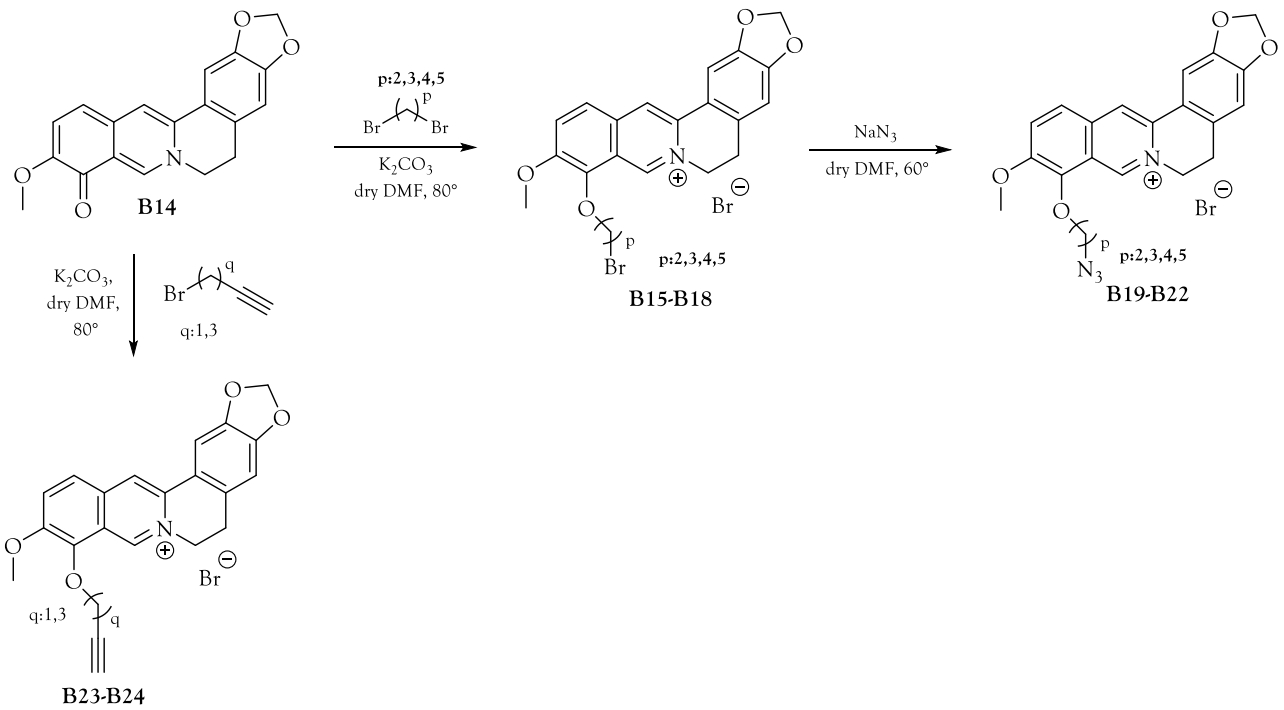

Scheme 9. Synthesis of azides **B19-B22** and alkynes **B23-B24** from berberrubine.

Sulfonamide hybrid derivatives were obtained using the click chemistry cited before. Our click conditions are composed by Sodium Ascorbate, Copper Sulfate in water and *tert*-Buthanol. To purify all compounds, we decided to quench all reaction with lipophilic ion hexafluorophosphate, in order to obtain final compounds more soluble in organic solvent and thus, have the ability to extract them in DCM to remove the various inorganic salts. Azides and alkynes of berberine were reacted with corresponding azides and alkynes of sulfonamides.

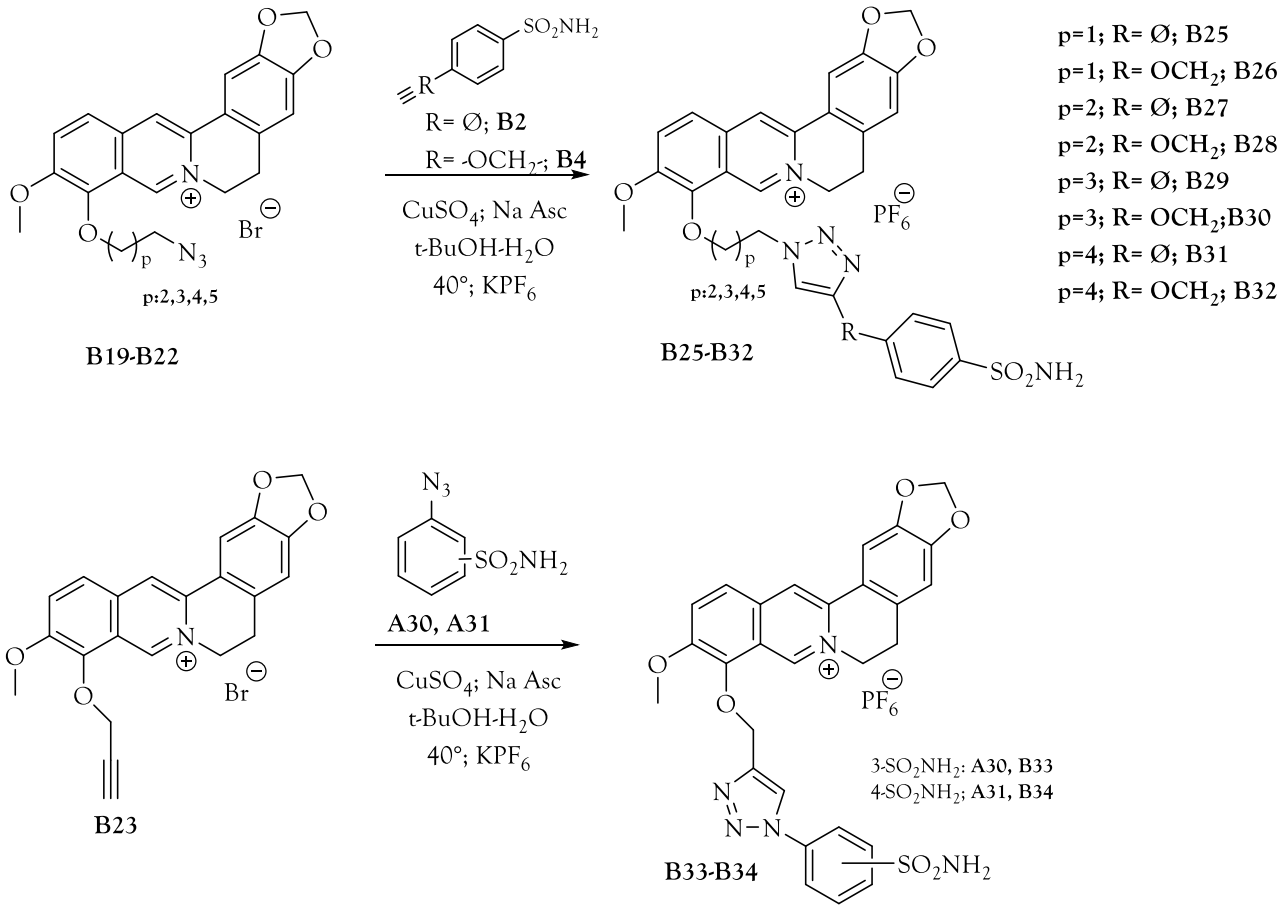

Scheme 10. Synthesis of hybrid derivatives berberine-triazolesulfonamides **B25-B34**.

Using the same strategy and the same click-conditions, we synthetized the coumarins derivatives starting from the azido and alkyno coumarins in complex with the same berberino-intermediates.

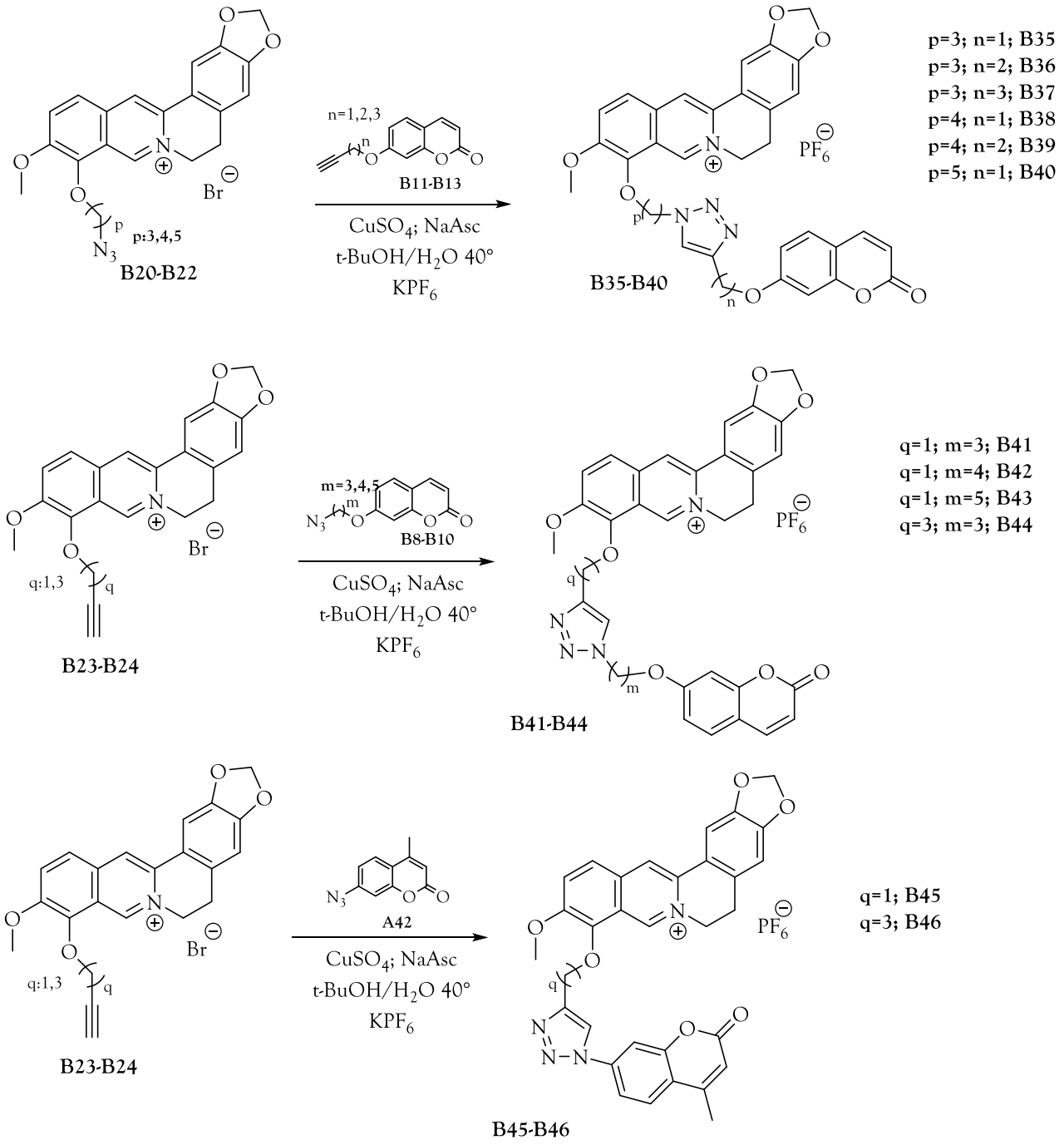

Scheme 11. Synthesis of hybrid derivatives berberine-triazolecoumarins **B35-B46.**

To concluse the synthesis part, we decided to realize an alkylsulfonamide. Berberrubine was reacted with propansultone in dry DMF at 60°; the reaction mixture, once cooled, was treated with Et2O, then filtering the precipitate obtained. The latter were then chlorinated into chloride of thionyl chloride using a drop of catalytic DMF, heating the reaction reflux for 2-3 hours. Once the excess SOCl2 was

brought to dryness, the crude was directly resolubilized in THF anhydrous and treated at 0°C with NH4OH (aq.) The crude obtained by filtration of the resulting suspension was purified by chromatographic column using as eluent various degrees of the TFA/ MeOH/ DCM mixture as eluent.

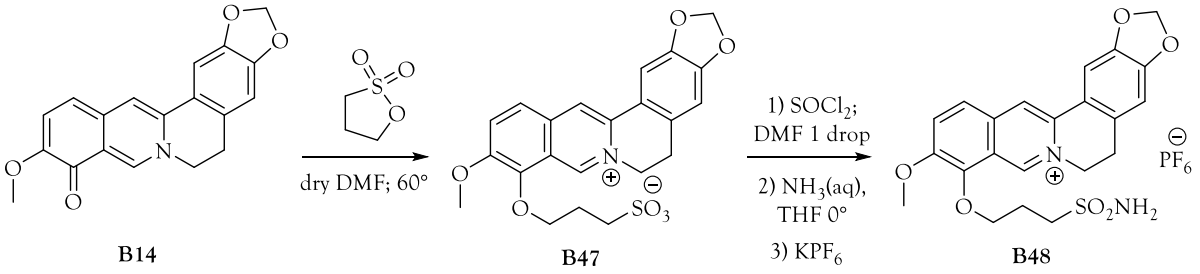

Scheme 12. Synthesis of hybrid derivative berberine-alkylsulfonamide **B48.**

Biological assay and results

All final compounds were assayed in vitro by Stopped-Flow technique for their ability to inhibit target CA isoforms IX/XII and off-target isoforms I and II compared with the classical sulfonamide inhibitor Acetazolamide (Table 8). The coumarins derivatives are incubated for 6h; while sulfonamide compounds for 15 minutes.

Table 8. Inhibition data for human CAs I, II, IX, and XII with the final hybrid sulfonamide compounds in comparison with the sulfonamide standard Acetazolamide (AAZ), obtained by CO2 hydration assay performed using the Stopped-Flow technique.

Compound	K_I[a] (nM)			
	CA I	CA II	CA IX	CA XII
Hybrids G4-CAI of the sulfonamide types				
B25	580.5	59.4	1.4	7.3
B26	940.2	6.0	0.65	4.4
B27	872.1	66.8	0.73	14.0
B28	805.0	62.3	0.56	31.2
B29	592.4	55.1	0.49	25.5
B30	915.6	71.5	0.70	7.2
B31	573.6	15.8	0.24	18.3
B32	219.5	41.1	0.54	2.9
B33	3670.2	90.1	3.9	24.8

B34	829.1	22.9	2.7	6.1
AAZ	250	12	25	5.7

a. Mean from 3 different assays (errors were in the range of ± 5-10 % of the reported values).

1)The ubiquitous isoform I was found to be the least inhibited from the entire set of hybrids made. The compounds inhibit in the mid-nanomolar to low micromolar range (inhibition constant, KI=219.5-5653.4 nM). Increasing the distance between benzenesulfonamide and the berberine core only slightly increases the inhibitory action. Meta-substitution on the benzenesulfonamide core is unfavorable for hCA I inhibitory action **(B33 vs B34)**

2) All sulfonamide derivatives of berberine show activity in the low nanomolar range towards this isoform (with KI from 6.0 to 90.1 nM). The nature and length of the spacer present in compound **B26** is the best to achieve efficacy towards hCA II (KI of 6.0 nM).

3) The hCA IX target isoform is effectively inhibited by most assayed derivatives (KI in the range 0.24-3.9nM), Notably, the inhibitory action improves with increasing length of the spacer linking CAI to the berberine scaffold. In fact, compounds bearing the shorter linker **B33, B34, B25** inhibit the enzyme up to 10-fold worse than longer-chain derivatives. In the case of derivatives with 4- and 5-carbon atom linkers between triazole and berberine (**B29-B32**), the inclusion of an additional oxymethylene spacer between triazole and benzenesulfonamide slightly worsens the inhibitory efficacy. The opposite effect occurs in the case of derivatives **B25-B28**, which have a 2- and 3-carbon atom spacer between triazole and berberine.

4) A rather flat inhibitory trend toward CA XII was detected for sulfonamide derivatives with KIs ranging from 2.9 to 31.2 nM, making it difficult to develop accurate SARs.

5) Both tumor-associated isoforms appear to be strongly inhibited by all berberine derivatives, especially hCA IX. Although the off-target isoform hCA II is also effectively inhibited by berberine scaffold sulfonamides, subnanomolar inhibition data measured toward hCA IX delineate hCA IX/II selectivity profiles (selectivity index, SI) that reach two orders of magnitude (>100-fold) for the target isoform. In detail, B28-B30 proved to be the most IX/II selective derivatives (IS of 111, 112, 102, respectively). The data in Table 1 show a lower hCA XII/II action selectivity for the same derivatives that reaches, however, approximately 10-fold, as in the

case of B30 (SI 9.9) and B32 (SI 14). The IX/I and XII/I selectivity indices are even higher for all berberine scaffold sulfonamide derivatives with action selectivity reaching three orders of magnitude. Interesting inhibitory profiles selective for tumor isoforms over hCA I and II are also found in the set of disulfonamide derivatives.

Table 9. Inhibition data for human CAs I, II, IX, and XII with the final hybrid coumarin compounds in comparison with the sulfonamide standard Acetazolamide (AAZ), obtained by CO2 hydration assay performed using the Stopped-Flow technique. 6h incubation to obtain the active open form of coumairns.

Compound	K_I[a] (nM)			
	CA I	CA II	CA IX	CA XII
Hybrids G4-CAI of the coumarin types				
B35	>10000	>10000	20,4	7,2
B36	>10000	>10000	24,0	6,3
B37	>10000	>10000	15,2	10,1
B38	>10000	>10000	17.3	8.4
B39	>10000	>10000	19,6	5,9
B40	>10000	>10000	12,9	3,4
B41	>10000	>10000	51.5	10.2
B42	>10000	>10000	48,2	7,7
B43	>10000	>10000	43,1	10,6
B44	>10000	>10000	29,7	8,3
B45	>10000	>10000	35.1	5.4
B46	>10000	>10000	18,6	6,9
B48	>10000	>10000	14,4	5,1
AAZ	250	12	25	5.7

a. Mean from 3 different assays (errors were in the range of ± 5-10 % of the reported values).

1-2) All coumarins do not inhibit off-target isoforms I and II below the 10 μM concentration, in agreement with literature data for this type of derivatives.

3) Coumarin derivatives effectively inhibit hCA IX in a range slightly higher than sulfonamide analogs (12.9-51.5 nM).

4) They demonstrate potent and selective CA XII inhibitory action (compared to hCA I and II). Indeed, these prodrugs show an inhibitory effect in the low nanomolar range (5.4-10.2 nM) against the target enzyme.

Binding experiments

Several techniques exist to assess ligand binding on g4 structures, the most widely used of which are shown below:

- UV-Vis spectroscopy acts on the basis of changes in absorption of the chromophore (ligand) when bound to the target. G-quadruplex structures tend to have a hypochromic effect, i.e. they lower the value of "ε" (molar extinction coefficient, specific for each molecule);
- circular dichroism offers the possibility to characterize conformations of nucleic acids and their complexes with proteins or other ligands. It has proven useful in distinguishing parallel from antiparallel filaments. Moreover, the circular dichroism does not recognize achiral molecules; often the ligands of G-Quadruplexes belong to this category but if they are bound to the nucleic acid, they undergo the phenomenon called induced circular dichroism. In summary, it can be understood if the binding between quartet and achiral molecule has occurred if the set orient the polarized light;
- 1H-NMR spectroscopy; in the case of G4 we study the hydrogens bound to the nitrogenous bases involved in Watson-Crick type bonds and Hoogsteen bonds. Usually, these hydrogens fall at 12.5 ppm but if implicated in Hoogsteen bonds they are found between 10.5 and 12 ppm, showing that they are involved in G-Quadruplex structures;
- X-ray crystallography has allowed the study of several different types of G-Quadruplexes as well as their complexes with ligands;
- FRET (Fluorescence Resonance Energy Transfer) exploits the transfer of energy from a molecule, capable of emitting fluorescence, to an adjacent molecule. It is useful in understanding the distance, therefore the bond, between two compounds. In this case between the ligand and the quartet.

In our case the technique of circular dichroism was used; to be precise an application of it called 'circular dichroism melting experiment'. It consists in evaluating the variation of the melting point of the various structures considered, after being incubated with a known amount

of our hybrids. The higher the melting point after incubation, the greater the stability that this compound confers to the non-canonical folding of DNA.

The research group of Professor Antonio Randazzo has been involved in doing this type of assay; evaluating the binding of our derivatives on 4 structures; 3 quadruplexes and one double helix. The structures that they have selected are: Tel23, typical telomeric sequence able to fold in g-4 structures; c-kit and c-myc, sequences of 22 nitrogenous bases detected in the protoncogenes just listed, also considered among the sequences that have the greatest ability to fold in g4 structures; finally, the hairpin structure, a double helix and is used as an off-target sequence because, in the organism, DNA is in the vast majority of cases double helix and we do not want our hybrids to interact with it, but only with g4 structures. The following spider-plot shows the obtained results. (Figure 37

Figure 37. Spider-plot of binding capacity of our synthetized hybrids.

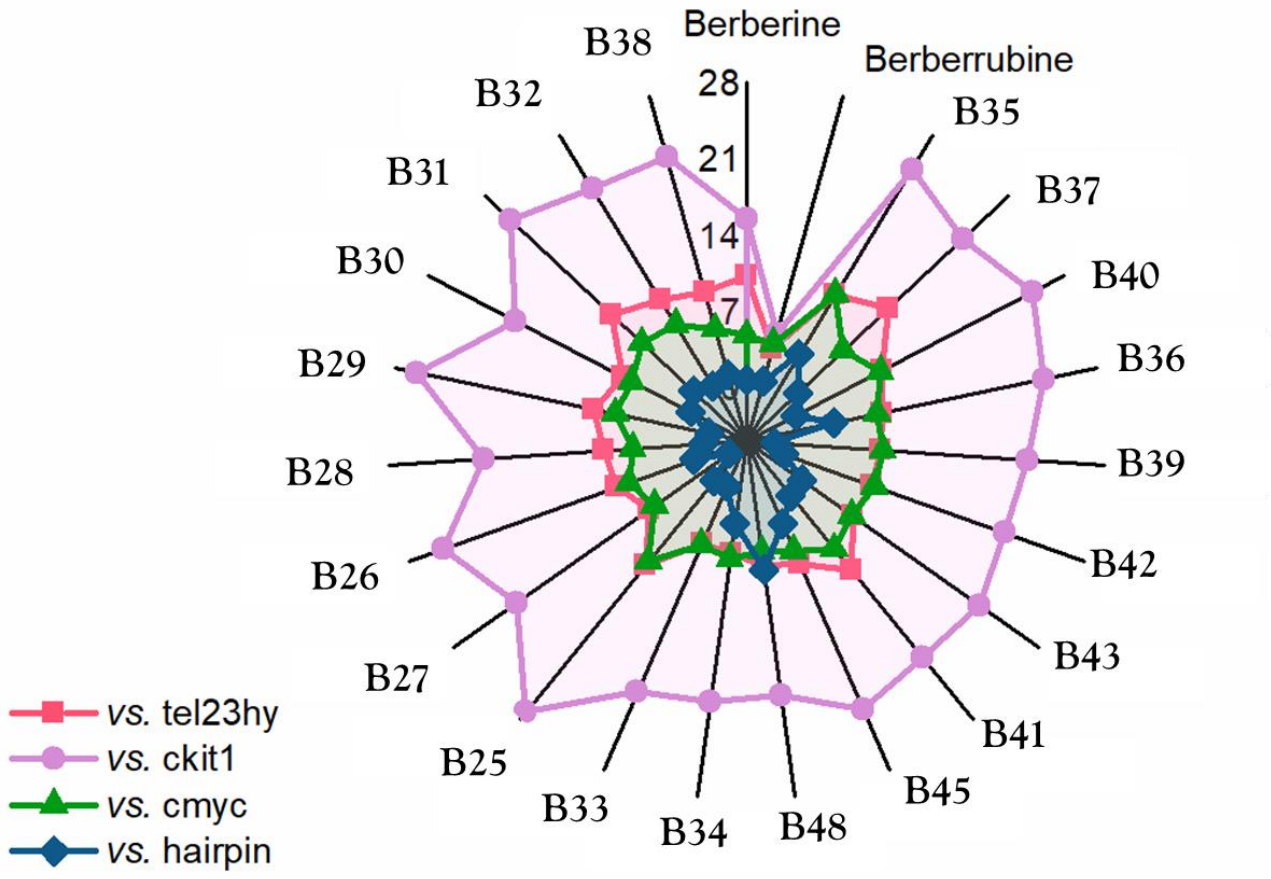

From the spider-plot, it can be seen that the most effectively stabilized sequence is largely that of c-kit. The notable compounds are **B25, B29, B35**, and **B40**. In detail we can see that

berberrubine, with its conformational change, stabilizes drastically worse than all other compounds; also, berberine despite being much more effective than its demethylated counterpart is also inferior in quality compared to all hybrids. This allows us to say that the hybridization of berberine with ca inhibitory portions increases the affinity towards the chosen target. Next, the stabilized sequences are tel23 and c-myc; which show very close values, but with a slight preference of tel 23, particularly in compounds **B31**, **B37** and **B41**. While towards c-myc, the most related compounds were found to be **B25** and **B35**. It is important to note that, towards the off-target sequence (Hairpin), the compounds stabilize in the least effective way; with the only exception of compound **B48** which, however, is the only one that does not present aromatic portions in the inhibitory CA portion and, it may be plausible that it has less chance of stacking, necessary to be a good ligand towards g-4 structures. The fact that there is no particular affinity of our compounds towards the hairpin is good news for us, as it means that our molecules do not readily interact with the DNA double helix.

Crystallization test

Intro

A large part of my thesis project is the various experiments done using the X-ray crystallography. This technique is the most widely used for understanding chemical systems at the atomic level. One of the major difficulties is that the results obtained in solution (binding assays or CA inhibition studies) do not always correspond to the results obtained in crystallography. However, it does provide information about intermolecular binding between dna and ligand that is obtainable in few other ways. There are several critical steps in order to obtain a valid crystallographic structure such as getting acceptable crystals, understanding what the right model is to have good phasing, and finally getting good data refinement.

The first challenge is to obtain sufficiently ordered crystals, since a crystal is defined as a sequence of physical entities arranged according to an ordered and defined lattice. To achieve this we rely on the graph that relates solubility to the concentration of the protein/nucleic acid. There are usually three phases of crystal formation: nucleation, which occurs in the supersaturation region and consists of the formation of an aggregate of a certain number of thermodynamically stable molecules; then there is crystal growth which occurs in the metastable

region where other molecules aggregate around the critical nucleus previously formed; Finally, there is the cessation of growth that occurs when the solution is now poor in proteins/nucleic acids or impurities have formed that block the development of new nucleations (Figure 38).[179]

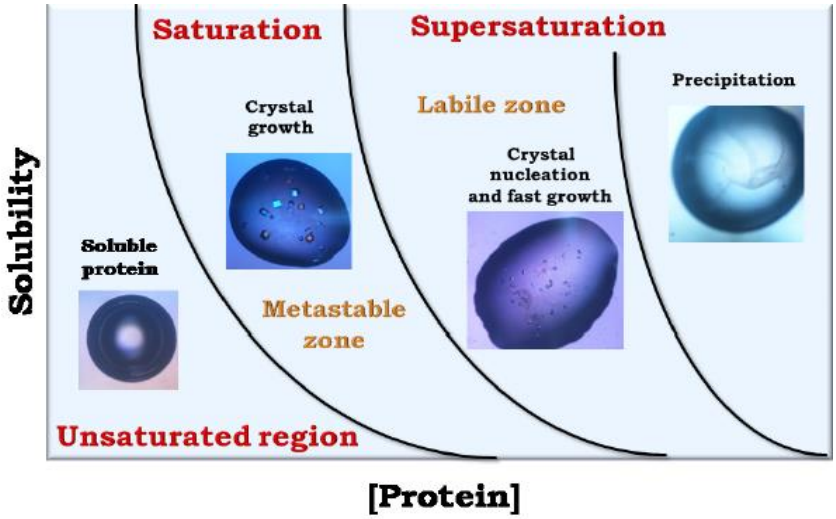

Figure 38. Graph of dependence of nucleic acid/protein concentration to solubility.

The variables that arise at this stage are many. In order to obtain a crystal, an enormous number of parameters must be taken into account, which are expressed in the figure below. (Figure 39).

Physical factors	Chemical factors	Biochemical factors
Temperature	Precipitant type	Sample purity
Pressure	Precipitant concentration	Sample homogeneity
Gravity	pH	Sequence modifications
Magnetic fields	Buffer type	Posttranslational modifications
Electric fields	Ionic strength	Chemical modifications
Dielectric properties	Sample concentration	Aggregation
Viscosity	Metal ions	Proteolysis
Vibrations and sound	Polyions	Sample pI
Time	Detergents	Ligands, co-factors, inhibitors
Equilibration rate	Heavy metals	
Nucleants	Small molecule impurities	
Methodology	Crosslinkers	
Surface of crystallization device	Reagent source	
Sample handling	Reagent formulation	

Figure 39. Physical, chemical and biochemical parameters to obtain a valid crystal growth.

Usually, a screening of conditions is created in which an attempt is made to compare as many parameters as possible; these screenings can be either purchased or created ad-hoc by the operator. Often it is necessary to optimize the conditions used at first, because it frequently happens that the crystal formed was not good enough. These conditions contain: salts useful for

the nucleation of the crystal; buffers useful because pH variations could lead to conformational changes especially of proteins that are very sensitive to these fluctuations; and then contain a precipitant that can be of organic nature such as MPD, a polymer such as PEG or a salt such as ammonium sulfate. It serves to reduce the solubility of the protein to favor nucleation and then crystallization of the desired species.[180]

The most common techniques for obtaining crystals are as follows: Counter-Diffusion in Gel, Gel Crystallization, Free Interface Diffusion, Dialysis, Batch and Vapor Diffusion. In my little experience I have used only the technique of Vapor Diffusion. This method consists in putting inside a minimum amount of solvent your macromolecule or adduct and it is balanced by a reservoir that contains the same salts of the solvent but at a higher concentration, this leads the drop to decrease in volume slowly bringing the macromolecule up to the point of supersaturation where the nucleation will begin. The fact that it requires small amounts of compounds makes it one of the most used techniques. There are 3 variations of it: sitting drop, hanging drop and sandwich drop. (Figure 40)

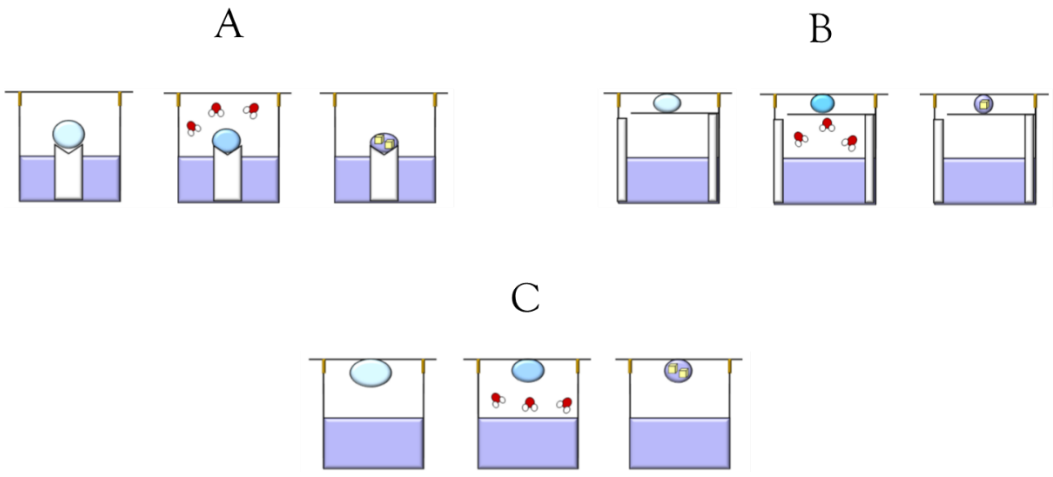

Figure 40. Variants of the vapour diffusion method. A) sitting drop (drop on a support); B) sandwich drop (drop between two surfaces); C) hanging drop (drop on a glass slide).

The difference between these three methods is only in the location of the drop that will contain the future crystals. In the sitting drop it is located inside a well and around it has the reservoir, in the sandwich drop it is located between the plate closure and a thin glass plate perforated on one side to allow the evaporation of the drop and in the hanging drop the drop is attached to

the wall that closes the plate thanks to its surface tension. Over the course of these 3 years I have used the sitting drop technique.[179-180]

Once the crystal is obtained it must be brought in a place that is able to shoot a X-rays beam to obtain the reflected images useful for the resolution of the structure. These structures are called synchrotrons and keep the crystal at a temperature of 100 Kelvin; from this it can be deduced that it is often necessary to create solutions, called cryoprotectants, to ensure that the crystal when placed at this temperature does not freeze and, therefore, lose its main characteristics. Usually, the solution is identical to that where the crystal was formed but with a higher percentage of precipitant because these substances are often viscous (eg MPD, glycerol, PEG) and their increase is at the expense of the percentage of water. Unfortunately, it can happen that the cryoprotectant dissolves the crystal.[181]

X-ray diffraction involves aiming a beam of electromagnetic waves at a known wavelength at the resulting crystal. Due to the ordered nature of crystal lattices, electromagnetic radiation can only be observed in specific directions where positive interference occurs; this leads to a pattern of reflections. The optimal wavelengths are between 0.4 and 2.0 Å since they roughly correspond to the interatomic distances of molecular bonds.[179] To make these measurements, the crystal is placed on a goniometer that has a loop capable of trapping the droplet of cryoprotectant in which the crystal itself resides. This goniometer rotates 0.5-1 degrees depending on how frequently we want to obtain the images; in addition, we choose to make it rotate on itself for 2-3 angles turns in order to have a certain redundancy of data that will then be reflected in the parameter of "completeness".[180] A small mention should also be given to the X-ray source, and conventional sources such as sealed X-ray tubes and rotating anode tubes are based on the emission of white light from a metal target at the incidence of accelerated electrons (30-60 kV). The intensity of the light is determined by the acceleration of the electrons and the nature of the metal that makes up the target. More specifically, the higher the atomic number of the metal, the more intense the resulting white light. However, these sources have been superseded by more recent and advanced technologies such as the synchrotron; it is a charged particles accelerator composed of a circular ring (beam line) in which electrons and positrons are accelerated to speeds close to those of light and kept under control by magnetic and electric fields. To compare with traditional X-ray sources, the standard closed tube

produced a brilliance of $0.6*10^9$ photons/mm^2/s, while the synchrotron reaches a brilliance of $1.9*10^{12}$. This has also led to a decrease in the time of the experiment, passed from several hours to a few tens of minutes. This beam power, however, leads to a decay of the quality of the crystal very fast.

At this point we arrive at the time of phasing. The collected data set must be processed in order to obtain preliminary information about the crystal cell. To do this there are a series of equivalent programs that are able to give us the necessary information; in our case we have used XDS[182]. Subsequently to try to solve the structure, exploiting the information coming from XDS, there are various techniques. The one we used is the molecular replacement (MR) that is based on models and structures already present in the literature used as a starting point for understanding the crystal we developed[183]. The programs we use for MR are Molrep and Phaser.[183-185] Finally, there is the refinement phase where the goal is to match as much as possible the calculated model called Fc with the observed model called Fo; also, in this step there are many programs that are able to help us and we have used more Refmac. Putting in relation Fc with Fo you get two parameters, Rfactor and Rfree, which establish the validity of your model. The equation that calculates Rfactor and is the same; the difference is only in the number of images that they use. In fact, Rfactor takes into account the whole sample of images received by the synchrotron, while Rfree uses only a small set of images chosen by the operator. Rfree is more reliable because it takes surely valid images of the crystal unlike Rfactor that can include even worse images because, as explained above, the crystal is wasted during the rotation on the goniometer. These values are smaller the more resolution has been done in the correct way.[179-185]

Plate deposition

In this process I have collaborated closely with Professor Carla Bazzicalupi of the Department of Chemistry, University of Florence. The deposition of the plates began with the choice of derivatives. Since we did not have preliminary binding studies, we opted to select compounds that had slightly different characteristics to each other. Thus, the compounds selected for the first crystallographic tests were **B26, B27, B28, B29, B31,** and **B38.** The other choice we had to make was what type of G-Quadruplex we wanted to interact with, and we chose Tel23; that

is, a sequence of 23 nitrogenous bases that mimics the G4 that forms in the single-stranded sequence of the telomere. These sequences are of commercial origin and, of course, are not already folded in the desired form but are also found in strand form. There are some well known protocols that are used to fold the sequence in order to obtain the G4; this step is called annealing and consists in solubilizing the lyophilized DNA in a solution composed of 0.02M potassium cacodylate buffer (pH 6.5) and 0.05 M KCl, heat it up to 85-90°, keep this heat for 15min and then let it cool down to room temperature. This process allows for G4 structures at a known concentration of 3mM. The hybrids on the other hand are solubilized in a known amount of DMSO at a concentration of 20mM to try to use as little solvent as possible. With these 2 stock solutions it is possible to form our desired adduct with DNA at known concentrations. We prepared 2 stock solutions with tel23-hybrid at concentrations of 2mM and 1mM; verified by means of the Nanodrop instrument.

The next step was to create a screening of conditions in which our adducts could crystallize. The choice fell on a screening found in the literature[186] that presents 24 conditions in which G4 were formed (table 10). It was not purchased but we reproduced it manually excluding the condition 17.

Tube	Salt	Buffer	Precipitant
1	0.1 M KCl	0.05 M K Caco pH 6.5	20% v/v MPD
2	0.3 M KCl	0.05 M K Caco pH 6.5	10% v/v MPD
3	0.1 M KF, 0.025 $MgSO_4$	0.05 M K Caco pH 6.5	25% v/v MPD
4	0.2 M KI	0.05 M K Caco pH 6.5	25% v/v MPD
5	0.1 M KF, 0.02 M $(NH_4)_2SO_4$	0.05 M Na Caco pH 6.5	15% v/v MPD
6	0.3 M NaCl	0.05 M Na Caco pH 6.5	30% v/v MPD
7	0.1 M NaI	0.05 M Na Caco pH 6.5	35% v/v MPD
8	0.3 M KF, 0.02 M $MgSO_4$	0.05 M K Caco pH 6.5	35% v/v MPD
9	0.15 M NaF, 0.15 M KF	0.05 M Na Caco pH 6.5	40% v/v MPD
10	0.1 M KCl, 0.1 M $(NH_4)_2SO_4$	0.05 M K Caco pH 6.5	20% v/v MPD
11	0.1 M NaI, 0.1 M NaF, 0.1 M NaCl	0.05 M Na Caco pH 6.5	30% v/v MPD
12	0.2 M KCl, 0.05 M KI	0.05 M K Caco pH 6.5	25% v/v PEG400
13	0.1 M KCl, 0.05 M $MgCl_2$	0.05 M K Caco pH 6.5	10% v/v PEG400
14	0.1 M Li_2SO_4	0.05 M K Caco pH 6.5	20% v/v PEG400
15	0.3 M KI	0.05 M K Caco pH 6.5	15% v/v PEG400
16	0.3 M NaI	0.05 M Na Caco pH 6.5	15% v/v PEG400
17	0.1 M KCl, 0.03 M $CaCl_2$	0.05 M K Caco pH 6.5	1.3 M ammonium sulphate
18	0.2 M KCl, 0.05 M Li_2SO_4	0.05 M K Caco pH 6.5	1.8 M ammonium sulphate
19	0.05 M Li_2SO_4, 0.05 M $MgSO_4$	0.05 M K Caco pH 6.5	20% v/v *iso*-propanol
20	0.2 M NaCl	0.05 M Na Caco pH 6.5	20% JEFF 2000
21	0.2 M NaCl, 0.1 M NaF	0.05 M Na Caco pH 6.5	10% JEFF 2000
22	0.05 M KI, 0.05 M $MgCl_2$	0.05 M K Caco pH 6.5	15% JEFF 2000
23	0.1 M NaCl, 0.05 M $MgCl_2$	0.05 M Na Caco pH 6.5	1 M ammonium sulphate
24	0.05 M Li_2SO_4	0.05 M Na Caco pH 6.5	1 M ammonium sulphate

Table 10. Screening condition from **Methods 2007.**

Using the sitting drop vapor diffusion technique, we deposited, in each individual plate (Greiner®96-well plates), the adduct at the two concentrations that became in the drop 1mM and 0.5mM, respectively. This is because the drop is formed by 1µL of adduct plus 1µL of condition; the reservoir is formed by 100 µL of condition. After a few weeks, the formation of numerous crystals, belonging to the **B26**-Tel23 and **B31**-Tel23 adduct, was observed. However, they led to a number of data collections, which gave rise to possible cells but upon reaching refinement we were unable to resolve the structure. Possible reasons for the failure can be attributed to the poor quality of the crystals, the small size of the crystal, or, of course, the inherent difficulties of resolving a DNA-derived structure. The classic strategy is to prepare a new condition screening starting from the wells in which the crystals had formed. In the case of **B26**, crystals had formed from conditions 1 and 3 in Table 10. While in the case of **B31**, crystals had formed in the wells with conditions 2 and 10 of Table 10. Through a program using the experimental design, the following optimizations were designed and targeted for each individual adduct.

Table 11. Optimization for **B26** from the original condition 1 and 3.

Condition N.	K^+ Salt	M^{2+}	Buffer	MPD %
1	0,1M KF	0,05 M MgSO4	0,05 M K Cacodyate	20
2	0,1M KF	0,05 M MgSO4	0,05 M K Cacodyate	25
3	0,1M KF	0,05 M MgSO4	0,05 M K Cacodyate	30
4	0,1M KCl	0,05 M MgSO4	0,05 M K Cacodyate	20
5	0,1M KCl	0,05 M MgSO4	0,05 M K Cacodyate	25
6	0,1M KCl	0,05 M MgSO4	0,05 M K Cacodyate	30
7	0,1M KCl	0,025 M MgSO4	0,05 M K Cacodyate	20
8	0,1M KCl	0,025 M MgSO4	0,05 M K Cacodyate	25
9	0,1M KCl	0,025 M MgSO4	0,05 M K Cacodyate	30
10	0,1M KF	0.05 M CaCl2	0,05 M K Cacodyate	20
11	0,1M KF	0.05 M CaCl2	0,05 M K Cacodyate	25
12	0,1M KF	0.05 M CaCl2	0,05 M K Cacodyate	30
13	0,1M KF	0,05 M SrCl2	0,05 M K Cacodyate	20
14	0,1M KF	0,05 M SrCl2	0,05 M K Cacodyate	25
15	0,1M KF	0,05 M SrCl2	0,05 M K Cacodyate	30
16	0,1M KCl	0.05 M CaCl2	0,05 M K Cacodyate	20
17	0,1M KCl	0.05 M CaCl2	0,05 M K Cacodyate	25
18	0,1M KCl	0.05 M CaCl2	0,05 M K Cacodyate	30
19	0,1M KCl	0,05 M SrCl2	0,05 M K Cacodyate	20

20	0,1M KCl	0,05 M SrCl2	0,05 M K Cacodyate	25
21	0,1M KCl	0,05 M SrCl2	0,05 M K Cacodyate	30
22	0,1M KCl	0,025 M CaCl2	0,05 M K Cacodyate	20
23	0,1M KCl	0,025 M CaCl2	0,05 M K Cacodyate	25
24	0,1M KCl	0,025 M CaCl2	0,05 M K Cacodyate	30
25	0,1M KCl	0,025 M SrCl2	0,05 M K Cacodyate	20
26	0,1M KCl	0,025 M SrCl2	0,05 M K Cacodyate	25
27	0,1M KCl	0,025 M SrCl2	0,05 M K Cacodyate	30

Table 12. Optimization for **B31** from the original condition 2 and 10.

Condition N.	K^+ Salt	M^{2+}	Buffer	MPD %
1	0,3 M KCl	0,1 M (NH3)2SO4	0,05 M K Cacodyate	10
2	0,3 M KCl	0,1 M (NH3)2SO4	0,05 M K Cacodyate	15
3	0,3 M KCl	0,1 M (NH3)2SO4	0,05 M K Cacodyate	20
4	0,2 M KCl	0,1 M (NH3)2SO4	0,05 M K Cacodyate	10
5	0,2 M KCl	0,1 M (NH3)2SO4	0,05 M K Cacodyate	15
6	0,2 M KCl	0,1 M (NH3)2SO4	0,05 M K Cacodyate	20

After a few weeks, new crystals had formed but in this second collection none of them diffracted. Nevertheless, in this expedition to the Elettra synchrotron in Trieste, there was also a crystal that had formed later from the first plates deposited with the original condition. The adduct **B28**-Tel23 had formed crystals with the original condition 2; the cryoprotectant had been decided by increasing the MPD to 30 (from 10% of the condition) so that the solution of the condition would not freeze. From it we were able to arrive at the resolution of the structure.

The data are as follows: the crystal was collected at a wavelength of 1 Å at a maximum resolution of 1.6 Å. The condition 2 from which it came contains 0.3M KCl, 0.05M K Caco as buffer and 10% v/v MPD as precipitant. Its cryoprotectant is identical to the original but with 30% v/v MPD. By analyzing the data within the XDS program package we were able to obtain the cell parameters; the crystal is part of space group C2 which is of monoclinic type with sides all different from each other and angles alpha=gamma=90° and beta different from 90°.

Table 13. Initial cell parameters.

Cell parameters	A(Å)	B(Å)	C(Å)	α (deg)	β(deg)	γ(deg)
	36.82	**72.72**	**27.03**	**90°**	**90.14°**	**90°**

Obtained these parameters we have used the programs of molecular replacement, Molrep and Phaser, and taking as a basic model the PDB code 6H5R we have reached a model on which we can start the refinements. Finally, we drew our **B28** ligand andtried to place it between 2 quadruplex structures where a significant electronic density was present. (Figure 41).

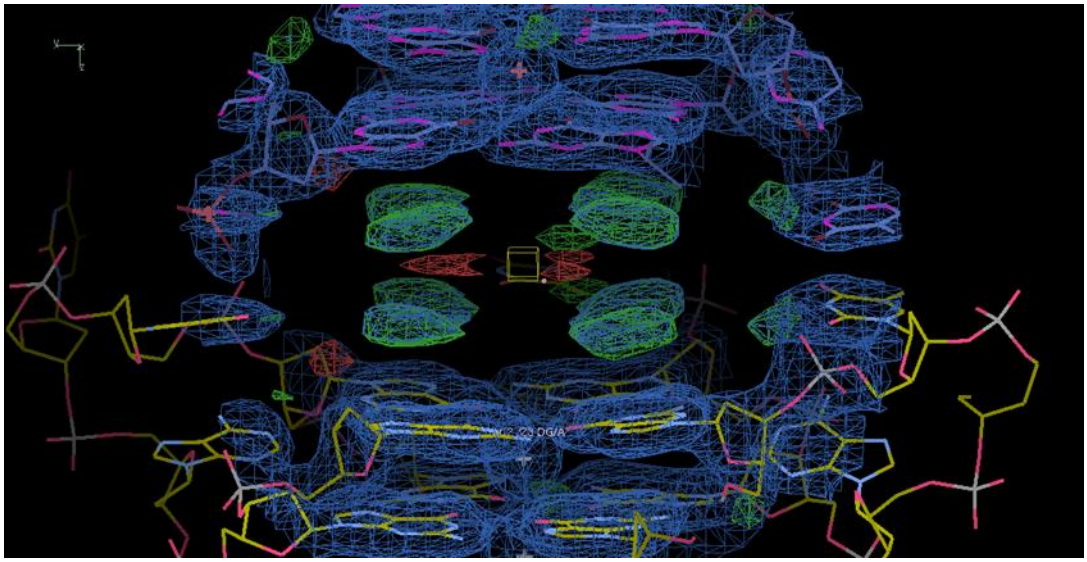

Figure 41. electron density map of B28 between 2 tetrads.

The hardest challenge was to understand the orientation of the ligand and after 49 cycles of refinement we came to the conclusion that it can be arranged in 2 different positions that we put at occupational factor 0.5 to explain that it is 50% of the time in one position and 50% in the other. The result of all our calculations is the OMIT map, shown here.

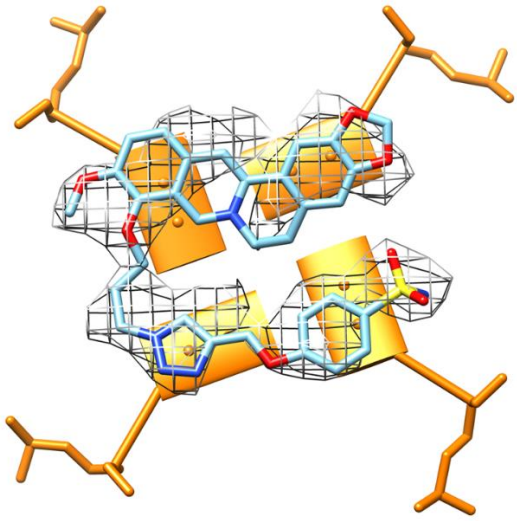

Figure 42. OMIT map of **B28.**

The entire structure with its final data is shown below. It has been deposited in the PDB with code 7PNL. (Figure 43)

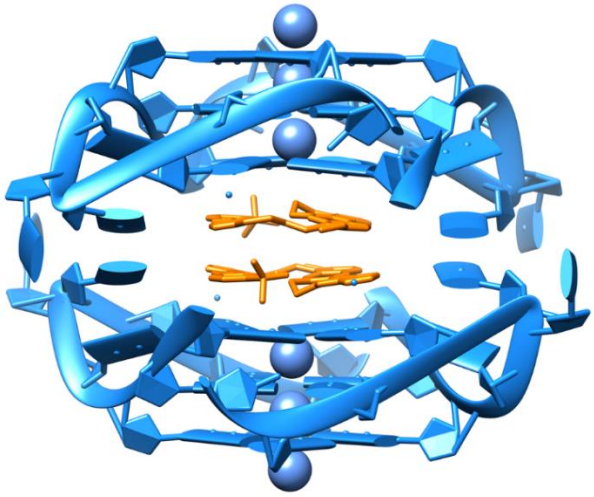

Data Collection	
Wavelength (Å)	1.000
Space group	C2
Cell dimension (Å/deg)	36.84 72.72 27.03 / 90 90.1 90
Limiting resolution (Å)	1.83
Unique reflections	5913
R_{merge}(%)	3.7
Multiplicity	2,93
Completeness overall (%)	99,24
<I/σ(I)>	13.7
Refinement	
Resolution range (Å)	36.36-1.83
Unique reflections, working/free	5913 / 336
Rfactor (%)	21.25
Rfree(%)	32.86
r.m.s.d. bonds(Å)	0,01
r.m.s.d. angles (°)	2,1

Figure 43. All structure with its final parameter.

Subsequently, binding data of our compounds to various types of quadruplexes arrived and as shown above C-kit seems to be the one most stabilized by our compounds. For this reason, we decided to test crystallizations with the best stabilizers of C-kit which are **B25, B29, B35,** and **B40**. The compounds are divided equally, 2 benzensulfonamide scaffold and two coumarin scaffold. To increase the number of chances of obtaining crystals of these adducts, we decided to use a commercial screening MD1-68 Helix from Molecular Dimension and we deposited them at 2 concentrations: 2mM and 1mM. Unfortunately, several weeks after deposition the plate wells were either clear or loaded with precipitate, showing a substantial inability to reach the supersaturation threshold to form the first nuclei. So, it was decided to try to use the screening that had led to the achievement of the resolved structure: the screening of Parkinson[186], also in this case we have laid the adducts at 2 concentrations. After a few weeks, some wells showed the presence of crystals. This information is particularly recent; therefore, we only have photos of the crystals, which have not yet been brought to the synchrotron. To date, we can say that we have been able to obtain crystals from both Tel23 and C-kit; but for the latter we do not yet have diffraction data.

3.4. Multitarget approach applied to hCA activators as hybrids with cholinesterase inhibitors: a new type of precognitive agents (Series C).

Dementia is mainly caused by Alzheimer's disease, which is a neurodegenerative disease; it is estimated that around 40 million people worldwide suffer from it, most of them over 60 years old, and as the world population grows and ages, the number of affected patients will increase. In fact, this figure is expected to double every 20 years, at least until 2050. However, despite decades of research, at present there are still no drugs that can offer a decisive cure or slow down the progression of the disease.[187-189] Dementia is characterized by a decline in memory, language, problem-solving skills, and other cognitive abilities that affect a person's ability to perform activities of daily living. It is a decline that occurs due to damage and destruction of nerve cells (neurons) in parts of the brain involved in cognitive function.[190]

The hippocampus is an essential area for the consolidation of short- and long-term memory information. Destruction of the hippocampal formation makes it impossible to store new memories. Thus, while the symptoms of Alzheimer's disease vary from individual to individual, in the early phase the most common symptom is a progressive deterioration in the ability to remember new information, often mistakenly associated with normal aging and only belatedly recognized as an early symptom of the disease.[191]

The following are the most common symptoms of Alzheimer's:
- Memory loss that disrupts daily life.
- Difficulty planning or solving problems.
- Difficulty completing familiar tasks at home, work or in leisure time.
- Confusion with time or place.
- Difficulty understanding visual imagery and spatial relationships.
- Problems with writing.
- Decreased or poor judgment.
- Changes in mood and personality, including apathy and depression.
- Increased anxiety, agitation, and sleep disturbances.

The pathophysiology is very complex however at the microscopic level there are some phenomena that occur constantly, and they are:

- Cortical amyloidogenesis, leading to extracellular deposits of toxic amyloid, mainly Aβ42, at the level of the extracellular and cerebrovascular parenchyma.
- Intraneuronal accumulation of neurofibrillary tangles (NFTs), which result from hyperphosphorylation of the tau protein.[192]

This pathogenic accumulation of proteins seems to be the cause, or at least the main factor leading to cognitive impairment and subsequently to neuronal dysfunction with death in essential areas, such as hippocampus and amygdala.

Recently it has been suggested that it may be more functional loss than neuronal cell loss that leads to cognitive impairment. The loss of synapses and dendritic spines itself correlates better with cognitive impairment than the simple loss of neurons.[193]

Amyloid hypothesis

Senile plaques consist of insoluble deposits of amyloid β-peptide (Aβ), among other components; its very pathogenic character has given rise to the "amyloid hypothesis" in which the formation and deposition of small Aβ peptides is believed to form long insoluble amyloid fibrils, which accumulate in senile plaques in critical regions of the brain, leading to the onset and progression of the disease.[193-194]

According to the amyloid cascade theory, brain accumulation of Aβ peptide, resulting from the imbalance between the production and clearance of this protein, is the main event causing the disease. The Aβ peptide, which has 36 to 43 amino acids, is derived from enzymatic proteolysis of the amyloid precursor protein (APP, consisting of 770 AA), a protein that plays an important role in brain homeostasis. The APP gene is located on chromosome 21, which explains the higher incidence of early-onset AD in individuals with trisomy 21 (Down syndrome). APP processing is divided into two pathways, one mediated by the nonamyloidogenic α-secretase and a mediated by amyloidogenic β- and γ-secretase.[195]

Cleavage of APP by α-secretase produces a soluble molecule, sAPPα, which has a likely neuroprotective function, playing an important role in neuronal plasticity and survival and protection against excitotoxicity.[195]

Peptide Aβ is produced by cleavage of APP by a β-secretase (mainly the enzyme BACE1), provides a soluble fragment of APP (sAPPβ, a mediator related to neuronal death) and a carboxy-terminal complex attached to the cell membrane. The latter is cleaved by a γ-secretase

complex composed of 4 proteins: presenilin 1 or 2, nicastrin, APH-1, and PEN-2 (presenilin enhancer-2), to give rise to Peptide Aβ.

Aβ peptides ranging in size from 38 to 43 amino acids are generated with predominance in the 40 amino acid form (Aβ 40), followed by 42 (Aβ 42) which accounts for 5-10%, and is considered more aggregating than Aβ40. Aβ42 thus represents the basis for the formation of larger oligomers and fibrils and ultimately for macroscopic amyloid plaques.[196-197]

Under physiological conditions, amyloidogenic and nonamyloidogenic pathways coexist in equilibrium, the latter preferentially favoured. High levels of Aβ can lead to the formation of aggregates (dimers, trimers, tetramers), either as cerebral amyloid angiopathy as in the case of Aβ1-42 that accumulates in brain vessels; or as senile plaques (SP) in the case of Aβ1-40, which will be deposited later in the disease process. [196-197]

AD is also characterized by the presence of NFTs, which are tangles resulting from hyperphosphorylation of the microtubule-associated protein τ. NFTs are helically coiled protein filament fragments in the cell cytoplasm of neurons. The τ protein has a binding domain for microtubules and co-assembles with tubulin to form mature and stable microtubules; interconnected bridges are formed between contiguous microtubules for greater stability. When the τ protein comes into contact with released kinases, due to the abundance of the Aβ peptide in the environment, hyperphosphorylation occurs, leading to its oligomerization. The tubule becomes unstable, due to dissociation of the tubular subunits, which flake off, and go on to form large pieces of τ filaments, which further aggregate into NFTs, fibrillar and highly insoluble, capable of leading initially to a loss of normal communication between neurons and eventually to apoptosis. Despite the presence of neurofibrillary foci in AD, no cases of AD secondary to mutations in the tau gene on chromosome 174 have been reported, although frontotemporal dementia with parkinsonism has been found in some families with that mutation.[198]

Cholinergic hypothesis

In addition to the amyloid theory, the other 2 theories to explain the onset of dementia and Alzheimer's are the dopaminergic theory, which we will not discuss in this thesis, and the cholinergic theory, which will be explained in this chapter.

In AD, there is a functional impairment of cholinergic neurons in the basal forebrain related to structural lesions in the same areas or regions that project to or from those areas. The

consequences are low levels of acetylcholine (ACh) and a loss of cholinergic transmission, resulting in learning and memory dysfunction. These related events have led to the so-called "cholinergic hypothesis," which is firmly supported by the fact that almost all drugs approved for the treatment of AD exploit as a target the acetylcholinesterase (AChE) that catalyzes the hydrolysis of ACh into acetate and choline.[199]

It appears that AChE is also implicated in the pathogenesis of AD through an influence on Aβ deposition; acting as a molecular chaperone, it accelerates the formation and increases the neurotoxicity of amyloid fibrils and stable complexes.

It has also been shown that APP processing is regulated by the cholinergic system, which in turn can be modulated by Aβ. This modulation appears to be age-dependent, as older neurons appear to be more sensitive to Aβ-mediated inhibition. However, the degenerative cholinergic loss is unknown whether it is primary or secondary to amyloid plaque pathology. The influence of neuroreceptors in AD has been intensively studied. Both muscarinic and nicotinic receptors are altered in patients with AD, and the early stages of the disease show a clear decrease in ACh and nicotinic receptor levels.

APP processing may also be affected by other factors, endogenous and exogenous, such as serotonin, glutamate, estrogen, testosterone, bradykinin, insulin, calmodulin, growth factors, copper, statins, and some plant extracts.[199]

Acetylcholinesterase (AChE) is the enzyme responsible for the degradation of ACh in the synaptic cleft of the neuromuscular junction, central nervous system (CNS) cholinergic synapses, and autonomic ganglia. The main biological role of acetylcholinesterase (AChE) is the disruption of impulse transmission at cholinergic synapses by rapid hydrolysis of the neurotransmitter acetylcholine (ACh).[200]

Consistent with this requirement, AChE possesses a remarkably high specific activity, operating at a rate approaching that of a diffusion-controlled reaction; it is one of the most efficient enzymes known. AChE is first acetylated by ACh, with concomitant release of choline. Then, a water molecule regenerates the free enzyme, with release of acetic acid. Because of its prominent role in the nervous system, AChE is the target of a variety of potent natural and synthetic compounds, ranging from synthetic organophosphorus nerve agents (OPs) and insecticides whose potent acute toxicity is primarily due to the fact that they are irreversible inhibitors, to the first generation of anti-Alzheimer's drugs.[200-201]

CA in CNS

CA II is expressed in the choroid plexus, oligodendrocytes, myelinated tracts, astrocytes and myelin sheaths in the vertebrates' brain.[202-203] CA III was shown to be present in the rat and human choroid plexus.[202] The membrane-associated CA IV has been identified on the luminal surface of cerebral capillaries, and associated with the blood-brain barrier, being also concentrated in layers III and VI in the cortex, hippocampus and thalamus [174,175]. Immunocytochemical studies demonstrated that astrocytes and in neurons express the mitochondrial CA VA.[202-203] The expression of CA VII and VIII are almost superimposable and are quite high in the cortex, hippocampus and thalamus. [202] Of note, CA VII is predominantly expressed in the brain and thus it is considered a brain-associated CA isoform being almost absent in most other tissues. [1-202] CA X is expressed in the myelin sheath, while CA XI is present in the neural cell body and astrocytes of few regions of the brain [170]. CA IX is overexpressed in many neurologic cancers such as glioma, ependymoma, hemangioblastoma, meningioma and choroid plexus tumors. [36] Likewise, brain tumors express CA XII [36-202], which is however also present in normal tissues and in the choroid plexus.[203] CA XIV is expressed in nuclei and nerve tracts associated with pontine, medullary and hippocampal functions. [203]

The cerebrospinal fluid (CSF) is produced by the epithelial cells of the choroid plexus by a process implicating the transport of Na^+, Cl^- and HCO_3^- from blood to the brain ventricles.[204] As a result of the formed osmotic gradient water is secreted into the CSF. Several transporters of HCO3- have a role in this process (anion exchangers (AEs) 1-3, Cl^-/HCO_3^- exchangers, Na^+/HCO_3^- cotransporters). A rather high amount of at least CA II, CA III and CA XII is present in the choroid plexus cells.[204]

The peripheral nervous system was also shown to possess a CA activity, whose distribution was assessed histochemically in rat cross-sections of peripheral nerves.[205] This survey indicated that high CA activity is found predominantly in large-calibre proprioceptive afferents showing that CAs have important roles are functionally related subpopulations of nerve fibers.[205] It has not been proven yet which CA isoforms are present in the peripheral nervous system.

Therapeutic use of CAA

In the introductory chapter the activators of carbonic anhydrase have already been explained as well as their mechanism of action. In order not to repeat ourselves we will talk about one of the possible therapeutic applications that they have. An interesting field of application for CAA is

related to the treatment of cognitive deficits, including dementia, including Alzheimer's disease. This application would result from the pharmacological enhancement of synaptic efficiency, spatial learning and memory; effects that from current experimental evidence seem to be achievable precisely by means of CAA.

CA1 pyramidal cells, present at the hippocampal level, on which spatial memory is based, receive three main inputs:

1. GABA-ergic interneurons
2. CA3 pyramidal cells (glutamatergic fibers)
3. Cholinergic neurons originating from the medial septum.

Activation of the same cholinergic neurons associated with that of GABA-ergic interneurons transforms the GABA-mediated inhibition of CA1 pyramidal neurons in the hippocampus into a depolarizing response, and this has been shown to be particularly so in the presence of CAA. This is due to the fact that the activation of CA determines an increase in intracellular levels of bicarbonate and consequently an increase in the efflux of the same, through the receptors channel of GABA, causing a sort of sympathetic switch. If in fact normally the effect of inhibition mediated by GABA is due to an increase in the conductance to Cl- through the receptor channel itself, with the increase in the intracellular concentration of bicarbonate, it follows an efflux, thus determining a depolarizing effect and no longer hyperpolarizing.[206-208] This excitatory response appears to persist for several hours resulting in sensitivity to CA or GABA receptor inhibition alone. If before synaptic transformation following CA activation, glutamatergic and cholinergic excitatory signals are as if filtered out by GABA-mediated inhibition, after synaptic switch there is instead a major amplification of the depolarizing signal; even small glutamatergic inputs that by themselves would be too weak to general an excitatory signal are amplified under such conditions to the point of resulting in an EPSP signal. [207]

CA activators facilitate the synaptic switch between excitatory/inhibitory effects mediated by the GABA receptor, therefore GABA-mediated responses on CA1 pyramidal neurons become excitatory, allowing signal enhancement, across the neuronal network involved in memory processes, in particular a subset of pyramidal neurons are activated, which appear to enhance associative memories. It has been observed through in vivo experiments (on rats) a significant increase in learning abilities following the administration of CAA; in particular it has been

shown the improved ability of these rats to learn tasks within an aquatic maze and remember the structure of the path itself. [206]

Carbonic anhydrase given its fundamental role in encoding and storing information possesses some signaling pathways that control its activity. Activation of ryanodine (RY) receptors in CA1 pyramidal cells, which is responsible for increased intracellular Ca^{2+} release, also appears to be involved in synaptic switching, mediated by GABA. In fact, the effect of increased intracellular Ca^{2+} concentration would seem to have an indirect effect on CA; in fact, some studies have shown that Ca^{2+} potentiates the activation of purified CA or gastric mucosal CA enzymes.

Experimentally it has been observed, more recently, that the administration of CAA (D-Phe) is also able to activate the extracellular kinase-regulated signaling cascade (ERK), which is involved in memory formation processes, both at the cortical and hippocampal levels, two brain areas crucial in memory processes. This effect is in turn antagonized by the simultaneous administration of a sulfonamide-type inhibitor (e.g., acetazolamide), but not by the administration of a CAI not able to pass the blood-brain barrier. The ERK pathway is a central cellular signaling pathway that links the numerous extracellular signals to membrane receptors, cascading down to transcription factors, ultimately controlling gene regulation; thus, representing a key step in both learning new stimuli and consolidating and persisting various types of long-term memory. However, the CA isoforms involved as well as the mechanism by which CA modulation induces an increase in ERK phosphorylation are still unknown. Some degree of fear memory impairment could also be observed in rats, which could also lead to a possible therapeutic application for the treatment of post traumatic stress disorder (PTSD) and various forms of phobia.[145-146]

Drug design

AD, which we have explained to be the first factor leading to dementia in humans, is an extremely complex disease. An innumerable series of factors are implicated in it, in fact, to date, an effective therapy has not yet been found either to prevent it or to significantly reduce the symptoms. Our strategy is to create a dual drug that can act on multiple fronts; an idea that is becoming increasingly popular in modern pharmaceutical chemistry. Especially with diseases like this one that involve a wide variety of factors and often occur in older patients already using substantial amounts of medication. In support of this theory there is an article from

August 2019;[146] which shows all the possible combinations of targets on which to go to act in the symptomatology of Alzehimer's disease.

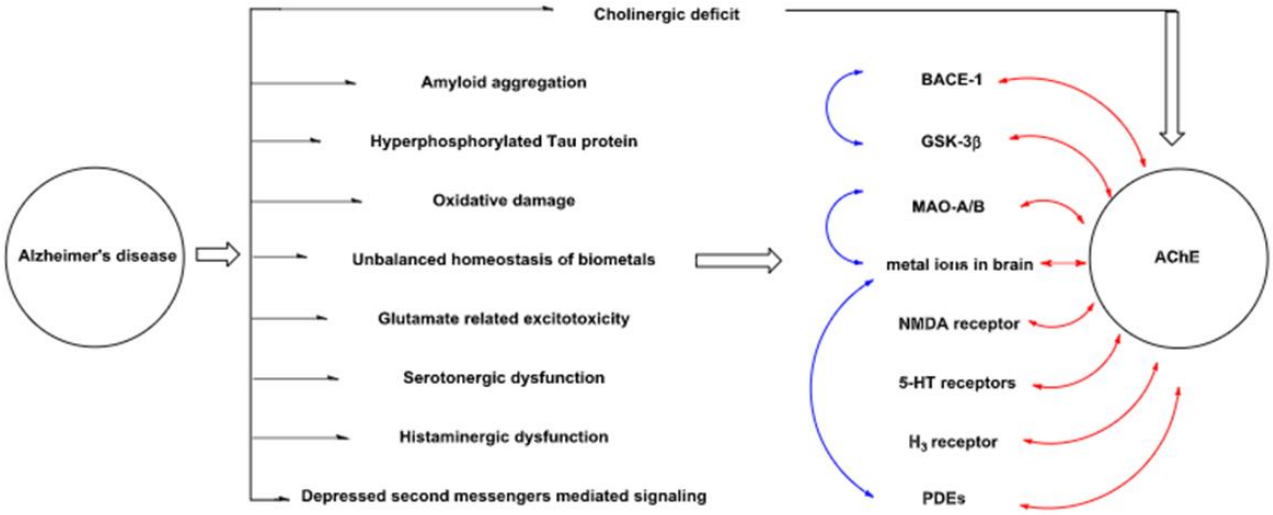

Figure 44. Possible multitarget approach for AD.

Also, in our project is used the multi target approach but acting on two different targets from those proposed. The first is the acetylcholinesterase, useful to fill the cholinergic deficit present in various forms of dementia. To inhibit this type of enzyme we have chosen as pharmacological lead the tacrinic scaffold. Tacrine is the first drug approved in the therapy of AD in 1993, later removed from the market due to its hepatotoxicity. However, it has been shown in several articles that functionalization at various positions of the scaffold reduces this toxicity.[209] The second portion is a new idea between the other proposed. We decided to interact with the Carbonic Anhydrases, because the activators improve memory process and prevent cognitions deficit. To interact with these seconds enzymes, we include in the scaffold various AA as Phe, Trp, Lys, His and one biogenic amine as Histamine; all demonstrated compounds activator of CA. To connect both moiety we use two kinds of linker; the amide one exploiting the carboxyl group af AA and the amine bridge, more valid to maintain the acid-base properties useful in CA activation.

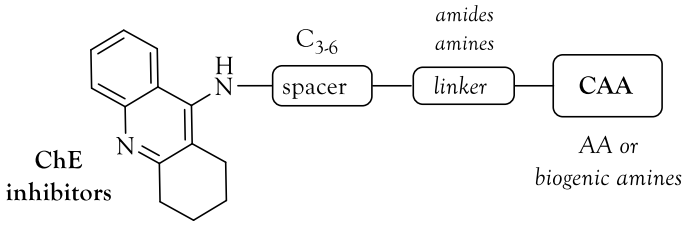

Figure 45. Drug design of all hybrids.

Synthesis

First series

Series 1 compounds were obtained by coupling reaction between aminoalkyl tacrines **C3-C5** and protected L-amino acids on amine function **C6-C9**. The intermediate 9-chloro-1,2,3,4-tetrahydroacridine **C2** was synthesized by condensation between anthranilic acid **C1** and cyclohexanone, in the presence of POCl3 at 115°C (Scheme 13) and subsequently treated with the appropriate 1-ω-diaminoalkane (1-3 diaminepropane, 1-4diaminebutane and 1-5 diaminepentane) in a sealed tube at 180°C in the presence of KI using phenol as solvent to give the aminoalkyl tacrines **C3-C5**.

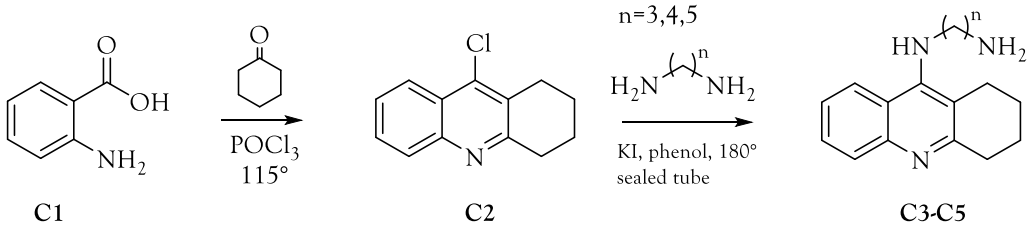

Scheme 13. Synthesis of amminotacrines **C3-C5.**

The L-amino acids **D-G** were protected with Boc on the amine function by reaction with di-tert-butyl dicarbonate in basic medium to give intermediates **C6-C9** (Scheme 14); specifically, TEA in methanol was used for the synthesis of the N-protected derivatives of L-Tryptophan and L-Histidine, while K2CO3 in 1,4-dioxane was used for the protected derivative of the amino acid L-Lysine bearing an N-ε-Cbz (carbobenzyloxy) protection. The amino acid bearing a different protection (Cbz) on the distal amine function than the carboxyl was chosen to assess any change in affinity to the target of the protected molecular hybrid. The amino acid L-Histidine was treated with twice as many reagent equivalents in order to obtain double protection, including on the NH of the imidazole core. For N-Boc-L-phenylalanine the commercial derivative was used.

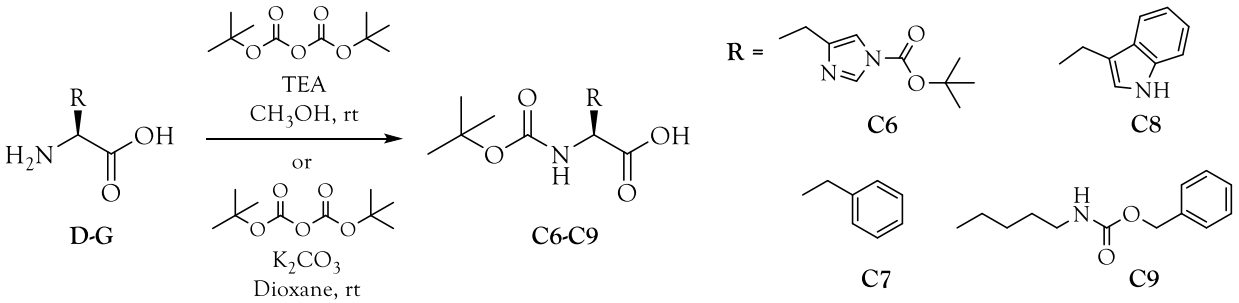

Scheme 14. Synthesis of protected L-AA **C6-C9.**

The amide coupling reactions between amines **C3-C5** and carboxylic acids **C6-C9** to obtain amides **C10-C22** were carried out using PyBOP as coupling agent in the presence of DIPEA and anhydrous DMF as solvent at room temperature for 24-48h (Scheme 15). Unexpectedly, an N-deprotection occurred totally in the reaction between intermediates **C4** and **C6**, and partially between intermediates **C5** and **C6**, losing the Boc group on the N-imidazole (derivatives **C11** and **C13**). Hybrid derivatives **C10-C22** were purified by chromatographic column using increasing gradients of MeOH in DCM as eluent.

The N-Boc **C10-C22** hybrids were subjected to a deprotection reaction using HCl 5M in MeOH to give the free chlorinated amines **C23-C31**. Unfortunately, this reaction applied to the **C10-C13** molecules damaged the structural integrity preventing the corresponding deprotected derivatives from being obtained.

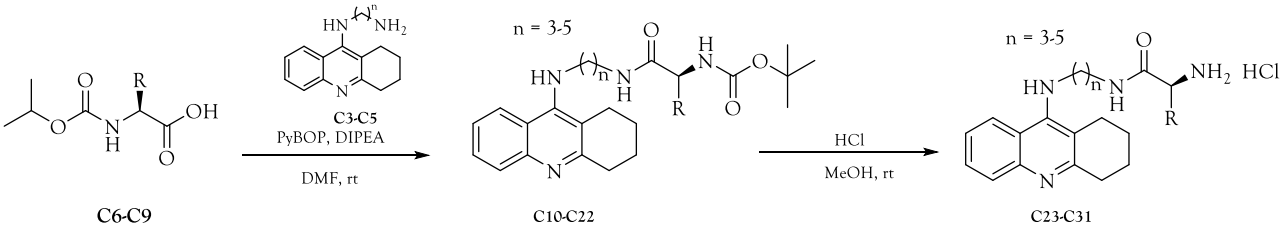

R / n	N-Boc	NH		NH	Cbz
3	C10	-	C14	C17	C20
4	-	C11	C15	C18	C21
5	C12	C13	C16	C19	C22

R / n		NH	Cbz
3	C23	C26	C29
4	C24	C27	C30
5	C25	C28	C31

Scheme 15. Synthesis of protected hybrids **C10-C22** and unprotected hybrids **C23-C31**.

Second series

Series 2 compounds were obtained by nucleophilic substitution reaction between bromoalkyl tacrins **C34** and **C36** and L-amino acids protected on carboxyl function **C37-C40**. Tacrine or 9-amino-1,2,3,4-tetrahydroacridine **C33** was obtained by condensation of 2-aminobenzonitrile **C32** with cyclohexanone in the presence of $AlCl_3$ at a temperature of 110°C for 24 hours. The nucleophilic substitution reactions of **C33** with the appropriate 1-ω-bromoalkanes were approached by different synthetic procedures. The use of KOH as a base and acetonitrile as a solvent gave poor or no product yields. In contrast, the use of NaH as a base and anhydrous DMF as a solvent produced derivative **C34** in good yields. Therefore, the realization of the bromoalkyl derivative **C36** with 6 carbon atoms in the spacer was chosen. It was synthesized using a different method than the 5-carbon-atom analog **C34**. Intermediate **C2** was treated 6-aminohexanol, in the presence of phenol and KI, at 180°C for 3h to obtain intermediate **C35**. Through an Appel reaction, alcohol **C35** was converted to the bromine derivative **C36** using CBr4 and PPh3 in anhydrous DCM (Scheme 16).

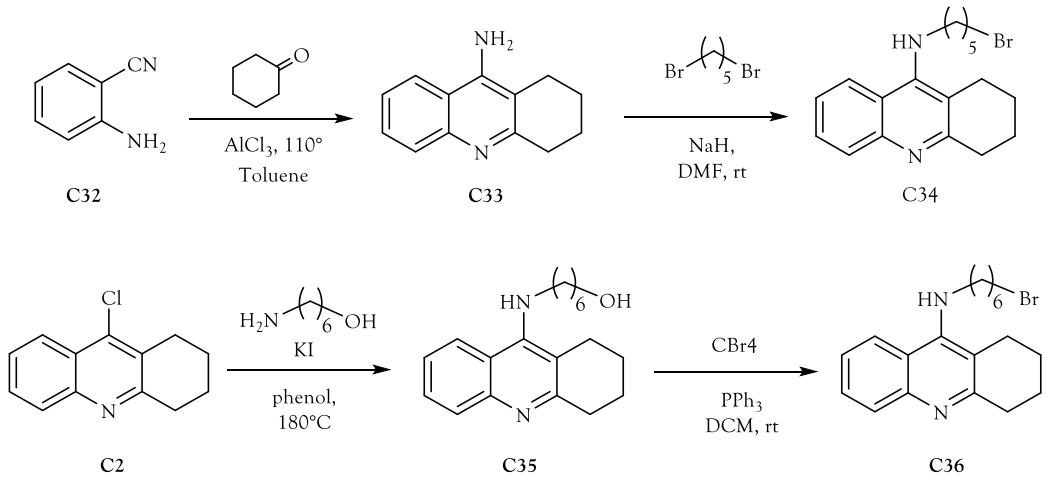

Scheme 16. Synthesis of bromotacrines **C34** and **C36.**

The L-amino acids **D-G** were protected on the carboxyl function by methyl esterification using SOCl2 in anhydrous methanol to give the **C37-C40** esters (Scheme 17). Again, the amino acid L-lysine bearing a Cbz protection on the amine function distal to the carboxyl was chosen. For compounds **C37** and **C40**, the commercial derivative was used.

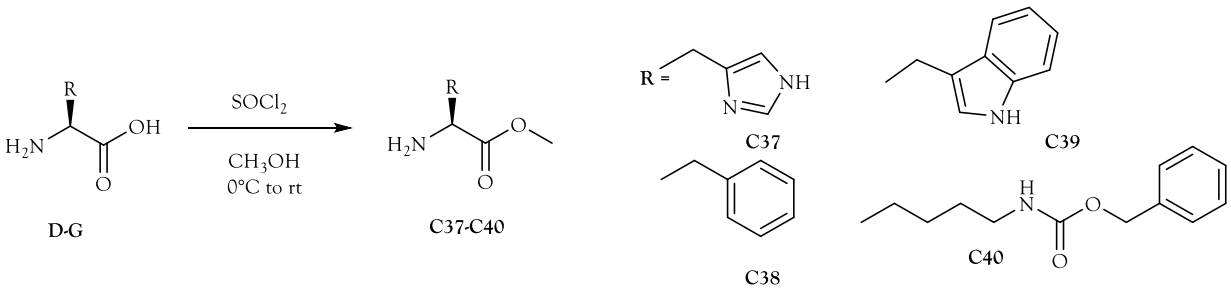

Scheme 17. Synthesis of esterified AA **C37-C40.**

The amines **C37-C40** were then treated with the bromine derivatives **C34** and **C36** under SN conditions using different reaction conditions, which, however, resulted in poor yields. The use of 18-Crown-6, K2CO3 in anhydrous acetonitrile or K2CO3, NaI in anhydrous acetonitrile gave poor reaction yields. In contrast, it was possible to obtain the **C41-C48** amine linker hybrids in excellent yields using K2CO3 and KI in anhydrous DMF. The **C41-C48** hybrid derivatives were purified by chromatographic column using increasing gradients of MeOH in DCM as eluent. Alkaline hydrolysis of the ester functions of derivatives **C41-C48** were attempted by two methods: 1) LiOH in a mixture of MeOH and THF at -20°C and 2) NaOH in MeOH. For the time being, the hydrolysis product was obtained only for derivative **C42** to give **C49**, whereas, for the other molecules the reactions were either unsuccessful or have not yet been attempted (Scheme 18).

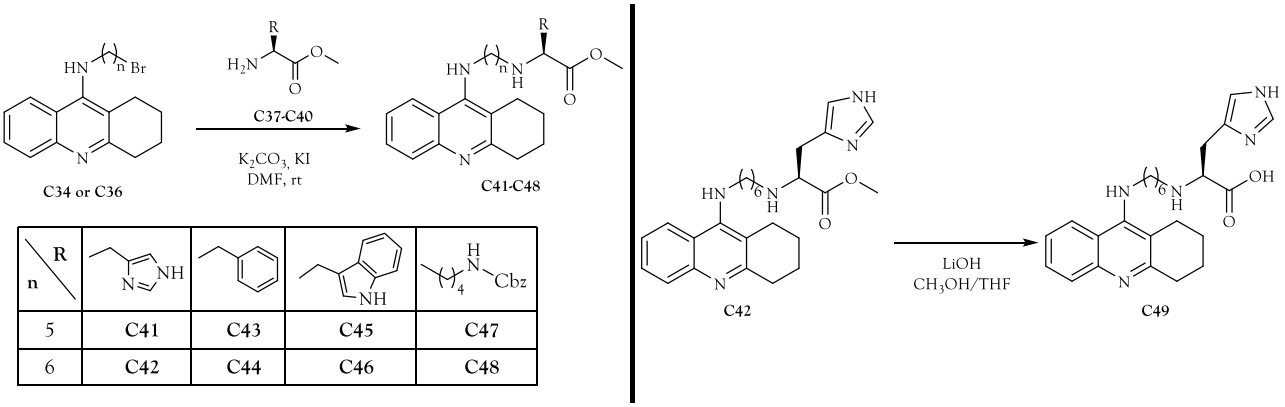

R / n	NH		NH	Cbz
5	C41	C43	C45	C47
6	C42	C44	C46	C48

Scheme 18. Synthesis of hybrids derivatives **C41-C49.**

Molecular hybrid **C50** was obtained from intermediate **C36** and histamine **H** by adopting similar SN conditions and salifying the product to hydrochloride with 1.25M HCl in MeOH (Scheme 19).

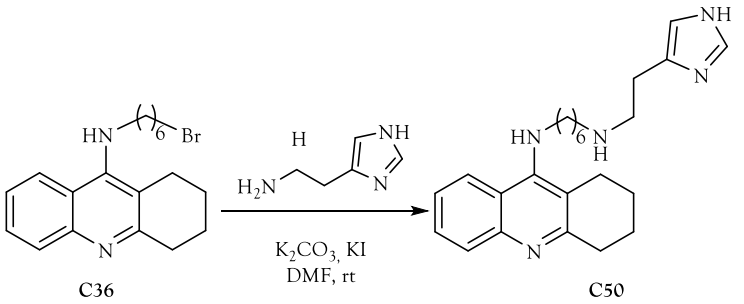

Scheme 19. Synthesis of hybrid derivative **C50.**

Biological assay and results

All final compounds were assayed in vitro by me using Stopped-Flow technique for their ability to activate a panel of CA present in brain. In details, I tested all compound against CA I, II, IV, Vb and VII. The found activation profiles are shown in Table 14 as activation constants (K_A).

Table 14. Activation profile of derivatives **C10-C31, C41-C50**, and tacrine **C32** toward hCAs I, II, IV, VB, and VII.

Cmpd	K_A (μM)[a]				
	CA I	CA II	CA IV	CA VB	CA VII
C10	NA	15.9	NA	NA	NA
C11	0.93	0.80	0.51	0.90	0.90
C12	NA	11.0	NA	9.05	NA
C13	1.01	0.97	0.69	0.93	0.91
C14	NA	NA	NA	NA	NA
C15	NA	NA	NA	NA	NA
C16	NA	NA	NA	NA	NA
C17	1.92	5.18	5.44	> 50	4.88
C18	2.62	7.65	2.14	8.64	5.21
C19	1.01	2.94	1.41	7.15	2.89
C20	NA	NA	NA	NA	NA
C21	NA	NA	NA	NA	NA
C22	NA	NA	NA	NA	NA
C23	0.89	0.82	0.36	0.97	4.28
C24	0.43	0.80	0.25	4.79	1.00
C25	0.98	0.96	0.20	5.32	0.89
C26	1.00	0.93	0.082	1.96	0.91

C27	0.54	0.062	0.080	0.70	0.90
C28	1.03	0.070	0.036	0.93	0.47
C29	0.99	1.20	0.082	4.95	0.91
C30	0.97	0.89	0.063	0.70	0.90
C31	0.73	0.99	0.064	0.96	0.90
C41	0.011	0.075	0.012	2.43	0.010
C42	0.026	0.105	0.009	0.49	0.012
C43	0.73	0.69	>50	5.20	0.89
C44	0.99	0.67	0.26	5.17	0.90
C45	0.005	0.24	0.033	0.47	0.049
C46	0.036	0.13	0.008	5.12	0.027
C47	7.12	6.04	4.75	9.38	8.95
C48	5.21	4.79	5.04	8.61	6.26
C49	0.007	0.089	0.45	0.92	0.096
C50	0.036	0.073	0.37	0.50	0.072
Tacrine	NA	NA	NA	NA	NA

a. Average of 3 experiments via a Stopped Flow technique (errors in the range 5-10 %). NA= activation not detected in the concentration range 1 nM - 10 mM.

Considering that tacrine **C32** showed no activatory action toward the tested isoforms, the following structure-activity relationships can be extrapolated.

Hybrid derivatives can be clearly distinguished between compounds with activating CA character and inactive compounds. In particular, compounds bearing the amino group of the protected aa (Boc) and having no other function capable of promoting activatory action, i.e., **C10, C12, C14-C16, C20-C22** (series 1) are inactive. However, the histidine twice protected derivatives **C10** and **C12** show weak activatory action toward hCA II and VB isoforms (K_A 9.05-15.9 μM) because the protected imidazole ring retains an acid-base character. Removal of imidazole N protection as in **C11** and **C13** (series 1) strongly promotes activatory action toward all isoforms tested up to a submicromolar range (K_A 0.51-1.01 μM). N-Boc derivatives with L-tryptophan as amino acid **C17-C19** (series 1) show activatory action in the low micromolar range toward all isoforms tested. Removal of protection on the α-NH2 group for derivatives **C14-C22** of series 1 significantly increases the activating power of compounds **C23-C31** compared with N-Boc analogs. Overall, K_A can be observed in the submicromolar towards hCA I, II, IV, and VII for most derivatives except L-phenylalanine derivative **C23** which activates hCA VII with a K_A of 4.28 μM. The hCA VB isoform appears to be the least activated by derivatives **C14-C22** with K_As that settle in the low micromolar and partly in the high submicromolar range (K_A 0.70-5.32 μM). In particular, in this subgroup show marked activatory

hCA II action the L-tryptophan derivatives **C27** (n=4) and **C28** (n=5) with K_A of 62 and 70 nM, respectively. Remarkable hCA IV activatory action, on the other hand, was found for L-tryptophan derivatives **C26-C28** (K_A 36-85 nM) and N-terminal-Cbz-L-lysine **C29-C31** (K_A 63-82 nM) in this subgroup of series 1. Overall, series 2 derivatives show a more pronounced CA activating action than series 1 compounds. Thus, it is possible to state that an amine-type linker between the two pharmacophoric portions promotes the proton transfer action required for enzyme activation. In detail, the derivatives of L-histidine **C41** and **C42** and L-tryptophan **C45** and **C46** turn out to be the most potent CAAs identified in this thesis work, together with the hydrolyzed derivative **C49**. Specifically, they activate the hCA VB isoform with medium potency (K_A 0.47-2.43 μM) and the hCA II isoform in the mid nanomolar range with K_A of 75-240 nM. On the other hand, these derivatives activate the other isoforms with great efficacy so much so that single digit nanomolar K_A in the range 5-36 nM vs hCA I, 8-45 nM vs hCA IV, and 10-96 nM vs hCA VII are achieved. Among them, derivatives 41 and 42 appear to be the most potent CAAs found here. Hydrolysis of the ester group of **C42** to carboxylic acid increases the CAA action of **C49** toward the hCA I (26 to 7 nM) and II (105 to 89 nM) isoforms but reduces it toward hCA IV (9 to 45 nM), VB (490 to 920 nM), and VII (12 to 96 nM). Series 2 scaffold derivatives L-phenylalanine **C43** and **C44** and N-ε-Cbz-L-lysine **C47** and **C48** exhibit less activatory action than the corresponding L-histidine and L-tryptophan derivatives mentioned above. In detail, derivatives **C47** and **C48** show activatory action in the low micromolar range toward all isoforms tested (K_A 4.75-9.38 μM), whereas **C43** and **C44** result in CAA action with K_A in the high nanomolar range toward hCA I, II, IV, and VII (K_A 0.26-0.99 μM). The histamine derivative **C50** exhibits potent CAA action in the low nanomolar range toward hCA I, II, and VII (K_A 36-72 nM), and worse toward CA IV, and VB. Overall, **C50** is less potent than histidine analogs **C42** and **C49.**

Overall, it is therefore possible to outline the following SARs:

- An amine linker between the two pharmacophores significantly increases the CAA action of the reported hybrid derivatives compared to an amide linker.
- The presence of free basic functions increases the CAA action of derivatives importantly compared to compounds with protected basic functions.

- Variations in spacer length between 3, 4, and 5 (series 1) or 5 and 6 (series 2) carbon atoms does not produce significant changes in the CAA action of the hybrid derivatives.

Inhibition data against cholinesterases

All final compounds were assayed in vitro by Professor Oscar Lopez from the department of chemistry of the University of Seville for their ability to inhibit both cholinesterase, AcetilCholinesterase and ButirrilCholinesterase (table 15).

Table 15. Inhibition profile of derivatives **C10-C31, C41-C50**, and tacrine **C32** toward AchE and BuChE. Three different inhibition types. M=Mixed. NC=Non-competitive. C=Competitive.

Cmpds	AChE-Ki (nM)	AchE Inh.	BuChE-Ki (nM)	BuchE Inh.
C10	Kia = 314 ± 46 Kib = 687 ± 208	M	Kia = 9.5 ± 1.8 Kib = 48 ± 3	M
C11	Kia = 574 ± 122 Kib = 280 ±	M	Kia = 15 ± 1 Kib = 61 ± 6	M
C12	Kia = 345 ± 15 Kib = 607 ±	M	Kia = 2.2 ± 0.1 Kib = 6.7 ± 7.7	M
C13	Kia = 134 ± 6 Kib = 79 ±	M	Kia = 1.2 ± 0.4 Kib = 6.3 ± 1.5	M
C14	Kia = Kib = 777 ± 86	NC	Kia = 1.6 ± 0.1 Kib = 5.2 ± 0.3	M
C15	Kia = 419 ± 82 Kib = 1342 ±	M	Kia = 2.4 ± 0.9 Kib = 4.8 ± 0.8	M
C16	Kia = 497 ± 15 Kib = 1320 ±	M	Kia = 1.1 ± 0.1 Kib = 4.1 ± 1.4	M
C17	Kia = Kib = 608 ± 129	NC	Kia = Kib = 608 ± 129	C
C18	Kia = 274 ± 51 Kib = 316 ±	M	Kia = 274 ± 51 Kib = 316 ± 64	M
C19	Kia = 107 ± 5 Kib = 284 ±	M	Kia = 107 ± 5 Kib = 284 ± 40	M
C20	Kia = 744 ± 79	C	Kia = 1.8 ± 0.3 Kib = 8.2 ± 2.2	M
C21	Kia = 1160 ± 225 Kib = 4720 ±	M	Kia = 1.1 ± 0.1 Kib = 7.1 ± 2.8	M
C22	Kia = 782 ± 38 Kib = 3947 ±	M	Kia = 8.4 ± 2.2 Kib = 28 ± 8	M
C23	Kia = Kib = 664 ± 30	NC	Kia = 9.1 ± 1.0 Kib = 23 ± 1	M
C24	Kia = 306 ± 1 Kib = 951 ± 96	M	Kia = 21 ± 2 Kib = 76 ± 1	M
C25	Kia = 235 ± 1 Kib = 619 ± 3	M	Kia = 15 ± 2 Kib = 59 ± 1	M
C26	Kia = 318 ± 32 Kib = 1417 ±	M	Kia = Kib = 17 ± 4	NC
C27	Kia = Kib = 137 ± 9	NC	Kia = 31 ± 6 Kib = 21 ±	M
C28	Kia = 86 ± 1 Kib = 224 ± 3	M	Kia = 18 ± 2 Kib = 33 ± 1	M
C29	Kia = 444 ± 37 Kib = 575 ±	M	Kia = 7.7 ± 0.2 Kib = 24 ± 4	M
C30	Kia = 825 ± 75 Kib = 933 ±	M	Kia = 26 ± 3 Kib = 48 ± 4	M
C31	Kia = 298 ± 35 Kib = 583 ±	M	Kia = 8.5 ± 1.6 Kib = 19 ± 1	M
C41	Kia = Kib = 223 ± 36	NC	Kia = Kib = 74 ± 3	NC
C42	Kia = 49 ± 13 Kib = 92 ±	M	Kia = 6.0 ± 1.0 Kib = 19.0 ± 5.5	M
C43	Kia = Kib = 370 ± 64	NC	Kia = 24 ± 6 Kib = 50 ± 3	M
C44	Kia = 46 ± 4 Kib = 152 ± 39	M	Kia = 1.9 ± 0.2 Kib = 2.6 ± 0.2	M
C45	Kia = 43 ± 2 Kib = 150 ± 19	M	Kia = 9.5 ± 1.0 Kib = 24 ± 3	M
C46	Kia = Kib = 52 ± 1	NC	Kia = Kib = 22 ± 2	NC
C47	Kia = 46 ± 3	C	Kia = 1.7 ± 0.6 Kib = 3.5 ± 0.9	M
C48	Kia = 29 ± 6 Kib = 68 ± 4	M	Kia = 1.7 ± 0.1 Kib = 4.0 ± 0.5	M

C49	Kia = 1670 ± 284 Kib = 3615 ±	M	Kia = 609 ± 121	C
C50	Kia = 11 ± 2 Kib = 27 ± 5	M	Kia = Kib = 11 ± 2	NC
Tacrine	Ki = 22.9	/	Ki = 17.2	/

The Professor Lopez and his research group identified three types of inhibition against Cholinesterases: competitive, where the ligand interacts with the free enzyme; mixed, where the ligand binds to both the free enzyme and the enzyme occupied by its natural substrate; and non-competitive, where the ligand inhibits the free enzyme and the occupied enzyme equally. In order to outline in the best way, the inhibitor profiles of the synthesized hybrids, it is necessary to divide them in the two series with which they have been synthesized. It is necessary to do this because, as for carbonic anhydrases, also in this case the two series show clear differences, while within the respective series the compounds follow a range of values rather similar. The first series, the amides, show an inhibitory capacity against Acetylcholinesterase in the high nano molar range about 2 units of magnitude worse than lead tacrine. Despite this difference with lead, there are some interesting considerations to make. In fact, the inhibition of these compounds is still significant as they are in the submicromolar range; but above all we can observe that the compounds **C12, C13, C16, C19, C22, C25, C28** and **C31**, sharing the 5 carbons atom spacer are those that work better than their counterparts with 3 and 4 carbon atoms. This can be explained by the fact that the active site where the tacrinic portion acts is well known and well defined; this leads to deduce that to go to interact with the other active site of AchE is necessary at least a spacer of 5 carbon atoms. Summarizing the best hybrids are compounds **C13, C19** and **C28** with values around 100 nM (87nM-134nM). The data on butyrylcholinesterase are certainly more intriguing. The amide series reaches the mid-low nanomolar range with almost all its derivatives. In many cases it reaches the value of tacrine or even exceeds it. The exception to this remarkable inhibitory potency is represented by the **C17-C19** derivatives that present the AA Trp, with values well above those of the other amides (107nM-608nM). All other His, Lys and Phe reach with some compounds the very low nanomolar like for example **C13** (1.2nM), **C16** (1.1nM) and **C21** (1.1nM). A peculiarity to underline is that the deprotected compounds **C23-C31** act an order of magnitude worse than their counterparts protected with Boc on amine. Turning to the description of the inhibitory profiles of the second series, the amines, to remain consistent with the last aspect observed, we

note that the only deprotected compound, namely the His derivative **C49**, is clearly the worst of the series even comparing it with its protected counterpart **C42**. This leads to a consideration: the deprotection that so favoured the activity against carbonic anhydrases, seems to dramatically disfavour the inhibition of cholinesterases. However, the data on the two enzymes agree that the amine series is the most effective. In fact, excluding the compound mentioned earlier, these hybrids inhibit acetylcholinesterase in a very similar manner to the tacrine compound **C32**. Even the **C50** derivative presenting the biogenic amine histamine achieves a better Ki than it (11nM). The higher affinity for butyrylcholinesterase is also confirmed in this series. In fact, almost all the derivatives can interact with it more effectively than tacrine. the other aspect that we evaluated for the first series was the length of the spacer. in this case, since the derivatives have spacers with 5 or 6 carbon atoms, there is no significant difference; confirming that 5 or more carbon atoms are suitable lengths to interact with this type of enzymes. the best example is represented by Trp derivatives **C45** and **C46** that have almost identical Ki (**C45**=43nM, **C46**=52nM).

***In vivo* test**

Professor Blandina and doctor Provensi for the University of Florence have performed *in vivo* test. We selected three compounds **C25**, **C28** and **C42** to evaluate their procogntive effect in mice. The choice fell on these 3 compounds because they summarize the general characteristics of all compounds. **C25** and **C28** are amides, while **C42** is an amine. spacers are at 5 carbon atoms as in the case of **C25** and **C28** or at 6 as in the case of **C42**; the 2 lengths that interacted better with cholinesterases as we had evaluated in previous tests. Also, presented as activators of carbonic anhydrases 3 different amino acids. **C25** has a phenylalanine, **C28** a tryptophan and **C42** a histidine, so we could evaluate which AA has a better effect in vivo.

The test is called social recognition test and it consist in three phases. It is necessary to explain all the phases to better understand the rationale behind this type of experiment.

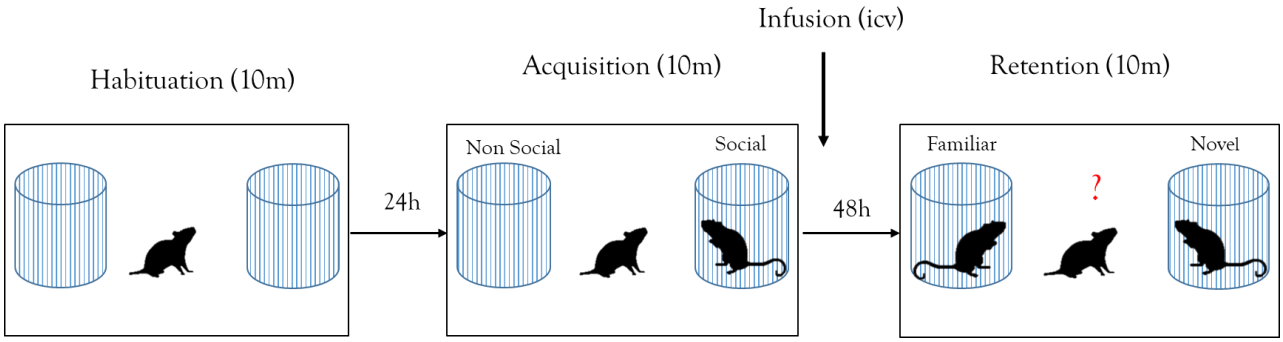

Figure 46. Three phases of social recognition test.

Phase 1: the mouse, on which the mnemonic abilities will be assessed, is placed inside a plastic box that contains 2 empty and transparent cylinders. The mouse will spend 10 minutes inside the box to familiarize itself with the environment of the experiment. This phase is called the habituation phase.

Phase 2: after 24 hours a second animal of the same species as the first is randomly inserted into one of the 2 cylinders. This phase, called acquisition, lasts 10 minutes. Here the time the animal spends getting to know the cylinder containing the second mouse is measured, compared to the time it spends looking at the empty cylinder. Given the remarkable sociability of this species, it is expected that the first mouse will spend most of its time becoming familiar with the second mouse.

Phase 3: after phase 2 the first mouse is injected intra cerebrovascularly with the drug that is supposed to be procognitive. After 48 hours from the acquisition phase, the first mouse is placed in the environment of the experiment where, in this case, it will find both cylinders full. In one cylinder there is the mouse it met in phase 2, while in the other cylinder there is a mouse of the same species but not previously known. In this phase, called retention phase, it is evaluated in 10 minutes how much time it takes to know the new mouse compared to the one already known. The premise of this type of test is that mice are a very sociable species (as shown in phase 2) and therefore it is assumed that the first mouse prefers to interact with the third and unknown mouse rather than the second. By spending 48 hours between phase 2 and phase 3 it is assumed that the mouse may forget who it interacted with previously; if the procognitive drug takes effect it will be seen that the mouse that received this type of drug will spend more

time with the new mouse while those that received nothing or received a drug that has no procognitive effect will spend roughly the same amount of time with both mice.

The first experiment was conducted comparing compound **C28** and with a known carbonic anhydrase activator, D-Phenylalanine, and lead **C32** tacrine.

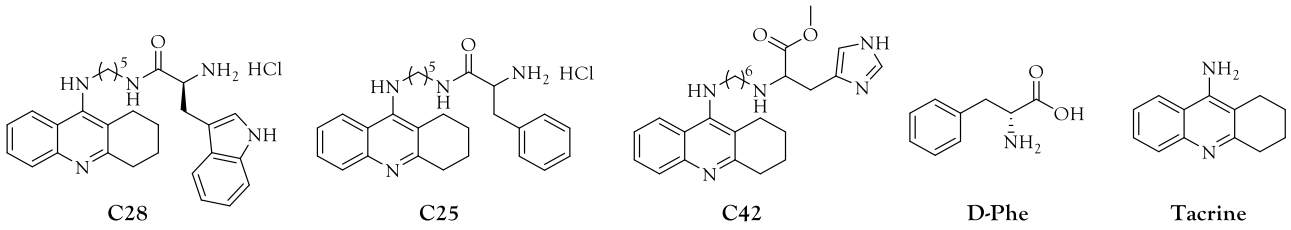

Figure 47. the compounds compared in all experiments.

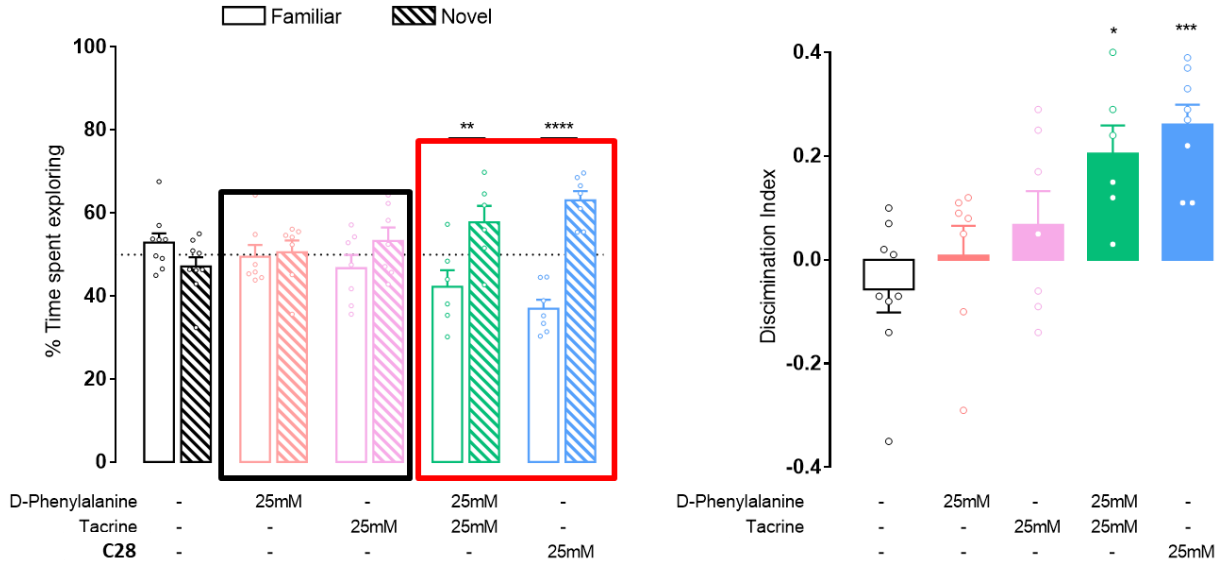

Figure 48. C28, **D-Phe** and **tacrine** were administered at the same concentration of 25mM. The graph on the left shows the time that the mouse spends with both cylinders in the retention phase. The graph on the right is the mathematic representation of the graph on the left.

This first experiment compares **C28** with tacrine, D-Phe and both co-administered. It is clear that our hybrid and the co-administration act at this concentration, while the single portion of molecule doesn't work. To better understand the graph on the left is important to explain that the two columns represent the two cylinders of the experiment; the white one is the column with the mouse that was inserted in phase 2. The other column represents the cylinder with the

third unknown mouse. For example, about the compound **C28** we can say that the first mouse spent 6 minutes to know the new one and only 4 minutes with the already known mouse.

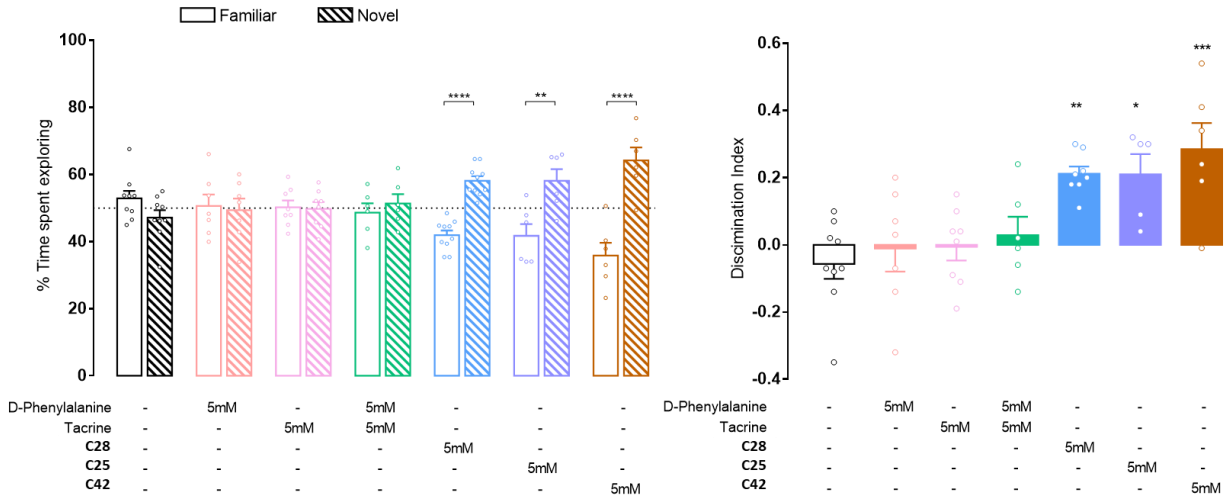

Figure 49. C28, C25, C42, D-Phe and **tacrine** were administered at the same concentration of 5mM.

In the second experiment, we decided to administer the drugs at lower concentration than before, 5mM. The results were really interesting because it is evident that the compound **C28** was still effective, while the co-administration loss is efficacy. This finding explains that the co-administration of two molecules on the same pharmacophore is more potent than the two lead co-administered simultaneously and it confirms that the multitarget approach is a great strategy. In the wake of these results, we tested a 5mM also the compound **C25** and **C42**. Again, both derivatives work at this concentration.

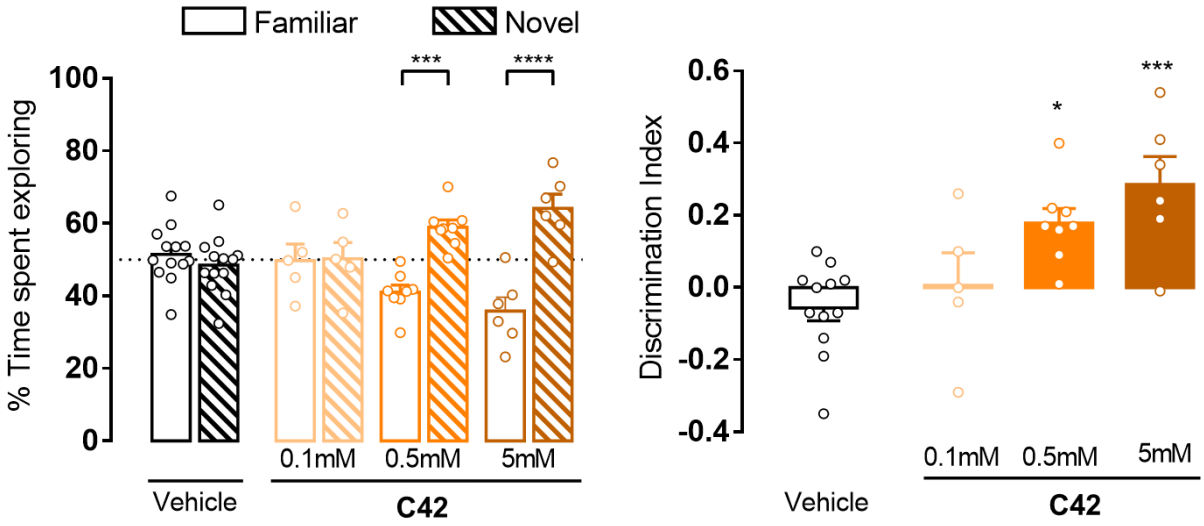

Figure 50. C42 was administered at three concentration 5mM, 0.5mM and 0.1mM.

The last experiment wants to evaluate up to what concentration these compounds can be effective. So, **C42** was administered at three different concentrations of 5mM, 0.5mM and 0.1mM. It has been shown to be effective down to the low concentration of 0.5mM, but not at 0.1mM.

CHAPTER 4. KINETIC CHARACTERIZATION OF THE FIRST ι-CLASS CA FROM THE GRAM-NEGATIVE BACTERIUM *BURKHOLDERIA TERRITORII.*

During my Ph.D. period I performed a multitude of kinetic studies with inhibitors and activators of several isoforms of CA belonging to the most classes. The kinetic assessments were conducted by a Stopped Flow Assay.[161] These studies allowed to draw up the inhibition or activation profiles of hundreds of derivatives from collaborators of us. Moreover, I performed the *ex-novo* complete kinetic characterization of the new CA classes ι identified in marine diatom *Thalassosira Pseudonana* and observed for the first time in a Gram-negative bacterium *Burkholderia territorii* and denominated BteCA*i*. These CA was produced by Dr. Clemente Capasso from the Institute of Biosciences and Bioresources, CNR of Naples.

4.1 Anions

I've performed the inhibition against the most common anions, simple and complex. The most common sulfonamide, simple and commercial. and I've performed the activation activity on the most common CA activators.

Table 16. Anion inhibition data of BteCA*ι* as determined by a stopped-flow CO2 hydrase assay. Inhibition of the human isoforms hCA I and II, and the bacterial *E. Coli* β-CA are also shown for comparison.

Anions	K_I (mM)*			
	hCA I	hCA II	*E. Coli* β-CA	BteCA*ι*
F^-	>300	>300	9.4	4.6
Cl^-	6	200	6.7	3.1
Br^-	4	63	3.8	4.8
I^-	0.3	26	>50	>50
CNO^-	0.0007	0.03	0.58	0.79
SCN^-	0.2	1.6	5.7	6.1
CN^-	0.0005	0.02	>50	>50
N_3^-	0.0012	1.51	>50	>50
NO_2^-	8.4	63	4.9	8.4
NO_3^-	7	35	2.4	6.2
HCO_3^-	12	85	0.81	0.94
CO_3^{2-}	15	73	0.89	4.4
HSO_3^-	18	89	3.7	8.4
SO_4^{2-}	63	>200	1.7	5.8

HS^-	0.0006	0.04	2.7	6.2
$NH_2SO_2NH_2$	0.31	1.13	0.011	0.086
NH_2SO_3H	0.021	0.39	0.0025	0.0062
$PhAsO_3H_2$	31.7	49	0.0061	0.008
$PhB(OH)_2$	58.6	23	0.0028	0.009
ClO_4^-	>200	>200	>50	>50
SnO_3^{2-}	0.57	0.83	0.52	0.094
SeO_4^{2-}	118	112	3.1	0.73
TeO_4^{2-}	0.66	0.92	0.51	0,71
OsO_5^{2-}	0.92	0.95	>50	>50
$P_2O_7^{2-}$	25.8	48	>50	>50
$V_2O_7^{2-}$	0.54	0.57	>50	>50
$B_4O_7^{2-}$	0.64	0.95	0.25	>50
ReO_4^-	0.11	0.75	>50	>50
RuO_4^-	0.101	0.69	9.5	>50
$S_2O_8^{2-}$	0.107	0.084	6.4	7.4
$SeCN^-$	0.085	0.086	3.1	6.6
$NH(SO_3)_2^{2-}$	0.31	0.76	1.5	>50
FSO_3^-	0.79	0.46	0.83	9.3
CS_3^{2-}	0.0087	0.0088	3.1	8.6
$EtNCS_2^-$	0.00079	0.0031	0.084	0.81
PF_6^-	nt	nt	>50	>50
$CF_3SO_3^-$	nt	nt	>50	>50

* Mean from 3 different assays, by a stopped flow technique (errors were in the range of ± 5-10 % of the reported values).

The data of Table 16 show the following interesting aspects for the inhibition of this poorly investigated CA class:

i. some anions, among which iodide, cyanide, azide, perchlorate, perosmate, diphosphate, divanadate, tetraborate, perrhenate, perruthenate, iminodisulfonate, hexafluorophosphate and trifluoromethanesulfonate, did not inhibit BteCA*ι* significantly up to 50mM concentration of inhibitor in the assay system. This is not unexpected for anions with low affinity for complexing metal ions, such as perchlorate, hexafluorophosphate and trifluoromethanesulfonate, but it is rather surprising for iodide, cyanide, and azide, which have quite a high affinity for metal ions in solution and in the active site of many metalloenzymes. Indeed, some of

these anions show a potent inhibitory action for other CAs, such as the isoform hCA I. As no X-ray crystallographic data are available so far for ι-CAs, it is impossible to rationalise these interesting and surprising data.

ii. The following inhibitors showed inhibitory action against BteCAι in the millimolar range: fluoride, chloride, bromide, thiocyanate, nitrite, nitrate, carbonate, bisulphite, sulphate, hydrogensulfide, peroxydisulfate, selenocyanate, fluorosulfonate and trithiocarbonate (KI values in the range of 3.1–9.3 mM). As above, some of these data stupefied us: sulphate, for example, is a highly inefficient inhibitor of many a-CAs (e.g. hCA I and II), but it inhibits efficiently the bacterial β - and ι-CAs shown in Table 16.

iii. Even more efficient inhibitory action against BteCAι was registered for the following anions: diethyldithiocarbamate, tellurate, selenate, bicarbonate and cyanate, which were submillimolar inhibitors with KI values ranging between 0.71 and 0.94mM (Table 16). The bicarbonate high affinity is of interest, since this anion is also a substrate/reaction product of the CA – catalysed reactions.

iv. The most efficient BteCAι inhibitors detected so far were stannate, sulphamic acid, phenylarsonic acid, phenylboronic acid and sulfamide, with KI values of 6.2–94 mM (Table 16). Some of these compounds, such as sulfamide and sulphamic acid, act as effective inhibitors of many other CAs (for example, see the E. coli b-CA inhibition data shown in Table 16). They also inhibit the human isoforms hCA I and II (although to lower levels compared to the bacterial enzymes). The stannate data is also quite interesting. This anion is an order of magnitude better as a BteCAι inhibitor compared to its inhibition level of other CAs investigated so far.

The experimental procedures are reported in Chapter 5 and the data and results of this research were published in A. Petreni, et al. *J. Med. Chem. J. Enzyme Inhib. Med. Chem.* **2021,** 36, 372-376.

4.2 Sulfonamides

Table 17. BteCA_ inhibition parameters for the catalyzed CO2 hydration reaction and their comparison with those determined for different CA classes (β, γ and ι). The inhibition measurements were carried out at 20°C and pH 7.5 in 10 mM HEPES buffer for the hCA I, hCA II, EcoCAγ and BteCA*ι*, while a different buffer was used for the EcoCAγ enzyme (20 mM TRIS, pH 8.3, containing 20 mM NaClO4).

Inhibitors	K_I (nM)*				
	hCA I	hCA II	EcoCA β	EcoCAγ	BteCA*ι*
1	28000	300	705	314	325
2	25000	240	790	193	477
3	79000	8	457	246	568
4	78500	320	3015	221	446
5	25000	170	2840	160	97
6	21000	160	3321	622	786
7	8300	60	>10000	605	481
8	9800	110	>10000	671	346
9	6500	40	2712	718	96
10	7300	54	8561	2577	357
11	5800	63	6246	1779	239
12	8400	75	4385	1953	329
13	8600	60	4122	197	303
14	9300	19	440	712	434
15	5500	80	6445	1013	540
16	9500	94	2340	4238	594
17	21000	125	502	1975	404
18	164	46	205	2064	467
19	109	33	416	1894	93
20	6	2	726	883	268
21	69	11	473	819	307
22	164	46	93	3501	365
23	109	33	322	4045	408
24	95	30	82	4262	698
AAZ	250	12	227	248	519
MZA	50	14	480	921	8466
EZA	25	8	557	5538	5024
DCP	1200	38	>10000	889	825
DZA	50000	9	629	2007	794
BRZ	45000	3	2048	4842	3703
BZA	15	9	276	94	724
TPM	250	10	3359	648	787
ZNS	56	35	3189	755	806

SLP	1200	40	97	914	958
IND	31	15	2392	387	638
VLX	54000	43	2752	891	934
CLX	50000	21	1894	944	960
SLT	374	9	285	446	954
SAC	18540	5959	6693	4903	7081
HCT	328	290	5010	3643	780
FAM	922	58	2769	274	943
EPA	8262	917	2560	744	955

* Mean from 3 different assays, by a stopped flow technique (errors were in the range of ± 5-10 % of the reported values).

From the data of Table 2, the following results can be observed:

1. Among the sulfonamides and sulfamate used to determine the BteCA*ι* inhibition profile, only three inhibitors resulted in a KI lower than 100 nM. This is the case of the compounds **5, 9** and **19**. These results confirm how different is the spatial organization of the catalytic pocket of the different CA classes. For the same compounds, the other two bacterial enzymes showed KI values in the range 160–2840 nM, while the corresponding KI values of two human isoforms were between 33–25,000 nM. The two human isoforms, hCA I and hCA II, resulted in a variegate behavior since hCAI was very susceptible to the inhibitors 9 and 19 with a KI values of 40 and 33 nM, respectively. Again, both human isoforms showed many nanomolar inhibitors with a KI below 100 nM, such as compounds **20, 21, 24, MZA, EZA, BZA, ZNS, IND**. Once more, there were compounds such as **3, 7, 10, 11, 12, 13, 14, 15, 16, DCP, DZA, BRZ, SLP, VLX** and **CLX**, which were potent inhibitors of hCA II with KI values in the range 3–94 nM but were very week inhibitors of hCA I (KIS > 5500 nM). Only the study of the three-dimensional structures of BteCA*ι* (not available at this moment) will explain the structural factors responsible for the KI variations.

2. Most of the inhibitors considered in Table 17 were moderate inhibitors of BteCA*i* with KIs in the range 239–955 nM, such as compounds **1, 2, 3, 4, 6, 7, 8, 10, 11, 12, 13, 14, 15, 16, 17, 20, 21, 22, 23, 24, AAZ, DCP, DZA, BZA, TMP, ZNS, SLP, SLT, IND, VLX, CLX, SLT, HTC, FAM and EPA**. A good number of these compounds, such as **1, 2, 3, 14, 20, 21, AAZ, BZA** and **SLT**, resulted in moderate inhibitors for the other two bacterial enzymes (EcoCA β and EcoCAγ), too. It is important to note that some of these inhibitors were very sensitive

versus the human isoform hCA II but not versus the human isoform hCA I (KIS > 10,000 nM). The zonisamide (**ZNS**), an aliphatic primary sulfonamide, was also a very weak inhibitor for the bacterial enzymes (KIs = 755–3189 nM) but effective towards the human isoenzymes (KIs = 35–56 nM).

3. Some substituted benzene-sulfonamides, such as **MZA, EZA, BRZ** and **SAC**, were rather ineffective, weak inhibitors of BteCA*ι*, showing KI values in the range of 5024–8466 nM. Moreover, **MZA** inhibited the *E. coli* EcoCA β and EcoCAγ enzymes with KI of 480 and 921 nM, respectively.

The experimental procedures are reported in Chapter 5 and the data and results of this research were published in V. De Luca, et al. *J. Med. Chem. J. Enzyme Inhib. Med. Chem.* **2021,** 36, 1000-1006.

4.3 Activators

Table 18. Activation of BteCA*ι*, hCA I and hCA II with amino acids and amines 1–24. Experiments were performed for the CO_2 hydration reaction, at 25 °C, and performed by a stopped-flow assay.

	Activators	K_A(uM)*		
		hCA I	hCA II	BteCA*ι*
1	L-His	0.03	10.9	8.6
2	D-His	0.09	43	6.2
3	L-Phe	0.07	0.013	36.5
4	D-Phe	86	0.035	9.4
5	L-DOPA	3.1	11.4	4.3
6	D-DOPA	4.9	7.8	11.7
7	L-Trp	44	27	10.2
8	D-Trp	41	12	6.1
9	L-Tyr	0.02	0.011	8.0
10	D-Tyr	0.04	0.013	7.3
11	4-H2N-L-Phe	0.24	0.15	6.9
12	Histamine	2.1	125	6.0
13	Dopamine	13.5	9.2	8.7
14	Serotonin	45	50	13.3
15	2-Pyridyl-methylamine	26	34	24.1
16	2-(2-Aminoethyl)pyridine	13	15	21.5
17	1-(2-Aminoethyl)-piperazine	7.4	2.3	3.9
18	4-(2-Aminoethyl)-morpholine	0.14	0.19	12.0
19	L-Adrenaline	0.09	96	9.7
20	L-Asn	11.3	0.011	45.6
21	L-Asp	5.20	>100	8.4
22	L-Glu	6.43	>100	18.4
23	D-Glu	10.7	>100	8.5
24	L-Gln	>100	>50	5.8

The following structure-activity relationship (SAR) data for the activation of BteCA*ι* may be noted fromthe data reported in Table 18:

i. Most of the tested activators showed an efficient and rather flat activating efficacy towards BteCA*ι*, with KA values ranging between 3.9 and 13.3 mM. Both amino acids (1, 2, 4–11, 21, 23 and 24) as well as amines (12–14, 17–19) showed this type of behaviour, with basically poor

SAR to be discussed due to the low range of activity variations. This condition is different from what observed for hCA I and hCA II activation, for which some activators also showed nanomolar activity, e.g., L-Phe, L- and D-Tyr (hCA I and hCA II), and L-adrenaline, L- and D-His (hCA I). For the enantiomeric pairs L-/D-His, L-/ D-Phe, L-/D-Trp and L-/D-Tyr, the D-enantiomer was always a better activator than the corresponding L-one. Only for DOPA the reverse was true, with L-DOPA being almost 3 times a more efficient activator compared to the corresponding D-enantiomer.

ii. Several compounds, among which L-Phe, the pyridyl-alkylamines 15 and 16, as well as L-Asn and L-Glu, showed rather weak CA activating effects against the i-class enzyme, with K_A values ranging between 18.4 and 45.6 mM. Also, for the L-/ D-Glu enantiomeric pair, the D-enantiomer was always a better activator than the corresponding L-one. When data of the L-Asp/L-Asn pair were evaluated, the amide derivative appeared a 5.42-fold weaker activator than the acid counterpart. These results highlight that rather small structural changes (even at the stereogenic center) in the assayed compounds can lead to rather important modifications of the corresponding CA activating properties.

iii. As already anticipated above, the activation profile of the i-class bacterial enzyme was very different from those of hCA I and hCA II.

The experimental procedures are reported in Chapter 5 and the data and results of this research were published in V. De Luca, et al. *Int J Mol Sci.* **2021**, 8, 571

Chapter 5. EXPERIMENTAL SECTION

General Protocols

Chemistry

Anhydrous solvents and all reagents were purchased from Sigma-Aldrich, Alfa Aesar and TCI. All reactions involving air- or moisture-sensitive compounds were performed under a nitrogen atmosphere using dried glassware and syringes techniques to transfer solutions. Nuclear magnetic resonance (^{1}H-NMR, ^{13}C-NMR, ^{19}F-NMR) spectra were recorded using a Bruker Advance III 400 MHz spectrometer in DMSO-d_6 or $CDCl_3$. Chemical shifts are reported in parts per million (ppm) and the coupling constants (*J*) are expressed in Hertz (Hz). Splitting patterns are designated as follows: s, singlet; d, doublet; t, triplet; q, quadruplet; sept, septet; m, multiplet; bs, broad singlet; dd, double of doubles, appt, apparent triplet, appq, apparent quartet. The assignment of exchangeable protons (O*H* and N*H*) was confirmed by the addition of D_2O. Analytical thin-layer chromatography (TLC) was carried out on Merck silica gel F-254 plates. Flash chromatography purifications were performed on Merck Silica gel 60 (230-400 mesh ASTM) as the stationary phase and ethyl acetate/*n*-hexane or MeOH/DCM were used as eluents. Melting points (m.p.) were measured in open capillary tubes with a Gallenkamp MPD350.BM3.5 apparatus and are uncorrected. HPLC was performed by using a Waters 2690 separation module coupled with a photodiode array detector (PDA Waters 996) and as column, a Nova-Pak C18 4 μm 3.9 mm × 150 mm (Waters), silica-based reverse phase column. Sample was dissolved in acetonitrile 10%, and an injection volume of 45 μL was used. The mobile phase, at a flow rate of 1 mL/min, was a gradient of water + trifluoroacetic acid (TFA) 0.1% (A) and acetonitrile + TFA 0.1% (B), with steps as follows: (A% : B%), 0−10 min 90:10, 10−25 min gradient to 60:40, 26:28 min isocratic 20:80, 29−35 min isocratic 90:10. TFA 0.1% in water as well in acetonitrile was used as counterion. All compounds reported here were >96% HPLC pure. The solvents used in MS measures were acetone, acetonitrile (Chromasolv grade), purchased from Sigma-Aldrich (Milan - Italy), and mQ water 18 MΩ, obtained from Millipore's Simplicity system (Milan-Italy). The mass spectra were obtained using a Varian 1200L triple quadrupole system (Palo Alto, CA, USA) equipped by Electrospray Source (ESI) operating in both positive and negative ions. Stock solutions of analytes were prepared in acetone at 1.0 mg

mL^{-1} and stored at 4°C. Working solutions of each analyte were freshly prepared by diluting stock solutions in a mixture of mQ H_2O/ACN 1/1 (*v*/*v*) up to a concentration of 1.0 μg mL^{-1} The mass spectra of each analyte were acquired by introducing, via syringe pump at 10 μL min^{-1}, of its working solution. Raw-data were collected and processed by Varian Workstation, version 6.8 software.

Stopped-flow kinetic assays

α-Cas and ι-Cas

An Applied Photophysics stopped-flow instrument has been used for assaying the CA catalysed CO_2 hydration activity.[169] Phenol red (at a concentration of 0.2 mM) has been used as a pH indicator, working at the absorbance maximum of 557 nm, with 20 mM Hepes (pH 7.5) as the buffer, and 20 mM Na_2SO_4 (for maintaining constant the ionic strength), following the initial rates of the CA-catalyzed CO_2 hydration reaction for a period of 10-100 s at 25°C.[169] The CO_2 concentrations ranged from 1.7 to 17 mM for the determination of the kinetic parameters and inhibition constants. For each inhibitor, at least six traces of the initial 5-10% of the reaction have been used for determining the initial velocity. The uncatalyzed rates were determined in the same manner and subtracted from the total observed rates. Stock solutions of inhibitor (0.1 mM) were prepared in distilled-deionized water and dilutions up to 0.01 nM were done thereafter with the assay buffer. Inhibitor and enzyme solutions were preincubated together for 15 min (sulfonamides) or 6h (coumarins) at room temperature prior to assay, in order to allow for the formation of the E-I complex. The inhibition constants were obtained by non-linear least-squares methods using PRISM 3 and the Cheng-Prusoff equation, as reported earlier,[169] and represent the mean from at least three different determinations. All hCA isofoms were recombinant ones obtained in-house as reported earlier,[1,2] while the α-CA SpiCA3, was obtained and purified by a diverse procedure as the one reported earlier in the thesis.

β-CAs

An Applied Photophysics stopped-flow instrument has been used for assaying the CA catalysed CO_2 hydration activity.[169] Bromothymol blue (at a concentration of 0.2 mM) has been used as a pH indicator, working at the absorbance maximum of 557 nm, with 10–20 mM TRIS (pH 8.3) as buffer, and 20 mM $NaBF_4$ for maintaining constant the ionic strength, following the initial

rates of the CA catalysed CO_2 hydration reaction for a period of 10–100 s at 25°C. The CO_2 concentrations ranged from 1.7 to 17 mM for the determination of the kinetic parameters and inhibition constants. For each inhibitor, at least six traces of the initial 5–10% of the reaction have been used for determining the initial velocity. The uncatalyzed rates were determined in the same manner and subtracted from the total observed rates. Stock solutions of inhibitor (10 mM) were prepared in distilled-deionized water and dilutions up to 0.01M were done thereafter with the assay buffer. Inhibitor and enzyme solutions were preincubated together for 15 min (sulfonamides) or 30 min (anions) at room temperature prior to assay, in order to allow for the formation of the E-I complex. The inhibition constants were obtained by non-linear least-squares methods using the Cheng-Prusoff equation whereas the kinetic parameters for the uninhibited enzymes from Lineweaver-Burk plots, as reported earlier,[169] and represent the mean from at least three different determinations. *Entamoeba histolytica* was a protein, obtained and purified by a diverse procedure as the one reported below in the thesis.

Inclusion of 5-fluorouracil moieties in nitrogenous base derivatives as human carbonic anhydrase IX and XII inhibitors produced a targeted action against MDA-MB-231 and T47D breast cancer cells. (Series A)

Synthesis of 2-(5-fluoro-2,4-dioxo-3,4-dihydropyrimidin-1(2H)-yl)acetic acid A2

An aqueous solution of chloroacetic acid (1.1 eq in 4 ml of water) was added dropwise to a solution of 5-fluorouracil **A1** (1.0 g, 1.0 eq) and KOH (3.0 eq) in water (4 ml) at 100°C. The reaction mixture was stirred for 2h at the same temperature, then cooled to r.t. and acidified to pH 2. The formed precipitate was collected by filtration and washed with water and Et_2O. The crude solid was recrystallized from the minimum amount of water to obtain the titled compound as a white powder. 82% yield; m.p. 280-282°C; silica gel TLC R_f 0.05 (MeOH/$CHCl_3$ 10 % v/v); δ_H (400 MHz, DMSO-d_6): 13.29 (s, 1H, exchange with D_2O, COO*H*), 11.96 (s, 1H, exchange with D_2O, CON*H*CO), 8.12 (d, *J* = 6.7 Hz, 1H, Ar-*H*), 4.40 (s, 2H, C*H*$_2$); δ_C (100 MHz, DMSO-d_6): 170.32, 158.51 (d, $J_{2\ CF}$ = 25.8 Hz), 150.72, 140.38 (d, $J_{2\ CF}$ = 228.9 Hz), 131.56 (d, $J_{2\ CF}$ = 33.9 Hz), 49.70; δ_F (376 MHz, DMSO-d_6): -170.04 (s); m/z (ESI negative) calcd for C6H4FN2O4 $[M-H]^-$ 187.0, found 186.9 .

General synthetic procedure of benzenesulfonamides A8-A12.

EDCI (2.0 eq) was added to a solution of 1-carboxymethyl 5-fluorouracil **A2** (0.2 g, 1.0 eq), HOBt (0.5 eq) and DMAP (0.03 eq) in dry DMF (2 ml) under a nitrogen atmosphere and the reaction mixture was stirred at r.t. until the consumption of the starting material (TLC monitoring). Thereafter the proper aminobenzenesulfonamide **A3-A7** (1.1 eq) was added to the reaction mixture, that was stirred at r.t. until the disappearance of the activated ester was observed (TLC monitoring) and then quenched with ice and $HCl_{(aq)}$ 2M. The formed precipitate was filtered under *vacuo* and recrystallized from the minimum amount of water to afford the titled compounds as white powders.

2-(5-Fluoro-2,4-dioxo-3,4-dihydropyrimidin-1(2H)-yl)-N-(4-sulfamoylphenyl)acetamide A8

Compound **A8** was obtained according the general procedure earlier reported using 1-carboxymethyl 5-fluorouracil **A2** (0.2 g, 1.0 eq), HOBt (0.5 eq), DMAP (0.03 eq) and 4-aminobenzenesulfonamide **A3** (1.1 eq) in dry DMF (2 ml). 36% yield; m.p. >300°C; silica gel TLC R_f 0.50 ($MeOH/CH_2Cl_2$ 10 % v/v); δ_H (400 MHz, DMSO-d_6): 11.98 (s, 1H, exchange with D_2O, CON*H*CO), 10.67 (s, 1H, exchange with D_2O, CON*H*), 8.14 (d, *J* = 6.7 Hz, 1H, Ar-*H*), 7.82 (d, *J* = 8.7 Hz, 2H, Ar-*H*), 7.76 (d, *J* = 8.8 Hz, 2H, Ar-*H*), 7.31 (s, 2H, exchange with D_2O, SO_2NH_2), 4.57 (s, 2H, CH_2); δ_C (100 MHz, DMSO-d_6): 166.89, 158.46 (d, $J_{2\ CF}$ =25.7 Hz), 150.74, 142.26, 140.21 (d, $J_{2\ CF}$ = 228.6 Hz). 139.70, 131.97 (d, $J_{2\ CF}$ = 34.0 Hz), 127.78, 119.70, 51.22; δ_F (376 MHz, DMSO-d_6): -170.40 (d, *J* = 5.7 Hz); m/z (ESI negative) calcd for C12H10FN4O5S $[M-H]^-$ 341.0, found 341.1.

2-(5-Fluoro-2,4-dioxo-3,4-dihydropyrimidin-1(2H)-yl)-N-(3-sulfamoylphenyl)acetamide A9

Compound **A9** was obtained according the general procedure earlier reported using 1-carboxymethyl 5-fluorouracil **A2** (0.2 g, 1.0 eq), HOBt (0.5 eq), DMAP (0.03 eq) and 3-aminobenzenesulfonamide **A4** (1.1 eq) in dry DMF (2 ml). 54% yield; m.p. >300°C; silica gel TLC R_f 0.25 ($MeOH/CH_2Cl_2$ 20 % v/v); δ_H (400 MHz, DMSO-d_6): 11.97 (s, 1H, exchange with D_2O, CON*H*CO), 10.62 (s, 1H, exchange with D_2O, CON*H*), 8.18 (d, *J* = 15.2 Hz, 1H, Ar-*H*), 8.14 (d, *J* = 6.5 Hz, 1H, Ar-*H*), 7.74 (s, 1H, Ar-*H*), 7.57 (s, 2H, Ar-*H*), 7.42 (s, 2H, exchange with D_2O, SO_2NH_2), 4.56 (s, 2H, CH_2); δ_C (100 MHz, DMSO-d_6): 166.73, 158.47 (d, $J_{2\ CF}$ = 25.8 Hz), 150.74, 145.70, 140.22 (d, $J_{2\ CF}$ = 228.5 Hz), 139.72, 131.98 (d, $J_{2\ CF}$ = 34.0 Hz), 130.57,

122.92, 121.62, 117.16, 51.19; δ_F (376 MHz, DMSO-d_6): -170.44 (d, J = 3.3 Hz); m/z (ESI negative) calcd for C12H10FN4O5S [M-H]$^-$ 341.0, found 341.1.

2-(5-Fluoro-2,4-dioxo-3,4-dihydropyrimidin-1(2H)-yl)-N-(4-sulfamoylbenzyl)acetamide A10

Compound **A10** was obtained according the general procedure earlier reported using 1-carboxymethyl 5-fluorouracil **A2** (0.2 g, 1.0 eq), HOBt (0.5 eq), DMAP (0.03 eq) and 4-(aminomethyl)benzenesulfonamide hydrochloride **A5** (1.1 eq) and DIPEA (1.1 eq) in dry DMF (2 ml). 25% yield; m.p. >300°C; silica gel TLC R_f 0.30 (MeOH/CH_2Cl_2 10 % v/v); δ_H (400 MHz, DMSO-d_6): 11.87 (s, 1H, exchange with D_2O, CON*H*CO), 8.79 (t, J = 5.8 Hz, 1H, exchange with D_2O, CON*H*), 8.10 (d, J = 6.8 Hz, 1H, Ar-*H*), 7.80 (d, J = 8.2 Hz, 2H, Ar-*H*), 7.47 (d, J = 8.2 Hz, 2H, Ar-*H*), 7.35 (s, 2H, exchange with D_2O, SO_2NH_2,), 4.41 (d, J = 5.8 Hz, 2H, CH_2), 4.38 (s, 2H, CH_2); δ_C (100 MHz, DMSO-d_6): 167.78, 158.68 (d, $J_{2\ CF}$ = 27.2 Hz), 150.74, 144.04, 143.65, 140.40 (d, $J_{2\ CF}$ = 238.7 Hz), 131.82 (d, $J_{2\ CF}$ = 45.1 Hz), 128.45, 126.58, 50.86, 42.75; δ_F (376 MHz, DMSO-d_6): -170.46 (d, J = 3.7 Hz); m/z (ESI negative) calcd for C13H12FN4O5S [M-H]$^-$ 355.1, found 355.0.

2-(5-Fluoro-2,4-dioxo-3,4-dihydropyrimidin-1(2H)-yl)-N-(4-sulfamoylphenethyl)acetamide A11

Compound **A11** was obtained according the general procedure earlier reported using 1-carboxymethyl 5-fluorouracil **A2** (0.2 g, 1.0 eq), HOBt (0.5 eq), DMAP (0.03 eq) and 4-(aminoethyl)benzenesulfonamide **A6** (1.1 eq) in dry DMF (2 ml). 63% yield; m.p. 258-260°C; silica gel TLC R_f 0.55 (MeOH/CH_2Cl_2 10 % v/v); δ_H (400 MHz, DMSO-d_6): 11.88 (s, 1H, exchange with D_2O, CON*H*CO), 8.33 (t, J = 5.3 Hz, 1H, exchange with D_2O, CON*H*), 8.05 (d, J = 6.7 Hz, 1H, Ar-*H*), 7.78 (d, J = 8.2 Hz, 2H, Ar-*H*), 7.45 (d, J = 8.2 Hz, 2H, Ar-*H*), 7.34 (s, 2H, exchange with D_2O, SO_2NH_2), 4.28 (s, 2H, CH_2), 3.35 (d, J = 15.0 Hz, 2H, CH_2), 2.80 (dd, J = 31.9, 24.9 Hz, 2H, CH_2); δ_C (100 MHz, DMSO-d_6): 167.50, 158.60 (d, $J_{2\ CF}$ = 35.1 Hz), 150.65, 144.43, 143.05, 140.23 (d, $J_{2\ CF}$ = 234.2 Hz), 131.99 (d, $J_{2\ CF}$ = 35.9 Hz), 130.11, 126.63, 50.61, 35.54; δ_F (376 MHz, DMSO-d_6): -170.66 (s); m/z (ESI negative) calcd for C14H14FN4O5S [M-H]$^-$ 369.1, found 369.0.

2-(5-Fluoro-2,4-dioxo-3,4-dihydropyrimidin-1(2H)-yl)-N-(2-hydroxy-5-sulfamoylphenyl)acetamide A12

Compound **A12** was obtained according the general procedure earlier reported using 1-carboxymethyl 5-fluorouracil **A2** (0.2 g, 1.0 eq), HOBt (0.5 eq), DMAP (0.03 eq) and 3-amino-4-hydroxybenzenesulfonamide **A7** (1.1 eq) in dry DMF (2 ml). 46% yield; m.p. >300°C; silica gel TLC R_f 0.20 ($MeOH/CH_2Cl_2$ 10 % v/v); δ_H (400 MHz, DMSO-d_6): 11.92 (s, 1H, exchange with D_2O, CON*H*CO), 10.85 (s, 1H, Ar-*H*), 9.82 (s, 1H, exchange with D_2O, O*H*), 8.49 (s, 1H, exchange with D_2O, CON*H*), 8.13 (d, *J* = 6.6 Hz, 1H, Ar-*H*), 7.45 (d, *J* = 8.1 Hz, 1H, Ar-*H*), 7.16 (s, 2H, exchange with D_2O, SO_2NH_2), 7.03 (d, *J* = 8.4 Hz, 1H, Ar-*H*), 4.71 (d, *J* = 52.0 Hz, 2H, CH_2); δ_C (100 MHz, DMSO-d_6): 166.85, 158.45 (d, $J_{2\ CF}$ = 25.7 Hz), 151.30, 150.74, 140.17 (d, $J_{2\ CF}$ = 227.7 Hz), 135.53, 132.07 (d, $J_{2\ CF}$ = 33.5 Hz), 126.63, 123.56, 120.60, 115.59, 51.24; δ_F (376 MHz, DMSO-d_6): -170.64 (d, *J* = 14.1 Hz); m/z (ESI negative) calcd for C12H10FN4O6S $[M-H]^-$ 357.0, found 356.9.

General synthetic procedure of benzenesulfonamides A19-A24.

EDCI (2.0 eq) was added to a solution of 1-carboxymethyl 5-fluorouracil **A2** (0.2 g, 1.0 eq), HOBt (0.5 eq) and DMAP (0.03 eq) in dry DMF (2 ml) under a nitrogen atmosphere and the reaction mixture was stirred at r.t. until the consumption of the starting material (TLC monitoring). Thereafter the proper aminobenzenesulfonamide **A13-A18** (1.5 eq) was added to the reaction mixture, that was stirred at r.t. until the disappearance of the activated ester was observed (TLC monitoring) and then quenched with ice and $HCl_{(aq)}$ 2M. The collected, water washed precipitate was triturated in MeOH to afford the pure titled compounds as powders.

N-Benzyl-2-(5-fluoro-2,4-dioxo-3,4-dihydropyrimidin-1(2H)-yl)-N-(4-sulfamoylphenethyl)acetamide A19

Compound **A19** was obtained according the general procedure earlier reported using 1-carboxymethyl 5-fluorouracil **A2** (0.2 g, 1.0 eq), HOBt (0.5 eq), DMAP (0.03 eq) and 4-(2-(benzylamino)ethyl)benzenesulfonamide **A13** (1.1 eq) in dry DMF (2 ml). 23% yield; m.p. 234-236°C; silica gel TLC R_f 0.75 ($MeOH/CH_2Cl_2$ 15 % v/v); δ_H (400 MHz, DMSO-d_6): 11.87 (s, 1H, exchange with D_2O, CON*H*CO), 8.09 (d, *J* = 6.8 Hz, 0.5H, Ar-*H*), 8.04 (d, *J* = 6.7 Hz, 0.5H, Ar-*H*), 7.80 (d, *J* = 8.1 Hz, 1H, Ar-*H*), 7.77 (d, *J* = 8.1 Hz, 1H, Ar-*H*), 7.51 (d, *J* = 8.2 Hz, 2H, Ar-*H*), 7.43 (m, 7H, partially exchange with D_2O, Ar-*H* + SONH_2), 4.72 (s, 1H, CH_2), 4.67 (s, 1H, CH_2), 4.60 (s, 1H, CH_2), 4.57(s, 1H, CH_2), 3.48 (m, 2H, CH_2), 3.02 (m, 1H, CH_2), 2.84

(m, 1H, C*H*$_2$); δ_C (100 MHz, DMSO-*d*$_6$): 167.47, 161.16, 158.57 (d, $J_{2\ CF}$ = 26.3 Hz), 150.82, 143.36, 140.39 (d, $J_{2\ CF}$ = 544.7 Hz), 138.41, 130.27, 129.82 (d, $J_{2\ CF}$ = 32.7 Hz), 129.38, 128.62, 128.10, 126.78, 50.94, 49.44 (d, $J_{2\ CF}$ = 28.2 Hz), 48.38 (d, $J_{2\ CF}$ = 15.2 Hz), 34.22 (d, $J_{2\ CF}$ = 95.9 Hz); δ_F (376 MHz, DMSO-*d*$_6$): -170.62; m/z (ESI negative) calcd for C21H20FN4O5S [M-H]$^-$ 459.1, found 459.1.

N-(4-Chlorobenzyl)-2-(5-fluoro-2,4-dioxo-3,4-dihydropyrimidin-1(2H)-yl)-N-(4-sulfamoylphenethyl)acetamide A20

Compound **A20** was obtained according the general procedure earlier reported using1-carboxymethyl 5-fluorouracil **A2** (0.2 g, 1.0 eq), HOBt (0.5 eq), DMAP (0.03 eq) and 4-(2-((4-chlorobenzyl)amino)ethyl)benzenesulfonamide **A14** (1.1 eq) in dry DMF (2 ml). 65% yield; m.p. 260-262°C; silica gel TLC R_f 0.80 (MeOH/CH_2Cl_2 20 % v/v); δ_H (400 MHz, DMSO-*d*$_6$: 11.86 (s, 1H, exchange with D_2O, CON*H*CO), 8.09 (d, *J* = 6.7 Hz, 0.5H, Ar-*H*), 8.04 (d, *J* = 6.7 Hz, 0.5H, Ar-*H*), 7.81 (d, *J* = 8.2 Hz, 1H, Ar-*H*), 7.77 (d, *J* = 8.2 Hz, 1H, Ar-*H*), 7.53 (d, *J* = 8.2 Hz, 1H, Ar-*H*), 7.50 (d, *J* = 8.4 Hz, 1H, Ar-*H*), 7.42 (m, 3H, Ar-*H*), 7.33 (m, 3H, partially exchange with D_2O, Ar-*H* + SON*H*$_2$), 4.72 (s, 1H, C*H*$_2$), 4.64 (s, 1H, C*H*$_2$), 4.62 (s, 1H, C*H*$_2$), 4.56 (s, 1H, C*H*$_2$), 3.53 (m, 1H, C*H*$_2$), 3.46 (m, 1H, C*H*$_2$), 3.03 (m, 1H, C*H*$_2$), 2.86 (m, 1H, C*H*$_2$); δ_C (100 MHz, DMSO-*d*$_6$): 167.62, 158.48 (d, $J_{2\ CF}$ = 23.7 Hz), 150.72, 143.32, 140.25 (d, $J_{2\ CF}$ = 243.4 Hz), 137.52, 132.86 (d, $J_{2\ CF}$ = 39.0 Hz), 130.52, 130.28, 129.97, 129.59, 129.32, 126.78, 50.03 (d, $J_{2\ CF}$ = 41.8 Hz), 49.20 (d, $J_{2\ CF}$ = 65.6 Hz), 48.45, 34.20 (d, $J_{2\ CF}$ = 108.8 Hz); δ_F (376 MHz, DMSO-*d*$_6$): -170.59; m/z (ESI negative) calcd for C21H19ClFN4O5S [M-H]$^-$ 493.1, found 493.0.

2-(5-Fluoro-2,4-dioxo-3,4-dihydropyrimidin-1(2H)-yl)-N-(4-fluorobenzyl)-N-(4-sulfamoylphenethyl)acetamide A21

Compound **A21** was obtained according the general procedure earlier reported using1-carboxymethyl 5-fluorouracil **A2** (0.2 g, 1.0 eq), HOBt (0.5 eq), DMAP (0.03 eq) and 4-(2-((4-fluorobenzyl)amino)ethyl)benzenesulfonamide **A15** (1.1 eq) in dry DMF (2 ml). 65% yield; m.p. 257-259°C; silica gel TLC R_f 0.83 (MeOH/CH_2Cl_2 20 % v/v); δ_H (400 MHz, DMSO-*d*$_6$): 11.91

(s, 1H, exchange with D_2O, CONHCO), 8.08 (d, *J* = 6.8 Hz, 0.5H, Ar-*H*), 8.02 (d, *J* = 6.7 Hz, 0.5H, Ar-*H*), 7.80 (d, *J* = 8.2 Hz, 1H, Ar-*H*), 7.77 (d, *J* = 8.2 Hz, 1H, Ar-*H*), 7.52 (d, *J* = 8.2 Hz, 1H, Ar-*H*), 7.32 (m, 7H, partially exchange with D_2O, Ar-*H* + $SONH_2$), 4.70 (s, 1H, CH_2), 4.66 (s, 1H, CH_2), 4.59 (s, 1H, CH_2), 4.55 (s, 1H, CH_2), 3.48 (m, 2H, CH_2), 3.01 (m, 1H, CH_2), 2.84 (m, 1H, CH_2); δ_C (100 MHz, DMSO-d_6): 167.55, 158.65 (d, $J_{2\ CF}$ = 14.0 Hz), 150.73, 143.99, 143.26 (d, $J_{2\ CF}$ = 22.8 Hz), 140.23 (d, $J_{2\ CF}$ = 212.0 Hz), 132.00 (d, $J_{2\ CF}$ = 40.0 Hz), 130.72 (d, $J_{2\ CF}$ = 7.9 Hz), 130.27, 129.98, 126.79, 116.53, 116.01, 50.04 (d, $J_{2\ CF}$ = 34.5 Hz), 49.12 (d, $J_{2\ CF}$ = 77.7 Hz), 48.28, 34.18 (d, $J_{2\ CF}$ = 112.8 Hz); δ_F (376 MHz, DMSO-d_6): -115.29, -170.13; m/z (ESI negative) calcd for $C_{21}H_{19}F_2N_4O_5S$ $[M-H]^-$ 477.1, found 477.2.

2-(5-Fluoro-2,4-dioxo-3,4-dihydropyrimidin-1(2H)-yl)-N-(4-methoxybenzyl)-N-(4-sulfamoylphenethyl)acetamide A22

Compound **A22** was obtained according the general procedure earlier reported using1-carboxymethyl 5-fluorouracil **A2** (0.2 g, 1.0 eq), HOBt (0.5 eq), DMAP (0.03 eq) and 4-(2-((4-methoxybenzyl)amino)ethyl)benzenesulfonamide **A16** (1.1 eq) in dry DMF (2 ml). 69% yield; m.p. 210-212°C; silica gel TLC R_f 0.63 ($MeOH/CH_2Cl_2$ 20 % v/v); δ_H (400 MHz, DMSO-d_6): 11.88 (s, 1H, exchange with D_2O, CONHCO), 8.07 (d, *J* = 6.8 Hz, 0.5H, Ar-*H*), 8.00 (d, *J* = 6.7 Hz, 0.5H, Ar-*H*), 7.77 (d, *J* = 8.2 Hz, 1H, Ar-*H*), 7.74 (d, *J* = 8.2 Hz, 1H, Ar-*H*), 7.48 (d, *J* = 8.2 Hz, 1H, Ar-*H*), 7.35 (d, *J* = 8.2 Hz, 1H, Ar-*H*), 7.29 (s, 2H, exchange with D_2O, SO_2NH_2), 7.28 (d, *J* = 8.2 Hz, 1H, Ar-*H*), 7.21 (d, *J* = 8.5 Hz, 1H, Ar-*H*), 6.96 (d, *J* = 8.6 Hz, 1H Ar-*H*), 6.90 (d, *J* = 8.6 Hz, 1H, Ar-*H*), 4.65 (s, 2H, CH_2), 4.48 (s, 1H, CH_2), 4.46 (s, 1H, CH_2), 3.76 (s, 1.5H, CH_2), 3.74 (s, 1.5H, CH_2), 3.44 (m, 2H, CH_2), 2.96 (m, 1H, CH_2), 2.79 (m, 1H, CH_2); δ_C (100 MHz, DMSO-d_6): 167.45, 159.75 (d, $J_{2\ CF}$ = 8.6 Hz), 150.86, 144.20, 143.53 (d, $J_{2\ CF}$ = 9.2 Hz), 143.26, 135.71 (d, $J_{2\ CF}$ = 243.0 Hz), 130.39, 130.11, 129.73, 126.92, 115.18, 114.94, 56.13, 49.79 (d, $J_{2\ CF}$ = 31.0 Hz), 48.73, 48.17 (d, $J_{2\ CF}$ = 21.2 Hz), 34.31 (d, $J_{2\ CF}$ = 104.7 Hz); δ_F (376 MHz, DMSO-d_6): -170.66; m/z (ESI negative) calcd for $C_{22}H_{22}FN_4O_6S$ $[M-H]^-$ 489.1, found 489.0.

N-(4-Cyanobenzyl)-2-(5-fluoro-2,4-dioxo-3,4-dihydropyrimidin-1(2H)-yl)-N-(4-sulfamoylphenethyl)acetamide A23

Compound **A23** was obtained according the general procedure earlier reported using1-carboxymethyl 5-fluorouracil **A2** (0.2 g, 1.0 eq), HOBt (0.5 eq), DMAP (0.03 eq) and 4-(2-((4-cyanobenzyl)amino)ethyl)benzenesulfonamide **A17** (1.1 eq) in dry DMF (2 ml). 43% yield; m.p. 230-232°C; silica gel TLC R_f 0.60 (MeOH/CH_2Cl_2 20 % v/v); δ_H (400 MHz, DMSO-d_6): 11.92 (s, 1H, exchange with D_2O, CON*H*CO), 8.02 (d, *J* = 6.7 Hz, 0.5H, Ar-*H*), 7.99 (d, *J* = 6.7 Hz, 0.5H, Ar-*H*), 7.86 (d, *J* = 8.2 Hz, 1H, Ar-*H*), 7.74 (m, 3H, Ar-*H*), 7.49 (m, 3H, Ar-*H*), 7.43 (d, *J* = 8.1 Hz, 1H, Ar-*H*), 7.36 (d, *J* = 8.2 Hz, 1H, Ar-*H*), 7.27 (s, 2H, exchange with D_2O, SO_2NH_2), 4.70 (s, 2H, CH_2), 4.62 (s, 1H, CH_2), 4.56 (s, 1H, CH_2), 3.53(m, 1H, CH_2), 3.44 (m, 1H, CH_2), 2.98 (m, 1H, CH_2), 2.82 (m, 1H, CH_2); δ_C (100 MHz, DMSO-d_6): 167.99, 158.68 (d, $J_{2\ CF}$ = 35.5 Hz), 150.86, 144.59, 143.92 (d, $J_{2\ CF}$ = 14.9 Hz), 140.33 (d, $J_{2\ CF}$ = 258.6 Hz), 133.70, 133.42, 130.46, 129.37, 126.91, 119.91, 111.00, 50.40 (d, $J_{2\ CF}$ = 96.5 Hz), 49.65, 49.01 (d, $J_{2\ CF}$ = 8.1 Hz), 34.35 (d, $J_{2\ CF}$ = 111.3 Hz); δ_F (376 MHz, DMSO-d_6): -170.34; m/z (ESI negative) calcd for C22H19FN5O5S $[M-H]^-$ 484.1, found 484.2.

N-(4-(Dimethylamino)benzyl)-2-(5-fluoro-2,4-dioxo-3,4-dihydropyrimidin-1(2H)-yl)-N-(4-sulfamoylphenethyl)acetamide A24

Compound **A24** was obtained according the general procedure earlier reported using1-carboxymethyl 5-fluorouracil **A2** (0.2 g, 1.0 eq), HOBt (0.5 eq), DMAP (0.03 eq) and 4-(2-((4-(dimethylamino)benzyl)amino)ethyl)benzenesulfonamide **A18** (1.1 eq) in dry DMF (2 ml). 28% yield; m.p. 188-190°C; silica gel TLC R_f 0.78 (MeOH/CH_2Cl_2 20 % v/v); δ_H (400 MHz, DMSO-d_6): 11.93 (s, 1H, exchange with D_2O, CON*H*CO), 9.24 (s, 1H, Ar-*H*), 7.82 (d, *J* = 7.7 Hz, 2H, Ar-*H*), 7.47 (d, *J* = 8.1 Hz, 2H, Ar-*H*), 7.36 (m, 4H, partially exchange with D_2O, Ar-*H* + SONH_2), 6.77 (d, *J* = 7.5 Hz, 2H, Ar-*H*), 4.68 (s, 1H, CH_2), 4.43 (s, 1H, CH_2), 4.06 (s, 2H, CH_2), 3.11 (s, 2H, CH_2), 2.95 (s, 6H, 2 x CH_3), 2.90 (m, 1H, CH_2), 2.79 (m, 1H, CH_2); δ_C (100 MHz, DMSO-d_6): 167.27, 151.79, 150.80 (d, $J_{2\ CF}$ = 13.9 Hz), 143.79, 143.37 (d, $J_{2\ CF}$ = 20.3 Hz), 142.47, 138.05 (d, $J_{2\ CF}$ = 215.0 Hz), 132.16, 130.21, 127.05, 126.88, 119.52, 113.05, 50.82, 49.86 (d, $J_{2\ CF}$ = 36.8 Hz), 48.47 (d, $J_{2\ CF}$ = 58.6 Hz), 47.56, 33.01 (d, $J_{2\ CF}$ = 160.3 Hz); δ_F (376 MHz, DMSO-d_6): -170.70; m/z (ESI negative) calcd for C23H25FN5O5S $[M-H]^-$ 502.2, found 502.1.

General synthetic procedure of azides.

The proper amine **A3, A4, A28, A29** and **A38** (0.5 g, 1.0 eq) was dissolved in a 2M HCl aqueous solution (5 ml). $NaNO_2$ (1.2 eq) was slowly added at 0°C and the reaction mixture was stirred at the same temperature for 0.5h. Thereafter NaN_3 (1.5 eq) was added portion-wise and the mixture was stirred at r.t. for 0.5h. The obtained precipitate was filtered-off and washed with water to afford the corresponding azides **A30-A33** and **A42**.

4-Azido-benzenesulfonamide A30

Compound **A30** was obtained according the general procedure earlier reported 4-aminobenzenesulfonamide **A3** (0.5 g, 1.0 eq), $NaNO_2$ (1.2 eq) and NaN_3 (1.5 eq) in a HCl 2M aqueous solution. 63% yield; m.p. 120-121°C; silica gel TLC *Rf* 0.47 (EtOAc/*n*-hexane 50 % *v/v*); δ_H (400 MHz, DMSO-d_6): 7.33 (d, *J* = 8.8, 2H, Ar), 7.41 (s, 2H, exchange with D_2O, SO_2NH_2), 7.87 (d, *J* = 8.8, 2H, Ar); δ_C (100 MHz, DMSO-d_6): 120.5, 128.6, 141.5, 143.9; m/z (ESI negative) calcd for C6H5N4O2S $[M-H]^-$ 197.0, found 197.1.

3-Azido-benzenesulfonamide A31

Compound **A31** was obtained according the general procedure earlier reported 3-aminobenzenesulfonamide **A4** (0.5 g, 1.0 eq), $NaNO_2$ (1.2 eq) and NaN_3 (1.5 eq) in a HCl 2M aqueous solution. 60% yield; m.p. 110°C; silica gel TLC *Rf* 0.35 (EtOAc/*n*-hexane 50 % *v/v*); δ_H (400 MHz, DMSO-d_6): 7.37 (m, 2H, Ar-*H*), 7.48 (s, 2H, exchange with D_2O, SO_2NH_2), 7.52 (s, 1H, Ar-*H*), 7.63 (m, 1H, Ar-*H*); δ_C (100 MHz, DMSO-d_6): 117.2, 123.1, 123.5, 131.8, 141.4, 146.9; m/z (ESI negative) calcd for C6H5N4O2S $[M-H]^-$ 197.0, found 197.1.

4-Azido-3-chlorobenzenesulfonamide A32

Compound **A32** was obtained according the general procedure earlier reported 4-amino-3-chlorobenzenesulfonamide **A28** (0.5 g, 1.0 eq), $NaNO_2$ (1.2 eq) and NaN_3 (1.5 eq) in a HCl 2M aqueous solution. 65% yield; m.p. 140-142°C; silica gel TLC *Rf* 0.38 (MeOH/CH_2Cl_2 10 % v/v); δ_H (400 MHz, DMSO-d_6): 8.23 (s, 1H, Ar-*H*), 7.63 (d, *J* = 8.8, 1H, Ar-*H*), 7.43 (d, *J* = 8.6, 1H, Ar-*H*), 7.23 (s, 2H, exchange with D_2O, SO_2NH_2); δ_C (100 MHz, DMSO-d_6): 141.1, 134.6, 130.5, 126.6, 125.4, 105.9; m/z (ESI negative) calcd for C6H4ClN4O2S $[M-H]^-$ 231.0, found 230.9.

4-Azido-3-bromobenzenesulfonamide A33

Compound **A33** was obtained according the general procedure earlier reported 4-amino-3-bromobenzenesulfonamide **A29** (0.5 g, 1.0 eq), $NaNO_2$ (1.2 eq) and NaN_3 (1.5 eq) in a HCl 2M aqueous solution. 70% yield; m.p. 154-156°C; silica gel TLC *Rf* 0.29 (MeOH/CH_2Cl_2 10 % v/v); δ_H (400 MHz, DMSO-d_6): 8.18 (s, 1H, Ar-*H*), 7.73 (d, *J* = 8.8, 1H, Ar-*H*), 7.38 (d, *J* = 8.6, 1H, Ar-*H*), 7.23 (s, 2H, exchange with D_2O, SO_2NH_2); δ_C (100 MHz, DMSO-d_6): 141.9, 134.8, 131.3, 129.5, 126.3, 117.7; m/z (ESI negative) calcd for C6H4BrN4O2S $[M-H]^-$ 274.9, found 274.8.

7-Azido-4-methyl-chromen-2-one A42

Compound **A42** was obtained according the general procedure earlier reported 7-amino-4-methyl-chromen-2-one **A38** (0.5 g, 1.0 eq), $NaNO_2$ (1.2 eq) and NaN_3 (1.5 eq) in a HCl 2M aqueous solution. 88% yield; m.p. 122-124°C; silica gel TLC R_f0.57 (EtOAc/*n*-hexane 20 % *v/v*); δ_H (400 MHz, DMSO-d_6): 7.83 (d, *J* = 8.4, 1H, Ar-*H*), 7.18 (m, 2H, Ar-*H*), 6.38 (d, *J* = 1.2, 1H, Ar-*H*), 2.46 (d, *J* = 1.2, 3H, CH_3); δ_C(100 MHz, DMSO-d_6): 160.4, 155.0, 153.8, 144.2, 127.9, 117.7, 116.5, 114.1, 107.7, 19.0; m/z (ESI positive) calcd for C10H8N3O2 $[M-H]^-$ 202.1, found 202.0.

Synthesis of 5-fluoro-1-(prop-2-yn-1-yl)pyrimidine-2,4(1H,3H)-dione A27

Propargyl bromide (1.0 eq) was added dropwise to a solution of 5-fluorouracil **A1** (0.5 g, 1.0 eq) and DBU (1.0 eq) in dry CH_3CN (7 ml) at 0°C under a nitrogen atmosphere. The reaction mixture was refluxed for 1.5h, then quenched with $HCl_{(aq)}$ 1M (15 ml) and extracted with EtOAc (25 ml). The organic layer was dried over Na_2SO_4, filtered-off and concentrated under *vacuo* to give a residue that was purified by silica gel coloumn chromatography eluting with 40 % EtOAc in *n*-hexane to afford the title compound **7** as white solid. 63% yield; m.p. 140-142°C; silica gel TLC R_f 0.20 (EtOAc/*n*-hexane 40 % v/v); δ_H (400 MHz, DMSO-d_6): 11.92 (s, 1H, exchange with D_2O, CONHCO), 8.17 (d, *J* = 6.6 Hz, 1H, Ar-*H*), 4.49 (d, *J* = 2.3 Hz, 2H, CH_2), 3.48 (t, *J* = 2.3 Hz, 1H, C*H*); δ_C (100 MHz, DMSO-d_6): 158.40 (d, $J_{2\ CF}$ = 25.9 Hz), 150.12, 140.87 (d, $J_{2\ CF}$ = 230.5 Hz), 129.96 (d, $J_{2\ CF}$ = 33.9 Hz), 79.18, 77.18, 38.05; δ_F (376 MHz, DMSO-d_6): -168.41; m/z (ESI negative) calcd for C7H4FN2O2 $[M-H]^-$ 167.0, found 167.1.

General synthetic procedure of triazoles A34-A37 and A43.

The proper azide **A30-A33** and **A42** (1.1 eq) was added to a solution of propargyl derivate **A27** (0.1 g, 1.0 eq) in H_2O/tBuOH 1/1 (8 ml) at r.t., followed by a suspension of $CuSO_4$ (0.1 eq) and Na ascorbate (0.5 eq) in water (0.5 ml). The reaction mixture was stirred at 40°C overnight, then quenched with H_2O (20 ml) and the formed precipitate was collected by filtration *in vacuo*. A solution of the residue in DMF (4 ml) was filtered-off through Celite521® and then poured on slush (20 ml). The precipitate was filtered *in vacuo* and washed with Et_2O to afford the titled compounds **A34-A37** and **A43** as powders**.**

4-(4-((5-Fluoro-2,4-dioxo-3,4-dihydropyrimidin-1(2H)-yl)methyl)-1H-1,2,3-triazol-1-yl)benzenesulfonamide A34

Compound **A34** was obtained according the general procedure earlier reported using 5-fluoro-1-(prop-2-yn-1-yl)pyrimidine-2,4(1H,3H)-dione **A27** (0.1 g, 1.0 eq), 4-azidobenzenesulfonamide **A30** (1.1 eq), $CuSO_4$ (0.1 eq) and Na ascorbate (0.5 eq) in H_2O/tBuOH 1/1 (8 ml). 73% yield; m.p. >300°C; silica gel TLC R_f 0.20 (MeOH/CH_2Cl_2 10 % v/v); δ_H (400 MHz, DMSO-d_6): 11.94 (s, 1H, exchange with D_2O, CON*H*CO), 8.95 (s, 1H, Ar-*H*), 8.28 (d, *J* = 6.7 Hz, 1H, Ar-*H*), 8.16 (d, *J* = 8.7 Hz, 2H, Ar-*H*), 8.05 (d, *J* = 8.6 Hz, 2H, Ar-*H*), 7.57 (s, 2H, exchange with D_2O, SO_2NH_2), 5.06 (s, 2H, CH_2); δ_C (100 MHz, DMSO-d_6): 158.61 (d, $J_{2\ CF}$ = 25.9 Hz), 150.53, 145.09, 144.98, 140.94 (d, $J_{2\ CF}$ = 225.6 Hz), 139.56, 130.95 (d, $J_{2\ CF}$ = 33.7 Hz), 128.57, 123.00, 121.34, 43.86; δ_F (376 MHz, DMSO-d_6): -168.94; m/z (ESI negative) calcd for C13H10FN6O4S $[M-H]^-$ 365.1, found 365.0.

3-(4-((5-Fluoro-2,4-dioxo-3,4-dihydropyrimidin-1(2H)-yl)methyl)-1H-1,2,3-triazol-1-yl)benzenesulfonamide A35

Compound **A35** was obtained according the general procedure earlier reported using 5-fluoro-1-(prop-2-yn-1-yl)pyrimidine-2,4(1H,3H)-dione **A27** (0.1 g, 1.0 eq), 3-azidobenzenesulfonamide **A31** (1.1 eq), $CuSO_4$ (0.1 eq) and Na ascorbate (0.5 eq) in H_2O/tBuOH 1/1 (8 ml). 67% yield; m.p. 255-257°C; silica gel TLC R_f 0.24 (MeOH/CH_2Cl_2 10 % v/v); δ_H (400 MHz, DMSO-d_6): 11.93 (s, 1H, exchange with D_2O, CON*H*CO), 8.94 (s, 1H, Ar-*H*), 8.39 (s, 1H, Ar-*H*), 8.27 (d, *J* = 6.6 Hz, 1H, Ar-*H*), 8.16 (d, *J* = 7.5 Hz, 1H, Ar-*H*), 7.96 (d, *J* = 7.3 Hz, 1H, Ar-*H*), 7.84 (t, *J* =

7.9 Hz, 1H, Ar-*H*), 7.62 (s, 2H, exchange with D_2O, SO_2NH_2), 5.06 (s, 2H, CH_2); δ_C (100 MHz, DMSO-d_6): 158.55 (d, $J_{2\ CF}$ = 38.3 Hz), 150.55, 146.85, 145.02, 140.86 (d, $J_{2\ CF}$ = 224.8 Hz), 137.70, 131.98, 130.95 (d, $J_{2\ CF}$ = 45.9 Hz), 126.65, 124.15, 123.11, 118.23, 43.85; δ_F (376 MHz, DMSO-d_6): -168.95; m/z (ESI negative) calcd for C13H10FN6O4S $[M-H]^-$ 365.1, found 365.0.

3-Chloro-4-(4-((5-fluoro-2,4-dioxo-3,4-dihydropyrimidin-1(2H)-yl)methyl)-1H-1,2,3-triazol-1-yl)benzenesulfonamide A36

Compound **A36** was obtained according the general procedure earlier reported using 5-fluoro-1-(prop-2-yn-1-yl)pyrimidine-2,4(1H,3H)-dione **A27** (0.1 g, 1.0 eq), 4-azido-3-chlorobenzenesulfonamide **A32** (1.1 eq), $CuSO_4$ (0.1 eq) and Na ascorbate (0.5 eq) in H_2O/tBuOH 1/1 (8 ml). 48% yield; m.p. 276-278°C; silica gel TLC R_f 0.30 (MeOH/CH_2Cl_2 10 % v/v); δ_H (400 MHz, DMSO-d_6): 11.91 (s, 1H, exchange with D_2O, CON*H*CO), 8.70 (s, 1H, Ar-*H*), 8.29 (s, 1H, Ar-*H*), 8.17 (d, *J* = 1.7 Hz, 1H, Ar-*H*), 8.01 (dd, *J* = 8.3, 1.8 Hz, 1H, Ar-*H*), 7.96 (d, *J* = 8.3 Hz, 1H, Ar-*H*), 7.76 (s, 2H, exchange with D_2O, SO_2NH_2), 5.08 (s, 2H, CH_2); δ_C (100 MHz, DMSO-d_6): 158.52 (d, $J_{2\ CF}$ = 37.0 Hz), 150.51, 147.61, 143.75, 140.96 (d, $J_{2\ CF}$ = 233.5 Hz), 137.73, 130.99 (d, $J_{2\ CF}$ = 33.9 Hz), 130.22, 129.97, 128.76, 126.86, 126.66, 43.66; δ_F (376 MHz, DMSO-d_6): -169.03; m/z (ESI negative) calcd for C13H9ClFN6O4S $[M-H]^-$ 399.0, found 399.1 .

3-Bromo-4-(4-((5-fluoro-2,4-dioxo-3,4-dihydropyrimidin-1(2H)-yl)methyl)-1H-1,2,3-triazol-1-yl)benzenesulfonamide A37

Compound **A37** was obtained according the general procedure earlier reported using 5-fluoro-1-(prop-2-yn-1-yl)pyrimidine-2,4(1H,3H)-dione **A27** (0.1 g, 1.0 eq), 4-azido-3-bromobenzenesulfonamide **A33** (1.1 eq), $CuSO_4$ (0.1 eq) and Na ascorbate (0.5 eq) in H_2O/tBuOH 1/1 (8 ml). 45% yield; m.p. 275-277°C; silica gel TLC R_f 0.28 (MeOH/CH_2Cl_2 10 % v/v); δ_H (400 MHz, DMSO-d_6): 11.91 (s, 1H, exchange with D_2O, CON*H*CO), 8.67 (s, 1H, Ar-*H*), 8.30 (s, 2H, Ar-*H*), 8.03 (d, *J* = 7.9 Hz, 1H, Ar-*H*), 7.90 (d, *J* = 8.2 Hz, 1H, Ar-*H*), 7.75 (s, 2H, exchange with D_2O, SO_2NH_2), 5.08 (s, 2H, CH_2); δ_C (100 MHz, DMSO-d_6): 158.58 (d, $J_{2\ CF}$ = 31.9 Hz), 150.49, 147.79, 143.65, 140.83 (d, $J_{2\ CF}$ = 230.1 Hz), 139.47, 131.73, 130.95 (d, J_2

$_{CF}$ = 37.0 Hz), 130.48, 127.10, 126.83, 120.16, 43.63; δ_F (376 MHz, DMSO-d_6): -169.02; m/z (ESI negative) calcd for C13H9BrFN6O4S [M-H]$^-$ 443.0, found 442.9.

5-Fluoro-1-((1-(4-methyl-2-oxo-2H-chromen-7-yl)-1H-1,2,3-triazol-4-yl)methyl)pyrimidine-2,4(1H,3H)-dione A43

Compound **A43** was obtained according the general procedure earlier reported using 5-fluoro-1-(prop-2-yn-1-yl)pyrimidine-2,4(1H,3H)-dione **A27** (0.1 g, 1.0 eq), 7-azido-4-methyl-chromen-2-one **A42** (1.1 eq), $CuSO_4$ (0.1 eq) and Na ascorbate (0.5 eq) in H_2O/tBuOH 1/1 (8 ml). 47% yield; m.p. 282-284°C; silica gel TLC R_f 0.30 (MeOH/CH_2Cl_2 10 % v/v); δ_H (400 MHz, DMSO-d_6): 11.93 (s, 1H, exchange with D_2O, CON*H*CO), 9.00 (s, 1H, Ar-*H*), 8.28 (d, *J* = 6.5 Hz, 1H, Ar-*H*), 8.00 (d, *J* = 9.3 Hz, 3H, Ar-*H*), 6.51 (s, 1H, Ar-*H*), 5.03 (s, 2H, C*H*$_2$), 2.51 (s, 3H, C*H*$_3$); δ_C (100 MHz, DMSO-d_6): 160.43, 158.71 (d, $J_{2\ CF}$ = 22.7 Hz), 154.68, 153.74, 150.53, 143.65 (d, $J_{2\ CF}$ = 311.3 Hz), 139.80, 139.44, 130.99 (d, $J_{2\ CF}$ = 42.8 Hz), 128.27, 122.96, 120.56, 116.45, 115.7, 108.45, 43.87, 19.15; δ_F (376 MHz, DMSO-d_6): -168.91; m/z (ESI negative) calcd for C17H11FN5O4 [M-H]$^-$ 368.1 found 368.0.

Synthesis of 2-(5-fluoro-2,4-dioxo-3,4-dihydropyrimidin-1(2H)-yl)-N-(4-methyl-2-oxo-2H-chromen-7-yl)acetamide A40

EDCI (2.0 eq) was added to a solution of 1-carboxymethyl 5-fluorouracil **A2** (0.2 g, 1.0 eq) and HOBt (0.5 eq) in dry DMF (2 ml) under a nitrogen atmosphere and the reaction mixture was stirred at r.t. until the consumption of the starting material (TLC monitoring). Thereafter 7-amino-4-methylcoumarin **A38** (1.5 eq) was added to the reaction mixture, that was stirred at r.t. until the disappearance of the activated ester was observed (TLC monitoring) and then quenched with ice and $HCl_{(aq)}$ 2M. The collected, water washed precipitate was triturated in MeOH to afford the pure titled compound **A40** as a powder. 24% yield; m.p. 274-276°C; silica gel TLC R_f 0.33 (MeOH/CH_2Cl_2 10 % v/v); δ_H (400 MHz, DMSO-d_6): 11.97 (s, 1H, exchange with D_2O, CON*H*CO), 10.76 (s, 1H, exchange with D_2O, CON*H*), 8.17 (s, 1H, Ar-*H*), 7.78 (s, 1H, Ar-*H*), 7.72 (d, *J* = 1.9 Hz, 1H, Ar-*H*), 7.53 (dd, *J* = 8.7, 2.0 Hz, 1H, Ar-*H*), 6.32 (d, *J* = 1.0 Hz, 1H, Ar-*H*), 4.59 (s, 2H, C*H*$_2$), 2.44 (s, 3H, C*H*$_3$).; δ_C (100 MHz, DMSO-d_6): 167.21, 160.99, 158.58 (d, $J_{2\ CF}$ = 25.8 Hz), 154.73, 154.11, 150.87, 142.78, 140.38 (d, $J_{2\ CF}$ = 228.7 Hz),

132.07 (d, $J_{2\ CF}$ = 33.8 Hz), 127.23, 116.43, 116.19, 113.59, 106.76, 51.43, 19.03; δ_F (376 MHz, DMSO-d_6): -170.35; m/z (ESI negative) calcd for C16H11FN3O5 $[M-H]^-$ 344.1, found 344.0.

Synthesis of 2-oxo-2H-chromen-7-yl 2-(5-fluoro-2,4-dioxo-3,4-dihydropyrimidin-1(2H)-yl)acetate A41

EDCI (2.0 eq) was added to a solution of 1-carboxymethyl 5-fluorouracil **A2** (0.2 g, 1.0 eq) and DMAP (0.03 eq) in dry DMF (2 ml) under a nitrogen atmosphere and the reaction mixture was stirred at r.t. until the consumption of the starting material (TLC monitoring). Thereafter 7-hydroxycoumarin **A39** (1.5 eq) was added to the reaction mixture, that was stirred at r.t. until the disappearance of the 1-carboxymethyl 5-fluorouracil was observed (TLC monitoring) and then quenched with ice and sodium bicarbonate. The collected, water-washed precipitate triturated with ethylacetate to afford the pure titled compound **A41** as a powder. 15% yield; m.p. 270-272°C; silica gel TLC R_f 0.45 ($MeOH/CH_2Cl_2$ 20 % v/v); δ_H (400 MHz, DMSO-d_6): 12.08 (s, 1H, exchange with D_2O, CON*H*CO), 8.17 (d, *J* = 6.7 Hz, 1H, Ar-*H*), 8.09 (d, *J* = 9.6 Hz, 1H, Ar-*H*), 7.80 (dd, *J* = 17.8, 8.5 Hz, 1H, Ar-*H*), 7.30 (s, 1H, Ar-*H*), 7.21 (dd, *J* = 8.5, 2.2 Hz, 1H, Ar-*H*), 6.51 (d, *J* = 9.6 Hz, 1H, Ar-*H*), 4.78 (d, *J* = 32.0 Hz, 2H, C*H*$_2$); δ_C (100 MHz, DMSO-d_6): 167.62, 160.66, 158.47 (d, $J_{2\ CF}$ = 25.8 Hz), 155.16, 153.26, 150.77, 144.80, 140.57 (d, $J_{2\ CF}$ = 230.2 Hz), 131.21 (d, $J_{2\ CF}$ = 34.7 Hz), 130.69, 119.25, 118.16, 116.95, 110.76, 49.85; δ_F (376 MHz, DMSO-d_6): -169.21; m/z (ESI negative) calcd for C15H8FN2O6 $[M-H]^-$ 331.0, found 331.0.

Design, synthesis and biological evaluation of CA inhibitors in complex with stabilizer of G-Quadruplex structures as antitumor drugs. (Series B)

Synthesis of azides and alkynes on various sulfonamides

Synthesis of 4-ethynylbenzenesulfonamide B2

$PdCl_2(PPh_3)_2$ (0.1 eq) and CuI (0.1 eq) were added to a solution of 4-bromobenzenesulfonamide **B1** (0.5 g, 1.0 eq), (trimethylsilyl)acetylene (1.2 eq) and Et_3N (10 eq.) in dry dioxane (5.0 mL) at r.t. under a nitrogen atmosphere. The reaction mixture was stirred at 100°C o.n., then quenched with slush and extracted with EtOAc (2x20ml). The collected organic layers were dried over anhydrous Na_2SO_4, filtered-off and concentrated *in vacuo* to give a residue that was

treated with a 1.0M solution of TBAF in THF (2.0 eq). The reaction mixture stirred at r.t. for 2h and thereafter concentrated under *vacuo*. The obtained residue was purified by silica gel chromatography eluting with 5% MeOH in DCM to afford **B2** as a white solid. 65% yield; silica gel TLC R_f 0.14 (EtOAc/n-Hex 30 % v/v); δ_H (400 MHz, DMSO-d_6): 4.47 (s, 1H, C*H*), 7.49 (s, 2H, exchange with D_2O, SO_2NH_2), 7.71 (d, *J* = 7.8, 2H, Ar), 7.85 (d, *J* = 7.8, 2H, Ar); δ_C (100 MHz, DMSO-d_6): 145.1, 133.1, 126.8, 125.9, 84.3, 83.2.

Synthesis of 4-prop-2-ynyloxy-benzenesulfonamide B4

Propargyl bromide (1.2 eq) was added to a suspension of the 4-hydroxybenzenesulfonamide **B3** (0.5 g, 1.0 eq) and K_2CO_3 (2.0 eq) in dry DMF (4 ml) under a nitrogen atmosphere and that was stirred at 60° for 5h. The obtained suspension was quenched with H_2O (20 ml) and stirred at r.t. o.n. The formed precipitate was filtered-off and purified by silica gel column chromatography eluting with 50 % EtOAc in *n*-hexane to afford **12** as a white solid. 71% yield; m.p. 131-132°C; silica gel TLC R_f 0.47 (EtOAc/*n*-hexane 50 % v/v); δ_H (400 MHz, DMSO-d_6): 3.66 (t, *J* = 2.4, 1H), 4.94 (d, *J* = 2.4, 2H), 7.17 (d, J= 8.8, 2H), 7.26 (s, 2H, exchange with D_2O, SO_2NH_2), 7.80 (d, *J* = 8.8, 2H); δ_C (100 MHz, DMSO-d_6): 160.4, 137.8, 128.6, 115.9, 79.7, 79.6, 56.7.

Synthesis of azides and alkynes on various coumarins

General procedure of azidocoumarins B8-B10

Dibromoalkane (5.0 eq) was added to a suspension of 7-hydroxy-2H-chromen-2-one **A39** (0.2g, 1.0 eq) and K_2CO_3 (2.0 eq) in dry DMF (5 ml) and the reaction mixture was stirred at 60°C until the consumption of the starting material (TLC monitoring). NaN_3 (5 mmol) was added and the reaction mixture was stirred at the same temperature for further 3h, quenched with H_2O and extracted with EtOAc (2x20ml). The combine organic layers were washed with brine (3x15ml), dried over Na_2SO_4, filtered-off, and concentrated *in vacuo* to give B8-B10 as a white powder.

Synthesis of 7-(3-azidopropoxy)-2H-chromen-2-one B8

Compound **B8** was obtained according the general procedure earlier reported using 1-3dibromopropane (5.0 eq), **A39** (0.2g, 1.0 eq) and NaN_3 (5 mmol) in DMF. 54% yield; m.p. 101°-102° C; δ_H (400 MHz, $CDCl_3$): 7.57 (d, *J* = 9.5 Hz, 1H), 7.31 (d, *J* = 8.3 Hz, 1H), 6.86 – 6.67 (m, 2H), 6.19 (d, *J* = 9.5 Hz, 1H), 4.11 (t, *J* = 5.8 Hz, 2H), 3.54 (t, *J* = 6.4 Hz, 2H), 2.29 (p, *J* = 6.1 Hz, 2H). δ_C (100 MHz, $CDCl_3$): 160.84, 160.11, 154.85, 142.32, 127.80, 112.29, 111.73, 100.55, 64.86, 30.95, 28.50.

Synthesis of 7-(4-azidobutoxy)-2H-chromen-2-one B9

Compound **B9** was obtained according the general procedure earlier reported using 1-4dibromobutane (5.0 eq), **A39** (0.2g, 1.0 eq) and NaN_3 (5 mmol) in DMF. 90% yield; silica gel TLC Rf 0.5 (EtOAc/Hex 30% v/v); δH (400MHz, DMSO-d6): 7.96 (d, *J* = 9.5 Hz, 1H, Ar-*H*), 7.59 (d, *J* =8.5 Hz, 1H, Ar-*H*), 6.94 (d, *J* = 2.1 Hz, 1H, Ar-*H*), 6.91 (dd, *J* = 8.5, 2.3 Hz, 1H, Ar-*H*), 6.27 (d, *J* = 9.5 Hz, 1H, Ar-*H*), 4.08 (t, *J* = 6.2 Hz, 2H, CH2), 3.41 (t, *J* = 6.8 Hz, 2H, CH2), 1.86 – 1.74 (m, 2H, CH2), 1.69 (dq, *J* = 9.7, 6.4 Hz, 2H, CH2) δC (100 MHz, DMSO-d6): 162.76, 161.33, 156.44, 145.28, 130.45, 113.68, 113.44, 113.34, 102.12, 68.78, 51.40, 26.75, 26.07.

Synthesis of 7-((5-azidopentyl)oxy)-2H-chromen-2-one B10

Compound **B10** was obtained according the general procedure earlier reported using 1-5dibromopentane (5.0 eq), **A39** (0.2g, 1.0 eq) and NaN_3 (5 mmol) in DMF. 90% yield; silica gel TLC Rf 0.5 (EtOAc/Hex 30% v/v); δH (400MHz, DMSO-d6): 7.98 (d, *J* = 9.5 Hz, 1H, Ar-*H*), 7.61 (d, *J* = 8.5 Hz, 1H, Ar-*H*), 6.96 (s, 1H, Ar-*H*), 6.95 – 6.89 (m, 1H, Ar-*H*), 6.28 (d, *J* = 9.5 Hz, 1H, Ar-*H*), 4.08 (dd, *J*= 11.6, 5.3 Hz, 2H, CH2), 3.36 (t, *J* = 3.3 Hz, 2H, CH2), 1.81 – 1.72 (m, 2H, CH2), 1.65 – 1.56 (m, 2H, CH2), 1.53 – 1.43 (m, 2H, CH2). δC (100 MHz, DMSO-d6): 162.89, 161.35, 156.48, 145.34, 130.49, 113.73, 113.43, 113.31, 102.14, 69.16, 51.63, 31.70, 29.02 (d, J= 1.8 Hz), 23.80.

General procedure of alkynocoumarins B11-B13

Alkynyl bromide (1.2 eq) was added to a solution of 7-hydroxy-2H-chromen-2-one **A39** (1.0 eq, 0,7 g) and K2CO3 (1.2 eq) in dry DMF (3 mL). The reaction mixture was stirred and heated up

to 80°C o.n. The mixture was quenched with slush and the precipitate obtained was filtered and washed with petrolium ether.

Synthesis of 7-(prop-2-yn-1-yloxy)-2H-chromen-2-one B11

Compound **B11** was obtained according the general procedure earlier reported using propargyl bromide (1.2 eq), **A39** (1.0 eq, 0,7 g) and K2CO3 (1.2 eq) in dry DMF (3 mL). 100% yield; m.p. 118°C; silica gel TLC Rf 0.5 (EtOAc/Hex 30% v/v); δH (400MHz, DMSO-d6): 8.01 (t, *J* = 9.4 Hz, 1H, Ar-*H*), 7.68 (d, *J* = 8.6 Hz, 1H, Ar-*H*), 7.07 (d, J = 2.1 Hz, 1H, Ar-*H*), 7.02 (dd, J = 8.6, 2.3 Hz, 1H, Ar-*H*), 6.35 (d, *J* = 9.5 Hz, 1H, Ar-*H*), 4.97 (d, *J* = 2.2 Hz, 2H, CH2), 3.69 (t, *J* = 2.1 Hz, 1H, CH). δC (100 MHz, DMSO-d6): 161.01, 161.25, 156.18, 145.26, 130.56, 114.02, 113.95, 113.92, 102.82, 79.96, 79.56, 57.17.

Synthesis of 7-(but-3-yn-1-yloxy)-2H-chromen-2-one B12

Compound **B12** was obtained according the general procedure earlier reported using 4-bromobut-1-yne (1.2 eq), **A39** (1.0 eq, 0,7 g) and K2CO3 (1.2 eq) in dry DMF (3 mL). 33% yield; m.p. 93°C; silica gel TLC Rf 0.5 (EtOAc/Hex 40% v/v); δH (400MHz, DMSO-d6): 8.03 (d, *J* = 9.5 Hz, 1H, Ar-*H*), 7.66 (d, *J* = 8.6 Hz, 1H, Ar-*H*), 7.03 (t, *J* = 3.9 Hz, 1H, Ar-*H*), 7.00 (dd, *J* = 8.6, 2.3 Hz, 1H, Ar-*H*), 6.33 (d, *J* = 9.5 Hz, 1H, Ar-*H*), 4.21 (t, *J* = 6.4 Hz, 2H, CH2), 2.71 (td, *J*= 6.3, 2.6 Hz, 2H, CH2). δC (100 MHz, DMSO-d6): 162.38, 161.32, 161.01, 156.42, 145.35, 130.60, 113.76, 113.69, 113.60, 102.36, 82.21, 73.61, 67.51, 19.79.

Synthesis of 7-(pent-4-yn-1-yloxy)-2H-chromen-2-one B13

Compound **B13** was obtained according the general procedure earlier reported using 5-bromopent-1-yne (1.2 eq), **A39** (1.0 eq, 0,7 g) and K2CO3 (1.2 eq) in dry DMF (3 mL). 86% yield; m.p. 103°C; silica gel TLC Rf 0.5 (EtOAc/Hex 30% v/v); δH (400MHz, DMSO-d6): 7.99 (t, *J* = 11.2 Hz, 1H, Ar *H*), 7.64 (d, *J* = 8.5 Hz, 1H, Ar-*H*), 7.00 (d, *J* = 1.9 Hz, 1H, Ar-*H*), 6.97 (dd, *J* = 8.6, 2.2 Hz, 1H, Ar-*H*), 6.31 (d, *J* = 9.5 Hz, 1H; CH), 4.17 (t, *J* = 6.1 Hz, 2H; CH2), 2.38 (td, *J* = 7.0, 2.4 Hz, 2H, CH2), 2.01 – 1.90 (m, 2H, CH2). δC (100 MHz, DMSO-d6): 162.70, 161.34, 161.01, 156.44, 145.34, 130.55, 113.68, 113.55, 113.44, 102.22, 84.55, 72.79, 67.81, 28.54, 15.50.

Synthesis of azides and alkynes on berberine scaffold.

Synthesis of berberrubine 14

Berberine hydrochloride (5.0g) was heated at 190°C under *vacuum* (20-30mm Hg) for 2h to obtain berberrubine **14** as a dark red solid; 90% yield; m.p. >300° C; silica gel TLC R_f 0.25 (MeOH/DCM 10% *v/v)*; δ_H (400 MHz, DMSO-d_6): 9.11 (s, 1H, Ar-*H*), 8.02 (s, 1H, Ar-*H*), 7.65 (s, 1H, Ar-*H*), 7.24 (d, *J* = 7.9 Hz, 1H, Ar-*H*), 7.00 (s, 1H, Ar-*H*), 6.38 (d, *J* = 7.8 Hz, 1H, Ar-*H*), 6.13 (s, 2H, CH_2), 4.51 (t, *J* = 5.9 Hz, 2H, CH_2), 3.76 (s, 3H, CH_3), 3.07 (t, *J* = 5.9 Hz, 2H, CH_2). δ_C (100 MHz, DMSO-d_6): 162.7, 149.6, 149.4, 148.0, 145.8, 134.0, 132.2, 129.2, 122.5, 121.4, 120.1, 118.2, 107.7, 106.9, 104.3, 101.8, 55.2, 54.1, 27.5.

General procedure for berberine azides B19-B22

The proper dibromoalkane (20.0 eq) was added to a solution of berberrubine (1.0 g, 1.0 eq) in dry DMF (10ml) and the reaction mixture was heated for at 60° o.n. The resulting suspension was treated with Et_2O (35ml) and the obtained precipitate was filtered-off and washed with further Et_2O. The crude (bromoalkyl)berberine (0.5 g, 1.0 eq) was dissolved in dry DMF (5ml) and NaN_3 (10.0 eq) was added. The mixture was stirred at 60° o.n., quenched with water and extracted with DCM (2x30ml). The combined organic layers were dried over anhydrous Na_2SO_4, filtered-off, concentrated *in vacuo* and triturated with Et_2O (30ml). The resulting solid was filtered and washed with additional Et_2O to afford the title compounds a red powder.

9-(2-Azidoethoxy)-10-methoxy-5,6-dihydro-[1,3]dioxolo[4,5-g]isoquinolino[3,2-a]isoquinolin-7-ium bromide B19

Compound **B19** was obtained according to general procedure previously reported using berberrubine (1.0 g, 1.0 eq), 1,2-dibromoethane (20.0 eq) and NaN_3 (10.0 eq). 72% yield; m.p. 215°-217° C; silica gel TLC R_f 0.50 (MeOH/DCM 10% *v/v)*; δ_H (400 MHz, DMSO-d_6): 9.85 (s, 1H, Ar-*H*), 8.98 (s, 1H, Ar-*H*), 8.25 (d, *J* = 9.2 Hz, 1H, Ar-*H*), 8.05 (d, *J* = 9.1 Hz, 1H, Ar-*H*), 7.84 (s, 1H, Ar-*H*), 7.13 (s, 1H, Ar-*H*), 6.21 (s, 2H, CH_2), 4.97 (t, *J* = 6.1 Hz, 2H, CH_2), 4.48 (m, 2H, CH_2), 4.11 (s, 3H, CH_3), 3.88 (m, 2H, CH_2), 3.25 (m, 2H, CH_2). δ_C (100 MHz, DMSO-d_6): 151.25, 150.79, 148.62, 146.15, 143.03, 138.46, 133.95, 131.58, 127.53, 124.77, 122.42, 121.32, 121.17, 109.34, 106.36, 103.02, 73.48, 58.02, 56.32, 51.50, 27.28.

9-(3-Azidopropoxy)-10-methoxy-5,6-dihydro-[1,3]dioxolo[4,5-g]isoquinolino[3,2-a]isoquinolin-7-ium bromide B20

Compound **B20** was obtained according to general procedure previously reported using berberrubine (1.0 g, 1.0 eq), 1,3-dibromopropane (20.0 eq) and NaN_3 (10.0 eq). 79% yield; m.p. 239-242° C; silica gel TLC R_f 0.50 (MeOH/DCM 10% *v/v*); δ_H (400 MHz, DMSO-d_6): 9.84 (s, 1H, Ar-*H*), 8.99 (s, 1H, Ar-*H*), 8.25 (d, *J* = 9.1 Hz, 1H, Ar-*H*), 8.05 (d, *J* = 9.1 Hz, 1H, Ar-*H*), 7.84 (s, 1H, Ar-*H*), 7.14 (s, 1H, Ar-*H*), 6.22 (s, 2H, CH_2), 4.99 (t, *J* = 5.9 Hz, 2H, CH_2), 4.41 (t, *J* = 6.2 Hz, 2H, CH_2), 4.11 (s, 3H, CH_2), 3.71 (t, *J* = 6.7 Hz, 2H, CH_2), 3.26 (t, *J* = 6.0 Hz, 2H, CH_2), 2.19 (m, 2H, CH_2). δ_C (100 MHz, DMSO-d_6): 151.25, 150.78, 148.63, 146.20, 143.49, 138.44, 133.98, 131.63, 127.62, 124.47, 122.46, 121.37, 121.16, 109.35, 106.38, 103.03, 72.42, 58.04, 56.24, 48.72, 29.97, 27.27.

9-(4-Azidobutoxy)-10-methoxy-5,6-dihydro-[1,3]dioxolo[4,5-g]isoquinolino[3,2-a]isoquinolin-7-ium bromide B21

Compound **B21** was obtained according to general procedure previously reported using berberrubine (1.0 g, 1.0 eq), 1,4-dibromobutane (20.0 eq) and NaN_3 (10.0 eq). 72% yield; m.p. 216-218° C; silica gel TLC R_f 0.50 (MeOH/DCM 10% *v/v*); δ_H (400 MHz, DMSO-d_6): 9.80 (s, 1H, Ar-*H*), 8.97 (s, 1H, Ar-*H*), 8.23 (d, *J* = 9.2 Hz, 1H, Ar-*H*), 8.03 (d, *J* = 9.1 Hz, 1H, Ar-*H*), 7.83 (s, 1H, Ar-*H*), 7.12 (s, 1H, Ar-*H*), 6.21 (s, 2H, CH_2), 4.98 (t, *J* = 6.1 Hz, 2H, CH_2), 4.34 (t, *J* = 6.4 Hz, 2H, CH_2), 4.09 (s, 3H, CH_3), 3.50 (t, *J* = 6.8 Hz, 2H, CH_2), 3.24 (m, 2H, CH_2), 1.96 (dd, *J* = 14.7, 6.5 Hz, 2H, CH_2), 1.84 (m, 2H, CH_2). δ_C (100 MHz, DMSO-d_6): 151.32, 150.77, 148.62, 146.21, 143.70, 138.39, 133.98, 131.60, 127.62, 124.34, 122.55, 121.37, 121.16, 109.34, 106.36, 103.02, 74.68, 58.00, 56.25, 51.45, 27.75, 27.29, 25.87.

9-((5-Azidopentyl)oxy)-10-methoxy-5,6-dihydro-[1,3]dioxolo[4,5-g]isoquinolino[3,2-a]isoquinolin-7-ium bromide B22

Compound **B22** was obtained according to general procedure previously reported using berberrubine (1.0 g, 1.0 eq), 1,5-dibromopentane (20.0 eq) and NaN_3 (10.0 eq). 72% yield; m.p. 219-222° C; silica gel TLC R_f 0.35 (MeOH/DCM 10% *v/v*); δ_H (400 MHz, DMSO-d_6): 9.80 (s, 1H, Ar-*H*), 8.98 (s, 1H, Ar-*H*), 8.24 (d, *J* = 9.2 Hz, 1H, Ar-*H*), 8.03 (d, *J* = 9.1 Hz, 1H, Ar-*H*),

7.84 (s, 1H, Ar-*H*), 7.13 (s, 1H, Ar-*H*), 6.21 (s, 2H, CH_2), 4.99 (t, *J* = 6.1 Hz, 2H, CH_2), 4.33 (t, *J* = 6.6 Hz, 2H, CH_2), 4.09 (s, 3H, CH_2), 3.43 (t, *J* = 6.7 Hz, 2H, CH_2), 3.30 – 3.16 (m, 2H, CH_2), 1.95 (m, 2H, CH_2), 1.69 (dd, *J* = 13.8, 6.9 Hz, H), 1.60 (m, 2H, CH_2). δ_C (100 MHz, DMSO-d_6): 151.33, 150.74, 148.60, 146.18, 143.78, 138.34, 133.97, 131.57, 127.58, 124.28, 122.57, 121.35, 121.14, 109.32, 106.35, 103.01, 74.98, 57.98, 56.25, 51.58, 29.93, 28.97, 27.29, 23.54.

Synthesis of 10-methoxy-9-(prop-2-yn-1-yloxy)-5,6-dihydro-[1,3]dioxolo[4,5-g]isoquinolino[3,2-a]isoquinolin-7-ium bromide B23

Propargyl bromide (0.111g, 2.0 eq) was added to a solution of berberrubine **14** (0.250g, 1.0 eq) in dry DMF (2ml) and the reaction mixture was stirred at 60°C o.n. and thereafter treated with Et_2O. The formed precipitate was filtered and purified by silica gel column chromatography eluting with MeOH/DCM 10% to afford **B23** as a yellow powder. 49% yield; m.p. >300° C; silica gel TLC R_f 0.52 (MeOH/DCM 10% *v/v)*; δ_H (400 MHz, DMSO-d_6): 9.91 (s, 1H, Ar-*H*), 9.00 (s, 1H, Ar-*H*), 8.27 (d, *J* = 9.2 Hz, 1H, Ar-*H*), 8.09 (d, *J* = 9.1 Hz, 1H, Ar-*H*), 7.84 (s, 1H, Ar-*H*), 7.14 (s, 1H, Ar-*H*), 6.22 (s, 2H, CH_2), 5.13 (d, *J* = 2.1 Hz, 2H, CH_2), 5.00 (t, *J* = 6.0 Hz, 2H, CH_2), 4.12 (s, 3H, CH_3), 3.65 (s, 1H, C*H*), 3.25 (m, 2H, CH_2). δ_C (100 MHz, DMSO-d_6): 151.20, 150.38, 148.19, 145.82, 141.19, 138.92, 133.42, 131.22, 127.03, 124.76, 122.58, 120.90, 120.79, 108.92, 105.96, 102.60, 80.30, 79.26, 61.44, 57.65, 55.79, 26.82.

10-Methoxy-9-(pent-4-yn-1-yloxy)-5,6-dihydro-[1,3]dioxolo[4,5-g]isoquinolino[3,2-a]isoquinolin-7-ium bromide B24

5-bromo-1-pentyne (2.0 eq) was added to a solution of berberrubine (1.0 eq, 0.5 g) and KI (1.2 eq) in dry DMF (3 mL). The reaction mixture was stirred and heated up to 60° o.n. The suspension was treated with Et2O and the obtained precipitate was filtered-off. 90% yield; m.p. 250°C; silica gel TLC Rf 0.36 (MeOH/DCM 5% v/v); δH (400MHz, DMSO-d6): 9.83 (s, 1H, Ar-*H*), 9.01 (s, 1H, Ar-*H*), 8.24 (d, *J* = 9.1 Hz, 1H, Ar-*H*), 8.04 (d, *J* = 9.1 Hz, 1H, Ar-*H*), 7.84 (s, 1H, Ar-*H*), 7.13 (s, 1H, Ar-*H*), 6.21 (d, *J* = 5.9 Hz, 2H, CH2), 4.99 (m, 2H, CH2), 4.41 (t, *J* = 6.3 Hz, 2H, CH2), 4.10 (s, 3H, CH3), 3.25 (m, 2H, CH2), 2.91 (m, 1H, CH), 2.53 (d, *J* = 6.5 Hz, 2H, CH2), 2.09 (m, 2H, CH2). δC (100 MHz, DMSO-d6): 151.00, 151.13, 148.75, 146.72,

143.98, 138.91, 134.37 – 133.84, 131.75, 127.78, 124.47, 122.90, 121.72, 121.34, 109.49, 106.50, 103.19, 84.99, 73.96, 72.79, 58.17, 56.40, 29.58, 27.38, 15.65.

Synthesis of benzensulfonamide-triazoles B25-B34

General procedure: Cu(I) catalysed azide-alkyne Huisgen cycloaddition reactions B25-B34

The appropriate alkyne (1.0-1.2 eq) was added to a suspension of azide (1.0-2.0 eq) in H_2O/t-BuOH 1/1 at r.t., followed by a suspension of $CuSO_4 \bullet 5H_2O$ (0.2 eq) and sodium ascorbate (0.7 eq) in H_2O. The suspension was stirred at 40°C for 24h, then quenched with KPF_6 1M acqueous solution (6.0 eq) and extracted with DCM. The organic layers were concentrated *in vacuo* and triturated with EtOAc to afford the title triazole derivative as a yellow-brown powder.

10-Methoxy-9-(2-(4-(4-sulfamoylphenyl)-1H-1,2,3-triazol-1-yl)ethoxy)-5,6-dihydro-[1,3]dioxolo[4,5-g]isoquinolino[3,2-a]isoquinolin-7-ium hexafluorophosphate(V) B25

Azide **B19** (1.0 eq, 0,2g) was added to a suspension of alkyne **B2** (1.0-2-0 eq) in H2O/t-BuOH 1/1 (12 mL) at r.t., followed by a suspension of CuSO4·5H2O (0.2 eq) and sodium ascorbate (0.7 eq) in H2O and it works as describe in general procedure to obtain the compounds **B25.** 59% yield; m.p. 212-215° C; silica gel TLC R_f 0.55 (MeOH/DCM 10% *v/v)*; δ_H (400 MHz, DMSO-d_6): 9.62 (s, 1H, Ar-*H*), 8.94 (s, 2H, Ar-*H*), 8.20 (s, 1H, Ar-*H*), 8.06 (s, 3H, Ar-*H*), 7.94 (s, 2H, Ar-*H*), 7.80 (s, 1H, Ar-*H*), 7.45 (s, 2H, exchange with D_2O, SO_2NH_2), 7.11 (s, 1H, Ar-*H*), 6.21 (s, 2H, CH_2), 5.04 (s, 2H, CH_2), 4.85 (s, 4H, 2 x CH_2), 4.04 (s, 3H, CH_3), 3.19 (s, 2H, CH_2). δ_C (100 MHz, DMSO-d_6): 151.03, 150.82, 148.65, 146.22, 145.88, 144.10, 142.67, 138.40, 134.64, 133.80, 131.43, 127.44, 127.38, 126.30, 124.83, 124.20, 122.25, 121.20, 121.05, 109.34, 106.31, 103.01, 72.89, 57.93, 56.35, 51.19, 27.17.

10-Methoxy-9-(2-(4-((4-sulfamoylphenoxy)methyl)-1H-1,2,3-triazol-1-yl)ethoxy)-5,6-dihydro-[1,3]dioxolo[4,5-g]isoquinolino[3,2-a]isoquinolin-7-ium hexafluorophosphate(V) B26

Azide **B19** (1.0 eq, 0,2g) was added to a suspension of alkyne **B4** (1.0-2-0 eq) in H2O/t-BuOH 1/1 (12 mL) at r.t., followed by a suspension of CuSO4·5H2O (0.2 eq) and sodium ascorbate (0.7 eq) in H2O and it works as describe in general procedure to obtain the compounds **B26.** 63% yield; m.p. 183-185° C; silica gel TLC R_f 0.56 (MeOH/DCM 10% *v/v)*; δ_H (400 MHz,

DMSO-d_6) : 9.52 (s, 1H, Ar-*H*), 8.94 (s, 1H, Ar-*H*), 8.46 (s, 1H, Ar-*H*), 8.20 (d, *J* = 8.8 Hz, 1H, Ar-*H*), 8.02 (d, *J* = 8.5 Hz, 1H, Ar-*H*), 7.82 (s, 1H, Ar-*H*), 7.76 (d, *J* = 8.5 Hz, 2H, Ar-*H*), 7.27 (s, 2H, exchange with D_2O, SO_2NH_2), 7.17 (d, *J* = 8.4 Hz, 2H, Ar-*H*), 7.13 (s, 1H, Ar-*H*), 6.22 (s, 2H, CH_2), 5.27 (s, 2H, CH_2), 4.98 (s, 2H, CH_2), 4.90 (s, 2H, CH_2), 4.79 (s, 2H, CH_2), 4.04 (s, 3H, CH_3), 3.25 (s, 2H, CH_2). δ_C (100 MHz, DMSO-d_6): 161.24, 151.00, 150.86, 148.68, 145.85, 143.42, 142.78, 138.41, 137.47, 133.79, 131.53, 128.59, 127.47, 126.36, 124.82, 122.19, 121.28, 121.12, 115.64, 109.39, 106.38, 103.06, 73.11, 62.29, 57.95, 56.40, 51.05, 27.26.

10-Methoxy-9-(3-(4-(4-sulfamoylphenyl)-1H-1,2,3-triazol-1-yl)propoxy)-5,6-dihydro-[1,3]dioxolo[4,5-g]isoquinolino[3,2-a]isoquinolin-7-ium hexafluorophosphate(V) B27

Azide **B20** (1.0 eq, 0,2g) was added to a suspension of alkyne **B2** (1.0-2-0 eq) in H2O/t-BuOH 1/1 (12 mL) at r.t., followed by a suspension of CuSO4·5H2O (0.2 eq) and sodium ascorbate (0.7 eq) in H2O and it works as describe in general procedure to obtain the compounds **B27.** 63% yield; m.p. 205-208° C; silica gel TLC R_f 0.50 (MeOH/DCM 10% *v/v)*; δ_H (400 MHz, DMSO-d_6): 9.88 (s, 1H, Ar-*H*), 8.96 (s, 1H, Ar-*H*), 8.85 (s, 1H, Ar-*H*), 8.22 (s, 1H, Ar-*H*), 8.06 (s, 3H, Ar-*H*), 7.93 (d, *J* = 7.1 Hz, 2H, Ar-*H*), 7.83 (s, 1H, Ar-*H*), 7.45 (s, 2H, exchange with D_2O, SO_2NH_2), 7.14 (s, 1H, Ar-*H*), 6.22 (s, 2H, CH_2), 5.01 (s, 2H, CH_2), 4.82 (s, 2H, CH_2), 4.38 (s, 2H, CH_2), 4.06 (s, 3H, CH_3), 3.34 (s, 2H, CH_2), 3.27 (s, 2H, CH_2). δ_C (100 MHz, DMSO-d_6): 151.26, 150.78, 148.62, 146.17, 146.12, 144.10, 143.32, 138.40, 134.85, 133.95, 131.61, 127.57, 127.38, 126.30, 124.53, 123.76, 122.42, 121.32, 121.09, 109.34, 106.33, 103.00, 71.92, 57.92, 56.14, 47.72, 31.05, 27.27.

10-Methoxy-9-(3-(4-((4-sulfamoylphenoxy)methyl)-1H-1,2,3-triazol-1-yl)propoxy)-5,6-dihydro-[1,3]dioxolo[4,5-g]isoquinolino[3,2-a]isoquinolin-7-ium hexafluorophosphate(V) B28

Azide **B20** (1.0 eq, 0,2g) was added to a suspension of alkyne **B4** (1.0-2-0 eq) in H2O/t-BuOH 1/1 (12 mL) at r.t., followed by a suspension of CuSO4·5H2O (0.2 eq) and sodium ascorbate (0.7 eq) in H2O and it works as describe in general procedure to obtain the compounds **B28**. 42% yield; m.p. 120-122° C; silica gel TLC R_f 0.45 (MeOH/DCM 10% *v/v)*; δ_H (400 MHz, DMSO-d_6): 9.88 (s, 1H, Ar-*H*), 8.98 (s, 1H, Ar-*H*), 8.42 (s, 1H, Ar-*H*), 8.22 (s, 1H, Ar-*H*), 8.05 (s, 1H, Ar-*H*), 7.84 (s, 1H, Ar-*H*), 7.78 (d, *J* = 8.3 Hz, 2H, Ar-*H*), 7.27 (s, 2H, exchange with D_2O, SO_2NH_2), 7.22 (d, *J* = 8.3 Hz, 2H, Ar-*H*), 7.14 (s, 1H, Ar-*H*), 6.22 (s, 2H, CH_2), 5.29 (s, 2H,

C*H*$_2$), 5.00 (s, 2H, C*H*$_2$), 4.77 (s, 2H, C*H*$_2$), 4.34 (s, 2H, C*H*$_2$), 4.06 (s, 3H, C*H*$_3$), 3.26 (s, 2H, C*H*$_2$), 2.51 (s, 2H, C*H*$_2$). δ_C (100 MHz, DMSO-*d*$_6$): 161.26, 151.26, 150.80, 148.65, 146.20, 143.31, 143.21, 138.45, 137.45, 133.98, 131.61, 128.58, 127.60, 125.89, 124.56, 122.43, 121.35, 121.17, 115.67, 109.36, 106.37, 103.02, 71.92, 62.36, 57.94, 56.21, 47.53, 31.17, 27.27.

10-Methoxy-9-(4-(4-(4-sulfamoylphenyl)-1H-1,2,3-triazol-1-yl)butoxy)-5,6-dihydro-[1,3]dioxolo[4,5-g]isoquinolino[3,2-a]isoquinolin-7-ium hexafluorophosphate(V) B29

Azide **B21** (1.0 eq, 0,2g) was added to a suspension of alkyne **B2** (1.0-2-0 eq) in H2O/t-BuOH 1/1 (12 mL) at r.t., followed by a suspension of CuSO4·5H2O (0.2 eq) and sodium ascorbate (0.7 eq) in H2O and it works as describe in general procedure to obtain the compounds **B29**. 74% yield; m.p. 183-185° C; silica gel TLC R_f 0.33 (MeOH/DCM 10% *v/v*); δ_H (400 MHz, DMSO-*d*$_6$): 9.81 (s, 1H, Ar-*H*), 8.96 (s, 1H, Ar-*H*), 8.84 (s, 1H, Ar-*H*), 8.23 (d, *J* = 7.7 Hz, 1H, Ar-*H*), 8.06 (d, *J* = 8.0 Hz, 3H, Ar-*H*), 7.94 (d, *J* = 8.1 Hz, 2H, Ar-*H*), 7.84 (s, 1H, Ar-*H*), 7.45 (s, 2H, exchange with D_2O, SO_2NH_2), 7.13 (s, 1H, Ar-*H*), 6.22 (s, 2H, C*H*$_2$), 4.99 (s, 2H, C*H*$_2$), 4.62 (s, 2H, C*H*$_2$), 4.37 (s, 2H, C*H*$_2$), 4.09 (s, 3H, C*H*$_3$), 3.25 (s, 2H, C*H*$_2$), 2.22 (s, 2H, C*H*$_2$), 1.94 (s, 2H, C*H*$_2$). δ_C (100 MHz, DMSO-*d*$_6$): 151.26, 150.76, 148.61, 146.13, 146.04, 144.04, 143.59, 138.35, 134.89, 133.94, 131.56, 127.50, 127.34, 126.25, 124.33, 123.60, 122.50, 121.33, 121.11, 109.32, 106.34, 103.01, 74.42, 57.95, 56.23, 50.38, 40.10, 27.45, 27.20.

10-Methoxy-9-(4-(4-((4-sulfamoylphenoxy)methyl)-1H-1,2,3-triazol-1-yl)butoxy)-5,6-dihydro-[1,3]dioxolo[4,5-g]isoquinolino[3,2-a]isoquinolin-7-ium hexafluorophosphate(V) B30

Azide **B21** (1.0 eq, 0,2g) was added to a suspension of alkyne **B4** (1.0-2-0 eq) in H2O/t-BuOH 1/1 (12 mL) at r.t., followed by a suspension of CuSO4·5H2O (0.2 eq) and sodium ascorbate (0.7 eq) in H2O and it works as describe in general procedure to obtain the compounds **B30**. 51% yield; m.p. 165-168° C; silica gel TLC R_f 0.31 (MeOH/DCM 10% *v/v*); δ_H (400 MHz, DMSO-*d*$_6$): 9.80 (s, 1H, Ar-*H*), 8.97 (s, 1H, Ar-*H*), 8.36 (s, 1H, Ar-*H*), 8.22 (s, 1H, Ar-*H*), 8.04 (s, 1H, Ar-*H*), 7.83 (s, 1H, Ar-*H*), 7.79 (d, *J* = 8.6 Hz, 2H, Ar-*H*), 7.27 (s, 2H, exchange with D_2O, SO_2NH_2), 7.22 (d, *J* = 8.5 Hz, 2H, Ar-*H*), 7.13 (s, 1H, Ar-*H*), 6.21 (s, 2H, C*H*$_2$), 5.27 (s, 2H, C*H*$_2$), 4.99 (s, 2H, C*H*$_2$), 4.55 (s, 2H, C*H*$_2$), 4.34 (s, 2H, C*H*$_2$), 4.08 (s, 3H, C*H*$_3$), 3.25 (s, 2H, C*H*$_2$), 2.14 (d, *J* = 10.6 Hz, 2H, C*H*$_2$), 1.89 (s, 2H, C*H*$_2$). δ_C (100 MHz, DMSO-*d*$_6$): 161.28,

151.29, 150.76, 148.62, 146.15, 143.61, 143.09, 138.37, 137.45, 133.94, 131.59, 128.59, 127.53, 125.72, 124.36, 122.51, 121.35, 121.13, 115.70, 109.33, 106.36, 103.01, 74.44, 62.38, 57.95, 56.24, 50.13, 40.16, 27.43, 27.30.

10-Methoxy-9-((5-(4-(4-sulfamoylphenyl)-1H-1,2,3-triazol-1-yl)pentyl)oxy)-5,6-dihydro-[1,3]dioxolo[4,5-g]isoquinolino[3,2-a]isoquinolin-7-ium hexafluorophosphate(V) B31

Azide **B22** (1.0 eq, 0,2g) was added to a suspension of alkyne **B2** (1.0-2-0 eq) in H2O/t-BuOH 1/1 (12 mL) at r.t., followed by a suspension of CuSO4·5H2O (0.2 eq) and sodium ascorbate (0.7 eq) in H2O and it works as describe in general procedure to obtain the compounds **B31**. 55% yield; m.p. 200-202° C; silica gel TLC R_f 0.44 (MeOH/DCM 10% *v/v*); δ_H (400 MHz, DMSO-d_6): 9.76 (s, 1H, Ar-*H*), 8.95 (s, 1H, Ar-*H*), 8.80 (s, 1H, Ar-*H*), 8.22 (d, *J* = 8.3 Hz, 1H, Ar-*H*), 8.04 (d, *J* = 8.1 Hz, 3H, Ar-*H*), 7.92 (d, *J* = 8.1 Hz, 2H, Ar-*H*), 7.83 (s, 1H, Ar-*H*), 7.44 (s, 2H, exchange with D_2O, SO_2NH_2), 7.13 (s, 1H, Ar-*H*), 6.22 (s, 2H, CH_2), 4.98 (s, 2H, CH_2), 4.53 (s, 2H, CH_2), 4.34 (s, 2H, CH_2), 4.08 (s, 3H, CH_3), 3.24 (s, 2H, CH_2), 2.01 (d, *J* = 31.6 Hz, 4H,2 x CH_2), 1.56 (s, 2H, CH_2). δ_C (100 MHz, DMSO-d_6): 151.27, 150.77, 148.63, 146.11, 145.98, 144.03, 143.73, 138.38, 134.88, 133.97, 131.59, 127.61, 127.32, 126.20, 124.21, 123.46, 122.53, 121.36, 121.13, 109.33, 106.36, 103.01, 74.88, 57.95, 56.24, 50.56, 32.23, 30.23, 29.80, 23.35.

10-Methoxy-9-((5-(4-((4-sulfamoylphenoxy)methyl)-1H-1,2,3-triazol-1-yl)pentyl)oxy)-5,6-dihydro-[1,3]dioxolo[4,5-g]isoquinolino[3,2-a]isoquinolin-7-ium hexafluorophosphate(V) B32

Azide **B22** (1.0 eq, 0,2g) was added to a suspension of alkyne **B4** (1.0-2-0 eq) in H2O/t-BuOH 1/1 (12 mL) at r.t., followed by a suspension of CuSO4·5H2O (0.2 eq) and sodium ascorbate (0.7 eq) in H2O and it works as describe in general procedure to obtain the compounds **B32**. 20% yield; m.p. 168-171° C; silica gel TLC R_f 0.38 (MeOH/DCM 10% *v/v*); δ_H (400 MHz, DMSO-d_6): 9.77 (s, 1H, Ar-*H*), 8.97 (s, 1H, Ar-*H*), 8.33 (s, 1H, Ar-*H*), 8.22 (s, 1H, Ar-*H*), 8.02 (s, 1H, Ar-*H*), 7.84 (s, 1H, Ar-*H*), 7.78 (d, *J* = 8.3 Hz, 2H, Ar-*H*), 7.26 (s, 2H, exchange with D_2O, SO_2NH_2), 7.21 (d, *J* = 8.2 Hz, 2H, Ar-*H*), 7.13 (s, 1H, Ar-*H*), 6.21 (s, 2H, CH_2), 5.25 (s, 2H, CH_2), 4.99 (s, 2H, CH_2), 4.48 (s, 2H, CH_2), 4.31 (s, 2H, CH_2), 4.08 (s, 3H, CH_3), 3.25 (s, 2H, CH_2), 1.97 (s, 4H,2 x CH_2), 1.52 (s, 2H, CH_2). δ_C (100 MHz, DMSO-d_6): 161.26, 151.32, 150.78, 148.64, 146.15, 143.74, 143.04, 138.40, 137.46, 133.98, 131.61, 128.57, 127.62,

125.58, 124.26, 122.57, 121.38, 121.16, 115.68, 109.35, 106.36, 103.01, 74.88, 62.38, 57.95, 56.24, 50.33, 30.35, 29.76, 27.28, 23.31.

10-Methoxy-9-((1-(3-sulfamoylphenyl)-1H-1,2,3-triazol-4-yl)methoxy)-5,6-dihydro-[1,3]dioxolo[4,5-g]isoquinolino[3,2-a]isoquinolin-7-ium hexafluorophosphate(V) B33

Azide **A30** (1.0 eq, 0,2g) was added to a suspension of alkyne **B23** (1.0-2-0 eq) in H2O/t-BuOH 1/1 (12 mL) at r.t., followed by a suspension of CuSO4·5H2O (0.2 eq) and sodium ascorbate (0.7 eq) in H2O and it works as describe in general procedure to obtain the compounds **B33**.34% yield; m.p. 195-198°; silica gel TLC R_f 0.45 (MeOH/DCM 10% *v/v)*; δ_H (400 MHz, DMSO-d_6): 9.81 (s, 1H, Ar-*H*), 9.22 (s, 1H, Ar-*H*), 8.99 (s, 1H, Ar-*H*), 8.42 (s, 1H, Ar-*H*), 8.28 (s, 1H, Ar-*H*), 8.17 (s, 1H, Ar-*H*), 8.08 (s, 1H, Ar-*H*), 7.99 (d, *J* = 7.2 Hz, 1H, Ar-*H*), 7.97 (d, *J* = 17.7 Hz, 1H, Ar-*H*), 7.86 (d, *J* = 17.7 Hz, 1H, Ar-*H*), 7.63 (s, 2H, exchange with D_2O, SO_2NH_2), 7.12 (s, 1H), 6.21 (s, 2H, CH_2), 5.61 (s, 2H, CH_2), 4.97 (s, 2H, CH_2), 4.16 (s, 3H, CH_3), 3.23 (s, 2H, CH_2). δ_C (100 MHz, DMSO-d_6): 151.69, 150.85, 148.67, 146.76, 146.15, 145.02, 142.63, 138.54, 137.60, 134.00, 131.97, 131.64, 127.58, 126.64, 125.01, 124.69, 124.18, 122.71, 121.35, 121.25, 118.31, 109.39, 106.39, 103.05, 67.39, 58.10, 56.41, 27.31.

10-Methoxy-9-((1-(4-sulfamoylphenyl)-1H-1,2,3-triazol-4-yl)methoxy)-5,6-dihydro-[1,3]dioxolo[4,5-g]isoquinolino[3,2-a]isoquinolin-7-ium hexafluorophosphate(V) B34

Azide **A31** (1.0 eq, 0,2g) was added to a suspension of alkyne **B23** (1.0-2-0 eq) in H2O/t-BuOH 1/1 (12 mL) at r.t., followed by a suspension of CuSO4·5H2O (0.2 eq) and sodium ascorbate (0.7 eq) in H2O and it works as describe in general procedure to obtain the compounds **B34**. 19% yield; m.p. 250°-253°; silica gel TLC R_f 0.26 (MeOH/DCM 10% *v/v)*; δ_H (400 MHz, DMSO-d_6): 9.80 (s, 1H, Ar-*H*), 9.20 (s, 1H, Ar-*H*), 8.99 (s, 1H, Ar-*H*), 8.29 (d, *J* = 8.9 Hz, 1H, Ar-*H*), 8.18 (d, *J* = 7.6 Hz, 2H, Ar-*H*), 8.08 (d, *J* = 7.6 Hz, 3H, Ar-*H*), 7.83 (s, 1H, Ar-*H*), 7.59 (s, 2H, exchange with D_2O, SO_2NH_2), 7.12 (s, 1H, Ar-*H*), 6.21 (s, 2H, CH_2), 5.61 (s, 2H, CH_2), 4.97 (s, 2H, CH_2), 4.15 (s, 3H, CH_3), 3.22 (s, 2H, CH_2). δ_C (100 MHz, DMSO-d_6): 151.79, 150.96, 148.78, 146.23, 145.11, 142.74, 139.58, 138.69, 134.10, 131.75, 128.61, 127.72, 127.69, 125.12, 124.69, 122.80, 121.56, 121.47, 121.35, 109.50, 106.50, 103.17, 67.50, 58.22, 56.56, 27.43.

Synthesis of coumarin-triazoles B35-B46

General procedure: Cu(I) catalysed azide-alkyne Huisgen cycloaddition reactions B35-B46

The general procedure is the same of the correspondent benzensulfonamide-triazole hybrids.

10-Methoxy-9-(3-(4-(((7-oxo-7,8-dihydronaphthalen-2-yl)oxy)methyl)-1H-1,2,3-triazol-1-yl)propoxy) 5,6-dihydro-[1,3]dioxolo[4,5-g]isoquinolino[3,2-a]isoquinolin-7-ium hexafluorophosphate(V) B35

Azide **B20** (1.0 eq, 0,2g) was added to a suspension of alkyne **B11** (1.0-2-0 eq) in H2O/t-BuOH 1/1 (12 mL) at r.t., followed by a suspension of CuSO4·5H2O (0.2 eq) and sodium ascorbate (0.7 eq) in H2O and it works as describe in general procedure to obtain the compounds **B35**. 85% yield; m.p. 140°C; silica gel TLC Rf 0.18 (MeOH/DCM 10%); δH (400MHz, DMSO-d6): 9.77 (s, 1H, Ar-*H*), 8.95 (s, 1H, Ar-*H*), 8.44 (s, 1H, Ar-*H*), 8.21 (d, *J* = 9.2 Hz, 1H, Ar-*H*), 8.02 (d, *J* = 4.5 Hz, 1H, Ar-*H*, 7.99 (d, *J* = 4.9 Hz, 1H, Ar-*H*), 7.83 (s, 1H, Ar-*H*), 7.62 (d, *J* = 8.6 Hz, 1H, Ar-*H*), 7.15 (d, *J* = 2.0 Hz, 1H, Ar-*H*), 7.13 (s, 1H, Ar-*H*), 7.01 (dd, *J* = 8.6, 2.2 Hz, 1H, Ar-*H*), 6.32 (d, *J* = 9.5 Hz, 1H, Ar-*H*), 6.22 (s, 2H, CH2), 5.32 (s, 2H, CH2), 4.98 (d, *J* = 5.7 Hz, 2H, CH2), 4.77 (t, *J* = 6.7 Hz, 2H, CH2), 4.32 (t, *J* = 5.8 Hz, 2H, CH2), 4.06 (s, 3H, CH3), 3.25 (d, *J* = 5.5 Hz, 2H, CH22), 2.52 – 2.47 (m, 2H, CH2). δC (100 MHz, DMSO d6): 161.92, 161.11, 156.13, 151.20, 150.80, 148.64, 146.17, 145.14, 143.23, 143.01, 138.42, 133.98, 131.59, 130.37, 127.56, 126.06, 124.65, 122.34, 121.32, 121.14, 113.80, 113.59, 113.45, 109.36, 106.34, 103.03, 102.4, 72.0, 62.57, 57.92, 47.66, 31.61, 31.13.

10-Methoxy-9-(3-(4-(2-((7-oxo-7,8-dihydronaphthalen-2-yl)oxy)ethyl)-1H-1,2,3-triazol-1-yl)propoxy)-5,6 dihydro-[1,3]dioxolo[4,5-g]isoquinolino[3,2-a]isoquinolin-7-ium hexafluorophosphate(V) B36

Azide **B20** (1.0 eq, 0,2g) was added to a suspension of alkyne **B12** (1.0-2-0 eq) in H2O/t-BuOH 1/1 (12 mL) at r.t., followed by a suspension of CuSO4·5H2O (0.2 eq) and sodium ascorbate (0.7 eq) in H2O and it works as describe in general procedure to obtain the compounds **B36**. 42% yield; m.p. 130°C; silica gel TLC Rf 0.2 (MeOH/DCM 5%); δH (400MHz, DMSO-d6): δ 9.80 (s, 1H, Ar-*H*), 8.92 (s, 1H, Ar-*H*), 8.20 (d, *J*= 9.2 Hz, 1H, Ar-*H*), 8.14 (s, 1H, Ar-*H*), 8.00 (d, *J* = 4.5 Hz, 1H, Ar-*H*), 7.98 (d, *J* = 4.9 Hz, 1H, Ar-*H*), 7.79 (s, 1H, Ar-*H*), 7.57 (t, *J* = 8.1 Hz, 1H,

Ar-*H*), 7.11 (s, 1H, Ar-*H*), 6.97 (d, *J* = 2.1 Hz, 1H, Ar-*H*), 6.89 (dd, *J* = 8.6, 2.3 Hz, 1H, Ar-*H*), 6.31 (d, *J* = 9.5 Hz, 1H, Ar-*H*), 6.21 (s, 2H, CH2), 5.04 – 4.96 (m, 2H, CH2), 4.73 (t, *J* = 6.7 Hz, 2H, CH2), 4.37 (t, *J* = 6.3 Hz, 2H, CH2), 4.29 (t, *J*= 5.7 Hz, 2H, CH2), 4.06 (s, 3H, CH3), 3.28 – 3.21 (m, 2H, CH2), 3.17 (t, *J* = 6.2 Hz, 2H, CH2), 2.51 – 2.43 (m, 2H, CH2). δC (100 MHz, DMSO-d6): 162.52, 161.29, 156.33, 151.40, 150.94, 148.77, 146.21, 145.31, 144.59, 143.37, 138.53, 134.02, 131.69, 130.51, 127.66, 124.68, 124.17, 122.5, 121.43, 121.28, 113.60, 113.56, 113.45, 109.49, 106.45, 103.18, 102.28, 72.13, 68.39, 58.04, 47.52, 31.31, 27.39, 26.41.

10-Methoxy-9-(3-(4-(3-((7-oxo-7,8-dihydronaphthalen-2-yl)oxy)propyl)-1H-1,2,3-triazol-1-yl)propoxy)-5,6-dihydro-[1,3]dioxolo[4,5-g]isoquinolino[3,2-a]isoquinolin-7-ium hexafluorophosphate(V) B37

Azide **B20** (1.0 eq, 0,2g) was added to a suspension of alkyne **B13** (1.0-2-0 eq) in H2O/t-BuOH 1/1 (12 mL) at r.t., followed by a suspension of CuSO4·5H2O (0.2 eq) and sodium ascorbate (0.7 eq) in H2O and it works as describe in general procedure to obtain the compounds **B37**. 30% yield; m.p. 145°C; silica gel TLC Rf 0.5 (MeOH/DCM 10%); δH (400MHz, DMSO-d6): 9.84 (s, 1H, Ar-*H*), 8.94 (s, 1H, Ar-*H*), 8.19 (t, *J* = 11.5 Hz, 1H, Ar-*H*), 8.06 (s, 1H, Ar-*H*), 8.01 (s, 1H, Ar-*H*), 7.99 (s, 1H, Ar *H*), 7.82 (s, 1H, Ar-*H*), 7.62 (d, *J*= 9.2 Hz, 1H, Ar-*H*), 7.12 (s, 1H, Ar-*H*, 6.94 (s, 1H, Ar-*H*), 6.93 (s, 1H, Ar-*H*), 6.31 (d, *J* = 9.5 Hz, 1H, Ar-*H*), 6.22 (s, 2H, CH2), 4.99 (d, *J* = 5.7 Hz, 2H, CH2), 4.70 (t, *J* = 6.7 Hz, 2H, CH2), 4.29 (t, *J* = 5.8 Hz, 2H, CH2), 4.13 (t, *J* = 6.3 Hz, 2H, CH2), 4.06 (s, 3H, CH3), 3.26 (d, *J* = 5.6 Hz, 2H, CH2), 2.84 (t, *J*= 7.3 Hz, 2H, CH2), 2.49 – 2.43 (m, 2H, CH2), 2.14 – 2.08 (m, 2H, CH2). δC (100 MHz, DMSO-d6): 162.15, 160.70, 155.80, 150.82, 150.34, 148.18, 145.70, 144.75, 142.79, 138.04, 133.45, 131.13, 129.92, 127.18, 124.15 – 123.95, 122.84, 122.00, 120.86, 120.74, 113.13, 112.90, 112.78, 108.96, 105.87, 102.58, 101.50, 71.52, 67.89, 57.47, 56.28, 46.82, 30.71, 28.68, 26.80, 21.95.

10-Methoxy-9-(4-(4-(((2-oxo-2H-chromen-7-yl)oxy)methyl)-1H-1,2,3-triazol-1-yl)butoxy)-5,6-dihydro-[1,3]dioxolo[4,5-g]isoquinolino[3,2-a]isoquinolin-7-ium hexafluorophosphate(V) B38

Azide **B21** (1.0 eq, 0,2g) was added to a suspension of alkyne **B11** (1.0-2-0 eq) in H2O/t-BuOH 1/1 (12 mL) at r.t., followed by a suspension of CuSO4·5H2O (0.2 eq) and sodium ascorbate

(0.7 eq) in H2O and it works as describe in general procedure to obtain the compounds **B38**. 45% yield; m.p. 108-110°C; silica gel TLC Rf 0.32 (MeOH/DCM 10% v/v); δH (400MHz, DMSO-d6): 9.78 (s, 1H, Ar-*H*), 8.95 (s, 1H, Ar-*H*), 8.38 (s, 1H, Ar-*H*), 8.22 (d, *J* = 8.6 Hz, 1H, Ar-*H*), 8.03 (d, *J* = 9.2 Hz, 1H, Ar-*H*), 7.83 (s, 1H, Ar-*H*), 7.67 (d, *J* = 8.5 Hz, 1H, Ar-*H*), 7.19 (s, 1H, Ar-*H*), 7.12 (s, 1H, Ar-*H*), 7.04 (d, *J* = 8.1 Hz, 1H, Ar-*H*), 6.34 (d, *J* = 9.4 Hz, 1H, Ar-*H*), 6.21 (s, 2H, CH2), 5.30 (s, 2H, CH2), 4.98 (s, 2H, CH2), 4.56 (s, 2H, CH2), 4.33 (s, 2H, CH2), 4.08 (s, 3H, CH3), 3.25 (s, 2H, CH2), 2.15 (s, 2H, CH2), 1.89 (s, 2H, CH2). δC (100 MHz, DMSO-d6): 161.93, 161.13, 156.17, 151.22, 150.72, 148.53, 145.76, 145.15, 143.61, 142.89, 138.33, 133.93, 131.61, 130.41, 127.48, 125.81, 124.39, 124.32, 122.56, 121.36, 121.03, 113.78, 113.56, 109.29, 106.34, 102.99, 102.47, 74.39, 62.67, 57.97, 56.18, 50.14, 41.09, 27.41, 27.28.

10-Methoxy-9-(4-(4-(2-((7-oxo-7,8-dihydronaphthalen-2-yl)oxy)ethyl)-1H-1,2,3-triazol-1-yl)butoxy)-5,6 dihydro-[1,3]dioxolo[4,5-g]isoquinolino[3,2-a]isoquinolin-7-ium hexafluorophosphate(V) B39

Azide **B21** (1.0 eq, 0,2g) was added to a suspension of alkyne **B12** (1.0-2-0 eq) in H2O/t-BuOH 1/1 (12 mL) at r.t., followed by a suspension of CuSO4·5H2O (0.2 eq) and sodium ascorbate (0.7 eq) in H2O and it works as describe in general procedure to obtain the compounds **B39**. 82% yield; m.p. 185°C; silica gel TLC Rf 0.2 (MeOH/DCM 5%); δH (400MHz, DMSO-d6): 9.76 (s, 1H, Ar-*H*), 8.91 (s, 1H, Ar-*H*), 8.19 (d, *J* = 9.1 Hz, 1H, Ar-*H*), 8.07 (s, 1H, Ar-*H*), 8.00 (s, 1H, Ar-*H*), 7.98 (s, 1H, Ar-*H*), 7.78 (s, 1H, Ar-*H*), 7.62 (d, *J* = 8.5 Hz, 1H, Ar-*H*), 7.10 (s, 1H, Ar-*H*), 7.00 (s, 1H, Ar-*H*), 6.96 (d, *J* = 8.5 Hz, 1H, Ar-*H*), 6.28 (t, *J* = 10.2 Hz, 1H Ar-*H*), 6.20 (s, 2H, CH2), 4.99 (s, 2H, CH2), 4.51 (t, *J* = 6.3 Hz, 2H, CH2), 4.36 (d, *J* = 6.1 Hz, 2H, CH2), 4.32 (d, *J* = 8.5 Hz, 2H, CH2), 4.07 (s, 3H, CH3), 3.24 (s, 2H, CH2), 3.15 (t, *J* = 6.1 Hz, 2H, CH2), 2.11 (dd, *J* = 20.3, 14.0 Hz, 2H, CH2), 1.88 (d, *J* = 5.6 Hz, 2H, CH2). δC (100 MHz, DMSO-d6): 162.56, 161.32, 156.37, 151.38, 150.90, 148.75, 146.23, 145.32, 144.32, 143.67, 138.51, 134.02, 131.71, 130.54, 127.63, 124.44, 123.95, 122.60, 121.46, 121.26, 113.61 (d, J=5.2 Hz), 113.58, 113.48, 109.46), 106.44, 103.17, 102.35, 74.52, 68.37, 58.04, 56.37, 50.07, 27.58, 27.43, 26.41.

10-Methoxy-9-((5-(4-(((7-oxo-7,8-dihydronaphthalen-2-yl)oxy)methyl)-1H-1,2,3-triazol-1-yl)pentyl)oxy)-5,6-dihydro-[1,3]dioxolo[4,5-g]isoquinolino[3,2-a]isoquinolin-7-ium hexafluorophosphate(V) B40

Azide **B22** (1.0 eq, 0,2g) was added to a suspension of alkyne **B11** (1.0-2-0 eq) in H2O/t-BuOH 1/1 (12 mL) at r.t., followed by a suspension of CuSO4·5H2O (0.2 eq) and sodium ascorbate (0.7 eq) in H2O and it works as describe in general procedure to obtain the compounds **B40**. 55% yield; m.p. 206°C; silica gel TLC Rf 0.2 (MeOH/DCM 5%); δH (400MHz, DMSO-d6): 9.74 (s, 1H, Ar-*H*), 8.93 (s, 1H, Ar-*H*), 8.35 (s, 1H, Ar-*H*), 8.21 (d, *J* = 9.2 Hz, 1H, Ar-*H*), 8.01 (s, 1H, Ar-*H*), 7.99 (s, 1H, Ar-*H*), 7.80 (s, 1H, Ar-*H*), 7.64 (d, *J* = 8.6 Hz, 1H, Ar-*H*), 7.15 (d, *J* = 2.1 Hz, 1H, Ar-*H*), 7.11 (d, *J* = 5.1 Hz, 1H, Ar-*H*), 7.02 (dd, *J* = 8.6, 2.3 Hz, 1H, Ar-*H*), 6.31 (d, *J* = 9.5 Hz, 1H, Ar-*H*), 6.21 (s, 2H, CH2), 5.28 (s, 2H, CH2), 5.03 – 4.95 (m, 2H, CH2), 4.49 (t, *J* = 6.8 Hz, 2H, CH2), 4.31 (dd, *J* = 12.2, 5.9 Hz, 2H, CH2), 4.07 (s, 3H, CH3), 3.29 – 3.20 (m, 2H, CH2), 2.00 (dd, *J* = 14.6, 7.3 Hz, 2H, CH2), 1.96 – 1.90 (m, 2H, CH2), 1.55 – 1.46 (m, 2H, CH2). δC (100 MHz, DMSO-d6): 162.13, 161.3, 156.32, 151.43, 150.90, 148.76, 145.30, 143.80, 142.98, 138.52, 134.06, 131.73, 130.55, 127.70, 125.86, 124.37, 122.66, 121.49, 121.28, 113.94, 113.73, 113.63, 109.47, 106.45, 103.17, 102.58, 74.97, 62.78, 58.05, 56.39, 50.46, 30.48, 29.90, 27.40, 23.45.

10-Methoxy-9-((1-(4-methyl-2-oxo-2H-chromen-7-yl)-1H-1,2,3-triazol-4-yl)methoxy)-5,6-dihydro-[1,3]dioxolo[4,5-g]isoquinolino[3,2-a]isoquinolin-7-ium hexafluorophosphate(V) B41

Azide **B8** (1.0 eq, 0,2g) was added to a suspension of alkyne **B23** (1.0-2-0 eq) in H2O/t-BuOH 1/1 (12 mL) at r.t., followed by a suspension of CuSO4·5H2O (0.2 eq) and sodium ascorbate (0.7 eq) in H2O and it works as describe in general procedure to obtain the compounds **B41**. 46% yield; m.p. 280-283°; silica gel TLC R_f 0.55 (MeOH/DCM 10% *v/v*); δ_H (400 MHz, DMSO-d_6): 9.79 (s, 1H, Ar-*H*), 9.24 (s, 1H, Ar-*H*), 8.98 (s, 1H, Ar-*H*), 8.28 (s, 1H, Ar-*H*), 8.05 (s, 4H, Ar-*H*), 7.83 (s, 1H, Ar-*H*), 7.12 (s, 1H, Ar-*H*), 6.55 (s, 1H, Ar-*H*), 6.21 (s, 2H, CH_2), 5.61 (s, 2H, CH_2), 4.96 (s, 2H, CH_2), 4.16 (s, 3H, CH_3), 3.23 (s, 2H, CH_2). δ_C (100 MHz, DMSO-d_6): 159.84, 154.10, 153.17, 151.17, 150.32, 148.19, 142.66, 142.16, 138.87, 138.14, 133.52, 131.15, 127.78, 127.13, 125.73, 124.51, 122.19, 120.86, 120.76, 120.09, 116.10, 115.28, 108.90, 108.08, 105.89, 102.60, 87.41, 83.42, 79.05, 58.72, 57.62, 18.57, 13.84.

10-Methoxy-9-((1-(3-((7-oxo-7,8-dihydronaphthalen-2-yl)oxy)propyl)-1H-1,2,3-triazol-4-yl)methoxy) 5,6-dihydro-[1,3]dioxolo[4,5-g]isoquinolino[3,2-a]isoquinolin-7-ium hexaflorophosphate(V) B42

Azide **B9** (1.0 eq, 0,2g) was added to a suspension of alkyne **B23** (1.0-2-0 eq) in H2O/t-BuOH 1/1 (12 mL) at r.t., followed by a suspension of CuSO4·5H2O (0.2 eq) and sodium ascorbate (0.7 eq) in H2O and it works as describe in general procedure to obtain the compounds **B42**. 78% yield; m.p. 117°C; silica gel TLC Rf 0,16 (MeOH/DCM 2,5%); δH (400MHz, DMSO-d6): 9.69 (s, 1H, Ar-*H*), 8.88 (s, 1H, Ar-*H*), 8.25 (s, 1H, Ar-*H*), 8.02 (d, *J*= 8.7 Hz,1H, Ar-*H*), 7.74 (s, 1H, Ar-*H*), 7.66 (d, *J*= 8.7 Hz, 1H, Ar-*H*), 7.08 (s, 1H, Ar-*H*), 7.03 (s, 1H, Ar-*H*), 6.99 (d,*J*= 6.5 Hz, 2H, Ar-*H*), 6.89 (s, 1H, Ar-*H*), 6.32 (d, *J*= 8.5 Hz, 1H, Ar-*H*), 6.20 (s, 2H, CH2), 5.51 (s, 2H, CH2), 4.92 (s, 2H, CH2), 4.58 (s, 2H, CH2), 4.13 (s, 3H, CH3), 4.00 (s, 2H, CH2), 3.21 (s, 2H, CH2), 2.30 (s, 2H, CH2). δC (100 MHz, DMSO-d6): 162.37, 161.30, 156.32, 151.86, 150.92, 148.74, 146.17, 145.29, 143.55, 142.65, 138.47, 133.94, 131.59, 130.53, 127.59, 126.35, 124.93, 122.94, 121.3, 121.30, 113.64, 113.55, 109.42, 106.39, 103.18, 102.28, 67.57, 66.35, 58.09), 56.81, 47.59, 30.28, 27.40.

10-Methoxy-9-((1-(4-((7-oxo-7,8-dihydronaphthalen-2-yl)oxy)butyl)-1H-1,2,3-triazol-4-yl)methoxy)-5,6 dihydro-[1,3]dioxolo[4,5-g]isoquinolino[3,2-a]isoquinolin-7-ium hexafluorophohphate(V) B43

Azide **B10** (1.0 eq, 0,2g) was added to a suspension of alkyne **B23** (1.0-2-0 eq) in H2O/t-BuOH 1/1 (12 mL) at r.t., followed by a suspension of CuSO4·5H2O (0.2 eq) and sodium ascorbate (0.7 eq) in H2O and it works as describe in general procedure to obtain the compounds **B43**. 51% yield; m.p. 124°C; silica gel TLC Rf 0.3 (MeOH/DCM 5%); δH (400MHz, DMSO-d6): 9.70 (s, 1H. Ar-*H*), 8.88 (s, 1H, Ar-*H*), 8.31 (d, *J* = 20.7 Hz, 1H, Ar-*H*), 8.24 (d, *J* = 9.1 Hz, 1H, Ar-*H*), 8.02 (s, 1H, Ar-*H*), 7.98 (d, *J* = 10.2 Hz, 1H, Ar-*H*), 7.69 (d, *J* = 9.0 Hz, 1H, Ar-*H*), 7.62 (d, *J* = 8.4 Hz, 1H. Ar-*H*), 7.02 (s, 1H, Ar-*H*), 6.90 (s, 1H, Ar-*H*), 6.88 (s, 1H, Ar-*H*), 6.31 (d, *J* = 9.5 Hz, 1H, Ar-*H*), 6.17 (s, 2H, CH2), 5.52 (s, 2H, CH2), 4.93 (s, 2H, CH2), 4.45 (t, *J* = 6.6 Hz, 2H, CH2), 4.14 (s, 3H, CH3), 3.98 (t, *J* = 6.1 Hz, 2H, CH2), 3.19 (s, 2H, CH2), 1.98 – 1.88 (m, 2H, CH2), 1.55 – 1.44 (m, 2H, CH2). δC (100 MHz, DMSO-d6): 162.48, 161.23, 156.26, 151.85, 150.75, 148.57, 146.04, 145.22, 143.16, 142.28, 138.30, 133.78, 131.41, 130.35,

127.45, 126.16, 124.85, 122.91, 121.17, 113.48, 113.37, 113.27, 109.27, 106.23, 103.0, 101.99, 68.43, 67.22, 60.70, 57.96, 49.95, 27.33, 26.16, 15.01.

10-Methoxy-9-((1-(3-((2-oxo-2H-chromen-7-yl)oxy)propyl)-1H-1,2,3-triazol-4-yl)methoxy)-5,6-dihydro-[1,3]dioxolo[4,5-g]isoquinolino[3,2-a]isoquinolin-7-ium hexafluorophohphate(V) B45

Azide **A42** (1.0 eq, 0,2g) was added to a suspension of alkyne **B23** (1.0-2-0 eq) in H2O/t-BuOH 1/1 (12 mL) at r.t., followed by a suspension of CuSO4·5H2O (0.2 eq) and sodium ascorbate (0.7 eq) in H2O and it works as describe in general procedure to obtain the compounds **B45**. 39% yield; m.p. 171-173°; silica gel TLC R_f 0.34 (MeOH/DCM 10% *v/v)*; δ_H (400 MHz, DMSO-d_6): 9.69 (s, 1H, Ar-*H*), 8.88 (s, 1H, Ar-*H*), 8.25 (s, 1H, Ar-*H*), 8.02 (d, *J* = 8.7 Hz, 1H, Ar-*H*), 7.74 (s, 1H, Ar-*H*), 7.66 (d, *J* = 8.7 Hz, 1H, Ar-*H*), 7.08 (s, 1H, Ar-*H*), 7.03 (s, 1H, Ar-*H*), 6.99 (d, *J* = 6.5 Hz, 2H, Ar-*H*), 6.89 (s, 1H, Ar-*H*), 6.32 (d, *J* = 8.5 Hz, 1H, Ar-*H*), 6.20 (s, 2H, CH_2), 5.51 (s, 2H, CH_2), 4.92 (s, 2H, CH_2), 4.58 (s, 2H, CH_2), 4.13 (s, 3H, CH_3), 4.00 (s, 2H, CH_2), 3.21 (s, 2H, CH_2), 2.30 (s, 2H, CH_2). δ_C (100 MHz, DMSO-d_6): 162.26, 161.15, 156.20, 151.77, 150.79, 148.61, 146.10, 145.21, 145.16, 143.39, 142.57, 138.38, 133.86, 131.48, 130.40, 127.61, 126.32, 124.80, 122.82, 121.24, 113.51, 113.43, 109.29, 106.29, 104.53, 103.00, 102.19, 67.46, 66.26, 57.96, 56.10, 47.44, 30.04, 27.33.

Synthesis of aliphatic berberine-sulfonamide

10-Methoxy-9-(3-sulfamoylpropoxy)-5,6-dihydro-[1,3]dioxolo[4,5-g]isoquinolino[3,2-a]isoquinolin-7-ium chloride B48

1,3-Propanesultone (2.0 eq) was added to a solution of berberrubine **B14** (1.0 eq, 0,5 g) in DMF dry at 60°C. The resulting suspension was quenched with Et2O and filtered. The powder was treated with SO2Cl2 (10 mL) and a drop of catalytic DMF and stirred o.n. at room temperature. The day after the reaction mixture was concentrated in vacuo and it was resolubilized in THF. NH4OH 30% (4.0 eq) was added to the solution at 0°C and the reaction was raised then to r.t. The reaction was quenched with water and filtered-off,and purified by silica gel chromatography (eluent: gradient of TFA/MeOH/DCM) to afford the compound **B48**. 4% yield; silica gel TLC Rf 0.3 (MeOH/DCM 5%); δH (400MHz, DMSO-d6): 9.84 (s, 1H, Ar-*H*), 8.98 (s, 1H, Ar-*H*), 8.25 (d, J = 8.1 Hz, 1H, Ar-*H*), 8.04 (d, J = 8.4 Hz, 1H, Ar-*H*),

7.84 (s, 1H, Ar-*H*), 7.14 (s, 1H, Ar-*H*), 6.95 (s, 2H, CH2), 6.21 (s, 2H, CH2), 4.98 (s, 2H, exchange with D2O, SO2NH2), 4.42 (s, 2H, CH2), 4.10 (s, 3H, CH2), 3.25 (s, 2H, CH2), 2.33 (s, 2H, CH2).

Experimental part of crystallization tests.

The chemical products used for the experiments have been purchased from Sigma-Aldrich with the exception of synthetic DNA oligonucleotides (table 19), bought from Metabion (Planegg, Germany) at HPLC purity, and ligand molecules. Synthetic and semi-synthetic compounds (table 7) have been synthesised by me as described before, while the alkaloid berberine hydrochloride was purchased from Fluorochem (Hadfield, UK).

Table 19. DNA sequences used for the experiments.

ID	Sequences
Tel 23	**TAG GGA TTG GGA TTG GGA TTG GG**
C-kit	**AGG GAG GGC GCT GGG AGG AGG G**

DNA oligonucleotides have been annealed prior to the experiments. Briefly, the lyophilized samples were dissolved in buffer and heated in a water bath under magnetic stirring up to 90-95°C for at least 15 minutes and then let cool overnight to room temperature. Human telomeric sequences were usually dissolved in 0.02 M potassium cacodylate buffer (pH 6.5), 0.05 M KCl to a concentration of either 0.001 M (Tel23 and c-kit). Stock solutions of the ligand molecules were prepared in DMSO at a concentration of 0.02M. MilliQ water from Millipore Water System (Millipore, USA) was used for the preparation of all solutions, including those of the crystallization screenings, which were also filtered through Sartorius Stedim Biotech filters of 0.2μm. Crystallization screenings for the adducts formed by DNA and ligand molecules were performed using the sitting drop vapour diffusion method. The screenings used for human telomeric DNA are reported in table 20 while the conditions used for the C-kit sequences are shown in table 21. The first one was found in literature(22 dal capitolo dei G4) and reproduced by myself, the second one was purchased from Molecular Dimension (Maumee,USA).

Table 20. Screening condition for Tel23 and, later for C-kit.

Tube	Salt	Buffer	Precipitant
1	0.1 M KCl	0.05 M K Caco pH 6.5	20% v/v MPD
2	0.3 M KCl	0.05 M K Caco pH 6.5	10% v/v MPD
3	0.1 M KF, 0.025 $MgSO_4$	0.05 M K Caco pH 6.5	25% v/v MPD
4	0.2 M KI	0.05 M K Caco pH 6.5	25% v/v MPD
5	0.1 M KF, 0.02 M $(NH_4)_2SO_4$	0.05 M Na Caco pH 6.5	15% v/v MPD
6	0.3 M NaCl	0.05 M Na Caco pH 6.5	30% v/v MPD
7	0.1 M NaI	0.05 M Na Caco pH 6.5	35% v/v MPD
8	0.3 M KF, 0.02 M $MgSO_4$	0.05 M K Caco pH 6.5	35% v/v MPD
9	0.15 M NaF, 0.15 M KF	0.05 M Na Caco pH 6.5	40% v/v MPD
10	0.1 M KCl, 0.1 M $(NH_4)_2SO_4$	0.05 M K Caco pH 6.5	20% v/v MPD
11	0.1 M NaI, 0.1 M NaF, 0.1 M NaCl	0.05 M Na Caco pH 6.5	30% v/v MPD
12	0.2 M KCl, 0.05 M KI	0.05 M K Caco pH 6.5	25% v/v PEG400
13	0.1 M KCl, 0.05 M $MgCl_2$	0.05 M K Caco pH 6.5	10% v/v PEG400
14	0.1 M Li_2SO_4	0.05 M K Caco pH 6.5	20% v/v PEG400
15	0.3 M KI	0.05 M K Caco pH 6.5	15% v/v PEG400
16	0.3 M NaI	0.05 M Na Caco pH 6.5	15% v/v PEG400
17	0.1 M KCl, 0.03 M $CaCl_2$	0.05 M K Caco pH 6.5	1.3 M ammonium sulphate
18	0.2 M KCl, 0.05 M Li_2SO_4	0.05 M K Caco pH 6.5	1.8 M ammonium sulphate
19	0.05 M Li_2SO_4, 0.05 M $MgSO_4$	0.05 M K Caco pH 6.5	20% v/v *iso*-propanol
20	0.2 M NaCl	0.05 M Na Caco pH 6.5	20% JEFF 2000
21	0.2 M NaCl, 0.1 M NaF	0.05 M Na Caco pH 6.5	10% JEFF 2000
22	0.05 M KI, 0.05 M $MgCl_2$	0.05 M K Caco pH 6.5	15% JEFF 2000
23	0.1 M NaCl, 0.05 M $MgCl_2$	0.05 M Na Caco pH 6.5	1 M ammonium sulphate
24	0.05 M Li_2SO_4	0.05 M Na Caco pH 6.5	1 M ammonium sulphate

Table 21. Screening condition Helix for C-kit.

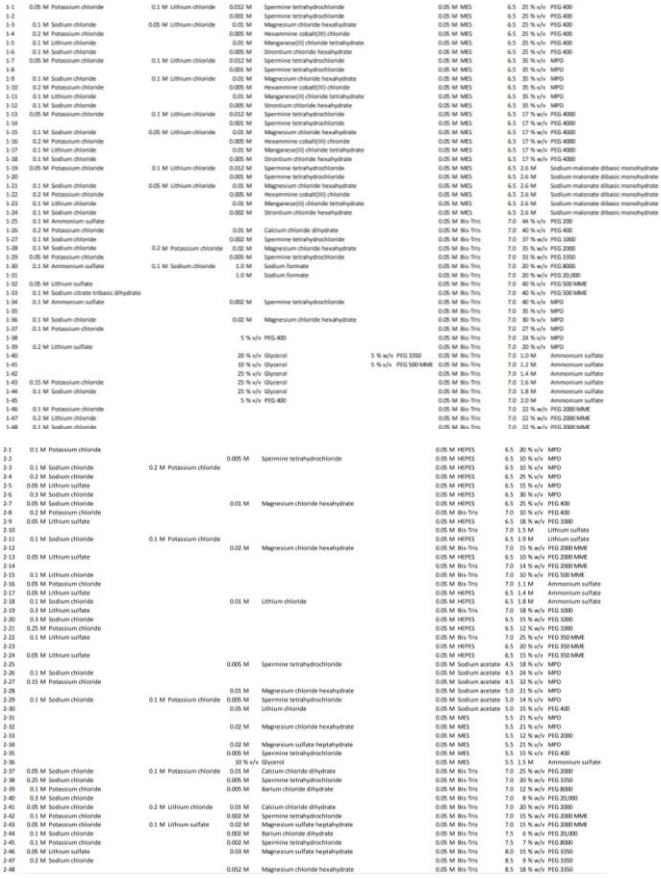

Crystallization trials were performed using Greiner®96-well plates designed for sitting drop experiments. The formation of adducts was achieved by mixing solutions of annealed DNA and ligands usually in 1:1 stoichiometric ratio. The solutions were then incubated for at least 20 minutes at 25°C. Every drop was formed by 1μL of the adduct solution and 1μL of each crystallization condition. The 100 μL reservoirs were composed either of the same condition used in the drop. At the end of drops deposition, the plates were hermetically sealed thanks to transparent adhesive tape and stored in an incubator at 23°C.

The plates were periodically checked by using an optical microscope. Crystals have been observed for most of the adducts studied and X-ray diffraction analyses were performed on them. Only few crystals showed good diffraction and, until now, the X-ray structures of the relative adducts were successfully solved only for **B28**-Tel23. The crystallization conditions from which the crystals were obtained are reported in table 22 along with the cryoprotecting solutions used. The crystals were analysed at an X-ray diffractometer with the experimental parameters reported in tables 23 and 24. All the experiments were carried out at the cryo temperature of 100 K. The analysis of diffraction images (indexing, integration, scaling) was performed by using the XDS software ([21] dal capitolo G4)

Table 22. Crystallization conditions and cryoprotecting solutions used for the DNA-ligand adducts. Only the increased concentration of precipitant or viscous chemicals is reported for the cryo solutions.

Adduct	Conditions	Reservoir	Cryo
B26-Tel23	0.1M KCl, 0.05M K Caco pH 6.5, 20% v/v MPD	Same as condition	30% v/v MPD
B26-Tel23	0.1M KF, 0.025M $MgSO_4$, 0.05M K Caco pH 6.5, 25% v/v MPD	Same as condition	30% v/v MPD
B31-Tel23	0.3M KCl, 0.05M K Caco pH 6.5, 10% v/v MPD	Same as condition	30% v/v MPD
B31-Tel23	0.1M KCl, 0.1M $(NH_4)_2SO_4$, 0.05M K Caco pH 6.5, 20% v/v	Same as condition	Not needed

	MPD		
B28-Tel23	0.3M KCl, 0.05M K Caco pH 6.5, 10% v/v MPD	Same as condition	30% v/v MPD

Table 23. Data collection statistics for X-ray diffraction experiments carried out on DNA-ligand crystals, part one.

Adduct	X-ray wavelength (Å)	Space group	Lattice	Cell parameters (Å,_)	Resolution range (Å)	Experimental apparatus
B26-Tel23	**1.000**	**P2**	**Monoclinic**	**37 53 37 / 90 120 90**	**50-2.8**	**XRD2 beamline Elettra**
B26-Tel23	**1.000**	**C2**	**Monoclinic**	**37.6 65.7 26.8/ 90 90.1 90**	**50-2.8**	**XRD2 beamline Elettra**
B31-Tel23	**1.000**	**C2**	**Monoclinic**	**37.4 64.9 26.1/ 90 90.1 90**	**50-2.8**	**XRD2 beamline Elettra**
B31-Tel23	**1.000**	**P2**	**Monoclinic**	**37.4 24.2 37.4/ 90 119.9 90**	**50-3.0**	**XRD2 beamline Elettra**
B28-Tel23	**1.000**	**C2**	**Monoclinic**	**36.84 72.72 27.03/ 90 90.1 90**	**36.36-1-83**	**XRD2 beamline Elettra**

Table 24. Data collection statistics for X-ray diffraction experiments carried out on DNA-ligand crystals, part two, only for adduct **B28**-Tel23.

Adduct	Unique reflections	Completeness %	Multeplicity	<I/σ(I)>	Rfree	Rfactor
B28-Tel23	5913	99,24	2,93	13.7	32.86	21.25

The structures of the adducts were solved in each case by themolecular replacement method using the program Phaser and Molrep.[183-184] Suitable coordinates of the previously reported structure without all heteroatoms were taken from the 6H5R model. The model was refined with the program Refmac5 from the CCP4 program suite.[185,210]

Multi-potent drugs formed by CA activators and Cholinesterase Inhibitors for the synthomatic treatment of Alzheimer's disease. (Series C)

Synthesis of 9-chlorotacrine C2

$POCl_3$ (50.97 g, 6 eq) was added dropwise to a mixture of anthranilic acid **C1** (7.5 g, 1 eq) and cyclohexanone (5.09 g, 0.95 eq) at 0°C. Then it was heated at reflux (115°C) for 3h; The reaction was monitored by TLC (EtOAc/hexane 20% *v/v*). An aqueous solution of NaOH 9M (30 ml) and ice were added to the mixture, and then it was neutralized with K_2CO_3. The mixture was then extracted with EtOAc, dried with Na_2SO_4, filtrated and evaporated under pressure. The oily residue was then purified with a flash column chromatography (EtOAc/hexane 40%). Yield 61%; silica gel R_f =0.35 (EtOAc/Hexane 10% *v/v*); 1H NMR (400 MHz, DMSO) δ: 8.16 (d, J = 7.9 Hz, 1H, Ar-H), 7.98 (d, J = 8.3 Hz, 1H, Ar-H), 7.79 (t, 1H, Ar-H), 7.68 (t, J = 7.2 Hz, 1H, Ar-H), 3.07 (m, 2H, CH_2), 3.00 (m, 2H, CH_2), 1.92 (m, 4H, 2 x CH_2). ^{13}C NMR ($CDCl_3$, 100 MHz) δ: 159.4, 146.5, 141.5, 129.2, 128.8, 128.5, 126.5, 125.3, 123.6, 34.1, 27.4, 22.61, 22.57.

General synthesis of N-(1,2,3,4- tetrahydroacridin-9-yl)alkane-1,ω-diamines C3-C5

The reaction mixture of phenol (2.6 g, 6.0 eq), 9- chlorotacrine **C2** (1.0 g, 1.0 eq), and KI (0,076 g, 0.1 eq) was heated at 90°C, for 10 minutes to form a liquid. The appropriate diamine (3 eq) was added and the mixture was refluxed at 180°C for 3h. The reaction was monitored by TLC. The mixture was cooled to rt and a 20% aqueous solution of KOH was added. The solution was extracted with EtOAc, and the combined organic layer were washed with brine,

dried over anhydrous sodium sulfate, filtrated and evaporated under pressure. The crude compound was purified by silica gel column chromatography using MeOH/CH_2Cl_2/NH_4OH (20:76:4) as mobile phase to give derivates **C3, C4** and **C5**.

***N*-(1,2,3,4-tetrahydroacridin-9-yl)propane-1,3-diamine C3**

Brown oil, Yield 93%; silica gel R_f 0.05 (MeOH/DCM 10% *v/v*); ^{1}H NMR ($CDCl_3$, 300 MHz) δ: 8.04 (m, 1H, Ar-H), 7.98 (d, *J* = 8.4Hz, 1H, Ar-H), 7.56 (m,1H, Ar-H), 7.33 (m, 1H, Ar-H), 3.68 (t, *J* = 6.5 Hz, 2H,CH_2), 3.07 (m, 2H, CH_2), 2.93 (t, *J* = 6.3 Hz 2H, CH_2), 2.70 (m, 2H, CH_2), 2.34 (s, 2H, CH_2), 1.90 (m, 4H, 2x CH_2), 1.82 (m, 2H, CH_2); ^{13}C NMR ($CDCl_3$, 100 MHz) δ: 158.4, 151.0, 147.4, 128.6, 128.3, 123.5, 122.9, 120.2, 115.9, 48.1, 40.5, 34.4, 34.0, 25.1, 23.1, 22.8.

***N*-(1,2,3,4-tetrahydroacridin-9-yl)butane-1,4-diamine C4**

Brown oil, Yield 76%; silica gel R_f 0.05 (MeOH/DCM 10% *v/v*); H NMR ($CDCl_3$) δ: 7.91 (m, 2H, Ar-H), 7.54 (m, 1H, Ar-H), 7.34 (m, 1H, Ar-H), 3.50 (t, J = 7.5Hz, 2H, CH_2), 3.07 (m, 2H, CH_2), 2.74 (m, 4H, 2x CH_2), 1.92 (m, 4H, 2x CH_2), 1.65 (m, 4H, 2x CH_2); ^{13}C NMR ($CDCl_3$) δ: 158.4, 150.7, 147.4, 128.7, 128.3, 123.6, 122.8, 120.2, 116.0, 53.4, 49.4, 41.8, 34.0, 29.1, 24.8, 23.0, 22.8.

***N*-(1,2,3,4-tetrahydroacridin-9-yl)pentane-1,5-diamine C5**

Brown oil, Yield 47%; silica gel R_f 0.05 (MeOH/DCM 10% *v/v*); H NMR($CDCl_3$) δ: 7.92 (m, 2H, Ar-H), 7.54 (m, 1H, Ar-H), 7.33 (m, 1H, Ar-H), 3.48 (t, J = 7.5Hz, 2H, CH_2), 3.05 (m, 2H, CH_2), 2.67 (m, 4H, 2x CH_2), 1.89 (m, 4H, 2x CH_2), 1.57 (m, 6H, 3x CH_2); ^{13}C NMR ($CDCl_3$) δ: 158.4, 150.8, 147.3, 128.6, 128.3, 123.6, 122.8, 120.2, 115.9, 49.4, 48.6, 41.9, 33.9, 33.3, 31.6, 24.8, 24.2, 22.7.

Synthesis of N_a,N_t-bis(tert-butoxycarbonyl)-D-histidine C6

The reaction mixture of L-Histidine (1.0 eq, 2.0 g), triethyl- amine (2.0 eq, 3.6 ml) and di-tert-butyl dicarbonate (Boc_2O, 2.3 eq, 6.5 g) was stirred in methanol (10 mL) under a nitrogen atmosphere at rt for 24h. The solvent was removed in vacuo to give compound **C6**. Yield: 92%; silica gel R_f =0.18 (MeOH/DCM 10% *v/v*); mp 73-75 °C; ^{1}H NMR (600 MHz, DMSO-d6): δH

8.06 (s, 1H, Ar-H), 7.29 (s, 2H, exchange with D_2O, N*H* + Ar-H), 4.25 (dd, J = 4, 8 Hz, 1H, CH), 3.08 (dd, J = 4, 15 Hz, 1H, CH), 2.87 (dd, J 8, 15 Hz, 1H, CH), 1.61 (s, 9H, 3x CH_3), 1.40 (s, 9H, 3x CH_3); ^{13}C NMR (600 MHz, CD_3OD) δ: 178.1, 157.5, 148.3, 141.1, 137.6, 116.1, 86.9, 80.1, 56.6, 31.1, 28.8, 28.1.

Synthesis of N-[(tert-butoxy) carbonyl]-L-tryptophan C8

The reaction mixture of L-tryptophan (1.0 eq, 1,5g), triethyl- amine (1.5 eq, 1,53ml) and di-tert-butyl dicarbonate (Boc_2O, 6.36 mmol) was stirred in methanol (10 mL) under a nitrogen atmosphere at rt for 24h. The solvent was removed in vacuo to give compound **C8**. Yield: 80%; silica gel R_f =0.15 (MeOH/DCM 10% *v/v*); ^1H NMR ($CDCl_3$) δ: 9.17 (s, 1H, exchange with D_2O, N*H*), 8.13 (s, 1H, Ar-H), 7.60 (m, 1H, exchange with D_2O, N*H*), 7.34 (m, 1H, Ar-H), 7.14 (m, 2H, Ar-H), 7.01 (s, 1H, Ar-H), 4.66 (s, 1H, CH), 3.36 (m, 2H, CH_2), 1.35 (m, 9H, 3x CH_3).

Synthesis of Nα-Boc-Nε-Cbz-L-lysine C9

N_6-Carbobenzyloxy-L-lysine (2.0 g, 1 eq) and K_2CO_3 (1.08 g, 1.1 eq) were dissolved in a mixture of water (22 mL) and 1,4-dioxane (9 mL). Then, a solution of Boc_2O (1.64g, 1.05eq) in 1,4-dioxane (9mL) was added dropwise and the mixture was stirred 24h at rt. After monitoring the reaction by TLC solvents were evaporated under vacuum, water (4mL) was added and then the mixture was acidified to pH 2-3 with an aqueous solution of HCl 1M. The mixture was extracted with EtOAc (30 mL x 3) and the collected organic layer was dried over Na_2SO_4 and evaporated under vacuum to give **C9**. Yellow oil, Yield 85%; silica gel R_f =0.28 (MeOH/DCM 10% *v/v*); ^1H NMR (CH2) δ: (ppm) 8.90 (s,1H, exchange with D_2O, N*H*), 7.30 (m, 5H, Ar-H), 6.18 (s, 1H, exchange with D_2O, N*H*), 5.01 (m, 3H, CH_2 + CH), 4.83 (s, 1H, CH), 4.12 (m, 1H, CH_2), 3.12 (m, 2H, CH_2), 1.60 (m, 13H, 3x CH_3 + 2x CH_2). ^{13}C-NMR (150 MHz CH2) δ: (ppm) 176.4, 156.8, 156.0, 136.6, 128.7, 128.3, 128.1, 80.4, 66.9, 53.3, 40.7, 32.0, 29.3, 29.5, 22.1.

General procedure for coupling reactions to obtain hybrids C10-C22

To a solution of compound **C6-C9** (1.0 eq) in dry DMF (3 mL), PyBOP (1-2 eq) and DIPEA (3eq) were added and the reaction mixture was stirred for 15min; then compound **C3-C5** (0.3 g, 1 eq) dissolved in dry DMF (3 mL) was added to the reaction mixture and stirred for 24h. After

monitoring by TLC (MeOH/DCM 5-15 % v/v), water (15 mL) was added, and the mixture was extracted with CH_2Cl_2 (3x30 mL). The combined organic layers were dried over Na_2SO_4 and the solvent was eliminated under reduced pressure. The crude was then purified by means of flash chromatography.

***Tert*-butyl 4-(2-((*tert*-butoxycarbonyl)amino)-3-oxo-3-((3-((1,2,3,4-tetrahydroacridin-9-yl)amino)propyl)amino)propyl)-1*H*-imidazole-1-carboxylate C10**

Starting from compound **C6** (0.41 g, 1.0 eq) PyBOP (0.61 g, 1.0 eq), DIPEA (0.61 mL, 3.0 eq) and compound **C3** (0.3 g, 1.0 eq), the title compound was obtained following the general procedure described above. The reaction was monitored by TLC (MeOH/CH_2Cl_2 10% *v/v*). The crude was purified by column chromatography (MeOH/CH_2Cl_2 20% v/v) to afford the title compound. Yield 20%; silica gel R_f 0.39 (MeOH/DCM 10% *v/v*); ^{1}H NMR (400 MHz, DMSO) δ: 8.36 (s, 1H, Ar-H), 8.11 (d, J = 10.6 Hz, 2H, Ar-H), 7.83 (s, 2H, Ar-H), 7.58 (s, 1H, Ar-H), 7.24 (s, 1H, exchange with D_2O, CON*H*), 6.96 (d, J = 8.4 Hz, 1H, exchange with D_2O, CON*H*), 3,45 (m, 1H, exchange with D_2O, CH), 3.01 (m, 2H, CH_2), 2.71 (m, 2H, CH_2), 1.82 (d, J = 42.0 Hz, 12H, 6 x CH_2), 1.56 (s, 9H, 3 x CH_3), 1.32 (s, 9H, 3x CH_3).

***Tert*-butyl (3-(1*H*-imidazol-4-yl)-1-oxo-1-((4-((1,2,3,4-tetrahydroacridin-9-yl)amino)butyl)amino)propan-2-yl)carbamate C11**

Starting from compound **C6** (0.395 g, 1.0 eq) PyBOP (0.58 g, 1.0 eq), DIPEA (0.58 mL, 3.0 eq) and compound **C4** (0.3 g, 1.0 eq), the title compound was obtained following the general procedure described above. The reaction was monitored by TLC (MeOH/CH_2Cl_2 10% *v/v*). The crude was purified by column chromatography (MeOH/CH_2Cl_2 20%v/v) to afford the title compound. Yield 19%; silica gel R_f 0.27 (MeOH/DCM 10% *v/v*); ^{1}H NMR (400 MHz, DMSO) δ: 11.90 (m, 1H, exchange with D_2O, N*H*), 8.18 (m, 1H, Ar-H), 7.77 (m, 2H, Ar-H), 7.59 (m, 2H, Ar-H), 7.41 (t, *J* = 7.6 Hz, 2H, Ar-H), 6.88 (d, *J* = 7.7 Hz, 1H, exchange with D_2O, CON*H*), 6.78 (s, 1H, exchange with D_2O, CON*H*), 5.61 (s, 1H, exchange with D_2O, N*H*), 4.15 (m, 1H, CH), 3.07 (d, *J* = 3.6 Hz, 2H, CH_2), 3.00 (m, 1H, CH), 2.95 (m, 2H, CH_2), 2.84 (s, 1H, CH), 2.74 (m, 2H, CH_2), 1.87 (s, 4H, 2x CH2), 1.79 (t, *J* = 6.4 Hz, 2H, CH_2), 1.56 (s, 2H, CH_2), 1.40 (m, 9H, 3x CH_3).

***Tert*-butyl 4-(2-((*tert*-butoxycarbonyl)amino)-3-oxo-3-((6-((1,2,3,4-tetrahydroacridin-9-yl)amino)pentyl)amino)propyl)-1*H*-imidazole-1-carboxylate C12**

Starting from compound **C6** (0.38g, 1.0 eq) PyBOP (0.55 g, 1.0 eq), DIPEA (0.55 mL, 3.0 eq) and compound **C5** (0.3 g, 1.0 eq), the title compound was obtained following the general procedure described above. The reaction was monitored by TLC ($MeOH/CH_2Cl_2$ 5% *v/v*). The crude was purified by column chromatography ($MeOH/CH_2Cl_2$ 20%v/v) to afford the title compound. Yield 18 %; silica gel R_f 0.18 (MeOH/DCM 5% *v/v*); 1H NMR (400 MHz, DMSO) δ: 8.36 (d, J = 8.6 Hz, 1H, Ar-H), 8.13 (d, 1H, Ar-H), 7.84 (m, J = 9.1 Hz, 3H, Ar-H), 7.57 (t, J = 7.3 Hz, exchange with D_2O, CON*H*), 7.22 (d, 1H, Ar-H), 6.87 (d, J = 8.3 Hz, 1H, exchange with D_2O, CON*H*), 3,45 (m, 1H, exchange with D_2O, CH), 3.00 (m, 2H, CH_2), 2.70 (m, 2H, CH_2), 1.87 (m, 4H, 2 x CH_2), 1.72 (m, 2H, CH_2), 1.57 (s, 9H, 3 x CH_3), 1.35 (m, 19H, 3x CH_3, 5 x CH_2).

Tert-butyl (S)-(3-(1H-imidazol-4-yl)-1-oxo-1-((5-((1,2,3,4-tetrahydroacridin-9-yl)amino)pentyl)amino)propan-2-yl)carbamate C13

Starting from compound **C6** (devoid of BOC on NH of imidazole) (0.395 g, 1.0 eq) PyBOP (0.58 g, 1.0 eq), DIPEA (0.58 mL, 3.0 eq) and compound **C5** (0.3 g, 1.0 eq), the title compound was obtained following the general procedure described above. The reaction was monitored by TLC ($MeOH/CH_2Cl_2$ 10% *v/v*). The crude was purified by column chromatography ($MeOH/CH_2Cl_2$ 20%v/v) to afford the title compound. Yield 37%; silica gel R_f 0.13 (MeOH/DCM 5% *v/v*); ^{1}H NMR (400 MHz, DMSO) δ: 13.10 (m, 1H exchange with D_2O, N*H*), 8.42 (d, *J* = 8.2 Hz, 1H, Ar-H), 8.17 (s, 1H, Ar-H), 7.89 (d, *J* = 6.5 Hz, 1H, Ar-H), 7.82 (s, 2H, Ar-H), 7.73 (s, 1H, exchange with D_2O, CON*H*), 7.63 (d, *J* = 7.6 Hz, 1H, Ar-H), 6.99 (m, 2H, exchange with D_2O, CON*H* + Ar-H), 4.14 (s, 4H, 2x CH_2), 3.87 (s, 2H, CH_2), 3.52 (m, 1H, CH), 3.07 (s, 2H, CH_2), 3.01 (s, 2H, CH_2), 2.91 (m, 1H, CH), 2.78 (m, 1H, CH_2), 2.69 (s, 2H, CH_2), 1.87 (s, 4H, 2x CH_2), 1.76 (s, 2H, CH_2), 1.36 (m, 9H, 3x CH_3).

***Tert*-butyl-(1-oxo-3-phenyl-1-((3-((1,2,3,4-tetrahydroacridin-9-yl)amino)propyl)amino)propan-2-yl)carbamate C14**

Starting from compound **C7** (0.31 g, 1.0 eq) PyBOP (0.61 g, 1.0 eq), DIPEA (0.61 mL, 3.0 eq) and compound **C3** (0.3 g, 1.0 eq), the title compound was obtained following the general procedure described above. The reaction was monitored by TLC ($MeOH/CH_2Cl_2$ 5% *v/v*). The crude was purified by column chromatography ($MeOH/CH_2Cl_2$) to afford the title compound. Yield 31%; silica gel R_f 0.19 (MeOH/DCM 5% *v/v*); 1H NMR (400 MHz, DMSO) δ: 8.29 (d, J = 8.6 Hz, 1H, Ar-H), 8.09 (t, J = 5.5 Hz, 1H, exchange with D_2O, CON*H*), 7.82 (d, J = 8.3 Hz, 1H, Ar-H), 7.71 (t, J = 7.6 Hz, 1H, Ar-H), 7.50 (t, J = 7.5 Hz, 1H, Ar-H), 7.24 (d, J = 27.9 Hz, 5H, Ar-H), 6.99 (d, J = 8.3 Hz, 1H, exchange with D_2O, CON*H*), 3,45 (m, 1H, exchange with D_2O, CH), 2.99 (m, 1H, CH_2), 2.76 (m, 1H, CH_2), 1.88 (m, 6H, 3 x CH_2), 1.76 (m, 2H, CH_2), 1.26 (m, 13H, 3 x CH_3, 2 x CH_2). ^{13}C NMR (100 MHz, DMSO) δ: 177.69, 172.60, 155.72, 155.06, 152.50, 140.09, 138.61, 132.17, 129.63, 128.46, 126.63, 125.25, 125.07, 112.62, 78.44, 56.47, 44.96, 40.27, 38.02, 36.09, 30.59, 29.49, 28.57, 24.65, 22.20, 21.18.

***Tert*-butyl-(1-oxo-3-phenyl-1-((4-((1,2,3,4-tetrahydroacridin-9-yl)amino)butyl)amino)propan-2-yl)carbamate C15**

Starting from compound **C7** (0.3 g, 1.0 eq) PyBOP (0.58 g, 1.0 eq), DIPEA (0.58 mL, 3.0 eq) and compound **C4** (0.3 g, 1.0 eq), the title compound was obtained following the general procedure described above. The reaction was monitored by TLC ($MeOH/CH_2Cl_2$ 5% *v/v*). The crude was purified by column chromatography ($MeOH/CH_2Cl_2$) to afford the title compound. Yield 17%; silica gel R_f 0.1 (MeOH/DCM 5% *v/v*); 1H NMR (400 MHz, DMSO) δ: 8.33 (d, 1H, Ar-H), 7.93 (m, 1H, Ar-H), 7.80 (m, 2H, exchange with D_2O, CON*H*), 7.55 (m, 1H, Ar-H), 7.25 (m, J = 16.3 Hz, 5H, Ar-H), 6.91 (d, J = 9.1 Hz, 1H, exchange with D_2O, CON*H*), 3,45 (m, 1H, exchange with D_2O, CH), 3.08 (m, 2H, CH_2), 2.99 (m, 2H, CH_2), 2.73 (m, 2H, CH_2), 1.88 (m, 4H, 2 x CH_2), 1.67 (m, 2H, CH_2), 1.47 (m, 2H, CH_2), 1.31 (m, 13H, 3 x CH_3, 2 x CH_2). ^{13}C NMR (100 MHz, DMSO) δ: 177.7, 177.69, 172.60, 155.72, 155.06, 152.50, 140.09, 138.61, 132.17, 129.63, 128.46, 126.63, 125.25, 125.07, 112.62, 78.44, 56.28, 47.54, 46.45, 38.62, 38.18, 28.58, 27.78, 26.49, 24.61, 22.29, 21.08.

***Tert*-butyl-(1-oxo-3-phenyl-1-((5-((1,2,3,4-tetrahydroacridin-9-yl)amino)pentyl)amino)propan-2-yl)carbamate C16**

Starting from compound **C7** (0.28 g, 1.0 eq) PyBOP (0.55 g, 1.0 eq), DIPEA (0.55 mL, 3.0 eq) and compound **C5** (0.3 g, 1.0 eq), the title compound was obtained following the general procedure described above. The reaction was monitored by TLC ($MeOH/CH_2Cl_2$ 5% *v/v*). The crude was purified by column chromatography ($MeOH/CH_2Cl_2$ 10% v/v) to afford the title compound. Yield 18%; silica gel R_f 0.05 (MeOH/DCM 10% *v/v*); 1H NMR (400 MHz, DMSO) **δ**: 8.25 (d, J = 8.6 Hz, 1H, Ar-H), 7.86 (t, 1H, exchange with D_2O, CON*H*), 7.78 (d, J = 8.2 Hz, 1H, Ar-H), 7.68 (t, 1H, Ar-H), 7.46 (t, 1H, Ar-H), 7.24 (m, 5H, Ar-H), 6.88 (d, J = 8.5 Hz, 1H, exchange with D_2O, CON*H*), 3,45 (m, 1H, exchange with D_2O, CH), 3.06 (m, 2H, CH_2), 2.93 (m, 2H, CH_2), 2.72 (m, 2H, CH_2), 1.85 (m, 4H, 2 x CH_2), 1.65 (m, 2H, CH_2), 1.30 (m, 17H, 3 x CH_3, 4 x CH_2).

***Tert*-butyl (3-(1*H*-indol-3-yl)-1-oxo-1-((3-((1,2,3,4-tetrahydroacridin-9 yl)amino)propyl)amino)propan-2-yl)carbamate C17**

Starting from compound **C8** (0.18 g, 1.0 eq) PyBOP (0.31 g, 1.0 eq), DIPEA (0.31 mL, 3.0 eq) and compound **C3** (0.15 g, 1.0 eq), the title compound was obtained following the general procedure described above. The reaction was monitored by TLC ($MeOH/CH_2Cl_2$ 5% *v/v*). The crude was purified by column chromatography ($MeOH/CH_2Cl_2$) to afford the title compound. Yield: 28%, silica gel R_f =0,15 (MeOH/DCM 10% *v/v*); mp 88.3-92.7°C. 1 H NMR (500 MHz, Methanol-d4) d: 8.05 (d, J= 8.5 Hz, 1H, Ar-H), 7.74 (m, 1H, Ar-H), 7.54 (m, 2H, Ar-H), 7.36 (m, 1H, Ar-H), 7.26 (d, J = 8.1 Hz, 1H, Ar-H), 7.06 (s, 1H, Ar-H), 6.98 (m, 2H, Ar-H), 4.28 (m, 1H, CH), 3.16 (m, 2H, CH_2), 2.95 (t, J = 6.0 Hz, 2H,), 2.69 (t, J = 5.9 Hz, 2H, CH_2), 1.92 (m, 4H, 2x CH_2), 1.88 (m, 2H, CH_2), 1.60 (m, 2H, CH_2), 1.34 (s, 9H, 3x CH_3), 1.18 (m, 2H, CH_2). ^{13}C NMR (100 MHz, Methanol-d4) d: 175.18, 172.95, 158.45, 157.52, 153.39, 147.02, 137.97, 130.11, 128.77, 127.18, 125.02, 124.55, 122.38, 120.96, 119.74, 119.41, 116.74, 112.22, 110.96, 80.62, 61.51, 57.28, 46.10, 37.52, 33.71, 31.62, 26.12, 23.97, 22.06, 20.85.

***Tert*-butyl (3-(1*H*-indol-3-yl)-1-oxo-1-((4-((1,2,3,4-tetrahydroacridin-9-yl)amino)butyl)amino)propan-2-yl)carbamate C18**

Starting from compound **C8** (0.18 g, 1.0 eq) PyBOP (0.31 g, 1.0 eq), DIPEA (0.31 mL, 3.0 eq) and compound **C4** (0.15 g, 1.0 eq), the title compound was obtained following the general procedure described above. The reaction was monitored by TLC ($MeOH/CH_2Cl_2$ 5% *v/v*). The

crude was purified by column chromatography (MeOH/CH_2Cl_2) to afford the title compound. Yield: 21%; silica gel R_f =0.14(MeOH/DCM 10% *v/v*); ^{1}H NMR (500 MHz, Methanol-d4) d: 8.02 (d, J = 8.5 Hz, 1H, Ar-H), 7.74 (dd, J = 8.5, 1.2 Hz, 1H, Ar-H), 7.52 (m, 2H, Ar-H), 7.33 (m, 1H, Ar-H), 7.26 (d, J = 8.0 Hz, 1H, Ar-H), 7.05 (s, 1H, Ar-H), 6.98 (m, 2H, Ar-H), 4.26 (m, 1H, CH), 3.38 (m, 2H, CH_2), 3.14 (m, 2H, CH_2), 2.94 (t, J = 6.1 Hz, 2H, CH_2), 2.67 (t, J = 5.8 Hz, 2H, CH_2), 1.86 (m, 4H, 2 x CH_2), 1.33 (m, 13H, 3x CH_3 + 2x CH_2), 1.18 (s, 2H, CH2). ^{13}C NMR (100 MHz, Methanol-d4) d: 174.65, 172.94, 159.10, 157.46, 153.03, 147.90, 137.98, 129.70, 128.82, 127.94, 124.73, 124.37, 122.37, 121.27, 119.74, 119.46, 116.80, 112.20, 110.98, 80.58, 61.51, 57.18, 39.95, 34.17, 29.39, 28.63, 27.54, 26.10, 24.07, 23.66, 20.85.

***Tert*-butyl (3-(1*H*-indol-3-yl)-1-oxo-1-((5-((1,2,3,4-tetrahydroacridin-9-yl)amino)pentyl)amino)propan-2-yl)carbamate C19**

Starting from compound **C8** (0.322 g, 1.0 eq) PyBOP (0.55 g, 1.0 eq), DIPEA (0.55 mL, 3.0 eq) and compound **C5** (0.3 g, 1.0 eq), the title compound was obtained following the general procedure described above. The reaction was monitored by TLC (MeOH/CH_2Cl_2 5% *v/v*). The crude was purified by column chromatography (MeOH/CH_2Cl_2) to afford the title compound. Yield: 20%; silica gel R_f 0.05 (MeOH/DCM 5% *v/v*); mp 73.3-76.8°C. 1 H NMR (300 MHz, Methanol-d4) d: 8.04 (m, 1H, Ar-H), 7.75 (m, 1H, Ar-H), 7.52 (m, 2H, Ar-H), 7.33 (m, 1H, Ar-H), 7.24 (d, J = 7.9 Hz, 1H, Ar-H), 6.97 (m, 3H, Ar-H), 4.25 (m, 1H, CH), 3.39 (m, 2H, CH2), 3.11 (m, 2H, CH_2), 2.94 (m, 4H, 2x CH_2), 2.69 (m, 2H, CH_2), 1.95 (m, 2H, CH_2), 1.87 (m, 6H, 3x CH_2), 1.50 (m, 2H, CH_2), 1.34 (s, 9H, 3x CH_3). ^{13}C NMR (100 MHz,Methanol-d4) d: 174.58, 172.92, 159.07, 157.44, 153.17, 147.91, 137.96, 129.71, 128.79, 127.93, 124.70, 124.42, 122.35, 121.30, 119.71, 119.42, 116.78, 112.18, 110.96, 80.55, 61.50, 57.14, 40.14, 34.16, 31.91, 29.83, 29.42, 26.09, 25.01, 24.07, 23.68, 20.85.

Benzyl *tert*-butyl (6-oxo-6-((3-((1,2,3,4-tetrahydroacridin-9-yl)amino)propyl)amino)hexane-1,5-diyl)dicarbamate C20

Starting from compound **C9** (0.45 g, 1.0 eq) PyBOP (0.61 g, 1.0 eq), DIPEA (0.61 mL, 3.0 eq) and compound **C3** (0.3 g, 1.0 eq), the title compound was obtained following the general procedure described above. The reaction was monitored by TLC (MeOH/CH_2Cl_2 5% *v/v*). The crude was purified by column chromatography (MeOH/CH_2Cl_2, 50% v/v) to afford the title

compound. Yield 29%; silica gel R_f 0.043 (MeOH/DCM 5% *v/v*); 1H NMR (400 MHz, DMSO) δ: 8.30 (d, J = 8.3 Hz, 1H, Ar-H), 7.98 (t, 1H, exchange with D_2O, CON*H*), 7.82 (d, J = 8.3 Hz, 1H,Ar-H), 7.75 (t, J = 7.1 Hz, 1H, Ar-H), 7.52 (t, J = 7.5 Hz, 1H, Ar-H), 7.36 (m, 5H, Ar-H), 7.26 (t, 1H, exchange with D_2O, CON*H*), 6.86 (d, J = 7.8 Hz, 1H, exchange with D_2O, CON*H*), 6.46 (t, 1H, exchange with D_2O, N*H*), 5.03 (s, 2H, CH_2), 3.83 (m, 1H, CH), 3.68 (m, 2H, CH_2), 3.19 (m, 2H, CH_2), 2.98 (m, 4H, 2 x CH_2), 2.73 (m, 2H, CH_2), 1.81 (m, 6H, 3 x CH_2), 1.51 (m, 2H, CH_2), 1.42 – 1.19 (m, 13H, 3x CH_3 + 2x CH_2). ^{13}C NMR (100 MHz, DMSO) δ: 172.53, 156.77, 155.75, 154.60, 137.81, 131.85, 128.80, 128.18, 128.14, 126.27, 125.10, 125.02, 124.95, 122.17, 117.40, 112.92, 79.01, 66.16, 55.71, 47.91, 45.73, 40.32, 36.53, 32.62, 31.39, 30.07, 29.10, 25.50, 23.97, 23.23, 22.27.

Benzyl *tert*-butyl (6-oxo-6-((4-((1,2,3,4-tetrahydroacridin-9-yl)amino)butyl)amino)hexane-1,5-diyl)dicarbamate C21

Starting from compound **C9** (0.41 g, 1.0 eq) PyBOP (1.12 g, 2.0 eq), DIPEA (0.56 mL, 3.0 eq) and compound **C4** (0.3 g, 1.0 eq), the title compound was obtained following the general procedure described above. The reaction was monitored by TLC ($MeOH/CH_2Cl_2$ 5% *v/v*). The crude was purified by column chromatography ($MeOH/CH_2Cl_2$, 50% v/v) to afford the title compound. Yield 32%; silica gel R_f 0.045 (MeOH/DCM 5% *v/v*); ^1H NMR (400 MHz, DMSO) δ: 8.36 (d, J = 8.5 Hz, 1H, Ar-H), 7.91 (d, J = 8.4 Hz, 1H, Ar-H), 7.82 (m, 2H, Ar-H + exchange with D_2O, CON*H*), 7.54 (t, J = 7.6 Hz, 1H, Ar-H), 7.36 (m, 5H, Ar-H), 7.26 (t, 1H, exchange with D_2O, CON*H*), 7.15 (s, 1H, exchange with D_2O, CON*H*), 6.77 (d, J = 7.8 Hz, 1H, exchange with D_2O, N*H*), 5.03 (s, 2H, CH_2), 3.83 (m, 1H, CH), 3.76 (m, 2H, CH_2), 3.09 (m, 2H, CH_2), 2.99 (m, 4H, 2 x CH_2), 2.71 (m, 2H, CH_2), 1.86 (m, 4H, 2 x CH_2), 1.70 (m, 2H, CH_2), 1.50 (m, 4H, 2 x CH_2), 1.38 (s, 9H, 3x CH_3), 1.26 (m, 4H, 2 x CH_2). ^{13}C NMR (100 MHz, DMSO) δ: 172.53, 156.77, 155.75, 154.60, 137.81, 131.85, 128.80, 128.18, 128.14, 126.27, 125.10, 125.02, 124.95, 122.17, 117.40, 112.92, 78.38, 65.57, 54.88, 47.59, 40.57, 40.16, 38.49, 32.21, 29.57, 28.63, 27.95, 26.82, 24.74, 23.26, 22.30, 21.36.

Benzyl *tert*-butyl (6-oxo-6-((5-((2-propylquinolin-4-yl)amino)pentyl)amino)hexane-1,5-diyl)dicarbamate C22

Starting from compound **C9** (0.40 g, 1.0 eq) PyBOP (0.55 g, 1.0 eq), DIPEA (0.55 mL, 3.0 eq) and compound **C5** (0.3 g, 1.0 eq), the title compound was obtained following the general procedure described above. The reaction was monitored by TLC ($MeOH/CH_2Cl_2$ 5% *v/v*). The crude was purified by column chromatography ($MeOH/CH_2Cl_2$, 50% v/v) to afford the title compound. Yield: 350mg, 52%; silica gel R_f =0.12 (MeOH/DCM 10% *v/v*); ^1H NMR (400 MHz, DMSO) δ: 8.21 (d, *J* = 8.4 Hz, 1H, Ar-H), 7.78 (m, 3H, 2Ar-H + exchange with D_2O, CON*H*), 7.64 (m, 1H, Ar-H), 7.40 (m, 5H, Ar-H), 7.26 (s, 1H, exchange with D_2O, CON*H*), 6.76 (d, *J* = 7.8 Hz, 1H, exchange with D_2O, CON*H*), 5.03 (m, 3H, exchange with D_2O, N*H* + CH_2), 3.84 (m, 2H, CH_2), 3.56 (m, 1H, CH), 3.38 (s, 4H, CH_2), 3.06 (m, 2H, 2x CH_2), 2.96 (m, 2H, 2x CH_2), 2.74 (m, 2H, 2x CH_2), 1.83 (m, 9H, 3x CH_3), 1.76 (m, 1H, CH), 1.64 (m, 1H, CH), 1.53 (m, 6H, 3x CH_2), 1.28 (m, 6H, 3x CH_2).

General procedure for the removal of the Nα Boc protection

To a solution of the appropriate intermediate in MeOH (2-8,5 mL), HCl 5M (1-4 mL) was added and the reaction mixture was stirred overnight at RT. After monitoring by TLC (MeOH/DCM 10% *v/v*), $NaHCO_3$ was added and the mixture was extracted with CH_2Cl_2 (30 mL x 3). The collected organic layer was dried over Na_2SO_4 and evaporated under vacuum. The crude compound was treated with HCl 1.25 M in MeOH (1.1 eq) to afford the title compound as hydrochloride salt.

2-amino-3-phenyl-*N*-(3-((1,2,3,4-tetrahydroacridin-9-yl)amino)propyl)propanamide C23

Yield 98%; silica gel R_f 0.11 (MeOH/DCM 10% *v/v*); ^1H NMR (400 MHz, DMSO) δ: 8.80 (s, 1H, Ar-H), 8.45 (d, *J* = 6.8 Hz, 1H, Ar-H), 8.33 (m, 1H, Ar-H), 7.92 (m, 2H, Ar-H), 7.79 (s, 1H, Ar-H), 7.61 (s, 1H, exchange with D_2O, CON*H*), 7.25 (M, 5H, Ar-H), 4.14 (s, 2H, CH_2), 3.98 (s, 1H, CH), 3.82 (s, 2H, CH_2), 3.47 (s, 2H, CH_2), 3.04 (s, 2H, CH_2), 2.71 (s, 2H, CH_2), 1.87 (m, 6H, 3x CH_2).

2-amino-3-phenyl-*N*-(4-((1,2,3,4-tetrahydroacridin-9-yl)amino)butyl)propanamide C24

Yield 82%; silica gel R_f 0.15 (MeOH/DCM 10% *v/v*); ^1H NMR (400 MHz, DMSO) δ: 8.27 (d, *J* = 8.6 Hz, 1H, Ar-H), 8.18 (s, 1H, Ar-H), 7.82 (d, *J* = 8.3 Hz, 1H, Ar-H), 7.71 (t, *J* = 7.5 Hz, 1H, Ar-H), 7.49 (t, *J* = 7.4 Hz, 1H, exchange with D_2O, CON*H*), 7.27 (m, 5H, Ar-H), 6.34 (s, 1H,

exchange with D_2O, N*H*), 3.69 (d, *J* = 6.8 Hz, 1H, CH2), 3.60 (d, *J* = 6.7 Hz, 2H, CH_2), 3.42 (s, 2H, CH_2), 3.06 (m, 1H, CH), 2.97 (m, 2H, CH_2), 2.85 (m, 1H, CH_2), 2.75 (s, 2H, CH_2), 1.88 (s, 4H,2xCH_2), 1.56 (m, 2H, CH_2), 1.42 (m, 2H, CH_2).^{13}C NMR (100 MHz, DMSO) δ: 170.35, 154.82, 153.50, 142.80, 136.80, 130.76, 129.84, 128.73, 128.50, 127.13, 124.63, 124.55, 118.33, 113.93, 54.98, 47.69, 46.40, 38.69, 31.15, 28.01, 26.58, 25.02, 22.58, 21.82.

2-amino-3-phenyl-*N*-(4-((1,2,3,4-tetrahydroacridin-9-yl)amino)pentyl)propanamide C25

Yield 79%; silica gel R_f 0.14 (MeOH/DCM 10% *v/v*); ^{1}H NMR (400 MHz, DMSO) δ: 8.44 (m, 2H, Ar-H), 7.87 (m, 2H, Ar-H), 7.59 (m, 2H, exchange with D_2O, CON*H* + Ar-H), 7.29 (m, 5H, Ar-H), 3.94 (t, *J* = 7.0 Hz, 1H, CH), 3.81 (m, 2H, CH_2), 3.46 (s, 2H, CH_2), 3.15 (m, 1H, CH), 3.02 (s, 2H, CH_2), 2.95 (m, 1H, CH), 2.71 (s, 2H, CH_2), 1.86 (s, 4H 2x CH_2), 1.71 (m, 2H, CH_2), 1.32 (m, 4H, 2x CH_2).

2-amino-3-(1*H*-indol-3-yl)-*N*-(3-((1,2,3,4-tetrahydroacridin-9-yl)amino)propyl)propanamide C26

Yield 66%; silica gel R_f 0.045 (MeOH/DCM 10% *v/v*); mp 148.8-152.0 °C. ^{1}H NMR (500 MHz, Methanol-d4) d: 8.28 (d, J ¼ 8.7 Hz, 1H, Ar-H), 7.81 (d, J ¼ 4.0 Hz, 2H, Ar-H), 7.54 (m, 2H, Ar-H), 7.23 (d, J ¼ 8.0 Hz, 1H, Ar-H), 7.10 (s, 1H, Ar-H), 6.94 (m, 2H, Ar-H), 4.28 (m, 1H, CH_2), 3.18 (m, 2H, CH_2), 3.02 (m, 2H, CH_2), 2.68 (m, 2H, CH_2), 1.94 (m, 8H, 4x CH_2), 1.80 (m, 2H, CH_2). ^{13}C NMR (100 MHz, Methanol-d4) d: 175.48, 157.91, 151.69, 139.64, 137.92, 133.98, 128.76, 126.44, 126.36, 124.68, 122.30, 120.12, 119.69, 119.40, 117.05, 112.95, 112.26, 110.85, 57.42, 45.69, 37.07, 31.27, 29.36, 28.64, 25.02, 23.01, 21.83.

2-amino-3-(1*H*-indol-3-yl)-*N*-(3-((1,2,3,4-tetrahydroacridin-9-yl)amino)butyl)propanamide C27

Yield 98%; silica gel R_f 0.048 (MeOH/DCM 10% *v/v*); mp 76.3-81.0°C. ^{1}H NMR (500 MHz, DMSO-d6) d: 10.78 (d, J = 2.4 Hz, 1H, exchange with D_2O, N*H*), 8.10 (d, J = 8.8 Hz, 1H, Ar-H), 7.83 (t, J = 5.7 Hz, 1H, Ar-H), 7.69 (dd, J = 8.3, 1.2 Hz, 1H, Ar-H), 7.55 (d, J = 7.9 Hz, 1H, Ar-H), 7.50 (ddd, J = 8.2, 6.7, 1.2 Hz, 1H, Ar-H), 7.32 (m, 2H, Ar-H), 7.10 (d, J = 2.3 Hz, 1H, exchange with D_2O, CON*H*), 6.99 (m, 2H, Ar-H), 6.67 (d, J = 8.3 Hz, 1H, Ar-H), 4.12 (m, 1H, CH), 3.02 (m, 2H, CH_2), 2.88 (m, 2H, CH_2), 2.70 (m, 2H, CH_2), 1.79 (m, 4H, 2x CH_2), 1.50 (m, 2H, CH_2), 1.38 (m, 2H, CH_2), 1.29 (m, 4H 2x CH_2). ^{13}C NMR (100 MHz,DMSO-d6) d: 171.92, 157.91, 155.26, 150.51, 146.89, 136.19, 128.25, 127.52, 123.74, 123.40, 123.23,

120.93, 120.31, 118.65, 118.25, 115.87, 111.37, 110.42, 78.05, 55.34, 47.83, 38.43, 33.57, 28.30, 26.64, 25.22, 22.90, 22.57.

2-amino-3-(1*H*-indol-3-yl)-*N*-(3-((1,2,3,4-tetrahydroacridin-9-yl)amino)pentyl)propanamide C28

Yield 98%; silica gel R_f 0.045 (MeOH/DCM 5% *v/v*); mp 118.5-121.1°C. ^{1}H NMR (300 MHz, D2O) d: (ppm) 7.73 (d, J = 8.6 Hz, 1H, Ar-H), 7.60 (m, 1H, Ar-H), 7.27 (m, 2H, Ar-H), 7.14 (m, 1H, Ar-H), 7.04 (m, 2H, Ar-H), 6.69 (m, 2H, Ar-H), 4.08 (m, 1H, CH), 3.65 (m, 2H, CH_2), 3.37 (m, 2H, CH_2), 3.03 (m, 2H, CH_2), 2.44 (m, 2H, CH_2), 2.22 (m, 4H, 2x CH_2), 1.65 (m, 4H, 2x CH_2), 1.41 (m, 2H, CH_2), 0.95 (m, 2H, CH_2). ^{13}C NMR (100 MHz,D2O) d: 168.82, 154.52, 148.87, 136.93, 135.46, 132.25, 126.23, 124.58, 124.51, 124.38, 121.14, 118.60, 118.18, 117.53, 114.21, 111.05, 110.34, 105.77, 57.28, 53.42, 46.97, 39.06, 30.10, 29.26, 27.11, 26.77, 22.93, 20.92, 19.80.

Benzyl(5-amino-6-oxo-6-((3-((1,2,3,4-tetrahydroacridin-9-yl)amino)propyl)amino)hexyl)carbamate C29

Yield 84%; silica gel R_f 0.052 (MeOH/DCM 10% *v/v*); ^{1}H NMR (400 MHz, DMSO) δ: 8.17 (d, *J* = 7.2 Hz, 1H, Ar-H), 7.99 (s, 1H, Ar-H), 7.75 (d, *J* = 8.2 Hz, 1H, Ar-H), 7.56 (t, *J* = 7.0 Hz, 1H, Ar-H), 7.38 (s, 5H, Ar-H), 7.24 (s, 1H, exchange with D_2O, CON*H*), 5.76 (s, 1H, exchange with D_2O, CON*H*), 5.60 (s, 1H, exchange with D_2O, N*H*), 5.03 (s, 2H, CH_2), 3.46 (s, 2H, CH_2), 3.24 (s, 1H, CH), 3.17 (m, 2H, CH_2), 3.09 (s, 1H, CH), 3.01 (m, 2H, CH_2), 2.94 (s, 2H, CH_2), 2.76 (s, 2H, CH_2), 1.85 (s, 4H, 2x CH_2), 1.71 (d, *J* = 5.6 Hz, 2H, CH_2), 1.57 (s, 1H, CH), 1.36 (m, 8H, 4x CH_2).^{13}C NMR (100 MHz, DMSO) δ: 175.34, 175.25, 158.37, 156.56, 150.70, 147.23, 128.81, 128.68, 128.42, 128.18, 124.01, 123.07, 120.67, 116.29, 98.40, 76.27, 65.60, 55.03, 45.55, 37.40, 36.22, 33.97, 31.16, 29.98, 25.68, 23.22, 23.02, 22.89.

Benzyl(5-amino-6-oxo-6-((3-((1,2,3,4-tetrahydroacridin-9-yl)amino)butyl)amino)hexyl)carbamate C30

Yield 85%; silica gel R_f 0.05 (MeOH/DCM 10% *v/v*); ^{1}H NMR (400 MHz, DMSO) δ: 8.52 (s, 1H, Ar-H), 8.33 (d, *J* = 8.5 Hz, 1H, Ar-H), 7.86 (d, *J* = 8.3 Hz, 1H, Ar-H), 7.75 (m, 1H, Ar-H), 7.50 (m, 1H, Ar-H), 7.35 (m, 5H, Ar-H), 7.26 (m, 1H, exchange with D_2O, CON*H*), 6.85 (s, 1H, exchange with D_2O, CON*H*), 5.02 (s, 2H, CH_2), 3.70 (s, 2H, CH_2), 3.63 (m, 1H, CH), 3.20

(m, 1H, CH), 3.10 (m, 1H, CH), 2.99 (s, 4H, 2x CH_2), 2.72 (s, 2H, CH_2), 1.85 (s, 4H, 2x CH_2), 1.70 (m, 4H, 2x CH_2), 1.51 (m, 2H, CH_2), 1.40 (m, 2H, CH_2), 1.27 (s, 2H, CH_2).^{13}C NMR (100 MHz, DMSO) δ: 175.34, 175.25, 158.37, 156.56, 150.70, 147.23, 128.81, 128.68, 128.42, 128.18, 124.01, 123.07, 120.67, 116.29, 98.40, 65.67, 58.38, 52.99, 47.61, 40.31, 39.46, 38.85, 29.49, 28.05, 26.80, 24.93, 22.51, 22.15, 21.72.

Benzyl(5-amino-6-oxo-6-((3-((1,2,3,4-tetrahydroacridin-9-yl)amino)pentyl)amino)hexyl)carbamate C31

Yield 79%; silica gel R_f 0.045 (MeOH/DCM 10% *v/v*); : ^{1}H NMR (400 MHz, DMSO) δ: 8.15 (d, *J* = 8.4 Hz, 1H, Ar-H), 7.87 (m, 2H, Ar-H + exchange with D_2O, CON*H*), 7.74 (d, *J* = 8.2 Hz, 1H, Ar-H), 7.55 (t, *J* = 7.4 Hz, 1H, Ar-H), 7.40 (m, 5H, Ar-H), 7,29 (s, 1H, exchange with D_2O, CON*H*), 5.44 (s, 1H, exchange with D_2O, N*H*), 5.03 (s, 2H, CH_2), 3.16 (d, *J* = 5.8 Hz, 1H, CH2), 3.04 (m, 4H, 2x CH2), 2.94 (t, *J* = 5.9 Hz, 2H, CH2), 2.74 (s, 2H, CH_2), 1.85 (m, 4H, 2x CH_2), 1.76 (m, 1H, CH), 1.68 (s, 1H, CH), 1.66 (s, 2H, CH_2), 1.59 (m, 2H, CH_2), 1.38 (m, 8H, 4x CH_2). ^{13}C NMR (100 MHz, DMSO) δ: 175.34, 175.25, 158.37, 156.56, 150.70, 147.23, 128.81, 128.68, 128.42, 128.18, 124.01, 123.07, 120.67, 116.29, 98.40, 65.56, 54.82, 48.46, 46.70, 43.64, 38.99, 38.80, 33.91, 30.88, 29.77, 29.24, 26.45, 25.15, 23.31, 22.77.

Synthesis of 9-aminotacrine C33

$AlCl_3$ (11.29 g, 1.0 eq) was added to the mixture of 2-cyanoaniline **C32** (10 g, 1.0 eq) and cyclohexanone (8.31g, 1.0 eq) in Toluene (250 ml), placed in a round bottom flask under N_2 fluss. The mixture was heated at refluss (110°C) for 24h under stirring. The reaction was monitored by TLC (MeOH/CH_2Cl_2 5% *v/v*). After cooling at RT, the suspension was filtrated and the remain solid was treated with NaOH 2M. The suspension was heated for 2h at refluss (100°C), and then was extracted with EtOAC (3 times). So, the result was dried with Na_2SO_4, filtrated and evaporated under pressure to give **C33** as an orange powder. Yield 77%. silica gel R_f =0.05 (MeOH/CH_2Cl_2 5% *v/v*); ^{1}H NMR (400 MHz, DMSO) δ: 8.16 (d, J = 8.3 Hz, 1H, Ar-H), 7.65 (d, J = 8.4 Hz, 1H, Ar-H), 7.51 (t, J = 11.0, 4.1 Hz, 1H, Ar-H), 7.31 (t, J = 11.1, 4.0 Hz, 1H, Ar-H), 6.32 (m, 2H, exchange with D_2O, NH_2), 2.86 (m, 2H, CH_2), 2.59 (t, J = 5.9 Hz, 2H, CH_2), 1.85 (m, 4H, 2 x CH_2).

Synthesis of *N*-(5-bromopentyl)-1,2,3,4-tetrahydroacridin-9-amine C34

To a solution of 9-aminotacrine **C33** (3.0 g, 1.0 eq) in DMF (18 ml), was added NaH (0.36 g, 1.0 eq), and the the result was stirred for 30min at RT. Then was added 1,5-dibromopentane (20.43 ml, 10 eq) at 0°C, and the mixture then was stirred for 48h at RT, under N_2 fluss. The reaction was monitored by TLC (MeOH/CH_2Cl_2, 10% *v/v*). The mixture was treated with an acid aqueous solution (40ml H_2O+20ml HCl 5M) and extracted with Et_2O (3 times). The aqueous solution was bringing to pH 10 with K_2CO_3 and extracted with CH_2Cl_2 (3x30mL). The organic layer was washed with Brine, dried over Na_2SO_4, filtrated, evaporated under vacuum and purified with a flash column chromatography (MeOH/CH_2Cl_2, 12%). Yield 42%; silica gel R_f 0.44 (MeOH/DCM 10% *v/v*); ^{1}H NMR ($CDCl_3$) δ: 8.38 (dd, *J* = 0.90, 8.59 Hz, 1H, Ar-H), 8.21 (d, *J* = 7.95 Hz, 1H, Ar-H), 7.66 (ddd, *J* = 1.03, 7.05, 8.34 Hz, 1H, Ar-H), 7.43 (ddd, *J* = 1.03, 7.12, 8.53 Hz, 1H, Ar-H), 3.92 (m, 2H, CH_2), 3.44 (t, *J* = 6.54 Hz, 2H, CH_2), 3.24 (m, 2H, CH_2), 2.69 (m, 2H, CH_2), 1.90 (m, 8H, 4x CH_2), 1.63 (m, 2H, CH_2), NH signal not detected.

Synthesis of *N*-(6-bromohexyl)-1,2,3,4-tetrahydroacridin-9-amine C36

The reaction mixture of phenol (5,2 g, 6.0 eq), 9-chlorotacrine **C2** (2.0 g, 1.0 eq), and KI (0,15 g, 0.1 eq) was heated at 90°C, for 10 minutes to form a liquid. To this mixture was added 6-aminohexan-1-ol (3.0 eq) and refluxed at 180°C for 3h. The reaction was monitored by TLC (MeOH/CH_2Cl_2 10% *v/v*). Then, the mixture was cooled to the room temperature and 20% aqueous solution of KOH was added. The solution was extracted with EtOAc and the resultant organic layer was washed with brine, dried over Na_2SO_4, filtrated and evaporated under vacuum. 6-((1,2,3,4-tetrahydroacridin-9-yl)amino)hexan-1-ol **C35** (7.61 g, 1.0 eq) was dissolved in CH_2Cl_2 dry (50 mL), and then CBr_4 (9.30 g, 1,1 eq) and PPh_3 (7.36 g, 1.1 eq) were added. The solution was stirred overnight, and after monitoring by TLC (MeOH/DCM 10% *v/v*) a 15% aqueous NaOH solution was added. The aqueous phase was extracted with CH_2Cl_2 (3x50 mL) and the combined organic layers were dried over Na_2SO_4, filtrated and evaporated under vacuum. The crude was then purified by column chromatography (MeOH/CH_2Cl_2, 20% v/v). Brow oil, Yield 24%; silica gel R_f 0.28 (MeOH/DCM 10% *v/v*); 1H NMR ($CDCl_3$) δ: 8.62 (d, *J*=8.7 Hz, 1H, Ar-H), 8.18 (d, *J* = 8.7 Hz, 1H, Ar-H), 7.73 (t, *J* = 7.7 Hz, 1H, Ar-H), 7.48 (t, *J* = 7.7 Hz, 1H, Ar-H), 4.10 (t, *J* = 6.5 Hz, 2H, CH_2), 3.94 (t, *J* = 6.9 Hz, 2H, CH_2), 3.45 (t, *J* = 6.5

Hz, 2H, CH_2), 3.37 (t, *J* = 5.6 Hz, 2H, CH_2), 2.62 (t, *J* = 5.3 Hz, 2H, CH_2),1.90 (m, 6H, 3x CH_2),1.55 (m, 4H, 2x CH_2).

General synthesis of amino acid derivatives C37-C40

A suspension of aminoacid (2.0 g, 1.0 eq) in MeOH (15-20 ml) cooled to 0°C, was stirred for 10 min. Then $SOCl_2$ (2-5 eq) was added dropwise and the mixture was stirred thoroughly for 24h at RT. After monitoring by TLC (MeOH/CH_2Cl_2, 5%v/v) the mixture was evaporated under vacuum. So, the remain solid was washed with Et_2O, and filtrated to obtain derivates **C37-C40**.

Methyl phenylalaninate C38

Starting from **E** (2.0 g, 1.0 eq), $SOCl_2$ (2.88 g, 2.0 eq) and MeOH(20 ml) the title compound was obtained following the general procedure described above. White solid, 1.90g, 88% Yield. silica gel R_f =0.23 (MeOH/CH_2Cl_2, 5%v/v); H NMR ($CDCl_3$) δ: 7.31 (m, 2H, Ar-H), 7.24 (tt, *J* = 7.2, 1.2 Hz, 1H, Ar-H), 7.19 (m, 2H, Ar-H), 3.74 (dd, *J* = 8.4, 5.4 Hz, 1H, CH), 3.70 (s, 3H, CH_3), 3.10 (dd, *J* = 13.2, 4.8 Hz, 1H, CH), 2.86 (dd, *J* = 13.2, 7.8 Hz, 1H, CH), 1.49 (s, 2H, exchange with D_2O, N*H*$_2$). ^{13}C NMR (151 MHz, CDCl3) δ: 175.5, 137.3, 129.3, 128.7, 126.9, 55.9, 52.1, 41.2.

Methyl tryptophanate C39

Starting from **F** (2.0 g, 1.0 eq), $SOCl_2$ (5.83 g, 5.0 eq) and MeOH(15 ml) the title compound was obtained following the general procedure described above. White solid, 70% Yield. silica gel R_f =0.21 (MeOH/CH_2Cl_2, 5%v/v); H NMR ($CDCl_3$) δ: 8.26 (s, 1H, exchange with D_2O, N*H*), 7.61 (d, *J* = 8.0 Hz, 1H, Ar-H), 7.35 (d, *J* = 8.0 Hz, 1H, Ar-H), 7.12 (m, 2H, Ar-H), 7.04 (d, *J* = 8.0 Hz, 1H, Ar-H), 3.84 (dd, *J* = 7.7, 4.8 Hz, 1H, CH), 3.71 (s, 3H, CH_3), 3.29 (dd, *J* = 14.4, 4.8 Hz, 1H, CH), 3.05 (dd, *J* = 14.8, 7.7 Hz, 1H, CH), 1.69 (s, 2H, exchange with D_2O, N*H*$_2$).

General procedure for the synthesis of hybrids C41-C48

To a solution of appropriate amino acid derivate **C37-C40**, (2-3 eq), in dry DMF (5-9 mL), K_2CO_3 (3-7 eq) was added. The mixture was stirred for 30min at RT, then tacrine derivate **C34** or **C36** (1.0 eq) and KI (1.0 eq) were added. The reaction was stirred at RT for 72h, under N_2 fluss. After monitoring by TLC, the mixture was extracted with CH_2Cl_2 (3x30 mL) and the

combined organic layers were dried over Na_2SO_4, filtrated and concentrated under vacuum. The crude was then purified by means of flash chromatography.

Methyl (5-((1,2,3,4-tetrahydroacridin-9-yl)amino)pentyl)histidinate C41

Starting from **C37** (0.3 g, 1.0 eq), **C34** (0.44 g, 3.0 eq), K_2CO_3 (0.84 g, 7.0 eq) and KI (0.14 g, 1.0 eq), the title compound was obtained following the general procedure described above. The reaction was monitored by TLC (MeOH/DCM 10% *v/v*); the crude was purified by column chromatography (MeOH/CH_2Cl_2 → MeOH 100%), to afford the title compound as a yellow oil. Yield 29%; silica gel R_f 0.04 (MeOH/DCM 10% *v/v*); ^{1}H NMR (400 MHz, DMSO) δ: 11.81 (s, 1H, exchange with D_2O, N*H*), 8.15 (d, J = 8.1 Hz, 1H, Ar-H), 7.75 (d, J = 8.3 Hz, 1H, Ar-H), 7.55 (m, 6.6 Hz, 2H, Ar-H), 7.38 (t, J = 7.3 Hz, 1H, Ar-H), 6.84 (d, 1H, Ar-H), 5.42 (t, 1H, exchange with D_2O, N*H*2), 3.59 (s, 3H, CH_3), 3.44 (m, 3H, CH_2 + CH), 2.95 (m, 2H, CH_2), 2.76 (m, 4H, 2 x CH_2), 2.42 (m, 2H, CH_2), 1.86 (m, 4H, 2 x CH_2),1.56 (m, 2H, CH_2), 1.35 (m, 4H, 2 x CH_2).

Methyl (6-((1,2,3,4-tetrahydroacridin-9-yl)amino)hexyl)histidinate C42

Starting from **C37** (0.37 g, 1.0 eq), **C36** (0.52 g, 3.0 eq), K_2CO_3 (0.99 g, 7.0 eq) and KI (0.17 g, 1.0 eq), the title compound was obtained following the general procedure described above. The reaction was monitored by TLC (MeOH/DCM 10% *v/v*) after stirring 96h; the crude was purified by column chromatography (MeOH/CH_2Cl_2 → MeOH 100%), to afford the title compound as a yellow oil. Yield 26%; silica gel R_f 0.05 (MeOH/DCM 10% *v/v*); ^{1}H NMR (400 MHz, DMSO) δ: 11.85 (s, 1H, exchange with D_2O, N*H*), 8.15 (d, J = 8.3 Hz, 1H, Ar-H), 7.74 (d, J = 8.2 Hz, 1H, Ar-H), 7.55 (m, 2H, Ar-H), 7.38 (t, J = 7.5 Hz, 1H, Ar-H), 6.84 (d, 1H, Ar-H), 5.45 (t, 1H, exchange with D_2O, N*H*2), 3.59 (s, 3H, CH_3), 3.44 (m, 3H, CH_2+ CH), 2.94 (m, 2H, CH_2), 2.75 (m, 4H, 2 x CH_2), 2.41 (m, 2H, CH_2), 1.85 (m, 4H, 2 x CH_2), 1.59 (m, 2H, CH_2), 1.28 (m, 6H, 3 x CH_2). ^{13}C NMR (100 MHz, DMSO) δ: 174.72, 154.20, 153.85, 130.93, 129.36, 128.66, 125.77, 124.68, 124.52, 123.45, 123.26, 118.04, 113.50, 60.22, 55.41, 51.72, 49.01, 47.87, 47.51, 30.62, 29.70, 26.74, 26.49, 24.96, 22.50, 21.66.

Methyl (5-((1,2,3,4-tetrahydroacridin-9-yl)amino)pentyl)phenylalaninate C43

Starting from **C38** (0.3 g, 1.0 eq), **C34** (0.31 g, 2.0 eq), K_2CO_3 (0.24 g, 2.0 eq) and KI (0.14 g, 1.0 eq), the title compound was obtained following the general procedure described above. The reaction was monitored by TLC (EtOH/DCM 15% *v/v*); the crude was purified by column chromatography (MeOH/CH_2Cl_2 40% v/v), to afford the title compound as a yellow oil. Yield 30%; silica gel R_f 0.33 (EtOH/DCM 15% *v/v*); 1H NMR (400 MHz, DMSO) δ: 8.13 (d, J = 8.4 Hz, 1H, Ar-H), 7.73 (d, J = 8.4 Hz, 1H, Ar-H), 7.55 (t, J = 7.5 Hz, 1H, Ar-H), 7.37 (t, J = 7.6 Hz, 1H, Ar-H), 7.21 (m, 5H, Ar-H), 5.44 (m, 1H, exchange with D_2O, N*H*$_2$), 3.54 (s, 3H, CH_3), 3,45 (m, 1H, exchange with D_2O, CH) 2.93 (m, 2H, CH_2), 2.83 (m, 2H, CH_2), 2.73 (m, 2H, CH_2), 2.39 (m, 2H, CH_2), 1.84 (m, 4H, 2 x CH_2), 1.54 (m, 2H, CH_2),1.31 (m, 6H, 3 x CH_2). ^{13}C NMR (100 MHz, DMSO) δ: 175.56, 173.46, 157.19, 152.79, 138.88, 138.52, 129.23, 129.12, 127.51, 127.30, 124.64, 124.59, 120.09, 115.64, 63.66, 55.95, 52.17, 48.07, 46.32, 30.68, 30.20, 25.81, 24.96, 24.66, 23.48, 22.97.

Methyl (6-((1,2,3,4-tetrahydroacridin-9-yl)amino)hexyl)phenylalaninate C44

Starting from **C38** (0.3 g, 1.0 eq), **C36** (0.45 g, 3.0 eq), K_2CO_3 (0.46 g, 4.0 eq) and KI (0.14 g, 1.0 eq), the title compound was obtained following the general procedure described above. The reaction was monitored by TLC (EtOH/DCM 7,5% *v/v*); the crude was purified by column chromatography (MeOH/CH_2Cl_2 40% v/v), to afford the title compound as a yellow oil. Yield 42%; silica gel R_f 0.09 (EtOH/DCM 7,5% *v/v*); ^{1}H NMR (400 MHz, DMSO) δ: 8.19 (d, J = 8.5 Hz, 1H, Ar-H), 7.76 (d, J = 8.4 Hz, 1H, Ar-H), 7.62 (t, J = 7.4 Hz, 1H, Ar-H), 7.41 (t, J = 7.5 Hz, 1H, AR-H), 7.22 (m, 4H, Ar-H), 5.87 (s, 1H, exchange with D_2O, N*H*$_2$), 3.63 (s, 1H, CH), 3.52 (m, 5H, CH_3 + CH_2), 2.94 (m, 2H, CH_2), 2.85 (m, 2H, CH_2), 2.73 (m, 2H, CH_2), 2.39 (m, 2H, CH_2), 1.85 (m, 4H, 2x CH_2), 1.59 (m, 2H, CH_2), 1.31 (m, 6H, 3x CH_2). ^{13}C NMR (100 MHz, DMSO) δ: 175.01, 156.67, 152.10, 138.32, 129.53, 129.45, 128.65, 128.55, 126.93, 126.73, 124.08, 124.01, 119.67, 115.29, 63.01, 55.38, 51.61, 48.25, 47.50, 32.68, 30.88, 29.85, 26.80, 26.51, 25.28, 22.92, 22.44.

Methyl (5-((1,2,3,4-tetrahydroacridin-9-yl)amino)pentyl)tryptophanate C45

Starting from **C39** (0.3 g, 1.0 eq), **C34** (0.21 g, 1.1 eq), K_2CO_3 (0.26 g, 2.2 eq) and KI (0.14 g, 1.0 eq), the title compound was obtained following the general procedure described above. The reaction was monitored by TLC (EtOH/DCM 15% *v/v*); the crude was purified by column

chromatography (MeOH/CH_2Cl_2 40% v/v), to afford the title compound as a yellow oil. Yield: 71%; silica gel R_f =0.12 (MeOH/CH_2Cl_2 10% v/v); ^{1}H NMR (400 MHz, DMSO) δ: 10.87 (s, 1H, exchange with D_2O, N*H*), 8.15 (d, J = 8.4 Hz, 1H,Ar-H), 7.75 (d, J = 8.2 Hz, 1H, Ar-H), 7.56 (t, J = 7.5 Hz, 1H, Ar-H), 7.50 (d, J = 7.9 Hz, 1H, Ar-H), 7.38 (t, J = 8.2 Hz, 2H, Ar-H), 7.10 (m, 2H, Ar-H), 7.00 (t, J = 7.4 Hz, 1H, Ar-H), 5.42 (t, J = 6.0 Hz, 1H, exchange with D_2O, N*H*), 3.54 (s, 3H, CH_3), 3.49 (t, J = 6.7 Hz, 1H, CH), 3.01 (m, 2H, CH_2), 2.95 (m, 2H, CH_2), 2.75 (m, 2H, CH_2), 2.44 (m, 2H, CH_2), 1.86 (m, 4H, 2xCH_2), 1.56 (m, 2H, CH_2), 1.34 (m, 6H, 3xCH_2).

Methyl (6-((1,2,3,4-tetrahydroacridin-9-yl)amino)hexyl)tryptophanate C46

Starting from **C39** (0.3 g, 1.0 eq), **C36** (0.54 g, 3.0 eq), K_2CO_3 (0.46 g, 4.0 eq) and KI (0.14 g, 1.0 eq), the title compound was obtained following the general procedure described above. The reaction was monitored by TLC (EtOH/DCM 15% *v/v*); the crude was purified by column chromatography (EtOH/CH_2Cl_2 25% v/v), to afford the title compound as a yellow oil. Yield 21%; silica gel R_f 0.18 (MeOH/DCM 15% *v/v*); ^{1}H NMR (400 MHz, DMSO) δ: 10.86 (s, 1H, exchange with D_2O, N*H*), 8.15 (d, J = 8.3 Hz, 1H, Ar-H), 7.74 (d, J = 8.3 Hz, 1H, Ar-H), 7.56 (t, 1H, Ar-H), 7.49 (d, J = 7.5 Hz, 1H, Ar-H), 7.37 (m, 2H, Ar-H), 7.08 (m, 2H, Ar-H), 6.98 (t, J = 7.2 Hz, 1H, Ar-H), 5.54 (m, 1H, exchange with D_2O, N*H*), 3.53 (s, 3H, CH_3), 3.47 (s, 1H, CH), 2.99 (m, 2H, CH_2), 2.94 (m, 2H, CH_2), 2.73 (m, 2H, CH_2), 2.41 (m, 2H, CH_2), 1.84 (m, 4H, 2x CH_2), 1.56 (m, 2H, CH_2), 1.26 (m, 8H, 4x CH_2). ^{13}C NMR (100 MHz, DMSO) δ: 175.32, 157.66, 151.36, 146.53, 136.56, 128.77, 127.86, 127.78, 123.92, 123.81, 123.73, 121.31, 120.29, 118.72, 118.63, 115.85, 111.83, 110.43, 62.67, 51.59, 48.36, 47.70, 33.45, 30.99, 29.96, 29.21, 26.87, 26.66, 25.42, 23.11, 22.73.

Methyl N^6-((benzyloxy)carbonyl)-N^2-(5-((1,2,3,4-tetrahydroacridin-9-yl)amino)pentyl)lysinate C47

Starting from **C40** (0.3 g, 1.0 eq), **C34** (0.28 g, 1.1 eq), K_2CO_3 (0.26 g, 2.2 eq) and KI (0.14 g, 1.0 eq), the title compound was obtained following the general procedure described above. The reaction was monitored by TLC (MeOH/DCM 10% *v/v*). The crude was purified by column chromatography (MeOH/CH_2Cl_2), to afford the title compound as a yellow oil. Yield 23%; silica gel R_f 0.35 (MeOH/DCM 10% *v/v*); ^{1}H NMR (400 MHz, DMSO) δ: 8.15 (d, J = 8.3 Hz,

1H, Ar-H), 7.75 (d, J = 8.3 Hz, 1H, Ar-H), 7.56 (t, J = 7.5 Hz, 1H, Ar-H), 7.38 (m, 6H, Ar-H, exchange with D_2O, CON*H*), 7.28 (t, 1H, Ar-H), 5.43 (t, 1H, exchange with D_2O, N*H*), 5.04 (s, 2H, CH_2), 3.65 (s, 3H, CH_3), 3.43 (d, J = 6.9 Hz, 3H, CH_2, CH), 3.00 (m, 2H, CH_2), 2.94 (m, 2H, CH_2), 2.75 (m, 2H, CH_2), 2.41 (m, 2H, CH_2), 1.85 (m, 4H, 2 x CH_2), 1.54 (m, 4H, 2 x CH_2), 1.34 (m, 8H, 4 x CH_2).

Methyl N^6-((benzyloxy)carbonyl)-N^2-(6-((1,2,3,4-tetrahydroacridin-9-yl)amino)hexyl)lysinate C48

Starting from **C40** (0.3 g, 1.0 eq), **C36** (0.73 g, 3.0 eq), K_2CO_3 (0.46 g, 4.0 eq) and KI (0.14 g, 1.0 eq), the title compound was obtained following the general procedure described above. The reaction was monitored by TLC (MeOH/EtOAc 15% *v/v*). The crude was purified by column chromatography (MeOH/CH_2Cl_2) to afford the title compound as a yellow oil. Yield 20%; silica gel R_f 0.11 (MeOH/EtOAc 10% *v/v*); ^{1}H NMR (400 MHz, DMSO) δ: 8.15 (d, J = 8.4 Hz, 1H, Ar-H), 7.75 (d, J = 8.4 Hz, 1H, Ar-H), 7.56 (t, J = 7.5 Hz, 1H, Ar-H), 7.40 (m, 6H, Ar-H), 7.29 (m, 1H, exchange with D_2O, CON*H*), 5.43 (t, J = 6.0 Hz, 1H, exchange with D_2O, N*H*), 3.65 (s, 3H, CH_3), 3,45 (m, 1H, exchange with D_2O, CH), 3.15 (m, 2H, CH_2), 3.00 (m, 2H, CH_2), 2.94 (m, 2H, CH_2), 2.76 (m, 2H, CH_2), 2.36 (m, 2H, CH_2), 1.86 (m, 4H, 2xCH_2), 1.55 (m, 4H, 2xCH_2), 1.33 (m, 12H, 6xCH_2). ^{13}C NMR (100 MHz, DMSO) δ: 175.88, 158.34, 156.56, 150.87, 147.37, 137.83, 128.82, 128.78, 128.34, 128.29, 128.17, 123.62, 123.51, 120.74, 116.28, 65.59, 61.35, 55.41, 51.71, 48.46, 47.71, 40.62, 34.01, 32.92, 31.11, 30.04, 29.70, 26.96, 26.74, 25.58, 23.27, 22.96.

Synthesis of (6-((1,2,3,4-tetrahydroacridin-9-yl)amino)hexyl)histidine C49

Lithium hydroxide monohydrate (0.0081 g, 3.0 eq) was dissolved in H_2O (1 mL) and added to a solution of **C42** in a 3:1 mixture of THF/MeOH (8 mL). The solution was then stirred overnight at -20°C. After monitoring by TLC (MeOH/DCM 10% *v/v*), the mixture was evaporated under vacuum. The resulting residue was acidified by the addition of HCl/MeOH 1.25M (0.65 ml, 7.2 eq) and then was evaporated under vacuum. The collected organic layer was dissolved in a mixture MeOH/CH_2Cl_2, 15% v/v (100 mL) and it was filtrated on CELITE to remove lithium salts. The organic layer was concentrated in vacuo to give an oil. Yield 31%; silica gel R_f = 0.15(MeOH/DCM 10% *v/v*); ^{1}H NMR (400 MHz, DMSO) δ: 8.17 (d, *J* = 8.0 Hz,

1H, Ar-H), 7.73 (d, *J* = 8.1 Hz, 1H, Ar-H), 7.55 (m, 1H, Ar-H), 7.37 (m, 1H, Ar-H), 6.94 (s, 1H, Ar-H), 6.38 (s, 1H, Ar-H), 5.46 (s,1H, exchange with D_2O, N*H*), 3.60 (s, 2H, CH_2), 2.93 (m, 2H, CH_2), 2.87 (s, 1H, CH), 2.75 (s, 2H, CH_2), 2.37 (s, 2H, CH_2), 2.05 (m, 2H, CH_2), 1.84 (s, 4H, 2X CH_2), 1.56 (m, 4H, CH_2), 1.42 (s, 2H, CH_2), 1.27 (s, 2H, CH_2).

Synthesis of *N*^{1}-(2-(1*H*-imidazol-4-yl)ethyl)-*N*^{6}-(1,2,3,4-tetrahydroacridin-9-yl)hexane-1,6-diamine C50

To a solution of **H**, (0.4 g, 3.0 eq), in dry DMF (6 mL), K_2CO_3 (0.70 g, 7.0 eq) was added. The mixture was stirred for 30min at RT, then tacrine derivate **C36** (0.26g, 1 eq) and KI (0.12 g, 1.0 eq) were added. The reaction was stirred at RT for 72h, under N_2 fluss. After monitoring by TLC (MeOH/CH_2Cl_2 10% *v/v*), the mixture was extracted with CH_2Cl_2 (3x30mL) and the combined organic layers were dried over Na_2SO_4, filtrated and concentrated under vacuum. The crude was then purified by means of flash chromatography. Yield 33%; silica gel R_f 0.045 (MeOH/DCM 10% *v/v*); ^{1}H NMR (400 MHz, DMSO) δ: 8.14 (d, *J* = 8.4 Hz, 1H, Ar-H), 7.73 (d, *J* = 8.3 Hz, 1H, Ar-H), 7.54 (m, 2H, Ar-H), 7.36 (m, 1H, Ar-H), 6.72 (m, 1H, Ar-H), 5.41 (s, 1H, exchange with D_2O, N*H*), 4.15 (s, 2H, CH_2), 2.94 (m, 2H, CH_2), 2.74 (m, 2H, CH_2), 2.62 (m, 2H, CH_2), 2.51 (m, 2H, CH_2), 1.82 (m, 4H, 2x CH_2), 1.59 (m, 2H, CH_2), 1.32 (m, 8H, 4CH_2).^{13}C NMR (100 MHz, DMSO) δ: 158.43, 151.11, 150.80, 147.46, 134.91, 128.82, 128.27, 123.85, 123.62, 123.51, 120.79, 116.34, 49.75, 49.44, 48.42, 34.03, 31.10, 29.73, 27.02, 26.75, 26.17, 25.56, 23.29, 23.00.

CHAPTER 6. CONCLUSIONS

During these three years of my PhD, my research has focused on the enzyme carbonic anhydrase. In this thesis it was demonstrated how its presence in most organs allows it to be particularly versatile against a wide range of pathologies. The other objective was to demonstrate how the multidrug approach is more effective than the administration of several drugs simultaneously. In addition, within the projects I have expanded my knowledge through the use of techniques such as crystallography, science that seeks to understand the inter and intramolecular bonds using solid phase studies; and I have used interesting tools such as the nanodrop and stopped-flow, the first allows you to assess the concentration of a sample of DNA or a protein using a single microliter of solution, while the second allows you to make measurements of enzyme kinetics.

Going into detail about the 3 major projects reported here, it can be concluded that:

- The first led to the development of new anticancer agents, with the aim of selectively targeting the IX and XII isoforms of carbonic anhydrase, which are those most involved in tumors. To do so, the compounds presented benzenesulfonamides, classical and non-specific inhibitors of CA, and coumarins, selective inhibitors of isoforms IX and XII. The other scaffold present on the hybrid is 5-fluorouracil, an antimetabolite used in many anticancer therapies. All compounds have been shown to be good inhibitors towards the target isoforms, in particular compounds **A12, A20, A22, A34** and **A40**. These were selected for in vitro testing to assess their ability to block growth in 8 cancer cell lines and showed good activity against MDA-MB-231 and T47D. To confirm if they had any apoptotic capacity, annexin V assay was performed with hybrids **A12** and **A22**, which proved to be excellent inducers of apoptosis.
- The second, as well as the main one, is also based on the molecular hybrid strategy and always aims to intervene in the context of cancer therapy. The CA IX and XII target is maintained also in this case while the counterpart is the berberin nucleus that is able to stabilize the G4 structures. They have become a very interesting target as if stabilized they are able to prevent telomerase from immortalizing tumor cells, furthermore G4 present in oncogene promoters, if stabilized, block transcription of proteins overexpressed in various types of tumors. All our hybrids have been evaluated for CA

inhibitory activity showing a remarkable selectivity. The research group of professor Antonio Randazzo of Federico II university of Naples has instead evaluated the binding capacity of our compounds on various G4 present in telomeres, in C-kit, in C-myc and towards the double helix DNA present in hairpins. They effectively stabilized the G4 of C-kit, then Tel and C-myc, while that of hairpins much less than the other sequences. Numerous crystallography assays were also done on these compounds using the sitting drop vapor diffusion technique. We were able to resolve the structure of the **B28**-Tel23 adduct by depositing it in the PDB with code 7PNL.

- The third project, also based on the multitarget approach, seeks to create compounds that can intervene in patients with dementia. The two portions of the hybrids are: an activator CA, can be either an amino acid or a biogenic amine, and tacrine. Activators are much less investigated than inhibitors, however, it has been observed in various studies that they are capable of having procognitive and memory-stimulating effects, whereas tacrine is a known drug in Alzheimer's symptomatic therapy. Two series were designed, one with amide linker and the other with amine linker. The inhibitory activity against both cholinesterases was evaluated by the research group of Professor Oscar Lopez of the University of Seville and it was noted that the amine linker promoted a better inhibition towards both AchE and BuchE. Also going to evaluate the activatory activity it was found that the compounds of the second series were generally better. Finally, Dr. G. Provensi conducted in vivo studies to evaluate the procognitive abilities of the C28, C25, and C42 hybrids and comparing them to the lead D-phenylalanines and tacrines. It was observed that the administration of the hybrids has a better procognitive effect and at lower dosages than the co-administration of the 2 leads demonstrating the validity of the multitarget approach.

Finally, I have also made enzyme kinetics measurements on hundreds of compounds from collaborators around the world evaluating their inhibitory and activating activities as appropriate. I have also characterized from scratch the iota-CA class, evaluating the inhibition of simple and complex anions, classical and commercial sulfonamides, and assessing the activation of the main activators known in the literature.

Through crystallography we also worked hard to obtain an adduct with berberine (the lead of the main project) and Holliday junction, another type of non-canonical DNA folding. After several optimizations we obtained a crystal of which we were able to solve the structure. It was, unfortunately, only DNA without berberine; however, that type of sequence had never been resolved at such a high resolution (0.95Å). It is a result not expected but nevertheless of remarkable workmanship.

REFERENCES

[1] Supuran, C.T. Carbonic anhydrases: novel therapeutic applications for inhibitors and activators. *Nat. Rev. Drug Discovery* **2008**, *7*, 168-181.

[2] Alterio, V.; Di Fiore, A.; D'Ambrosio, K.; Supuran, C.T.; De Simone, G. Multiple binding modes of inhibitors to carbonic anhydrases: how to design specific drugs targeting 15 different isoforms? *Chem. Rev.* **2012**, *112*, 4421-4468.

[3] Nocentini, A.; Supuran, C.T. Advances in the structural annotation of human carbonic anhydrases and impact on future drug discovery. *Expert Opin. Drug Discov.* **2019**, *14*, 1175-1197.

[4] Xu, Y.; Feng, L.; Jeffrey, P. D.; Shi, Y.; Morel, F. M. Structure and metal exchange in the cadmium carbonic anhydrase of marine diatoms. *Nature* **2008**, *452*, 56-61.

[5] Jensen, E.L.; Clement, R.; Kosta, A.; Maberly, S.C.; Gontero, B. A new widespread subclass of carbonic anhydrase in marine phytoplankton. *ISME J.* **2019**, *13*, 2094-2106.

[6] Maren, T. H. Carbonic anhydrase: chemistry, physiology, and inhibition. *Physiol. Rev.* **1967**, *47*, 595-781.

[7] Del Prete, S.; Vullo, D.; Fisher, G.M.; Andrews, K.T.; Poulsen, S.A.; Capasso, C.; Supuran, C.T. Discovery of a new family of carbonic anhydrases in the malaria pathogen Plasmodium falciparum-the η-carbonic anhydrases. *Bioorg. Med. Chem. Lett.* **2014**, *24*, 4389-4396.

[8] Tripp, B. C.; Smith, K.; Ferry, J. G. Carbonic anhydrase: new insights for an ancient enzyme. *J. Biol. Chem.* **2001**, *276*, 48615-48618.

[9] Ferry, J. F. The gamma class of carbonic anhydrases. *Biochim. Biophys. Acta* **2010**, 1804, 374-381.

[10] Smith, K.S.; Jakubzick, C.; Whittam, T. S.; Ferry, J.G. Carbonic anhydrase is an ancient enzyme widespread in prokaryotes. *Proc. Natl. Acad. Sci. U.S.A.* **1999**, *96*, 15184–15189.

[11] Kikutani, S.; Nakajima, K.; Nagasato, C.; Tsuji, Y.; Miyatake, A.; Matsuda, Y. Thylakoid luminal θ-carbonic anhydrase critical for growth and photosynthesis in the marine diatom Phaeodactylum tricornutum. *Proc. Natl. Acad. Sci. U.S.A.* **2016**, *113*, 9828–9833.

[12] Capasso, C.; Supuran, C.T. An overview of the alpha-, beta- and gamma-carbonic anhydrases from Bacteria: can bacterial carbonic anhydrases shed new light on evolution of bacteria? *J. Enzyme Inhib. Med. Chem.* **2015**, *30*, 325–332.

[13] Petreni A.; De Luca V.; Scaloni A.; Nocentini A.; Capasso C.; Supuran CT. Anion inhibition studies of the Zn(II)-bound ι-carbonic anhydrase from the Gram-negative bacterium *Burkholderia territorii*. *J. Enzyme Inhib. Med. Chem.* **2021,** 36, 372-376.

[14] De Luca V.; Petreni A.; Carginale V.; Scaloni A.; Supuran CT.; Capasso C. Effect of amino acids and amines on the activity of the recombinant ι-carbonic anhydrase from the Gram-negative bacterium *Burkholderia territorii*. *J. Enzyme Inhib. Med. Chem.* **2021,** 36,1000-1006.

[15] De Luca V.; Petreni A.; Nocentini A.; Scaloni A.; Supuran CT.; Capasso C. Effect of Sulfonamides and Their Structurally Related Derivatives on the Activity of ι-Carbonic Anhydrase from *Burkholderia territorii*. *Int J Mol Sci.* **2021**, 8, 571.

[16] Supuran, C.T. Structure and function of carbonic anhydrases. *Biochem. J.* **2016**, *473*, 2023-2032.

[17] Supuran, C.T.; Scozzafava, A.; Casini, A. Carbonic anhydrase inhibitors. *Med. Res. Rev.* **2003**, *23*, 146-189.

[18] Supuran, C.T.; Scozzafava, A. Carbonic anhydrases as targets for medicinal chemistry. *Bioorg. Med. Chem.* **2007**, *15*, 4336-4350.

[19] Temperini, C.; Scozzafava, A.; Supuran, C.T. In Drug Design of Zinc-Enzyme Inhibitors: Functional, Structural, and Disease Applications; Supuran, C.T., Winum, J.-Y., Eds.; Wiley: Hoboken, NJ, **2009**; p 473.

[20] Gao, B. B.; Clermont, A.; Rook, S.; Fonda, S. J.; Srinivasan, V. J.; Wojtkowski, M.; Fujimoto, J. G.; Avery, R. L.; Arrigg, P. G.; Bursell, S. E.; Aiello, L. P.; Feener, E. P. Extracellular carbonic anhydrase mediates hemorrhagic retinal and cerebral vascular permeability through prekallikrein activation. *Nat. Med.* **2007**, *13*, 181-188.

[21] Mincione, F.; Scozzafava, A.; Supuran, C.T. The development of topically acting carbonic anhydrase inhibitors as antiglaucoma agents. *Curr. Pharm. Des.* **2008**, *14*, 649-654.

[22] Supuran, C.T. Diuretics: from classical carbonic anhydrase inhibitors to novel applications of the sulfonamides. *Curr. Pharm. Des.* **2008**, *14*, 641-648.

[23] De Simone, G.; Scozzafava, A.; Supuran, C.T. Which carbonic anhydrases are targeted by the antiepileptic sulfonamides and sulfamates? *Chem. Biol. Drug Des.* **2009**, *74*, 317-321.

[24] Basnyat, B.; Gertsch, J. H.; Johnson, E. W.; Castro-Marin, F.; Inoue, Y.; Yeh, C. Efficacy of low-dose acetazolamide (125 mg BID) for the prophylaxis of acute mountain sickness: a prospective, double-blind, randomized, placebo-controlled trial. *High Alt. Med. Biol.* **2003**, *4*, 45-52.

[25] Nocentini, A.; Supuran, C.T. Carbonic anhydrase inhibitors as antitumor/antimetastatic agents: a patent review (2008-2018). *Expert Opin. Ther. Pat.* **2018,** *28*, 729-740

[26] Barreiro, E.; Hussain, S. N. A. Protein carbonylation in skeletal muscles: impact on function. *Antioxid. Redox Signal.* **2010**, *12*, 417-429.

[27] Nishimori, I.; Minakuchi, T.; Kohsaki, T.; Onishi, S.; Takeuchi, H.; Vullo, D.; Scozzafava, A.; Supuran, C.T. Carbonic anhydrase inhibitors: the beta-carbonic anhydrase from Helicobacter pylori is a new target for sulfonamide and sulfamate inhibitors. *Bioorg. Med. Chem. Lett.* **2007**, *17*, 3585-3594.

[28] Capasso, C.; Supuran, C.T. Bacterial, fungal and protozoan carbonic anhydrases as drug targets. *Expert Opin. Ther. Targets.* **2015**, *19*, 1689-1704.

[29] Del Prete, S.; Nocentini, A.; Supuran, C.T.; Capasso, C. Bacterial ι-carbonic anhydrase: a new active class of carbonic anhydrase identified in the genome of the Gram-negative bacterium Burkholderia territorii. *J. Enzyme Inhib. Med. Chem.* **2020**, 35, 1060-1068.

[30] Supuran, C.T.; De Simone, G. In Carbonic Anhydrases as Biocatalysts; Supuran C.T., De Simone G., Eds.; *Elsevier: Walthman*, MA, **2015**, p. 3.

[31] Berman, H.M.; Westbrook, J.; Feng, Z.; Gilliland, G.; Bhat, T.N.; Weissig, H.; Shindyalov, I.N.; Bourne, P.E.The Protein Data Bank. *Nucleic Acids Research*, **2000**, *28*, 235-242. www.rcsb.org

[32] De Simone, G.; Supuran, C.T. Carbonic anhydrase IX: Biochemical and crystallographic characterization of a novel antitumor target. *Biochim. Biophys. Acta* **2010**, *1804*, 404-409.

[33] Whittington, D. A.; Waheed, A.; Ulmasov, B.; Shah, G. N.; Grubb, J. H.; Sly, W. S.; Christianson, D. W. Crystal structure of the dimeric extracellular domain of human carbonic anhydrase XII, a bitopic membrane protein overexpressed in certain cancer tumor cells. *Proc. Natl. Acad. Sci. U.S.A.* **2001**, *98*, 9545-9550.

[34] Schlicker, C.; Hall, R. A.; Vullo, D.; Middelhaufe, S.; Gertz, M.; Supuran, C.T.; Muehlschlegel, F. A.; Steegborn, C. Structure and Inhibition of the CO2-Sensing Carbonic Anhydrase Can2 from the Pathogenic Fungus Cryptococcus neoformans. *J. Mol. Biol.* **2009**, *385*, 1207-1220.

[35] Alber, B.E.; Ferry, J.G. A carbonic anhydrase from the archaeon Methanosarcina thermophila. *Proc Natl Acad Sci U S A.* **1994**, *91*, 6909-6913.

[36] Supuran C.T. Carbonic anhydrase activators. *Future Med Chem.* **2018**, *10*, 561-573.

[37] Masini, E.; Carta, F.; Scozzafava, A.; Supuran, C.T. Antiglaucoma carbonic anhydrase inhibitors: a patent review. *Expert Opin Ther Pat* **2013**, *23*, 705–716.

[38] Matsui, H.; Murakami, M.; Wynns, G. C.; Conroy, C. W.; Mead, A.; Maren, T. H.; Sears, M. L. Membrane carbonic anhydrase (IV) and ciliary epithelium. Carbonic anhydrase activity is present in the basolateral membranes of the non-pigmented ciliary epithelium of rabbit eyes. *Exp. Eye Res.* **1996**, 62, 409-417.

[39] Tang, Y.; Xu, H.; Du, X.; Lit, L.; Walker, W.; Lu, A.; Ran, R.; Gregg, J. P.; Reilly, M.; Pancioli, A.; Khoury, J. C.; Sauerbeck, L. R.; Carrozzella, J. A.; Spilker, J.; Clark, J.; Wagner, K. R.; Jauch, E. C.; Chang, D. J.; Verro, P.; Broderick, J. P.; Sharp, F. R. Gene expression in blood changes rapidly in neutrophils and monocytes after ischemic stroke in humans: a microarray study. *J. Cereb. Blood Flow Metab.* **2006**, 26, 1089-1102.

[40] De Simone, G.; Supuran, C.T. In Drug Design of Zinc-Enzyme Inhibitors: Functional, Structural, and Disease Applications; Supuran, C.T., Winum, J.-Y., Eds.; *Wiley: Hoboken, NJ,* **2009**; p 241.

[41] Liu, C.; Wei, Y.; Wang, J.; Pi, L.; Huang, J.; Wang, P.; Carbonic anhydrases III and IV autoantibodies in rheumatoid arthritis, systemic lupus erythematosus, diabetes, hypertensive renal disease, and heart failure. *Clin. Dev. Immunol.* **2012**, 354594.

[42] Margheri, F.; Ceruso, M.; Carta, F.; Laurenzana, A.; Maggi, L.; Lazzeri, S.; Simonini, G.; Annunziato F.; Del Rosso M.; Supuran C.T.; Cimaz, R. Overexpression of the transmembrane carbonic anhydrase isoforms IX and XII in the inflamed synovium. *J. Enzyme Inhib. Med. Chem.* **2016,** 31, 60-63.

[43] De Simone, G.; Di Fiore, A.; Supuran, C.T. Are carbonic anhydrase inhibitors suitable for obtaining antiobesity drugs? *Curr. Pharm. Des.* **2008**, 14, 655-660.

[44] De Simone, G.; Supuran, C.T. Antiobesity carbonic anhydrase inhibitors. *Curr. Top. Med.* Chem. **2007**, 7, 879-884.

[45] Supuran, C.T.; Di Fiore, A.; De Simone, G. Carbonic anhydrase inhibitors as emerging drugs for the treatment of obesity. *Expert Opin. Emerg. Drugs*. **2008**, 13, 383-392.

[46] Nishimori, I.; Minakuchi, T.; Onishi, S.; Vullo, D.; Scozzafava, A.; Supuran, C.T. Carbonic anhydrase inhibitors. DNA cloning, characterization, and inhibition studies of the human secretory isoform VI, a new target for sulfonamide and sulfamate inhibitors. *J. Med. Chem.* **2007**, 50, 381-388.

[47] Kivelä, J.; Parkkila, S.; Parkkila, A.K.; Rajaniemi, H. A low concentration of carbonic anhydrase isoenzyme VI in whole saliva is associated with caries prevalence. *Caries Res.* **1999**, 33, 178-184.

[48] Ruusuvuori, E.; Li, H.; Huttu, K.; Palva, J.M.; Smirnov, S.; Rivera, C.; Kaila, K.; Voipio, J. Carbonic anhydrase isoform VII acts as a molecular switch in the development of synchronous gamma-frequency firing of hippocampal CA1 pyramidal cells. *J. Neurosci.* **2004**, 24, 2699-2707.

[49] Aspatwar, A.; Tolvanen, M.E.; Ortutay, C.; Parkkila, S. Carbonic anhydrase related protein VIII and its role in neurodegeneration and cancer. *Curr. Pharm. Des.* **2010**, 16, 3264-3276.

[50] Nishimori, I. In Carbonic Anhydrase: Its Inhibitors and Activators; Supuran, C.T., Scozzafava, A., Conway, J., Eds.; *CRC Press: Boca Raton*, FL, **2004**; p 25.

[51] Neri, D.; Supuran, C.T. Interfering with pH regulation in tumours as a therapeutic strategy. *Nat. Rev. Drug Discov*. **2011**, 10, 767-777.

[52] Pastorekova, S.; Parkkila, S.; Zavada, J. Tumor-associated carbonic anhydrases and their clinical significance. *Adv. Clin. Chem*. **2006**, 42, 167-216.

[53] Dai, H.T.; Hong, C.C.; Liang, S.C; Yan, M.D.; Lai, G.M., Cheng, A.L.; Chuang S.E. Carbonic anhydrase III promotes transformation and invasion capability in hepatoma cells through FAK signaling pathway. *Mol Carcinog* **2008**, 47, 956–963.

[54] Battke, C.; Kremmer, E.; Mysliwietz, J.; Gondi, G.; Dumitru, C.; Brandau, S.; Lang, S.; Vullo, D.; Supuran, C.T.; Zeidler, R. Generation and characterization of the first inhibitory antibody targeting tumour-associated carbonic anhydrase XII. *Cancer Immunol. Immunother*. **2011**, 60, 649-658.

[55] Liao, S.Y.; Ivanov, S.; Ivanova, A.; Ghosh, S.; Cote, M.A.; Keefe, K.; Coca-Prados, M.; Stanbridge, E. J.; Lerman, M. I. Expression of cell surface transmembrane carbonic anhydrase genes CA9 and CA12 in the human eye: overexpression of CA12 (CAXII) in glaucoma. *J. Med. Genet*. **2003**, 40, 257-261.

[56] Pastorek, J.; Pastorekova, S. Hypoxia-induced carbonic anhydrase IX as a target for cancer therapy: From biology to clinical use. *Semin. Cancer Biol*. **2015**, 31, 52–64.

[57] Monti, S. M.; Supuran, C.T.; De Simone, G. Anticancer carbonic anhydrase inhibitors: a patent review (2008 -2013). *Expert Opin. Ther. Pat*. **2013**, 23, 737–749.

[58] Lehtonen, J.; Shen, B.; Vihinen, M.; Casini, A.; Scozzafava, A.; Supuran, C.T.; Parkkila, A. K.; Saarnio, J.; Kivelä, A. J.; Waheed, A.; Sly, W. S.; Parkkila, S. Characterization of CA XIII, a novel member of the carbonic anhydrase isozyme family. *J. Biol. Chem*. **2004**, 279, 2719-2727.

[59] Shah, G. N.; Ulmasov, B.; Waheed, A.; Becker, T.; Makani, S.; Svichar, N.; Chesler, M.; Sly, W. S. Carbonic anhydrase IV and XIV knockout mice: roles of the respective carbonic anhydrases in buffering the extracellular space in brain. *Proc. Natl. Acad. Sci .U.S.A.* **2005**, 102, 16771-16776.

[60] Ogilvie, J.M.; Ohlemiller, K.K.; Shah, G. N.; Ulmasov, B.; Becker, T.A.; Waheed, A.; Hennig, A.K.; Lukasiewicz, P. D.; Sly, W. S. Carbonic anhydrase XIV deficiency produces a functional defect in the retinal light response. *Proc. Natl. Acad. Sci. U.S.A.* **2007**, 104, 8514-8519.

[61] Alterio, V.; Di Fiore, A.; D'Ambrosio, K.; Supuran, C.T.; De Simone, G. In Drug Design of Zinc-Enzyme Inhibitors: Functional, Structural, and Disease Applications; Supuran, C.T., Winum, J.-Y., *Eds.; Wiley: Hoboken, NJ*, **2009;** p 73.

[62] Eriksson, A. E.; Kylsten, P. M.; Jones, T. A.; Liljas, A. Crystallographic studies of inhibitor binding sites in human carbonic anhydrase II: a pentacoordinated binding of the SCN- ion to the zinc at high pH. *Proteins* **1988**, 4, 283-293.

[63] Boriack-Sjodin, P.A.; Heck, R.W.; Laipis, P.J.; Silverman, D.N.; Christianson, D.W. Structure determination of murine mitochondrial carbonic anhydrase V at 2.45-A resolution: implications for catalytic proton transfer and inhibitor design. *Proc. Natl. Acad. Sci. U.S.A.* **1995**, 92, 10949-10953.

[64] Eriksson, A. E.; Liljas, A. Refined structure of bovine carbonic anhydrase III at 2.0 A resolution. *Proteins* **1993**, 16, 29-42.

[65] Stams, T.; Nair, S.K.; Okuyama, T.; Waheed, A.; Sly, W.S.; Christianson, D.W. Crystal structure of the secretory form of membrane-associated human carbonic anhydrase IV at 2.8-A resolution. *Proc. Natl. Acad. Sci. U.S.A.* **1996**, 93, 13589-13594.

[66] Angeli, A.; Vaiano, F.; Mari, F.; Bertol E.; Supuran, C.T. Psychoactive substances belonging to the amphetamine class potently activate brain carbonic anhydrase isoforms VA, VB, VII, and XII. *J Enzyme Inhib Med Chem.* **2017**, 32, 1253-1259.

[67] Whittington, D.A.; Grubb, J.H.; Waheed, A.; Shah, G.N.; Sly, W.S.; Christianson, D.W. Expression, assay, and structure of the extracellular domain of murine carbonic anhydrase XIV: implications for selective inhibition of membrane-associated isozymes. *J. Biol. Chem.* **2004**, 279, 7223-7228.

[68] Duda, D.M.; Tu, C.; Fisher, S.Z.; An, H.; Yoshioka, C.; Govindasamy, L.; Laipis, P.J.; Agbandje-McKenna, M.; Silverman, D. N.; McKenna, R. Human carbonic anhydrase III: structural and kinetic study of catalysis and proton transfer. *Biochemistry* **2005**, 44, 10046-10053.

[69] Di Fiore, A.; Monti, S. M.; Hilvo, M.; Parkkila, S.; Romano, V.; Scaloni, A.; Pedone, C.; Scozzafava, A.; Supuran, C.T.; De Simone, G. Crystal structure of human carbonic anhydrase XIII and its complex with the inhibitor acetazolamide. *Proteins* **2008,** 74, 164-175.

[70] Alterio, V.; Hilvo, M.; Di Fiore, A.; Supuran, C.T.; Pan, P.; Parkkila, S.; Scaloni, A.; Pastorek, J.; Pastorekova, S.; Pedone, C.; Scozzafava, A.; Monti, S.M.; De Simone, G. Crystal structure of the catalytic domain of the tumor-associated human carbonic anhydrase IX Proc. *Natl. Acad. Sci. U.S.A*. **2009**, 106, 16233-16238.

[71] Di Fiore, A.; Truppo, E.; Supuran, C.T.; Alterio, V.; Dathan, N.; Bootorabi, F.; Parkkila, S.; Monti, S. M.; De Simone, G. Crystal structure of the C183S/C217S mutant of human CA VII in complex with acetazolamide. *Bioorg. Med. Chem. Lett*. **2010**, 20, 5023-5026.

[72] Capasso, C.; Supuran C.T. Anti-infective carbonic anhydrase inhibitors: a patent and literature review. *Expert Opin. Ther. Pat*. **2013**, 23, 693-704.

[73] Chirica, L.C.; Petersson, C.; Hurtig, M.; Jonsson, B.H.; Borén, T.; Lindskog, S. Expression and localization of alpha- and beta-carbonic anhydrase in Helicobacter pylori. *Biochim. Biophys. Acta*. **2002**, 1601, 192-199.

[74] Nishimori, I.; Minakuchi, T.; Morimoto, K.; Sano, S.; Onishi, S.; Takeuchi, H.; Vullo, D.; Scozzafava, A.; Supuran, C.T. Carbonic anhydrase inhibitors: DNA cloning and inhibition studies of the alpha-carbonic anhydrase from Helicobacter pylori, a new target for developing sulfonamide and sulfamate gastric drugs. *J. Med. Chem*. **2006**, 49, 2117-2126.

[75] Shahi, D.R.; Zdeh, R.; Opekun, A.; Shiotani, A; Graham D.Y. Effect of the carbonic anhydrase inhibitor, acetazolamide, on Helicobacter pylori infection in vivo: a pilot study. *Helicobacte*r **2005**, 10, 136-138.

[76] Del Prete, S.; Isik, S.; Vullo, D.; De Luca, V.; Carginale, V.; Scozzafava, A.; Supuran C.T.; Capasso, C. DNA cloning, characterization, and inhibition studies of an alpha-carbonic anhydrase from the pathogenic bacterium Vibrio cholerae. *J. Med. Chem.* **2012**, 55, 10742-10748.

[77] Vullo, D.; Isik, S.; Del Prete, S.; De Luca, V.; Carginale, V.; Scozzafava, A.; Supuran, C.T.; Capasso, C. Anion inhibition studies of the alpha-carbonic anhydrase from the pathogenic bacterium Vibrio cholerae. *Bioorg. Med. Chem. Lett.* **2013**, 23, 1636-1638.

[78] Innocenti, A.; Hall, R.A.; Schlicker, C.; Scozzafava, A.; Steegborn, C.; Mühlschlegel, F.A.; Supuran, C.T. Carbonic anhydrase inhibitors. Inhibition and homology modeling studies of the fungal beta-carbonic anhydrase from Candida albicans with sulfonamides. *Bioorg. Med. Chem.* **2009**, 17, 4503-4509.

[79] Monti, S.M.; Maresca, A.; Viparelli, F.; Carta, F.; De Simone, G.; Mühlschlegel, F.A.; Scozzafava, A.; Supuran, C.T. Dithiocarbamates are strong inhibitors of the beta-class fungal carbonic anhydrases from Cryptococcus neoformans, Candida albicans and Candida glabrata. *Bioorg. Med. Chem. Lett.* **2012**, 22, 859-862.

[80] Cottier, F.; Leewattanapasuk, W.; Kemp, L.R.; Murphy, M.; Supuran, C.T.; Kurzai, O.; Mühlschlegel, F. A. Carbonic anhydrase regulation and CO(2) sensing in the fungal pathogen Candida glabrata involves a novel Rca1p ortholog. *Bioorg. Med. Chem.* **2013**, 21, 1549-1554.

[81] Davis. R.A.; Hofmann, A.; Osman, A.; Hall, R.A.; Mühlschlegel, F.A.; Vullo, D.; Innocenti, A.; Supuran, C.T.; Poulsen, S.A. Natural product-based phenols as novel probes for mycobacterial and fungal carbonic anhydrases. *J. Med. Chem.* **2011**, 54, 1682-1692.

[82] Isik, S.; Kockar, F.; Arslan, O.; Guler, O.O.; Innocenti, A.; Supuran, C.T. Carbonic anhydrase inhibitors. Inhibition of the beta-class enzyme from the yeast Saccharomyces cerevisiae with anions. *Bioorg. Med. Chem. Lett.* **2008**, 18, 6327-6331.

[83] Hewitson, K.S.; Vullo, D.; Scozzafava. A.; Mastrolorenzo, A.; Supuran, C.T. Molecular cloning, characterization, and inhibition studies of a beta-carbonic anhydrase from Malassezia globosa, a potential antidandruff target. *J. Med. Chem.* **2012**, 55, 3513-3520.

[84] Krungkrai, J.; Scozzafava, A.; Reungprapavut, S.; Krungkrai, S. R.; Rattanajak, R.; Kamchonwongpaisan, S.; Supuran C.T. Carbonic anhydrase inhibitors. Inhibition of Plasmodium falciparum carbonic anhydrase with aromatic sulfonamides: towards antimalarials with a novel mechanism of action? *Bioorg. Med. Chem*. **2005**, 13, 483-489.

[85] Krungkrai, S. R; Suraveratum, N.; Rochanakij, S.; Krungkrai, J. Characterisation of carbonic anhydrase in Plasmodium falciparum. *Int. J. Parasitol* **2001**, 31, 661-668.

[86] Supuran C.T.; Capasso C. The eta-class carbonic anhydrases as drug targets for antimalarial agents. *Expert Opin. Ther. Targets* **2015**, 19, 551-563.

[87] Pan, P.; Vermelho, A.B.; Capaci Rodrigues, G.; Scozzafava, A.; Tolvanen, M.E.; Parkkila, S.; Capasso, C.; Supuran, C.T. Cloning, characterization, and sulfonamide and thiol inhibition studies of an alphacarbonic anhydrase from Trypanosoma cruzi, the causative agent of Chagas disease. *J. Med. Chem*. **2013**, 56, 1761-1771.

[88] Guzel-Akdemir, O.; Akdemir, A.; Pan, P.; Vermelho, A.B.; Parkkila, S.; Scozzafava, A.; Capasso, C.; Supuran, C.T. A class of sulfonamides with strong inhibitory action against the alpha-carbonic anhydrase from Trypanosoma cruzi. *J. Med. Chem.* **2013**, 56, 5773-5781.

[89] Syrjanen, L.; Vermelho, A.B.; Rodrigues Ide, A.; Corte-Real, S.; Salonen, T.; Pan, P.; Vullo, D.; Parkkila, S.; Capasso, C.; Supuran, C.T. Cloning, characterization, and inhibition studies of a beta-carbonic anhydrase from Leishmania donovani chagasi, the protozoan parasite responsible for leishmaniasis. *J. Med. Chem* **2013**, 56, 7372-7381.

[90] Supuran, C.T. Structure-based drug discovery of carbonic anhydrase inhibitors. *J. Enzyme Inhib. Med. Chem.* **2012**, 27, 759–772.

[91] Supuran, C.T. Carbonic anhydrase inhibitors. *Bioorg. Med. Chem. Lett.* **2010**, 20, 3467–3474.

[92] Carta, F.; Supuran, C.T.; Scozzafava, A. Sulfonamides and their isosters as carbonic anhydrase inhibitors. *Future Med. Chem.* **2014**, 6, 1149-1165.

[93] Winum, J.-Y.; Supuran, C.T. Recent advances in the discovery of zinc-binding motifs for the development of carbonic anhydrase inhibitors. *J. Enzyme Inhib. Med. Chem*. **2015**, 30, 321-324.

[94] Supuran, C.T. How many carbonic anhydrase inhibition mechanisms exist? *J. Enzyme Inhib. Med. Chem*. **2016**, 31, 345-360.

[95] Keilin, D.; Mann, T. Carbonic anhydrase. Purification and nature of the enzyme. *Biochem. J.* **1940**, 34, 1163-1176.

[96] Winum, J.-Y.; Monter, J,-L.; Scozzafava, A.; Supuran, C.T. In Drug Design of Zinc-Enzyme Inhibitors: Functional, Structural, and Disease Applications; Supuran, C.T., Winum, J.-Y., Eds.; *Wiley: Hoboken, NJ*, **2009**; p 39.

[97] Supuran, C.T.; De Simone, G. Carbonic Anhydrases as Biocatalysts: From Theory to Medical and Industrial Applications; Supuran, C.T., De Simone, G. Eds.; *Elsevier*. **2015**.

[98] Bozdag, M.; Ferraroni, M.; Nuti, E.; Vullo, D.; Rossello, A.; Carta, F.; Scozzafava, A.; Supuran, C.T. Combining the tail and the ring approaches for obtaining potent and isoform-selective carbonic anhydrase inhibitors: solution and X-ray crystallographic studies. *Bioorg. Med. Chem*. **2014**, 22, 334−340.

[99] Scozzafava, A.; Menabuoni, L.; Mincione, F.; Briganti, F.; Mincione, G.; Supuran, C.T. Carbonic anhydrase inhibitors. Synthesis of water-soluble, topically effective, intraocular pressure-lowering aromatic/heterocyclic sulfonamides containing cationic or anionic moieties: Is the tail more important than the ring? *J. Med. Chem*. **1999**, 42, 2641−2650.

[100] Menchise, V.; De Simone, G.; Alterio, V.; Di Fiore, A.; Pedone, C.; Scozzafava, A.; Supuran, C.T. Carbonic anhydrase inhibitors: stacking with Phe131 determines active site binding region of inhibitors as exemplified by the X-ray crystal structure of a membrane-impermeant antitumor sulfonamide complexed with isozyme II. *J. Med. Chem*. **2005**, 48, 5721-5727.

[101] Scozzafava, A.; Briganti, F.; Ilies, M.A.; Supuran, C.T. Carbonic anhydrase inhibitors: synthesis of membrane-impermeant low molecular weight sulfonamides possessing in vivo selectivity for the membrane-bound versus cytosolic isozymes. *J. Med. Chem.* **2000**, 43, 292-300.

[102] Pacchiano, F.; Carta, F.; McDonald, P.C.; Lou, Y.; Vullo, D.; Scozzafava, A.; Dedhar, S.; Supuran, C.T. Ureido-substituted benzenesulfonamides potently inhibit carbonic anhydrase IX and show antimetastatic activity in a model of breast cancer metastasis. *J. Med. Chem.* **2011**, 54, 1896−1902.

[103] ClinicalTrials.gov, https://clinicaltrials.gov/ct2/results?term=slc-0111Search=Search (Accessed on October 10th 2019); https://clinicaltrials.gov/ct2/show/NCT03450018 (last updated on March 1, 2018); last accessed on October 10th, 2019.

[104] Carta, F.; Aggarwal, M.; Maresca, A.; Scozzafava, A.; McKenna, R.; Supuran, C.T. Dithiocarbamates: a new class of carbonic anhydrase inhibitors. Crystallographic and kinetic investigations. *Chem. Commun. (Camb)*. **2012**, 48, 1868-1870.

[105] Carta, F.; Aggarwal, M.; Maresca, A; Scozzafava, A.; McKenna, R.; Masini, E.; Supuran, C.T. Dithiocarbamates strongly inhibit carbonic anhydrases and show antiglaucoma action in vivo. *J. Med. Chem.* **2012**, 55,1721-1730.

[106] Carta, F.; Akdemir, A.; Scozzafava, A.; Masini, E; Supuran, C.T. Xanthates and trithiocarbonates strongly inhibit carbonic anhydrases and show antiglaucoma effects in vivo. *J. Med. Chem.* **2013**, 56, 4691-4700.

[107] Vullo, D.; Durante, M.; Di Leva, F. S.; Cosconati, S.; Masini, E.; Scozzafava, A.; Novellino, E.; Supuran, C.T.; Carta, F. Monothiocarbamates Strongly Inhibit Carbonic Anhydrases in Vitro and Possess Intraocular Pressure Lowering Activity in an Animal Model of Glaucoma. *J. Med. Chem.* **2016**, 59, 5857-5867.

[108] Mori, M.; Cau, Y.; Vignaroli, G.; Laurenzana, I.; Caivano, A.; Vullo, D.; Supuran, C.T.; Botta, M. Hit recycling: discovery of a potent carbonic anhydrase inhibitor by in silico target fishing. *ACS Chem. Biol.* **2015**, 10, 1964–1969.

[109] Innocenti, A.; Vullo, D.; Scozzafava, A.; Casey, J.R.; Supuran, C.T. Carbonic anhydrase inhibitors. Interaction of isozymes I, II, IV, V and IX with carboxylates. *Bioorg. Med. Chem. Lett.* **2005**, 15, 573–578.

[110] Scozzafava, A.; Supuran, C.T. Hydroxyurea is a carbonic anhydrase inhibitor. *Bioorg. Med. Chem.* **2003**, 11, 2241–2246.

[111] Di Fiore, A.; Maresca, A.; Supuran, C.T.; De Simone, G. Hydroxamate represents a versatile zinc binding group for the development of new carbonic anhydrase inhibitors. *Chem. Commun. (Camb.)* **2012**, 48, 8838–8840.

[112] Nocentini, A.; Gratteri, P.; Supuran, C.T. Phosphorus versus Sulfur: Discovery of Benzenephosphonamidates as Versatile Sulfonamide-Mimic Chemotypes Acting as Carbonic Anhydrase Inhibitors. *Chemistry*. **2019**, 5, 1188-1192.

[113] Alterio, V.; Cadoni, R.; Esposito, D., Vullo, D.; Fiore, A.D.; Monti, S.M.; Caporale, A.; Ruvo, M.; Sechi, M.; Dumy, P.; Supuran, C.T.; De Simone, G.; Winum J.Y. Benzoxaborole as a new chemotype for carbonic anhydrase inhibition. *Chem Commun (Camb).* **2016**, 52, 11983-11986.

[114] Angeli, A.; Tanini, D.; Nocentini, A., Capperucci, A.; Ferraroni, M.; Gratteri, P.; Supuran, C.T. Selenols: a new class of carbonic anhydrase inhibitors. *Chem Commun (Camb).* **2019**, 55, 648-651.

[115] Nair, S. K.; Ludwig, P. A.; Christianson, D. W. Two-site binding of phenol in the active site of human carbonic anhydrase II: structural implications for substrate association. *J. Am. Chem. Soc.* **1994**, 116, 3659–3660.

[116] Innocenti, A.; Vullo, D.; Scozzafava, A.; Supuran, C.T. Carbonic anhydrase inhibitors. Interactions of phenols with the 12 catalytically active mammalian isoforms (CA I–XIV). *Bioorg. Med. Chem. Lett.* **2008**, 18, 1583–1587.

[117] Carta, F.; Temperini, C.; Innocenti, A.; Scozzafava, A.; Kaila, K.; Supuran, C.T. Polyamines inhibit carbonic anhydrases by anchoring to the zinc-coordinated water molecule. *J. Med. Chem.* **2010**, 53, 5511–5522.

[118] Innocenti, A.; Ozturk Sarkaya, S.B.; Gulcin, I.; Supuran, C.T. Carbonic anhydrase inhibitors. Inhibition of mammalian isoforms I-XIV with a seriess of natural product polyphenols and phenolic acids. *Bioorg. Med. Chem.* **2010**, 18, 2159–2164.

[119] Davis, R.A.; Hofmann, A.; Osman, A.; Hall, R. A.; Mühlschlegel, F.A.; Vullo, D.; Innocenti, A.; Supuran, C.T.; Poulsen, S. A. Natural product-based phenols as novel probes for mycobacterial and fungal carbonic anhydrases. *J. Med. Chem.* **2011**, 54, 1682–1692.

[120] Martin, D.P.; Cohen, S.M. Nucleophile recognition as an alternative inhibition mode for benzoic acid based carbonic anhydrase inhibitors. *Chem. Commun. (Camb.)* **2012**, 48, 5259–5261.

[121] Tars, K.; Vullo, D.; Kazaks, A.; Leitans, J.; Lends, A.; Grandane, A.; Zalubovskis, R.; Scozzafava, A.; Supuran, C.T. Sulfocoumarins (1,2- benzoxathiine-2,2-dioxides): a class of potent and isoform-selective inhibitors of tumor-associated carbonic anhydrases. *J. Med. Chem.* **2013**, 56, 293–300.

[122] Buchieri, M.V.; Riafrecha, L.E.; Rodrıguez, O. M.; Vullo, D.; Morbidoni, H. R.; Supuran, C.T.; Colinas, P. A. Inhibition of the b-carbonic anhydrases from Mycobacterium tuberculosis with C-cinnamoyl glycosides: identification of the first inhibitor with anti-mycobacterial activity. *Bioorg. Med. Chem. Lett.* **2013**, 23, 740–743.

[123] Maresca, A.; Temperini, C.; Vu, H.; Pham, N.B.; Poulsen, S.A.; Scozzafava, A.; Quinn, R.J. Supuran, C.T. Non-zinc mediated inhibition of carbonic anhydrases: coumarins are a new class of suicide inhibitors. *J. Am. Chem. Soc.* **2009**, 131, 3057–3062.

[124] Maresca, A.; Temperini, C.; Pochet, L.; Masereel, B.; Scozzafava, A.; Supuran, C.T. Deciphering the mechanism of carbonic anhydrase inhibition with coumarins and thiocoumarins. *J. Med. Chem.* **2010**, 53, 335–344.

[125] Temperini, C.; Innocenti, A.; Scozzafava, A.; Parkkila, S.; Supuran, C.T. The coumarin binding site in carbonic anhydrase accommodates structurallydiverse inhibitors: the antiepileptic lacosamide as an example and lead molecule for novel classes of carbonic anhydrase inhibitors. *J. Med. Chem.* **2010**, 53, 850–854.

[126] Touisni, N.; Maresca, A.; McDonald, P.C.; Lou, Y.; Scozzafava, A.; Dedhar, S.; Winum, J.Y.; Supuran, C.T. Glycosyl coumarin carbonic anhydrase IX and XII inhibitors strongly attenuate the growth of primary breast tumors. *J. Med. Chem.* **2011**, 54, 8271–8277.

[127] Bonneau, A; Maresca, A.; Winum, J.-Y.; Supuran, C.T. Metronidazolecoumarin conjugates and 3-cyano-7-hydroxy-coumarin act as isoform-selective carbonic anhydrase inhibitors. *J. Enzyme Inhib. Med. Chem.* **2013**, 28, 397–401.

[128] Sharma, A.; Tiwari, M.; Supuran, C.T. Novel coumarins and benzocoumarins acting as isoform-selective inhibitors against the tumor-associated carbonic anhydrase IX. *J. Enzyme Inhib. Med. Chem.* **2014**, 29, 292–296.

[129] Maresca, A.; Supuran, C.T. Coumarins incorporating hydroxy- and chloro- moieties selectively inhibit the transmembrane, tumor-associated carbonic anhydrase isoforms IX and XII over the cytosolic ones I and II. *Bioorg. Med. Chem. Lett.* **2010**, 20, 4511–4514.

[130] Maresca, A.; Scozzafava, A.; Supuran, C.T. 7,8-Disubstituted- but not 6,7-disubstituted coumarins selectively inhibit the transmembrane, tumor-associated carbonic anhydrase isoforms IX and XII over the cytosolic ones I and II in the low nanomolar/subnanomolar range. *Bioorg. Med. Chem. Lett.* **2010**, 20, 7255–7258.

[131] D'Ambrosio, K.; Carradori, S.; Monti, S.M.; Buonanno, M.; Secci, D.; Vullo, D.; Supuran, C.T.; De Simone, G. Out of the active site binding pocket for carbonic anhydrase inhibitors. *Chem Commun* **2015**, 51, 302–305.

[132] D'Ascenzio, M.; Carradori, S.; De Monte, C.; Secci, D.; Ceruso, M.; Supuran, C.T. Design, synthesis and evaluation of N-substituted saccharin derivatives as selective inhibitors of tumor-associated carbonic anhydrase XII. *Bioorg Med Chem* **2014**, 22, 1821–1831.

[133] De Monte, C.; Carradori, S.; Secci, D.; D'Ascenzio, M.; Vullo, D.; Ceruso, M.; Supuran, C.T. Cyclic tertiary sulfamates: selective inhibition of the tumor-associated carbonic anhydrases IX and XII by N- and O-substituted acesulfame derivatives. *Eur J Med Chem* **2014**, 84, 240–246.

[134] Parkkila, S.; Innocenti, A.; Kallio, H.; Hilvo, M.; Scozzafava, A.; Supuran, C.T. The protein tyrosine kinase inhibitors imatinib and nilotinib strongly inhibit several mammalian a-carbonic anhydrase isoforms. *Bioorg Med Chem Lett* **2009**, 19, 4102–4106.

[135] Briganti, F.; Mangani, S.; Orioli, P.; Scozzafava, A.; Vernaglione, G.; Supuran, C.T. Carbonic anhydrase activators: x-ray crystallographic and spectroscopic investigations for the interaction of isozymes I and II with histamine. *Biochemistry* **1997**, 36, 10384–10392.

[136] Supuran, C.T. Carbonic anhydrases: from biomedical applications of the inhibitors and activators to biotechnologic use for CO2 capture. *J. Enzyme Inhib Med Chem* **2013**, 28, 229–230.

[137] Temperini, C.; Scozzafava, A.; Supuran, C.T. Carbonic anhydrase activation and the drug design. *Curr Pharm Des*. **2008**, 14, 708-715.

[138] Temperini, C.; Scozzafava, A.; Vullo, D.; Supuran, C.T. Carbonic anhydrase activators. Activation of isozymes I, II, IV, VA, VII, and XIV with l- and d-histidine and crystallographic analysis of their adducts with isoform II: engineering proton-transfer processes within the active site of an enzyme. *Chemistry*. **2006**, 12, 7057-7066.

[139] Temperini, C.; Scozzafava, A.; Puccetti, L.; Supuran, C.T. Carbonic anhydrase activators: X-ray crystal structure of the adduct of human isozyme II with L-histidine as a platform for the design of stronger activators. *Bioorg Med Chem Lett*. **2005**, 15, 5136-5141.

[140] Temperini, C.; Scozzafava, A.; Supuran, C.T. Carbonic anhydrase activators: the first X-ray crystallographic study of an adduct of isoform I. *Bioorg Med Chem Lett*. **2006**, 16, 5152-5156.

[141] Csermely, P.; Agoston, V.; Pongor, S. The efficiency of multi-target drugs: the network approach might help drug design. *Trends Pharmacol. Sci*. **2005**, 26, 178-182.

[142] Espinoza-Fonseca, L.M. The benefits of the multi-target approach in drug design and discovery. *Bioorg. Med. Chem*. **2006**, 14, 896-897.

[143] Zimmermann, G. R.; Lehár, J.; Keith, C. T. Multi-target therapeutics: when the whole is greater than the sum of the parts. *Drug Discov. Today*. **2007**, 12, 34-42.

[144] Sikazwe, D. M. N. The multi-target drug design era is here, consider it. *Drug Design* **2012**, 1, 1000-1101.

[145] P. Blandina, G. Provensi, M. B. Passani, C. Capasso, C. T. Supuran Carbonic anhydrase modulation of emotional memory. Implications for the treatment of cognitive disorders, *Jour. of Enz. Inh. and Med. Chem*. **2020**, 35:1, 1206-1214.

[146] Zhang P.; Xu S.; Zhu Z.; Multi-target design strategies for the improved treatment of Alzheimer's disease. *Eur. J. Med. Chem*. **2019**, 176, 228-242.

[147] M.L. Taddei, E. Giannoni, G. Comito, P. Chiarugi, Microenvironment and tumor cell plasticity: an easy way out, *Cancer Lett.* **2013**, 341, 80–96.

[148] E.C. Finger, A.J. Giaccia, Hypoxia, inflammation, and the tumor microenvironment in metastatic disease. *Cancer Metastasis Rev*. **2010**, 29, 285–293.

[149] R.A. Gatenby, K. Smallbone, P.K. Maini, F. Rose, J. Averill, R.B. Nagle, L. Worrall, R.J. Gillies, Cellular adaptations to hypoxia and acidosis during somatic evolution of breast cancer, Br. *J. Cancer.* **2007**, 97, 646–653.

[150] A. Nocentini, C.T. Supuran, Carbonic Anhydrases: An Overview. In Carbonic Anhydrases; Nocentini, A.; Supuran CT. Amsterdam: *Elsevier;* **2019**. p. 3-16.

[151] C.T. Supuran, V. Alterio, A. Di Fiore, K. D' Ambrosio, F. Carta, S.M. Monti, G. De Simone, Inhibition of carbonic anhydrase IX targets primary tumors, metastases, and cancer stem cells: Three for the price of one. *Med. Res. Rev*. **2018**, 38,1799-1836.

[152] C.L. Lomelino, J.T. Andring, R. McKenna, Crystallography and its impact on carbonic anhydrase research, *Int. J. Med. Chem*. 2018, 2018, 9419521.

[153] https://clinicaltrials.gov/ct2/show/NCT03450018. Last access on January 9, **2020**.

[154] A. Nocentini, S. Bua, C.L. Lomelino, R. McKenna, M. Menicatti, G. Bartolucci, B. Tenci, L. Di Cesare Mannelli, C. Ghelardini, P. Gratteri, C.T. Supuran, Discovery of new sulfonamide carbonic anhydrase IX inhibitors incorporating nitrogenous bases, *ACS Med. Chem. Lett*. **2017**, 8, 1314-1319.

[155] A. Palasz, Ciez. Dariusz, In search of uracil derivatives as bio-active agents. Uracils and fused uracils: Synthesis, biological activity and applications, *Eur. J. Med. Chem*. **2015**, 97, 582-611.

[156] M. Legraverend, D. S. Grierson, The purines: Potent and versa-tile small molecule inhibitors and modulators of key biological targets, *Bioorg. Med. Chem*. **2006**, 14, 3987-4006.

[157] W. B. Parker, Enzymology of Purine and Pyrimidine Antimetabolites Used in the Treatment of Cancer, *Chem. Rev.* **2009**, 109, 2880-2893.

[158] J. Calderón-Arancibia, C. Espinosa-Bustos, A. Cañete-Molina, R.A. Tapia, M. Faúndez, M.J. Torres, A. Aguirre, M. Paulino, C.O. Salas, Synthesis and Pharmacophore Modelling of 2,6,9-Trisubstituted Purine Derivatives and Their Potential Role as Apoptosis-Inducing Agents in Cancer Cell Lines, *Molecules.* **2015**, 20, 6808-6826.

[159] B. Daniel, D. Longley, Harkin Paul, G. Patrick, Johnston, 5-Fluorouracil: mechanisms of action and clinical strategies, *Nature Reviews Cancer*. **2003**, 3, 330–338.

[160] L.K. Gediya, V.C. Njar, Promise and challenges in drug discovery and development of hybrid anticancer drugs, *Expert Opin. Drug Discov*. **2009**, 4, 1099-1111.

[161] R.G. Khalifah, The carbon dioxide hydration activity of carbonic anhydrase, *J. Biol. Chem.* **1971**, 246, 2561−2573.

[162] Y. Mo, Probing the nature of hydrogen bonds in DNA base pairs. *J. Mol. Model.* **2006**, 12, 665-672.

[163] Y. Liu, S.C. West, Happy Hollidays: 40th anniversary of the Holliday Junction. *Nat. Rev. Mol. Cell. Biol.* **2004**, 5, 937-944.

[164] S. Burge, G. N. Parkinson, P. Hazel, A. K. Todd, S. Neidle, Quadruplex DNA: sequence, topology and structure. *Nucleic Acids Res*. **2006**, 34, 5402-5415.

[165] A. T. Phan, Human telomeric G-quadruplex: structures of DNA and RNA sequences. *The FEBS journal*. **2010,** 277, 1107-1117.

[166] N. Zhang, A. Gorin, A. Majumdar, V. Kettani, V. Chernichenko, E. Skripkin, D. J. Patel, V-shaped scaffold: a new architectural motif identified in an A·(G·G·G·G) pentad-containing dimeric DNA quadruplex involving stacked G(anti)·G(anti)·G(anti)·G(syn) tetrads. *J. Mol. Biol.* **2001**, 311, 1063-1079.

[167] S. Niedle, Quadruplex nucleic acids as novel therapeutic targets. *J. Med. Chem*. **2016**, 59, 5987-6011.

[168] R. Hansel, S. Foldynova-Trantirkova, F. Lohr, J. Buck, V. Bongartz, E. Bamberg, H. Schwalbe, V. Dotsch, L. Trantirek, Evaluation of parameters critical for observing nucleic acids inside living Xenopus laevis oocytes by in-cell NMR spectroscopy. *JACS*. **2009**, 131, 15761-15768.

[169] R. Hänsel-Hertsch, M. Di Antonio, S. Balasubramanian, DNA G-quadruplexes in the human genome: detection, functions and therapeutic potential. *Nat. Rev. Mol. Cell. Biol*. **2017**, 18, 279-284.

[170] J.H. Tan, L.Q. Gu, J.Y. Wu, Design of selective G-quadruplex ligands as potential anticancer agents. *Mini Rev. Med. Chem*. **2008**, 8, 1163-78.

[171] O. Tian-miao, L. Yu-jing, T. Jia-heng, H. Zhi-shu, W. Kwok-Yin, G. Lian-quan, G-Quadruplexes: Targets in Anticancer Drug Design. *ChemMedChem*. **2008**, 3, 690-713;

[172] J. Liang, Y.L. Wu, B. J. Chen, W. Zhang, Y. Tanaka, H. Sugiyama, The C-Kit Receptor-Mediated Signal Transduction and Tumor-Related Diseases. *Int. J. Biol. Sci.* **2013,** 9, 435-443.

[173] Y. Yarden, W.J. Kuang, T. Yang-Feng, L. Coussens, S. Munemitsu, T.J. Dull, E. Chen, J. Schlessinger, U. Francke, A. Ullrich, Human proto-oncogene c-kit: a new cell surface receptor tyrosine kinase for an unidentified ligand. *EMBO J.* **1987,** 6, 3341-3351

[174] C.R. Antonescu, The GIST paradigm: lessons for other kinase-driven cancers. *J Pathol.* **2011**, 223, 251-261.

[175] M. Heinrich, C.D. Blanke, B.J. Druker, C.L. Corless, Inhibition of KIT tyrosine kinase activity: a novel molecular approach to the treatment of KIT-positive malignancies. *J Clin Oncol.* **2002**, 20, 1692-1703.

[176] H.Q. Shen, Y.M. Tang, S.L.Yang, B.Q. Qian, H. Song, S.W. Shi, W.Q. Xu, Analysis of CD117 expression on leukemia cells. *Chinese Journal of Hematology.* **2003**, 24, 516-5

[177] X. Jiang, X. Hao, L. Jing, G. Wu, D. Kang, X. Liu, P. Zhan, Recent applications of click chemistry in drug discovery. *Expert Opin Drug Discov*. **2019**, 14, 779-789.

[178] C. Bazzicalupi, M. Ferraroni, A.R. Bilia, F. Scheggi, P. Gratteri, The crystal structure of human telomeric DNA complexed with berberine: an interesting case of stacked ligand to G-tetrad ratio higher than 1:1. *Nucleic Acids Res*. **2013**, 41, 632-8.

[179] I. Russo Krauss, A. Merlino, A. Vergara, F. Sica, "An overview of biological macromolecule crystallization", *International journal of molecular sciences* **2013**, 14, 11643–11691.

[180] B.H. Mooers, Crystallographic studies of DNA and RNA. *Methods*. **2009**, 47, 168-76.

[181] R. Henderson, "Cryo-protection of protein crystals against radiation damage in electron and X-ray diffraction", *Proceedings: Biological Sciences* **1990**, 6–8.

[182] W. Kabsch, "Xds", *Acta Crystallographica Section D: Biological Crystallography* **2010**, 66, 125–132.

[183] A. J. McCoy, R. W. Grosse-Kunstleve, P. D. Adams, M. D. Winn, L. C. Storoni, R. J. Read, "Phaser crystallographic software", *Journal of applied crystallography* **2007**, 40, 658–674.

[184] A. Vagin, A. Teplyakov, "MOLREP: an automated program for molecular replacement", *Journal of applied crystallography* **1997**, 30, 1022–1025.

[185] G. N. Murshudov, A. A. Vagin, E. J. Dodson, "Refinement of macromolecular structures by the maximum-likelihood method", *Acta Crystallographica Section D: Biological Crystallography* **1997**, 53, 240–255.

[186] N.H. Campbell, G.N. Parkinson, Crystallographic studies of quadruplex nucleic acids. *Methods.* **2007**, 43, 252-63.

[187] C. A. Lane, J. Hardy, Schott, Alzheimer's disease. *Eur.J. Neurol.* **2018**, 25, 59–70.

[188] R. Hodson, Alzheimer's disease. *Nature*. **2018**, 559, S4-S7.

[189] Alzheimer's disease. Lancet 2016;388(10043):505-17. Alzheimer's Association Report. 2016 Alzheimer's disease facts and figures. *Alzheimer's Dement*. **2016**, 12, 459-509.

[190] H. Jahn, Memory loss in Alzheimer's disease. *Dialogues Clin. Neurosci*. **2013**, 15, 445-454.

[191] J.M. Roldán-Peña, V. Romero-Real, J. Hicke, I. Maya, A. Franconetti, I. Lagune,s J.M. Padrón, S. Petralla, E. Poeta, M. Naldi, M. Bartolini, B. Monti, M.L Bolognesi, Ó. López, J.G. Fernández-Bolaños, Tacrine-O-protected phenolics heterodimers as multitarget-directed ligands against Alzheimer's disease: Selective subnanomolar BuChE inhibitors. *Eur.J. Med. Chem*. **2019**, 181, 111550.

[192] A. Torres, M. Söllhuber, M. Fernandez, J.M. Sanchez-Montero, Multi-Target-Directed Ligands and other Therapeutic Strategies in the Search of a Real Solution for Alzheimer's Disease. *Curr. Neuropharmacol.* **2014**, 12, 2-36.

[193] A.S. Schachter, K.L. Davis, Alzheimer's disease. *Dialogues Clin. Neurosci*. **2000**, 2, 91–100.

[194] A. Serrano-Pozo, M.P. Frosch, E. Masliah, B.T. Hyman, Neuropathological Alterations in Alzheimer Disease. *Cold Spring Harb Perspect Med*. **2011**, 1, 006189.

[195] M. Vinícius Ferreira Silva, C.D.M. Gomide Loures, L.C.V. Alves, L.C. de Souza, K.B.G. Borges, M.D.G. Carvalho, Alzheimer's disease: risk factors and potentially protective measures. *J. Biomed. Sci*. **2019**; 26:33.

[196] S. Tiwari, V. Atluri, A. Kaushik, Alzheimer's disease: pathogenesis, diagnostics, and therapeutics. *Int. J. Nanomed*. **2019**, 14, 5541–5554.

[197] M. Robinson, B.Y. Lee, F.T. Hane, Recent Progress in Alzheimer's Disease Research, Part 2: Genetics and Epidemiology. *J. Alzheimer's Dis*. **2017**, 57, 317–330.

[198] C. Qiu, M. Kivipelto, E. Von Strauss, Epidemiology of Alzheimer's disease: occurrence, determinants, and strategies toward intervention. *Dialogues Clin. Neurosci*. **2009**, 11, 111–128.

[199] G.D. Stanciu, A. Luca, R.N. Rusu, V. Bild, S.I. Beschea Chiriac, C. Solcan, W. Bild, D.C. Ababei, Alzheimer's Disease Pharmacotherapy in Relation to Cholinergic System Involvement. *Biomolecules.* **2020**, 10:40.

[200] Y. Xu, S. Cheng, J.L. Sussman, I. Silman, H. Jiang, Computational Studies on Acetylcholinesterases. *Molecules.* **2017**, 22, 1324.

[201] M.K. Sun, D.L. Alkon, Pharmacological enhancement of synaptic efficacy, spatial learning, and memory through carbonic anhydrase activation in rats. *J. Pharmacol. Exp. Ther.* **2001**, 297, 961–967.

[202] A. Aspatwar, M.E. Tolvanen, S. Parkkila, An update on carbonic anhydrase-related proteins VIII, X and XI. *J Enzyme Inhib Med Chem* **2013**, 28, 1129–42.

[203] P. Halmi, S. Parkkila, J. Honkaniemi, Expression of carbonic anhydrases II, IV, VII, VIII and XII in rat brain after kainic acid induced status epilepticus. *Neurochem Int* **2006**, 48, 24-30.

[204] C.T. Supuran, Acetazolamide for the treatment of idiopathic intracranial hypertension. *Expert Rev Neurother*. **2015**, 15, 851-6.

[205] P.D. Brown, S.L. Davies, T. Speake, I.D. Millar, Molecular mechanisms of cerebrospinal fluid production. *Neuroscience* **2004**, 129, 957-970.

[206] M.K. Sun, D.L. Alkon, Carbonic anhydrase gating of attention: memory therapy and enhancement. *Trends Pharmacol. Sci*. **2002**, 23, 83–89.

[207] S. P. Wiebe, U.V. Staubli, Recognition memory correlates of hippocampal theta cells. *J. Neurosci. Off. J. Soc. Neurosci.* **2001**, 21, 3955–3967.

[208] L. Canto de Souza, G. Provensi, D. Vullo, F. Carta, A. Scozzafava, A. Costa, S.D. Schmidt, M.B. Passani, C.T. Supuran, P. Blandina, Carbonic anhydrase activation enhances object recognition memory in mice through phosphorylation of the extracellular signal-regulated kinase in the cortex and the hippocampus. *Neuropharmacology*. **2017**, 118, 148–156.

[209] M. Rossi, M. Freschi, L. Nascente, A. Salerno, S. de Melo, V.T.F. Nachon, F. Chantegreil, O. Soukup, L. Prchal, M. Malaguti, C. Bergamini, M. Bartolini, C.Angeloni, S. Hrelia, L.A.S. Romeiroand, M.L. Bolognesi, Sustainable Drug Discovery of Multi-Target-Directed Ligands for Alzheimer's Disease. *J Med Chem*. **2021**, 64, 4972-4990.

[210] M.D. Winn, C.C. Ballard, K.D. Cowtan, E.J. Dodson, P. Emsley, P.R. Evans, R.M. Keegan, E.B. Krissinel, A.G. Leslie, A. McCoy, S.J. McNicholas, G.N. Murshudov, N.S. Pannu, E.A. Potterton, H.R. Powell, R.J. Read, A. Vagin, K.S. Wilson, "Overview of the CCP4 suite and current developments", *Acta Crystallographica Section D: Biological Crystallography* **2011**, 67, 235–242.